

THE FAILURE OF THERMAL BARRIER COATINGS AT ELEVATED TEMPERATURES

by

Nazik Meltem Yanar

BS, Middle East Technical University, 1995

MS, Middle East Technical University, 1998

Submitted to the Graduate Faculty of
the School of Engineering in partial fulfillment
of the requirements for the degree of
Doctor of Philosophy

University of Pittsburgh

2004

UNIVERSITY OF PITTSBURGH
SCHOOL OF ENGINEERING

This dissertation was presented

by

Nazik Meltem Yanar

It was defended on

April 1, 2004

and approved by

Jack Beuth, Professor, Department of Mechanical Engineering

Judith Yang, Assistant Professor, Department of Materials Science and Engineering

Scott Mao, Professor, Department of Mechanical Engineering

Gerald H. Meier, Professor, Department of Materials Science and Engineering
Dissertation Director

Frederick S. Pettit, Professor, Department of Materials Science and Engineering
Dissertation Director

THE FAILURE OF THERMAL BARRIER COATINGS AT ELEVATED TEMPERATURES

Nazik Meltem Yanar, PhD

University of Pittsburgh, 2004

In this study, the current state of the art thermal barrier coating (TBC) systems (heavy grit blasted Pt aluminide and NiCoCrAlY Bond Coats with EBPVD TBCs) were investigated first followed by TBC systems which were modified based upon the results obtained on the failure of the state of the art TBC systems. The specimens were subjected to cyclic oxidation testing, mostly at 1100°C in a bottom loading furnace in laboratory air. Optical and scanning electron microscopy (SEM) were used for characterization of the as-processed and failed specimens.

The state of the art TBC systems with NiCoCrAlY bond coats failed in the presence of defects which were identified as TBC defects, transient oxides, surface defects and reactive element (RE) rich oxide protrusions. On the other hand, the failure of the state of the art TBC systems with Pt aluminide bond coats were due to deformation of the bond coat by a mechanism known as ratcheting. The stored strain energy in the TGO was also a factor that contributed to the failure of both systems. Most of the modifications performed on the state of the art TBC systems improved their lives to some extent. In the case of NiCoCrAlY systems, elimination or at least minimization of the identified defects was responsible for the improvements whereas the prevention of the ratcheting type of failure was the main reason for the improvement in lives in the case of Pt aluminide systems. On the other hand, other issues such as slower growth of the

TGO as well as improved interfacial toughesses with some of the modifications were observed to be contributing factors in the improved lives.

Based on the observations on the failure of both the state of the art as well as the modified TBC systems, the surface condition of the bond coats as well as the morphology of the TBCs close to the TGO were found to have a first order effect on the failure of TBC systems. The characteristics of the TGO, such as composition, growth rate and adherence both to the bond coat and the TBC, as well as the characteristics of the bond coats were also observed to have an effect on the failures. Recommendations for future work that should be pursued to better define the conditions necessary for optimized TBC performances are given .

TABLE OF CONTENTS

ACKNOWLEDGEMENTS.....	xxi
1.0 INTRODUCTION	1
2.0 BACKGROUND	5
2.1 THERMAL BARRIER COATINGS.....	5
2.1.1 Fabrication Procedures.....	7
2.1.1.1 Plasma Sprayed TBCs	7
2.1.1.2 EBPVD TBCs	10
2.2 BOND COATS	11
2.2.1 Diffusion Aluminide Coatings.....	11
2.2.1.1 Fabrication Procedures	12
2.2.1.2 Microstructural Evolution	13
2.2.1.3 Performance of Diffusion Aluminide Bond Coats	15
2.2.2 MCrAlY Bond Coats	17
2.2.2.1 Fabrication Procedures	17
2.2.2.3 Performance of MCrAlY Bond Coats	19
2.3 THERMALLY GROWN OXIDE (TGO)	21
2.3.1 Transient Oxidation	22
2.3.2 Growth and Adherence of TGO.....	23
2.3.3 Stresses Generated During Oxidation.....	25

2.4 FAILURE MECHANISMS OF TBC SYSTEMS	26
3.0 EXPERIMENTAL DETAILS	33
4.0 RESULTS AND DISCUSSION	39
4.1 STUDIES OF BOND COATS WITHOUT TBCS	39
4.1.1 NiCoCrAlY Bond Coats	39
4.1.2 Platinum Aluminide Bond Coats	54
4.2 TBC INVESTIGATIONS.....	67
4.2.1 TBC Failure Premises	67
4.2.2 Defects in TBC systems.....	71
4.2.2.1 Transient Oxides	71
4.2.2.2 TBC defects	76
4.2.2.3 Surface defects	97
4.2.2.4 Reactive Element Oxide protrusions	100
4.2.2.5 Intermixed zone	100
4.2.2.6 Contamination	114
4.2.2.7 Voids	115
4.2.2.8 Grain boundary ridges	116
4.2.2.9 Abnormal Defects	116
4.2.3 Failure of Current State-of-the-Art TBC Systems.....	125
4.2.3.1 NiCoCrAlY Bond Coats	126
4.2.3.2 Platinum Modified Aluminide Bond Coats	140
4.2.4 Modified TBC Systems.....	157
4.2.4.1 NiCoCrAlY Bond Coats	157

4.2.4.2 Platinum Aluminide Bond Coats	201
4.2.4.3 No Bond Coat Systems	235
4.3 SOME MICROSTRUCTURAL OBSERVATIONS.....	248
4.4 IMPORTANT CONDITIONS NECESSARY FOR OPTIMIZED PERFORMANCES AND RECOMMENDATIONS FOR FUTURE WORK.....	264
5.0 CONCLUSIONS	269
5.1 BOND COATS WITH NO TBCS.....	269
5.2 CURRENT STATE OF THE ART TBC SYSTEMS.....	270
5.3 MODIFIED TBC SYSTEMS	270
5.4 NO BOND COAT TBC SYSTEMS.....	272
BIBLIOGRAPHY.....	274

LIST OF TABLES

Table 1 Compositions of NiCoCrAlY bond coats (wt %)	36
Table 2 Summary of the development of intermixed zone for various TBC systems	103
Table 3 Failure Times for the current state of the art TBC systems	126
Table 4 Failure times for the TBC systems with modified NiCoCrAlY Bond Coats	158
Table 5 Failure Times for TBC systems with modified Pt Aluminide Bond Coats	202
Table 6 Failure Times for no Bond Coat TBC systems	237

LIST OF FIGURES

Figure 1 A schematic showing the various layers in a TBC system.....	3
Figure 2 Scanning electron micrographs showing the typical microstructures of (a) EBPVD and (b)APS YSZ Thermal Barrier Coatings.....	4
Figure 3 A diagram showing the improvement of temperature capabilities of superalloys by the use of TBCs [1].....	6
Figure 4 The Zirconia-Yttria phase diagram [3].....	8
Figure 5 Schematics illustrating the equipment used for (a) plasma spray, and (b) EBPVD processes.	9
Figure 6 (a) Schematic to show the typical configuration of the specimens used in this study.	37
Figure 7 Macrographs showing the typical TBC failures, (a) and (b).	38
Figure 8 The surface, (a), and cross-sectional micrographs, (b), of NiCoCrAlY bond coats showing the presence of surface defects as well as porosity and oxide inclusions in the as processed condition. The phases present in NiCoCrAlY-A and NiCoCrAlY-B coatings are labeled in (c) and (d) respectively.....	43
Figure 9 Scanning electron micrographs showing the degradation of NiCoCrAlY-A bond coats after 209, (a), 955, (b and c), and 3031, (d), cycles of exposure at 1100°C.....	45
Figure 10 Scanning electron micrographs showing the degradation of NiCoCrAlY-B coatings after 209, (a), 955, (b), and 3031 cycles, (c), of exposure at 1100°C.....	47
Figure 11 Cross sectional micrographs from a NiCoCrAlY-A bond coat in the as processed condition, (a), and after 209, (b), and 955, (c), cycles of exposure at 1100°C showing the roughening of the surface. The surface became smoother after 3031 cycles of exposure (d).	49
Figure 12 (a) Surface micrograph of the NiCoCrAlY-A bond coat after exposure at 1080°C for 2 hrs in air showing the transient oxides developed and the spallation of the oxide scale. (b) Surface micrograph showing the purer and more adherent alumina scale developed after the	

bond coat was preoxidized in an Ar-4% H_2 atmosphere at 1100°C for 100 hrs and then exposed in air under the same conditions as in (a).	50
Figure 13 (a) Surface micrograph of the NiCoCrAlY-B bond coats after exposure at 1080°C for 2 hrs in air showing the transient oxides developed and the spallation of the oxide scale. (b) Surface micrograph showing the purer and more adherent alumina scale developed after the bond coat was preoxidized in an Ar-4% H_2 atmosphere at 1100°C for 100 hrs and then exposed in air under the same conditions as in (a).	51
Figure 14 Scanning electron micrographs showing the surface of a hand polished NiCoCrAlY-A bond coat after exposure at 1100°C for 100 cycles at (a) low and (b) high magnifications.	52
Figure 15 Scanning electron micrographs showing the surface of a heavy grit blasted NiCoCrAlY-A bond coat after exposure at 1100°C for 100 cycles at (a) low and (b) high magnifications.	53
Figure 16 Optical micrographs of the Pt-Aluminide bond coat a) in the as processed condition, b) after exposure at 1200°C for 20 cycles showing the γ' that nucleated preferentially at the β phase grain boundaries, (c) Scanning electron micrograph showing a β phase grain boundary enriched in refractory metal rich particles, (d) optical micrograph of the TBC system with the Pt aluminide bond coat, which failed at 1200°C after 132 cycles, showing the development of a continuous layer of γ' in β phase.	58
Figure 17 Cross-sectional micrographs showing the degradation of Pt aluminide bond coats after exposure at 1200°C for 40, (a), 60, (b), 80, (c), 100, (d), 130, (e), and 200 cycles, (f), respectively. The arrows point to the large cavities formed at the later stages of oxidation in the bond coat, (e), and at the bond coat/oxide interface, (f).	61
Figure 18 Scanning electron micrographs from the surface of Pt aluminide bond coats showing a) the ridges that developed at the grain boundaries of the bond coat , b) the cracks that formed on these grain boundary ridges after exposure at 1200°C for 40 cycles, c) the absence of ridges after grit blasting operation, which is generally applied prior to TBC deposition.	63
Figure 19 Scanning electron micrographs from the surface of the Pt aluminide bond coat, which was exposed at 1200°C for 15 hours, showing the cracks that developed due to volume reduction following the phase transformation from metastable to stable alumina, (a), and the oxide ridges developing at these cracks, (b).	64
Figure 20 a) Scanning electron micrograph from the surface of the Pt-Aluminide bond coat, which was highly rumpled after exposure at 1100°C for 955 cycles. Cross sectional scanning electron micrographs showing (b) the large cavities formed at the bond coat/oxide interface after exposure at 1100°C for 3031 cycles. (c) the alumina formed on the surface of the large cavities, (arrow), as a result of oxygen diffusion through the cracks present at	

the initially formed alumina,(d) the spinel phase formed on the alumina scale in these cavities.	66
Figure 21 The plot of inverse of the failure times (t) versus reciprocal temperature (T) for the state of the art TBC systems with NiCoCrAlY and Pt aluminide bond coats.	69
Figure 22 Scanning electron micrographs showing that dense TBCs can be a source of crack initiation (a) and / or propagation sites (b), probably due to relatively high stored energy in the TBC.....	70
Figure 23 Schematic diagram summarizing the TBC failures based on experimental results. ...	71
Figure 24 Scanning electron micrographs showing the presence of a dense and uniform TGO when it is pure alumina, (a), and the porous and non uniform TGO when oxides other than alumina are present, (b).....	73
Figure 25 Scanning electron micrographs showing the poor adherence between the transient oxides and the TBC, arrow in (a), as well as between the transient oxides and the alumina, arrow in (b). The adherence between the TBC and the TGO is stronger when it is pure alumina, arrow in (c) and also when the transient oxide is relatively thin, arrow in (d) . .	75
Figure 26 Scanning electron micrograph showing cracks initiated in the vicinity of defects, which were referred to as “points of separation in the TBC”.....	80
Figure 27 Scanning electron micrograph showing a corn kernel type of defect in the TBC.....	80
Figure 28 Scanning electron micrographs of a specimen with many TBC defects, which were referred to as “points of separation in the TBC”, in the as processed condition, (a), and after the failure, (b) and (c).....	82
Figure 29 Scanning electron micrograph showing another example to “points of separation in the TBC” in the as processed condition (a). The failure propagated mainly in the TBC in the vicinity of these defects as can be seen from the fracture surface (b), and the cross section (c) of the failed specimens.	84
Figure 30 Scanning electron micrograph of a specimen with small openings in the TBC in the as processed condition, (a).These openings enlarged with exposure resulting in the formation of so-called “vertical separations” in the TBC, (b).....	85
Figure 31 Scanning electron micrographs showing the morphology of the TBC in the as-processed condition for the specimens that did not (a) and that did develop vertical separations in the TBC with exposure (b).....	86
Figure 32 High magnification scanning electron micrographs from areas (a) close to the interface, (b) middle and (c) the top of the TBC of an as processed TBC system which did not develop vertical separations in the TBC.	88

Figure 33 High magnification micrographs from areas (a) close to the interface, (b) middle and (c) the top of the TBC of an as processed TBC system which developed vertical separations in the TBC.....	90
Figure 34 Top views of TBCs in the as-processed condition for the specimens (a) which developed vertical separations in the TBC and (b) which did not. The columns in (a), which had a fine morphology, got sintered during exposure resulting in the formation of vertical separations (c), whereas the denser columns, (b), remained almost the same (d).	92
Figure 35 Top views of TBCs for specimens that developed vertical separations after exposure at (a) 1000°C for 780 cycles and (b) 1150°C for 15 cycles. The vertical separations were more well developed after exposure at 1150°C.	93
Figure 36 Cross sectional micrographs showing vertical separations and cracks in their vicinity at (a) low and (b) high magnifications.	94
Figure 37 Scanning electron micrograph showing a large number of vertical separations in a TBC system which had a significantly long life.	95
Figure 38 Scanning electron micrographs showing (a) spits in the TBC and (b) cracks initiating in the vicinity of a spit.	96
Figure 39 Top view of a TBC showing a hole and cracks passing through it.	97
Figure 40 (a) Scanning electron micrographs showing oxide inclusions that cut the surface at various angles. In some areas, the alloy was undercut by these oxide inclusions, (b).	98
Figure 41 Scanning electron micrographs from the fracture surfaces of specimens with surface defects showing the development of a discontinuous oxide in the vicinity of oxide inclusions, (a) and voids around some of these oxide inclusions , (b).....	99
Figure 42 Scanning electron micrograph showing stringers of reactive element rich oxides encapsulated in alumina.	104
Figure 43 (a) Scanning electron micrograph showing the fracture surface of a specimen where the failure cut through RE rich oxide protrusions. (b) Cross sectional examination showed the presence of cracks in the vicinity of these oxide protrusions.	105
Figure 44 Scanning electron micrograph showing the presence of a thick TGO which had incorporated RE rich oxides.....	106
Figure 45 Scanning electron micrographs showing a discontinuous, (a), and a continuous layer of intermixed zone, (b).....	107

- Figure 46 Scanning electron micrographs from a specimen in the as-processed condition (a), as well as after exposure at 1100°C for 10, (b) , 60 (c), 100 , (d), and 880 cycles, (e), showing the development of the intermixed zone with time. 110
- Figure 47 Scanning electron micrographs of the fracture surfaces, (a) and (b) , and cross sections, (c) and (d) , of specimens that developed intermixed zones. See text for details. 112
- Figure 48 Scanning electron micrographs showing a buckle, (a), and cracking in the vicinity of a buckle along the TGO/intermixed zone interface, (b). Significant amount of failure was sometimes observed to propagate along this TGO/intermixed zone interface, (c)..... 114
- Figure 49 Scanning electron micrographs of the fracture surface of a specimen showing an Fe rich contamination and re-oxidation around it at (a) low and (b) high magnifications. Accelerated oxidation and penetration of the bond coat was evident in the vicinity of a contamination site, (c). Other examples of reoxidation and accelerated oxidation for different specimens in the vicinity of contamination sites are given in (d) and (e), respectively. 119
- Figure 50 Scanning electron micrographs (a) from the fracture surface and (b) the cross sections of the specimens that developed voids along the TGO/BC and BC/superalloy interface, respectively. These voids were usually associated with the grain boundaries, (c), and reoxidized areas were present around some of these voids, (d)..... 121
- Figure 51 Scanning electron micrographs showing the grain boundary ridges on the surface of a Pt aluminide bond coat without a TBC, (a) and Pt aluminide bond coat with a TBC, (b). Upon exposure, the surface of a Pt aluminide bond coat without a TBC, (c), and cross section of a TBC system, (d), showed cracks in the vicinity of grain boundary ridges. 123
- Figure 52 Scanning electron micrographs showing examples of abnormal defects, above which buckles developed..... 125
- Figure 53 Scanning electron micrographs showing the typical state of the art TBC systems with NiCoCrAlY bond coats in the as processed condition. The bond coat consisted of porosity and oxide inclusions throughout the coating, (a), and β , γ as well as Cr and RE rich phases, (b). Surface defects (c), as well as TBC defects (d), were present. 131
- Figure 54 Scanning electron micrographs showing the fracture surfaces of state of the art NiCoCrAlY bond coats. The failure was mainly along the TGO/BC interface with numerous excursions into the TGO and TBCs (a). The typical features observed on the fracture surfaces were RE rich oxide protrusions (b), oxide inclusions (c), transient oxides (d), and TBC segments (e)..... 134
- Figure 55 Scanning electron micrograph of a TBC system with state of the art NiCoCrAlY bond coat showing a significant amount of separation along the TGO/TBC interface followed by buckling..... 135

Figure 56 Optical micrograph of a TBC system with state of the art NiCoCrAlY bond coat after failure showing that a significant amount of Al-rich β phase was present at the time of failure.....	136
Figure 57 Scanning electron micrographs from the fracture surfaces of the TBC systems with the state of the art NiCoCrAlY bond coats after an indentation test has been performed on the as-processed specimens (a), as well as on the ones which were exposed at 1100°C for 10 (b), and 25 cycles (c). The fracture surfaces of the specimens, which failed after 102 cycles of exposure is also shown in (d). Dark areas correspond to the TGO and the TBC while white areas correspond to the bare bond coat.	138
Figure 58 A simple schematic summarizing the failure behavior of the state of the art TBC systems with NiCoCrAlY bond coats. See text for details.....	139
Figure 59 Scanning electron micrographs of typical state of the art TBC systems with Pt aluminide bond coats in the as processed condition. The microstructure consisted of only β phase with Pt, Cr and Co in solid solution (a). Corn Kernel TBC defects were present (b).	145
Figure 60 Scanning electron micrographs from the fracture surface of a state of the art TBC system with Pt Aluminide bond coat at (a) low and (b) high magnifications. A significant amount of failure was above the TGO/BC interface.	146
Figure 61 Scanning electron micrographs of TBC systems with state of the art Pt aluminide bond coats before (a), and after failure (b), both of which give examples to deformation of the bond coat with thermal exposure. Cracks initiate in the vicinity of the deformed areas (c).	148
Figure 62 Scanning electron micrographs of state of the art TBC systems with Pt aluminide bond coats showing (a) ratcheting in the vicinity of corn kernel defects, (b) a TBC segment that was pulled from the TBC due to ratcheting at a corn kernel defect, (c) presence of a smooth interface in the absence of corn kernel defects.	150
Figure 63 Scanning electron micrographs of a state of the art TBC system with Pt aluminide bond coat, which failed relatively early compared to its counterparts. There were significant amounts of ratcheting, (a), which were believed to be associated with the different TBC morphologies in the as processed condition, (b). This specimen also developed vertical separations in the TBC, (c).	152
Figure 64 Optical micrographs of state of the art TBC systems with Pt aluminide bond coats with fine (a, b) and coarser grain size (c, d) at low and high magnifications. The amount of ratcheting was more pronounced for the specimens with finer grain size.....	154
Figure 65 Scanning electron micrographs of state of the art TBC systems with Pt aluminide bond coats showing a marked difference in the amount of ratcheting for specimens which were subjected to cyclic, (a) and isothermal test, (b).	155

Figure 66 schematic diagram summarizing the failure behaviour of state of the art Pt Aluminide bond coats. See text for details	156
Figure 67 Scanning electron micrographs of a TBC system with a Pt overlayer on NiCoCrAlY bond coat in the as processed condition showing (a) highly irregular interface with associated TBC defects, (b) defective areas in the vicinity of large embedded grit blast particles, (c) very uniform and continuous TGO.....	163
Figure 68 Composition profile away from the TGO/TBC interface for an as processed TBC system with Pt overlayer on NiCoCrAlY bond coat.....	164
Figure 69 Fracture surface of the TBC system with Pt overlayer on the NiCoCrAlY bond coat showing that the failure was mainly along the TGO/TBC interface, as well as in the TBC and in the TGO (a). A higher magnification micrograph from the fracture surface is presented in (b).	165
Figure 70 Scanning electron micrographs of the TBC system with Pt overlayer on the NiCoCrAlY bond coat after exposure at 1100 °C for 40 cycles showing that the cracks that initiated at TBC defects, (a), either linked up, (b), or missed each other, (c), causing a layered alumina scale, (d).	167
Figure 71 Scanning electron micrograph of the TBC system with Pt overlayer on the NiCoCrAlY bond coat after it failed, showing the extensive amount of oxidation along the initial bond coat/ Pt overlayer interface	168
Figure 72 Scanning electron micrographs of the TBC systems with Pt overlayer on the media finished NiCoCrAlY bond coats. The interface was highly irregular with associated TBC defects, (a), from which significant amounts of failure were observed to propagate, (b). The interface of the specimen that was given media finish after Pt deposition was still irregular, (c)	170
Figure 73 The TGO thickness vs square root of time for the TBC systems with Pt overlayer on NiCoCrAlY bond coat and state of the art NiCoCrAlY bond coat at 1100°C showing that the growth of the pure alumina underneath the intermixed zone for specimens with Pt overlayers was slower compared to the growth of the TGO on the state of the art NiCoCrAlY systems.	171
Figure 74 Scanning electron micrographs of the TBC systems on NiCoCrAlY bond coats with Pt underlayers in the as processed condition. Surface as well as TBC defects were evident, (a). The TGO was very non-uniform, (b).....	174
Figure 75 Scanning electron micrographs of TBC systems on NiCoCrAlY bond coats with Pt underlayers after failure showing the fracture path (a), as well as typical features observed on the fracture surfaces such as RE rich oxides, (b), oxide inclusions, (c), transient oxides and TBC segments, (d). A cross sectional micrograph indicating damage in the vicinity of	

transient oxides and TBC defects is presented in (e). It is also possible to get separation along the..... 177

Figure 76 TGO thickness vs square root of time at 1100°C. The TGO growth rate on the state of the art TBC systems with NiCoCrAlY bond coats and the ones with Pt underlayers were similar, whereas the TGO growth on TBC systems with aluminized NiCoCrAlY bond coats were slower. 178

Figure 77 Scanning electron micrographs from TBC systems with state of the art NiCoCrAlY bond coats, (a), and the NiCoCrAlY bond coats with Pt underlayers, (b), after 20 cycles of exposure at 1100°C before failure. The absence of separation during metallographic preparation for the specimen with Pt underlayer suggests improved interfacial toughness. 179

Figure 78 Scanning electron micrograph of a TBC system with aluminized NiCoCrAlY bond coat in the as processed condition showing the presence of a relatively defect free interface with more uniform TGO compared to the state of the art TBC systems. However, the interface was still irregular..... 181

Figure 79 Scanning electron micrographs of TBC systems with aluminized NiCoCrAlY bond coats after failure. (a) The interface became more irregular with time, (b) Significant amount of failure was along or close to TGO/TBC interface, (c) There were indications of separation and reformation of the alumina prior to failure, (d) Al rich nitrides were observed at these sites where separation occurred prior to failure 183

Figure 80 Scanning electron micrographs of TBC systems with aluminized NiCoCrAlY bond coats after failure showing the development of (a) vertical separations in the TBC, (b) voids in the bond coat. 184

Figure 81 Scanning electron micrographs of a TBC system with hand polished NiCoCrAlY bond coat in the as processed condition, at (a) low and (b) high magnifications, showing a very smooth interface which is free of many defects identified for the state of the art systems except at some localized areas where the continuity of the TGO is interrupted above the Cr rich phases, (c), and where the porosity in the bond coat intersected the surface, (d). 190

Figure 82 SEM micrographs of a TBC system with hand polished NiCoCrAlY bond coat after 1520 cycles of exposure at 1100°C before failure showing the presence of a very thick TGO with significant amounts of RE rich oxide protrusions, (a). The TGO/TBC interface was almost free of defects, (b), except at localized areas with transient oxides, (c), and small buckles along the TGO/intermixed zone interface, (d), which seemed to develop by linking up of small voids along this interface, (e). Cracks were present in the vicinity of RE rich oxide protrusions, (f) 193

- Figure 83 Scanning electron micrographs of TBC systems on hand polished NiCoCrAlY bond coats which failed after 720 cycles of exposure at 1100°C. Spits, (a), as well as an abnormal defect, (b), were observed..... 194
- Figure 84 Scanning electron micrographs of a TBC system on hand polished NiCoCrAlY bond coat which failed after 220 cycles of exposure at 1100°C. Significant amount of failure was along the TGO/intermixed zone interface as can be seen at (a) low and (b) high magnification micrographs from the fracture surface, as well as cross sectional micrographs, (c) and (d). Transient oxides were also present embedded in the intermixed zone, (e).197
- Figure 85 Scanning electron micrographs of a TBC system with vibro finished NiCoCrAlY bond coat in the as processed condition showing large TBC defects, (a). There were also smooth areas along the interface, (b). 198
- Figure 86 Scanning electron micrographs of a TBC system with vibro finished NiCoCrAlY bond coat from the fracture surface, (a), and cross section, (b), showing failure in the vicinity of pronounced TBC defects. 199
- Figure 87 Scanning electron micrograph from a TBC systems with media finished NiCoCrAlY bond coat in the as processed condition showing the presence of TBC defects..... 200
- Figure 88 Optical micrographs of TBC systems with as aluminized Pt aluminide bond coats with varying thicknesses of Pt and Aluminide layers after exposure at 1100°C. The bond coat with normal thickness of Pt and aluminide layers consisted of significant amounts of γ' phase after 1080 cycles, (a), whereas the specimens with double thickness of aluminide, (b), and with double thickness of Pt and aluminide layers, (c), after 1240 and 860 cycles of exposure, respectively, had much less γ' phase. 204
- Figure 89 Scanning electron micrographs of TBC systems with as aluminized Pt aluminide bond coats in the as processed condition showing grain boundary ridges, (a), dense TBC with parallel row of pores, (b) and small openings in the TBC above the ridges, (c), which enlarge with exposure resulting in the formation of vertical separations in the TBC, (d).209
- Figure 90 Macrographs of a TBC system on as aluminized Pt aluminide bond coat after exposure at 1100°C for 360 (a), 680 (b) and 860 cycles, (c), showing propagation of failure with time. The SEM micrograph in (d) shows the buckles in cross section. 211
- Figure 91 Scanning electron micrographs of TBC systems on as aluminized Pt aluminide bond coats after failure. The failure was mainly in the TBC, (a), and cracks were present at the grain boundary ridges as can be seen from the fracture surface, (b), as well as cross section, (c). Cracks at the ridges were also present in the absence of vertical separations in the TBC, (d). 213
- Figure 92 Scanning electron micrographs of TBC systems on as aluminized Pt aluminide bond coats with TBCs deposited by different companies. There was not any evidence of an

intermixed zone for one set of specimens, (a), whereas there was a continuous layer of intermixed zone for the other set of specimens, (b).....	214
Figure 93 Scanning electron micrographs of TBC systems with as aluminized Pt aluminide bond coats after failure showing a highly deformed bond coat surface, (a), except at areas where the bond coat was still in contact with the TBC at the time of failure, (b).	215
Figure 94 Scanning electron micrographs of TBC systems with as aluminized Pt aluminide bond coats showing vertical crack formation at the ridges, (a), and their propagation along the TGO/bond coat interface, (b), followed by reoxidation along this interface, (c). Preferential oxidation, usually at the grain boundaries, was observed in some areas, (d).	217
Figure 95 Scanning electron micrographs of TBC systems with as aluminized Pt aluminide bond coats after exposure under 15 hr cycles, (a), as well as under isothermal conditions, (b). Separation along the TGO/bond coat interface followed by reoxidation was not observed for these specimens. Cracking at the grain boundary ridges was not evident for the isothermally tested specimen.	218
Figure 96 Scanning electron micrograph of a TBC system with light grit blasted Pt aluminide bond coat in the as processed condition showing a relatively smooth interface compared to the interfaces of heavy grit blasted Pt aluminides.	223
Figure 97 Scanning electron micrographs of TBC systems with light grit blasted Pt aluminide bond coats after failure showing that the failure was mainly along the TGO/bond coat interface,.....	225
Figure 98 Scanning electron micrograph of a TBC system with media finished Pt aluminide bond coat in the as processed condition showing the presence of remnants of grain boundary ridges.....	226
Figure 99 Scanning electron micrographs of a TBC system with media finished Pt aluminide bond coat after failure. The failure was mainly along the TGO/bond coat interface, (a), and the interface was relatively smooth compared to heavy grit blasted Pt aluminides except at areas of preferential oxidation which were usually observed to be along the grain boundaries, (b) and.....	228
Figure 100 Scanning electron micrographs of a TBC system with media finished Pt aluminide bond coat after failure showing buckles above areas with pronounced amounts of preferential oxidation, (a) and (b). The macrograph of this specimen after failure also indicated failure initiation at localized areas, (c).	230
Figure 101 Macrographs of TBC systems with hand polished Pt aluminide bond coats showing buckles formed close to the center of the specimens, (a) and (b). Examination of the fracture surface, (c), as well as underside of the TBC, (d), under these buckles showed a grain boundary network.	232

Figure 102 Scanning electron micrographs of TBC systems with hand polished Pt aluminide bond coats after failure. The TGO/TBC interface remained smooth, (a), whereas the TGO/bond coat interface was irregular due to thickness variations in the TGO, (b). Small pore like openings developed in the TBC, (c), which then linked up causing larger separations which were followed by deformation of the bond coat underneath, (d)..... 234

Figure 103 Scanning electron micrographs of no bond coat TBC systems in the as processed condition. The specimens from the first batch did not develop a continuous layer of TGO, (a), whereas the ones from the second batch did, (b). Some irregularity of the interface was evident as a result of grit blasting, (c)..... 239

Figure 104 Scanning electron micrographs from no bond coat TBC systems after 140 cycles, 242

Figure 105 Scanning electron micrograph from a no bond coat TBC system after 1840 cycles of exposure before failure showing the presence of a very smooth interface. 243

Figure 106 Scanning electron micrographs of no bond coat TBC systems with Pt overlayers in the as processed condition. The specimens from the first batch did not develop a continuous layer of TGO, (a), whereas the ones from the second batch did, (b)..... 244

Figure 107 Scanning electron micrographs of no bond coat TBCs with Pt overlayers from the first batch showing the presence of voids, (a), and transient oxides, (b), after failure. .. 245

Figure 108 Scanning electron micrographs of second batch of no bond coat TBCs with Pt overlayers after 2300 cycles of exposure before failure. The TGO was rather pure, (a), with intermittent areas of transient oxides, (b). Numerous vertical separations were present in the TBC, (c). 247

Figure 109 Scanning electron micrograph from the underside of a spalled TBC showing the ridge like morphology of the alumina that developed above voids. 251

Figure 110 Scanning electron micrograph from the fracture surface of a specimen showing a ridge like alumina morphology which indicates that the TGO was not in contact with the TBC at the time of failure. 252

Figure 111 Scanning electron micrographs showing examples to sintering between the spalled and the reformed alumina. The arrows point to the interfaces where sintering occurred... 253

Figure 112 Scanning electron micrograph showing an example to thickness variations in the TGO. 254

Figure 113 Scanning electron micrographs from the fracture surface, (a), cross section, (b) and underside of the spalled TBC of a specimen which developed bond coat protrusions. The failure sometimes cut through these bond coat protrusions leaving them isolated in the TGO as can be seen in (b) and (c)..... 256

Figure 114 Scanning electron micrographs from a specimen which had a highly irregular interface in the as processed condition, (a). Upon exposure, thickness variations in the TGO developed as a result of the initially irregular interface, (b)...... 257

Figure 115 Scanning electron micrographs from the fracture surface of a specimen showing grain imprints of the original TGO, (a), as well as the grain imprints of the reformed and then spalled TGO, (b). The grain imprints of the original and reformed TGO can be seen side by side in (c). 259

Figure 116 Optical micrographs showing the effect of cooling rate on the formation of γ' phase. 261

Figure 117 Scanning electron micrographs showing cracking along the β grain boundaries and/or β/γ' phase boundaries during metallographic sample preparation. 262

Figure 118 Scanning electron micrograph showing TBC segmentation. 263

ACKNOWLEDGEMENTS

Firstly, I would like to express my sincere gratitudes to my advisors, Dr Pettit and Dr Meier, for their continued support, guidance, encouragement and advice throughout my studies. I feel very lucky to have a chance to work with them. I also very much appreciate their patience and understanding throughout the hard times that I had during this study.

I would like to thank my committee members, Dr Beuth, Dr Yang and Dr Mao, for their participation and guidance in my studies.

I would like to express my gratitude to Monica Marissida, Igor Garcia, Matt Stiger, Scott Laney, Dave Helmick and Julie Hammer for their friendship and collaboration. And my special thanks go to Kivilcim Onal, who always stood by me and made this working place very enjoyable with her valuable friendship.

I wish to thank Albert Stewart and George McManus for their technical assistance and support. The technical support of Earl Hewitt will also not be forgotten. I also would like to thank our administrative assistants,Carolynn Wilson, Nora Siewiorek and Carol McFadden, who were always willing to help us on any subject.

I would like to acknowledge ONR/MURI for their financial support and also Praxair, Howmet and GE for supplying the specimens. This work would not be possible without the close collaboration and invaluable suggestions of Tom Taylor, Ann Bolcavage and Bruce Warnes.

My last, but not least, thanks go to my beloved family. Even though they were so far away from me, I was able to feel their endless support and love at every moment of this long process. I also owe a lot to my best friend and love, my husband Cagatay, for giving me the strength and encouragement to go through difficult times during this period of my life and for everything else...

1.0 INTRODUCTION

Thermal barrier coatings (TBCs) are increasingly used in gas turbine components, which are subjected to high temperatures. TBC systems are typically composed of an oxidation resistant metallic bond coat and an insulative ceramic coating (TBC). A TBC schematic is presented in Figure 1. As a result of its low thermal conductivity, the TBC reduces the temperature to which the metal components are subjected. Thus, higher gas temperatures can be used which leads to improved efficiency and performance. However, the open and porous structure of the TBC does not provide oxidation protection, which necessitates the application of an oxidation resistant metallic bond coat beneath it. During deposition of the TBC, a slow growing, thermodynamically stable alumina scale develops along the bond coat/TBC interface by reaction of oxygen with the aluminum in the bond coat. This oxide scale, which is referred to as thermally grown oxide (TGO), provides the oxidation protection by acting as a physical barrier between the substrate and the detrimental gaseous environment. It becomes thicker during exposure at high temperatures due to easy penetration of oxygen through the open and porous structure of the TBC.

The current state-of-the-art TBC systems consist of yttria stabilized zirconia (YSZ) deposited either by air plasma spray (APS) or electron beam physical vapor deposition (EBPVD) processes with platinum modified diffusion aluminide or MCrAlY bond coats. Single crystal Ni-base superalloys, which have high strength at elevated temperatures, are usually used as the

substrate. Figures 2a and 2b present typical cross sectional micrographs of EBPVD and APS thermal barrier coatings, respectively.

The substantial improvement obtained in the efficiency and performance of gas turbines by the development of TBC systems is limited by the failure of these systems. Thus, there is a need for the development of more durable TBC systems to fully utilize the benefits obtained from them. However, a thorough understanding of the failure mechanisms of different TBC systems under various operating conditions is first necessary in order to improve their performance. Even though a substantial amount of research has been performed to understand the failure of TBC systems, the exact failure mechanisms are still not clear due to the contribution of many factors in their failures. The fact that the type and the fabrication procedures of the bond coats as well as the TBCs result in different failure behaviors complicates the understanding of TBC failures even more. Therefore, there is still a need for more research on the failure of TBC systems.

The principle objective of this study was to contribute to the understanding of TBC failures so that the performance of TBC systems could be improved through making modifications. For this purpose, the failure behavior of the state of the art TBC systems were investigated first. Based on the tentative failure mechanisms formulated for the state of the art TBC systems, modified TBC systems were prepared and then tested. Failure characterization of these TBC systems elaborated the findings obtained from the state of the art TBCs. A particular emphasis was given to identification of various defects as well as important factors that contributed to the failure of TBC systems. Moreover, important conditions necessary for optimized performances of TBC systems were determined.

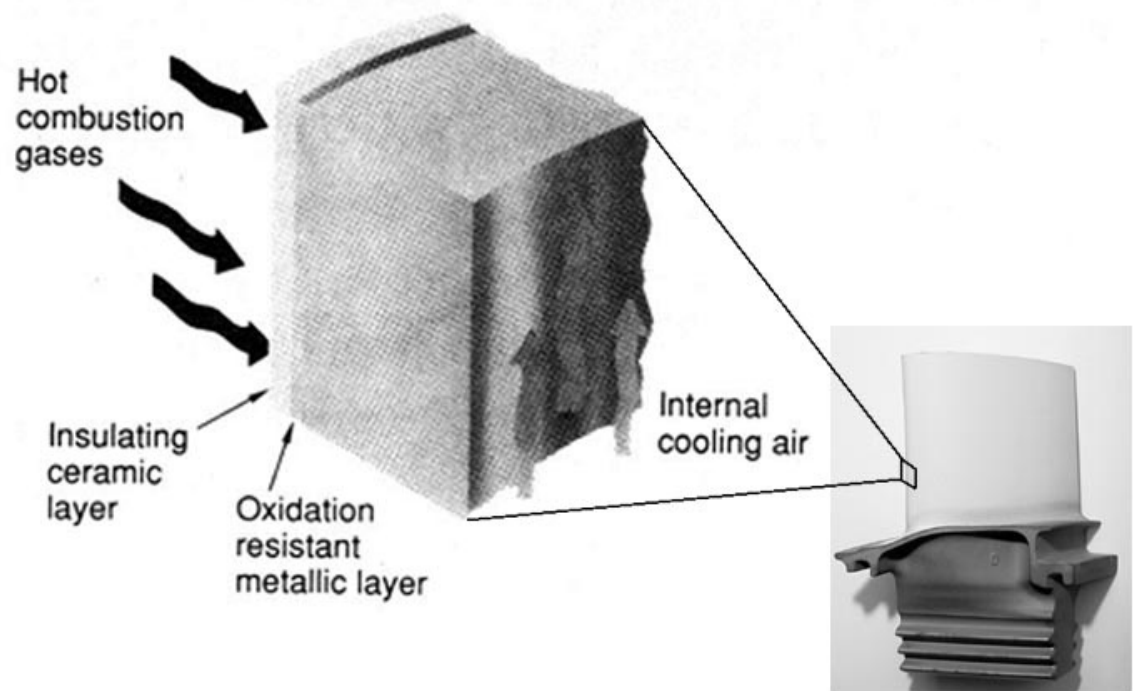
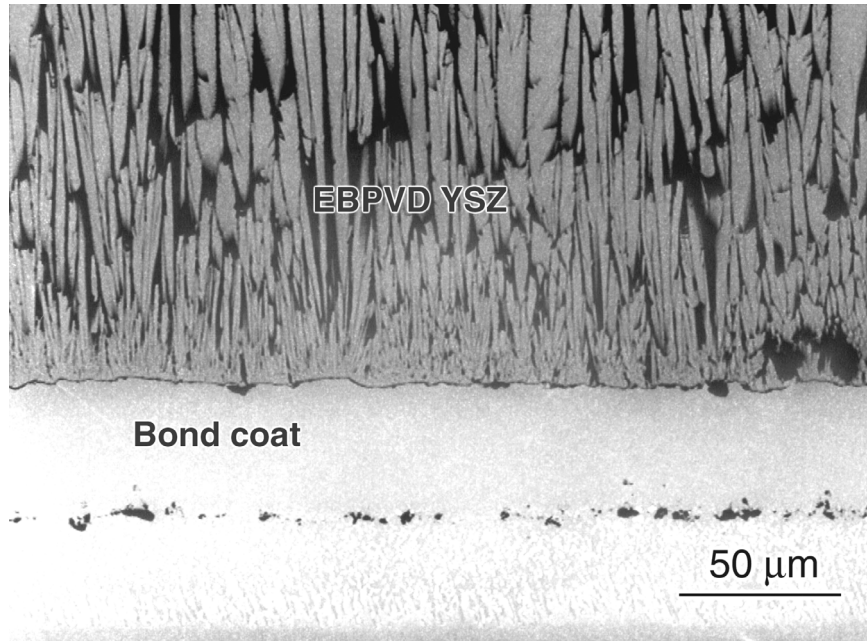
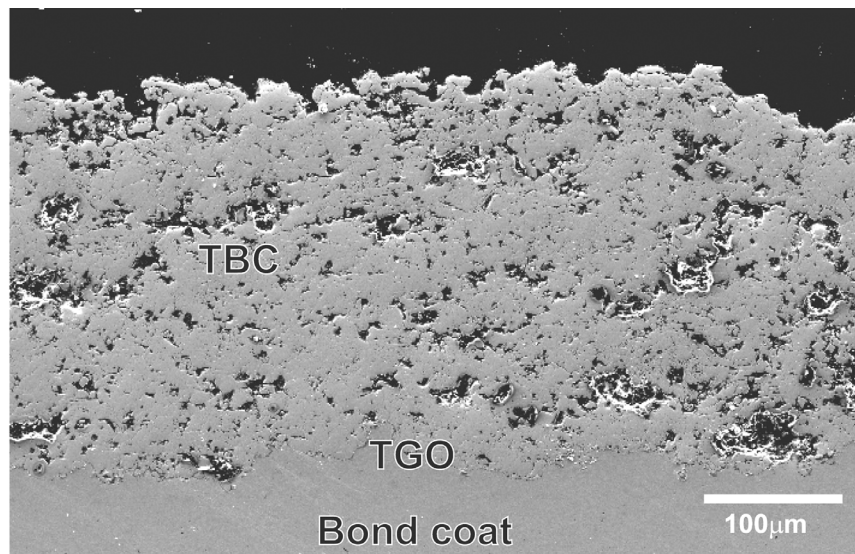


Figure 1 A schematic showing the various layers in a TBC system.



(a)



(b)

Figure 2 Scanning electron micrographs showing the typical microstructures of (a) EBPVD and (b) APS YSZ Thermal Barrier Coatings.

2.0 BACKGROUND

2.1 THERMAL BARRIER COATINGS

Superalloys are usually used in aircraft gas turbine components, which must withstand very oxidizing environments and high temperatures resulting from the hot combustion environment. They have been developed to obtain high strength and creep resistance at elevated temperatures. However, the temperature of the desired combustion gas environment for optimum power and efficiency exceeds the melting temperature of these superalloys which causes structural failure of these components by melting, creep, oxidation, thermal fatigue and numerous other mechanisms [1]. In order to prevent these kinds of structural failures, compressed air had previously been used to cool the components. However, the requirement of using higher gas temperatures to increase the efficiency and performance of gas turbines has limited the protection provided by air cooling [2]. This led to the development of thermal barrier coatings (TBC), which reduce the temperature to which the metal components are subjected. Figure 3 is a diagram showing the improvement of temperature capabilities of superalloys by the use of TBCs over the years. As can be seen from this diagram, temperature differentials as much as 167°C can be obtained by the use of TBCs, which are higher than the total improvement obtained by developing more advanced superalloys [1]

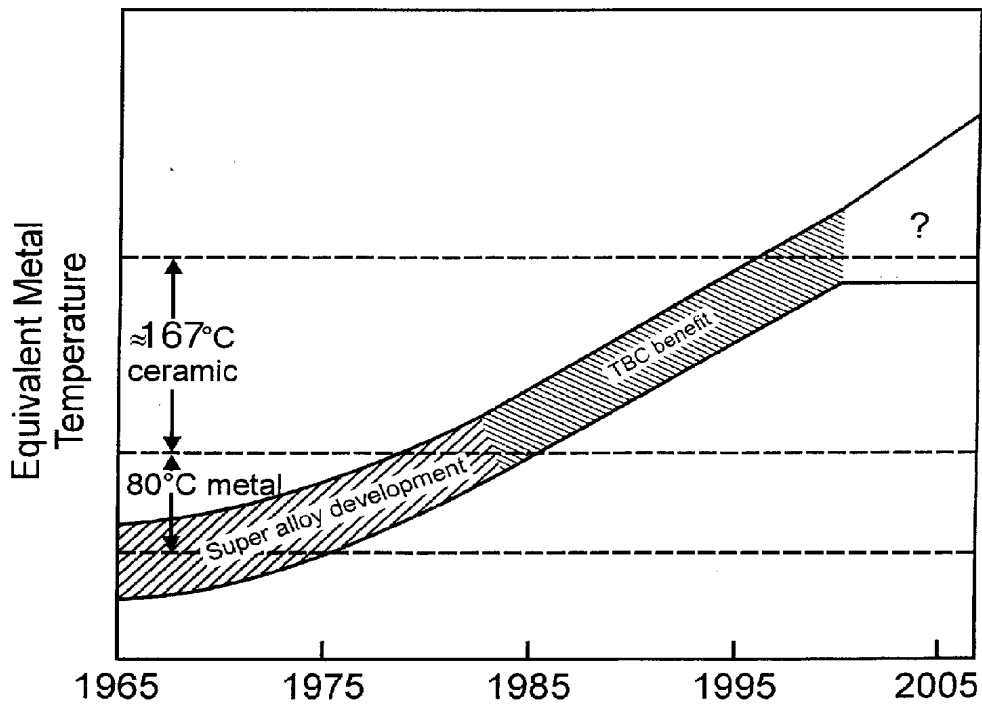


Figure 3 A diagram showing the improvement of temperature capabilities of superalloys by the use of TBCs [1].

TBCs are ceramic coatings with low thermal conductivity, which makes them appropriate coatings to be used as thermal insulators. They are also thermal shock resistant, which is important for their durability under rapid thermal cyclic conditions as experienced in gas turbines.

Zirconia (ZrO_2) stabilized with certain other oxides has been used over the years as the ceramic material for TBCs. Pure ZrO_2 is a polymorphic material showing the following sequence of transformations:



The polymorphic transformation from tetragonal to monoclinic upon cooling is followed by a volume increase which is detrimental to the integrity of these coatings by causing stress

build up in the coating during thermal cycling conditions. Thus, certain stabilizers are used in order to inhibit the transformation from a tetragonal to a monoclinic phase. Yttria is the most widely used stabilizer for ZrO_2 . As can be seen from the ZrO_2 - Y_2O_3 phase diagram in Figure 4 [3], formation of a monoclinic phase is possible by adding around 6.5 - 9 wt % Y_2O_3 , but the actual microstructure consists of cubic and non-transformable tetragonal phase. For TBC applications, 7-9 wt % Y_2O_3 stabilized zirconias are usually used. Lower amounts of Y_2O_3 do not inhibit the formation of the monoclinic phase whereas higher amounts cause complete stabilization of the cubic phase which is known to have poorer thermal shock resistance when compared to partially stabilized zirconias containing both cubic and tetragonal phases [4].

2.1.1 Fabrication Procedures

The current state-of-the-art TBCs are deposited either by air plasma spray (APS) or electron beam physical vapor deposition (EBPVD) techniques. These processes are suitable for deposition of TBCs due to their ability to obtain open and porous structures, which are required for low thermal conductivity and high thermal shock resistance.

2.1.1.1 Plasma Sprayed TBCs Plasma spraying is a coating process where a high temperature plasma gas stream created inside a plasma gun is used to melt prealloyed powder that is injected into the gun. The melted powder is then accelerated towards the substrate by use of a high velocity plasma and the coating develops as the molten metal or ceramic impacts and spreads out over the surface [5]. A simple schematic summarizing the plasma spray process is given in Figure 5a.

Plasma spray coatings necessitate a rough surface to maintain the initial adhesion of the coating to the substrate, which results from mechanical interlocking at the interface. When applied on smooth surfaces, plasma sprayed coatings spall easily due to low interface toughness [6].

The presence of porosity incorporated into the ceramic coating as well as subcritical microcracks make air plasma sprayed YSZ coatings very strain tolerant.

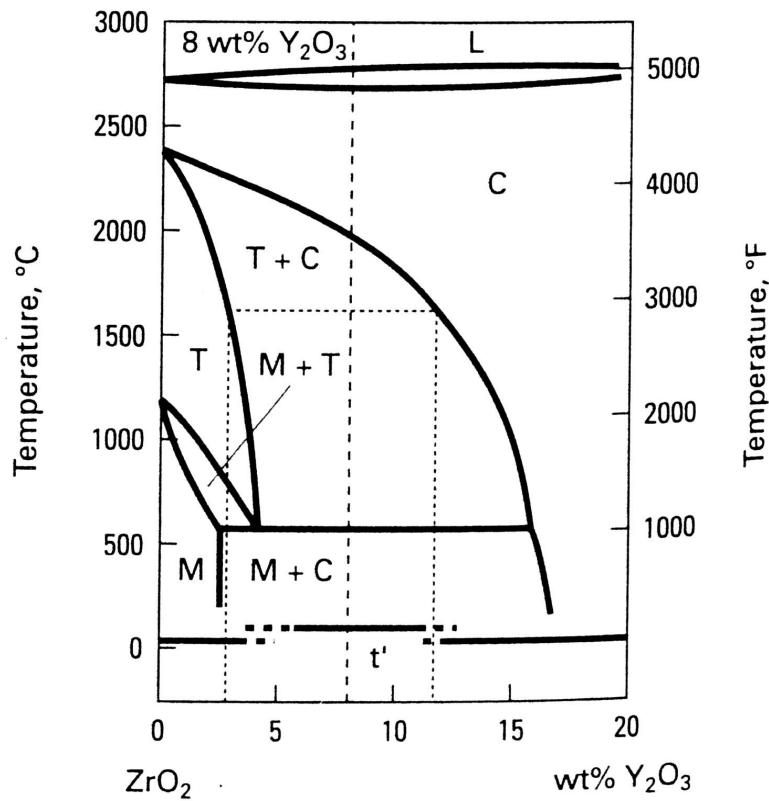
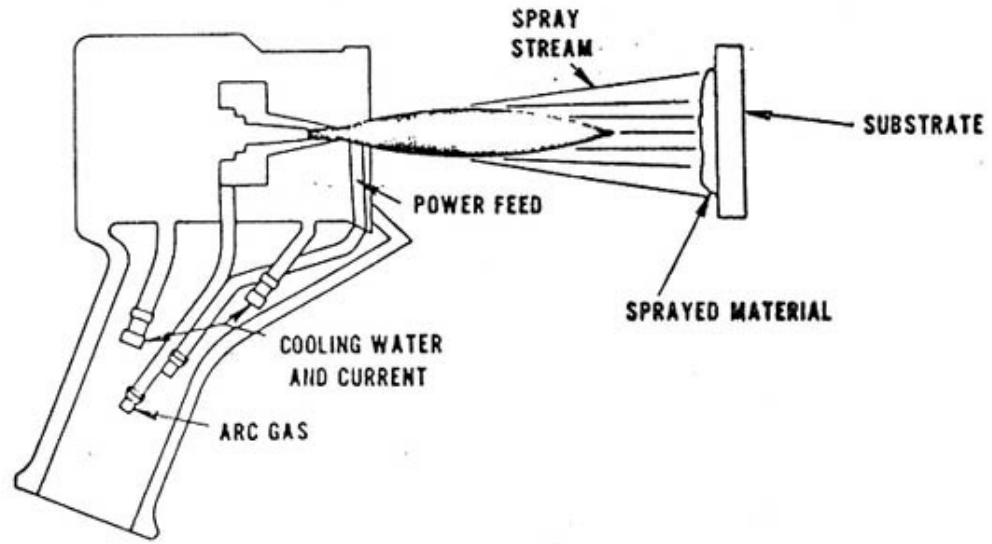
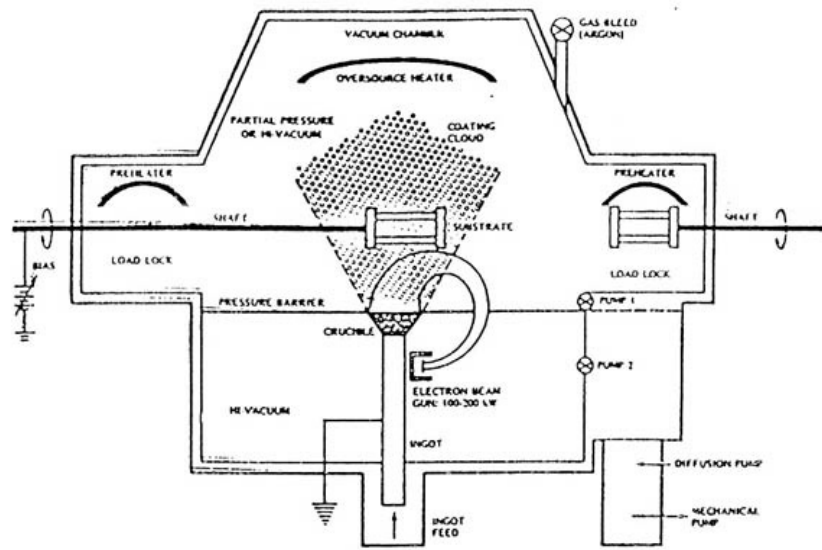


Figure 4 The Zirconia-Yttria phase diagram [3].



(a)



(b)

Figure 5 Schematics illustrating the equipment used for (a) plasma spray, and (b) EBPVD processes.

2.1.1.2 EBPVD TBCs EBPVD is an alternative coating process to plasma spray where an ingot of the target material is evaporated by use of a high energy electron beam. The resulting vapor travels along the line of sight to the preheated substrate whereby the coating develops by the condensation of these vapors onto the substrate [5]. A schematic of an EBPVD coater is shown in Figure 5b. This process can be used to deposit metallic or ceramic coatings. Zirconia becomes oxygen deficient when evaporation and recombination occur at low oxygen pressures. Thus, in order to maintain the stoichiometry of the ZrO_2 , the coating process is performed under low partial pressure of oxygen [7].

The EBPVD coatings require a smooth surface in contrast to rough surfaces required for plasma spray coatings. The adhesion between the coating and the substrate is obtained by chemical bonding which necessitates higher deposition temperatures and post coating heat treatments [6].

The microstructure of EBPVD coatings can vary depending on the nucleation and film growth characteristics which can be adjusted by altering the processing conditions such as deposition temperature, deposition rate, angle of incidence, gas pressure, etc...[8]. In the initial stages of the deposition process, an interfacial boundary first develops in the YSZ at the substrate surface. This layer is necessary for the development of the chemical bond between the substrate and the coating. As the film grows, the surface roughens due to rapid diffusion along grain boundaries and dislocations or preferential growth of some crystallographic planes. When this interfacial boundary layer reaches an appreciable thickness, the surface roughness and surface mobility of the atoms determine the growth mode. If the surface is rough enough, atoms coming from all directions can condense on the projections of the surface shadowing the valley parts.

The shadowing effects, combined with the low surface mobility of condensing atoms, results in preferential growth on projections leading to development of a columnar structure. Development of columnar structures can thus be favored by decreasing the surface mobility of atoms, which is possible by using low deposition temperatures and high gas pressures, and also by increasing the shadowing effect by using lower angles of incidence of the vapor stream.

For TBC applications, the microstructure of EBPVD coatings consists of columnar grains which are poorly bonded to neighbouring grains. However the bonding between the columnar grains and the substrate is strong under proper processing conditions [1]. This type of morphology is favored for strain accommodation within the coating, which causes a significant reduction in the stress generated during cyclic conditions.

2.2 BOND COATS

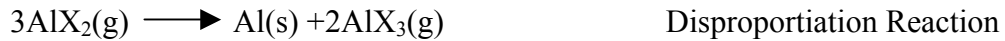
The open and porous structure of the ceramic coating does not provide oxidation protection which necessitates the application of an oxidation resistant metallic bond coat beneath it.

The current state of the art TBC systems consist of MCrAlY and platinum modified diffusion aluminide bond coats, the characteristics of which are summarized below.

2.2.1 Diffusion Aluminide Coatings

Diffusion aluminide coatings form by reaction of aluminum with the substrate resulting in formation of an oxidation resistant NiAl phase. The adhesion of this coating is provided by elemental interdiffusion between the substrate and the coating material.

2.2.1.1 Fabrication Procedures Pack cementation and chemical vapor deposition are the two processes which are widely used for the deposition of diffusion aluminide coatings. Both processes are essentially similar where aluminum is provided to the alloy surface in the form of gaseous aluminum halides. The coating develops by reaction of Al(s) with the substrate surface which results from one of the following deposition reactions where X refers to halides:



In the case of platinum modified diffusion aluminide coatings, platinum is first electroplated or deposited by some other technique on the substrate surface followed by one of the aluminizing processes mentioned above.

•Pack Cementation Process - The pack cementation techniques have been described in the literature [5, 9, 10] and can be summarized as follows. In such processes, the substrate to be coated is placed in the pack, which consists of an inert filler material, metal powder and activator. The pack is heated in an inert gas atmosphere. The metal powder consists of aluminum and some other elements like Cr and Ni which are added to control the activity of aluminum in the pack. The aluminum activity in the pack plays an important role in the microstructural development of these coatings as will be discussed later. Ammonium or sodium halides are usually used as the activator, which react with aluminum in the pack upon heating to form gaseous aluminum halides. The aluminum halides diffuse through the porous pack towards the alloy surface as a result of partial pressure gradient between the pack and the substrate surface. When they reach the surface, one of the deposition reactions, described above, takes place leading to coating formation.

It has been indicated by C. Duret and R. Pichoir [10] that transportation of aluminum towards the substrate is also possible through a metallic vapor phase, solid state diffusion as a result of contact between the pack and the substrate, and by inclusion of metallic particles in the coating.

•**Chemical Vapor Deposition (CVD)** - In the CVD process, aluminum halides are generated separately outside the coating chamber and then introduced into the coating chamber to form the coating by a similar mechanism as explained for the pack cementation process.

The CVD process has been reported to produce cleaner diffusion coatings as compared to other aluminizing processes [11] and the better oxidation resistance of these coatings was attributed to the removal of impurities which resulted in formation of slower growing, purer alumina scales with improved adhesion.

Punola et al. [12] also reported several advantages of CVD processes over pack cementation processes such as higher ductility coatings, enhanced uniformity and repairability, more precise control due to automation of the equipment, capability to coat more complex shapes and faster overall processing.

2.2.1.2 Microstructural Evolution Goward and Boone [13] classified diffusion aluminide coatings as "outward diffusion" or "inward diffusion" type coatings based on their microstructural development. The activity of aluminum in the pack or in the gas phase in case of a CVD process as well as temperature determine whether the diffusion aluminide coating is "outward diffusion" or "inward diffusion" type. The details of the development of these microstructures, which are summarized below, can also be found elsewhere[9, 10, 14].

High temperature low activity (HTLA) and low temperature high activity (LTHA) aluminizing are the two methods of pack aluminizing where temperature refers to the

temperature at which aluminizing is carried out and activity refers to the aluminum concentration in the aluminum-containing powder used in the pack or the activity of aluminum in the gas phase for the CVD process.

HTLA is a single step process at which the aluminizing is carried out at a high temperature ($> 1000^{\circ}\text{C}$) for a certain amount of time which is typically 3-4 hours. The coating develops by outward diffusion of nickel from the substrate and its subsequent reaction with aluminum at the surface. This results in the formation of an outward growing NiAl layer above the initial substrate interface. On the other hand, a nickel deficient region develops just below the initial substrate interface due to outward nickel diffusion. Various substrate elements that are initially-present in solid solution in the substrate precipitate out due to their low solubility in this nickel deficient region. This nickel deficient region, which is rich in metal rich precipitates, is known as the interdiffusion zone.

LTHA aluminizing is a 2 step process where the aluminizing is carried out at a low temperature ($700\text{-}850^{\circ}\text{C}$) followed by a diffusion heat treatment above 1000°C . After the first step the coating microstructure consists of an aluminum rich phase (Ni_2Al_3 or $\text{Ni}_2\text{Al}_3\text{+Al}$ rich NiAl), embedded carbides and precipitates of various substrate elements. The development of this microstructure results from the inward diffusion of aluminum which causes the formation of an inwardly growing layer below the initial substrate interface. After the second step, which is the diffusion heat treatment, a NiAl layer forms by outward diffusion of nickel from the substrate in a similar way to the HTLA process. The reaction of nickel with Al from the initially formed Al rich layer results in Al deficiency in the outer coating layer causing Al rich phases to transform into NiAl. The nickel deficiency below the initial coating layer-substrate interface causes the formation of the interdiffusion zone as explained before. Thus the final microstructure

consists of an outer layer of $\beta(\text{NiAl})$ with embedded carbides and substrate element precipitates, an NiAl layer in the middle that is free of any carbides and substrate element precipitates and an interdiffusion zone .

It has been reported that the presence of a platinum layer on the surface enhances aluminum uptake during aluminizing and this is attributed to the Al activity coefficient on the surface which is lower in the presence of the platinum layer [15]. However, it has also been shown that the aluminum uptake is independent of the amount of platinum unless it is below a certain critical value [16]. In this study, the microstructure of the platinum modified diffusion aluminide coatings, when the initial Pt layer thickness is between a certain range (2.5-10 μm), has been found to consist of a two phase mixture of NiAl and PtAl_2 at the outer surface and an intermediate NiAl layer followed by an interdiffusion zone. At higher thicknesses of the initial Pt layer, the microstructure consisted of a continuous layer of Pt rich phase at the outermost layer and a two phase layer ($\text{NiAl}+\text{PtAl}_2$) underneath followed by a layer of NiAl and the interdiffusion zone. The formation of the continuous Pt rich phase at the surface is attributed to the excess amount of Pt in which case the two phase mixture of NiAl and PtAl_2 is not the equilibrium constituent. Below a certain thickness of Pt layer ($< 2.5 \mu\text{m}$), the microstructure consisted of NiAl with Pt in solid solution. It has been concluded that the microstructural development in these coatings depends on the Pt concentration in various layers throughout the coating, which is determined by the diffusion heat treatment given prior to aluminizing.

2.2.1.3 Performance of Diffusion Aluminide Bond Coats Diffusion aluminide coatings are oxidation resistant due to the presence of the NiAl phase in their microstructures, which provides the aluminum required to form the thermodynamically stable Al_2O_3 scale at elevated temperatures. This oxide scale protects the surface by acting as a barrier between the substrate

and the detrimental gaseous environment. However, due to the stresses generated during oxidation, which will be explained later, the oxide layer cannot be maintained as a continuous layer for long periods of time. Cracking and spalling of the scale, followed by reformation of Al_2O_3 results in depletion of aluminum in the coating. Interdiffusion with the substrate also plays a role in aluminum depletion. When this aluminum depletion becomes so pronounced that the continuous alumina scale cannot be formed anymore, the coating starts to degrade rapidly. Aluminum levels below about 4-5 wt% have been reported to be insufficient to form continuous alumina scales [5]. Thus, the coatings ability to maintain the alumina scale for long periods of time becomes a critical issue for their oxidation resistance.

Straight diffusion aluminides have been known to form a continuous Al_2O_3 scale but they cannot maintain it for long periods of time due to the lack of adequate alumina adherence to the coating [17]. However, application of a platinum layer before aluminizing overcomes this problem, resulting in a significant improvement in scale adherence. Many other beneficial effects of Pt modified aluminide coatings were reported by other investigators [18-22]. These can be summarized as follows:

The high affinity of platinum for aluminum promotes the selective oxidation of aluminum resulting in purer alumina scales with slower growth rates.

Pt acts as a physical barrier restricting the outward transport of substrate elements to the surface which may be detrimental to the performance of these coatings. Diffusional stability of these coatings is improved as a result of lowered aluminum activity that decreases the driving force for diffusion.

Due to their advantages over straight diffusion aluminides, Pt modified diffusion aluminides have been used as the current state of the art bond coats. However, the beneficial

effects obtained by platinum modified diffusion aluminides have been shown to be reduced after exposure at high temperatures where interdiffusion between the substrate and the coating becomes pronounced [20]. The degradation of these coatings was accelerated after a substantial reduction in platinum concentration due to interdiffusion.

2.2.2 MCrAlY Bond Coats

Binary alloys such as Ni-Al, Fe-Al, Co-Al can form protective alumina scales upon exposure to air provided that the aluminum content is above a critical value [23]. However, addition of elements like Cr and reactive elements such as Y to these binary alloys has been found to have beneficial effects which have led to the development of oxidation resistant MCrAlY (M=Ni, Fe, Co..) type bond coats.

2.2.2.1 Fabrication Procedures Thermal spray processes are usually used for the deposition of MCrAlY bond coats. There are various types of thermal spray processes. However, the basic idea is the same. In each case, any material that can be prepared in the form of powder is fed into a torch or a gun and heated close to their melting temperatures by various sources. The coating then develops as the molten particles, which are accelerated towards the substrate, impact and solidify on the surface. Compositional flexibility is one of the major advantages of thermal spray coatings. Moreover, due to very little diffusion at the substrate-coating interface, the unacceptable coatings can be stripped and the substrate can be recoated without affecting properties [24].

Even though there are various thermal spray processes, only the plasma spray and detonation gun techniques, which are widely used for the deposition of MCrAlY bond coats, will be explained below.

- **Plasma Spray** - The plasma spraying process has been summarized before for deposition of TBCs. In the case of deposition of TBCs, the plasma spraying process is performed in air. However, deposition of MCrAlY bond coats is usually done in an inert atmosphere in order to minimize the oxidation of the highly reactive constituents. Argon gas is usually used as an inert atmosphere and the process is named the argon shrouded plasma spray process. Another type of plasma spray process, known as low pressure plasma spray (LPPS), is performed in a low pressure chamber. Deposition of plasma sprayed coatings under a low pressure atmosphere results in increased particle velocity and minimum oxidation during deposition [25]. Thus, the coatings produced by the low pressure plasma spray process exhibit high quality with dense and homogeneous structures with minimal oxidation.

- **Detonation Gun Technique** - The detonation gun is one type of thermal spray process where the particle velocity is very high compared to other conventional plasma spray processes [25]. Thus, the detonation gun technique can produce very dense microstructures with very high bond strengths owing to the high particle velocity. In this process, the powder is heated by a detonation wave, which is produced by detonating a mixture of oxygen and acetylene along with a pulse of powder by using a spark. The melted particles are then accelerated onto the substrate with a very high velocity. Each detonation produces a circle of coating 25 mm in diameter and 1 μ m thick. Thus the process is repeated until the desired coating thickness is obtained. After each cycle, the gaseous combustion products are swept out by nitrogen flushing [24].

2.2.2.2 Microstructural Development As previously mentioned, thermal sprayed coatings develop as the molten particles impact on the surface and spread out parallel to the surface. Molten particles take a lamellar shape as they hit the surface and they bond to the surface as they contract during rapid cooling. Thus the microstructure of thermal sprayed coatings consists of overlapped lamellar splats parallel to the surface [24]. Depending on the processing parameters, varying amounts of porosity and internal oxide inclusions are observed. The processes performed under either inert gas or low pressure atmospheres by using high particle velocity produce the densest microstructures with less internal oxidation

After the post coat heat treatment, the interfaces between the lamellar splats become invisible and usually a two phase microstructure develops [5]. The microstructures of MCrAlY bond coats usually consist of β (NiAl) and γ (Ni solid solution) or γ' (Ni₃Al) phases depending on their composition. They may also contain some other phases such as ∞ -Cr and yttrides in their microstructures.

2.2.2.3 Performance of MCrAlY Bond Coats The MCrAlY coatings have less aluminum when compared with aluminide coatings. However oxidation protection is provided by the presence of Cr which permits the selective oxidation of Al at low aluminum concentrations and oxygen active elements such as yttrium that improve the adherence of the alumina scale [5]. The effect of Cr in promoting selective oxidation of aluminum has been explained to result from the prevention of oxygen entering into the alloy by Cr acting as a getter [26]. However, this explanation has been questioned by Stott [27] due to the absence of detectable Cr₂O₃ above alumina scales in most cases.

MCrAlY bond coats have better mechanical properties compared to diffusion aluminides owing to the lower concentration of Al in their composition [28]. Reactive elements are known

to improve oxidation behaviour of these coatings. Extensive studies have been done in order to fully understand the effects of reactive elements [29-31]. However the mechanisms responsible for the beneficial effects of reactive elements are not clear and there are still controversial ideas on the proposed mechanisms. Some of the proposed mechanisms for the reactive element effects can be summarized as below:

- Reactive element oxides develop close to the oxide-substrate interface and serve as rapid oxygen transport paths. Oxygen reacts with aluminum in the substrate around these oxides resulting in preferential growth of alumina encapsulating these oxides. The oxide protrusions formed this way improve the scale adherence by mechanically keying the oxide to the substrate .
- They improve the alloy-scale bond strength by preventing the segregation of harmful elements such as sulfur to the alloy- scale interface. These elements are known to weaken the bonds at the interface.
- They act as vacancy sinks preventing the formation of voids at the alloy-scale interface.
- The presence of reactive elements reduces the oxidation rate by altering the scale growth mechanism. They diffuse out from the substrate to the scale gas interface in the presence of an oxygen potential gradient. They prefer the scale grain boundaries for diffusion. Since the diffusion of reactive element ions is slower than the other elements in the alloy (Cr,Al), they inhibit the outward transport of cations along grain boundaries causing reduction in the parabolic rate constant. They improve the scale plasticity by modifying the scale microstructure.

The beneficial effects of reactive elements are widely accepted. However, it has also been reported that the amount and distribution of reactive elements has a significant effect on the performance of MCrAlY coatings[31, 32].

Fabrication procedure is another important factor that affects the performance of these coatings. Gupta and Duvall [33] compared the relative performance of NiCoCrAlY bond coats deposited by 4 different fabrication procedures, namely air plasma, argon shrouded plasma, low pressure plasma spray, and EBPVD. The performance of NiCoCrAlY bond coats deposited by the low pressure plasma spray process was better compared to air and argon shrouded plasma sprayed coatings. However, the EBPVD NiCoCrAlY coatings performed the best. These results show the importance of fabrication procedures on the properties of these coatings.

2.3 THERMALLY GROWN OXIDE (TGO)

The oxidation resistance of most bond coats is developed by the selective oxidation of aluminum in the bond coat to form a slow growing, thermodynamically stable alumina scale. This oxide scale which is referred to as thermally grown oxide (TGO) when present with TBCs, forms along the TBC/bond coat interface during TBC deposition and becomes thicker during exposure at high temperatures.

The characteristics of the TGO such as growth mechanism, growth rate and microstructure, as well as its adherence to the bond coat and TBC, are critical factors that affect the durability of TBC systems. The best oxidation protection is provided in the presence of a pure alumina scale with the slowest possible growth rate and good adherence. However, establishment of a pure alumina scale is not always possible due to transient oxidation effects, which are explained below.

2.3.1 Transient Oxidation

When an alloy is exposed to an oxidizing atmosphere, oxides of every element in the alloy can form providing that the free energy change for their formation is negative in that environment [28]. Formation of more than one type of oxide during the initial stages of oxidation is known as transient oxidation and it plays a significant role in the oxidation behavior of alloys. At the later stages of oxidation, the more thermodynamically stable oxide usually predominates. However, kinetic factors also come into play at this stage and determine whether a continuous scale of more thermodynamically stable oxide can be established or not.

Giggins and Pettit [34] investigated the oxidation behavior of Ni-Cr-Al alloys with varying amounts of Cr and Al. At the very early stages of oxidation, the surfaces of all alloys were observed to consist of NiO and spinel phases due to rapid uptake of oxygen by the alloy. Due to rapid transport of oxygen through these oxides, the oxygen activity established at the scale-alloy interface was higher than that required for formation of Cr_2O_3 and Al_2O_3 . This caused diffusion of oxygen into the alloy. Cr_2O_3 and Al_2O_3 particles then formed below the outer scale where the critical oxygen activity was reached. Due to a lower oxygen activity required for Al_2O_3 formation, the alumina particles extended deeper into the alloy. As the oxidation proceeded, the volume fractions of Cr_2O_3 and Al_2O_3 , which depend on the amount of Cr and Al in the original alloy, determined the steady state oxide. For alloys with high Cr and Al concentrations, the volume fraction of Cr_2O_3 and Al_2O_3 was sufficient to prevent the further diffusion of oxygen into the alloy resulting in formation of a continuous scale of either Cr_2O_3 or Al_2O_3 as the steady state scale. However, the alloys with lower amounts of Cr and Al were unable to form continuous Al_2O_3 or Cr_2O_3 scales exhibiting higher oxidation rates.

Even though α -Al₂O₃ is the thermodynamically favored oxide, its establishment as a continuous steady state scale depends on some other factors. First of all, the concentration of aluminum in the alloy must be larger than a critical value as shown by the study of Giggins and Pettit. Conditions which cause rapid transport of aluminum to the surface and restrict inward oxygen transport favor the establishment of a steady state alumina scale [23]. Thus, the alloy interdiffusion coefficient and oxygen solubility and diffusivity in the alloy become factors important for selective oxidation of aluminum. For example, establishment of a continuous layer of α -Al₂O₃ is easier on a FeCrAl alloy due to its high alloy interdiffusion coefficient, which allows rapid transport of aluminum to the surface, and low oxygen solubility in this alloy. The comparative growth rates of various oxides formed at the initial stages of oxidation are also critical for the ease of establishment of Al₂O₃ scales.

Formation of less stable oxides, such as NiO and spinels, is not desirable since they are not as protective as alumina scales due to their rapid growth rate. Thus the prevention or at least minimization of transient oxidation is a very important issue for the oxidation behavior of alloys.

2.3.2 Growth and Adherence of TGO

Even though the growth and adherence of alumina scales have been recognized as critically important to the development of more oxidation resistant superalloys and coatings, including thermal barrier coatings, the exact details of alumina growth and adherence are not fully understood, or at least not universally accepted. All alloys undergo transient oxidation as discussed in the previous section. Alumina scales develop beneath the transient oxides and the thickness of the transient layer is greater for MCrAlY bond coats compared to aluminide and platinum aluminide bond coats. In some cases the initial alumina that forms is not the stable α -

Al_2O_3 but metastable phases. Tolpygo and Clarke [35] studied the transformation from $\theta\text{-Al}_2\text{O}_3$ to $\alpha\text{-Al}_2\text{O}_3$ on platinum modified diffusion aluminide coatings. They observed that the temperature and the surface condition are important factors that affect the development of metastable aluminas. The transformation from $\theta\text{-Al}_2\text{O}_3$ to $\alpha\text{-Al}_2\text{O}_3$ was observed to be much faster on rough surfaces compared to smooth surfaces. This faster transformation was attributed to more nucleation sites available for $\alpha\text{-Al}_2\text{O}_3$ on rough surfaces. It was also indicated that higher temperatures resulted in faster $\theta\text{-Al}_2\text{O}_3$ to $\alpha\text{-Al}_2\text{O}_3$ transformation by increasing the growth rate of individual $\alpha\text{-Al}_2\text{O}_3$ nuclei. In summary, low temperatures and smooth surfaces were observed to favor metastable $\theta\text{-Al}_2\text{O}_3$ formation. However, $\alpha\text{-Al}_2\text{O}_3$ eventually develops on the surfaces of the bond coats.

It is well established that the $\alpha\text{-Al}_2\text{O}_3$ grows by the inward diffusion of oxygen along grain boundaries. There is some question about the importance of an outward growth component involving aluminum diffusion. A number of studies have indicated that there is a small outward growth component and that reactive elements can decrease or eliminate this growth [13]. It is not clear if the aluminum that participates in the outward growth diffuses through bulk grains or along grain boundaries in the $\alpha\text{-Al}_2\text{O}_3$ scales.

The microstructure of alumina scales also affects the oxidation behavior of the alloys. Studies by Felten and Pettit [36] on the development, growth and adhesion of Al_2O_3 on platinum-aluminum alloys indicated that the growth rate of alumina is highly dependent on its microstructure. They observed that the alumina scale grew faster when its grain size was smaller. This observation was consistent with the proposed mechanism that alumina scales grow predominantly by inward oxygen transport along grain boundaries. The authors have also shown

that the microstructure of alumina scales are dependent on factors such as the phases present originally on the alloy surface, temperature and time of oxidation and the oxygen pressure.

It is very well documented that reactive elements improve the adherence of α - Al_2O_3 scales. As discussed previously, a number of mechanisms have been proposed to account for the improved adherence. It is clear that mechanisms involving removal of sulfur from the α - Al_2O_3 /bond coat interface must be important because α - Al_2O_3 scales are extremely adherent to low sulfur alloys with no reactive elements. It is also evident that the reactive element concentration and distribution in the bond coat are important factors in optimizing α - Al_2O_3 adherence as mentioned previously. Gupta and Duvall [33] investigated the oxidation behavior of NiCoCrAlY+Hf+Si bond coats. Hf was added to improve the oxide scale adherence whereas Si was added to reduce the oxide scale growth rate. A substantial improvement in oxide scale adherence was observed due to combined beneficial effects of these elements.

The adherence of α - Al_2O_3 on platinum aluminide bond coats is significantly better than on aluminide bond coats. Platinum does improve α - Al_2O_3 adherence significantly. The mechanism by which platinum improves this adherence is not well established. Some investigators have proposed that it removes sulfur from the interface but the arguments are not convincing [37]. Others have proposed that residual stresses in the α - Al_2O_3 may be smaller on platinum aluminide bond coats [38] but work is required to substantiate this.

2.3.3 Stresses Generated During Oxidation

One of the major causes that leads to spalling of oxides is the generation of stresses during oxidation. These stresses can be classified into two types: Growth stresses and thermal stresses.

Growth stresses form during isothermal formation of the scale and various mechanisms were proposed to explain the origin of these stresses. The important ones are the volume difference between the oxide and the metal that is consumed for the formation of oxide, oxide formation within an oxide, epitaxial stresses, compositional changes in the alloy or scale, and specimen geometry [28].

Thermal stresses are generated during cyclic oxidation and they result from differences in the thermal expansion coefficients of alloy and the oxide.

Thermal and growth stresses in the TGO were determined to be compressive. Thermal stresses ranged from 3 to 6 GPa [39] whereas the growth stresses were much smaller ranging from 0 to 1 GPa [40, 41]. However, Evans indicated that imperfections, such as undulations on the surface and localized thickness variations in the TGO, cause deviations from these average values [42].

The mechanisms for accommodation of these stresses vary depending on the properties of the system [28]. When the stored elastic strain energy, which is directly proportional to the scale thickness and the residual stress in the scale, exceeds the fracture resistance of the interface, the oxide scale spalls following either buckling or wedge crack formation. However, if the alloy is not strong enough and the fracture resistance of the interface is high, the compressive stresses can be accommodated by plastic deformation of the substrate and the scale .

2.4 FAILURE MECHANISMS OF TBC SYSTEMS

The beneficial effects obtained by using TBC systems strongly depend on the durability of these systems under various operating conditions. Many studies have been performed to understand the failure mechanisms of TBC systems in order to be able to improve their durability. However, the fact that many factors contribute to the failure of TBC systems complicates the

characterization of possible failure mechanisms. This is why the mechanisms that lead to failure of these systems are still not clear.

The oxidation behavior of the bond coats, which is strongly influenced by the continuity of the TGO layer, has been reported to be the most critical factor in TBC failures [43]. Thus both the growth of the TGO and its adherence to the TBC and bond coat, play important roles in the durability of the TBC system performance. Many other factors can also influence TBC system performance. These include: thickness, structure, chemistry, thermal expansion, phase stability and creep strength of the ceramic; thermal expansion, phase transformations, thermal fatigue, creep/stress relaxation of the bond coat and bond coat/substrate interactions [44].

There is data in the literature that indicates better performance of EBPVD TBCs compared to APS TBCs [1]. The coating spallation mechanisms were reported to be different for these coatings. The APS TBCs fail by cracking in the TBC close to the TGO-TBC interface [45, 46] whereas EBPVD TBCs fail by cracking along the TGO/bond coat interface or within the oxide layer [47, 48].

Failure of EBPVD TBCs that occur along the BC-TGO-TBC interfaces and within the TGO indicates that the characteristics of the TGO are a critical issue in the durability of these TBC systems. However, the influence of oxidation on the failure of APS TBCs is not very clear since the fracture occurs within the TBC. De Masi Marcin et al [49] proposed that the ceramic spallation may result from progressive link up of subcritical cracks within the APS TBC. Although these investigators could not find a direct link between crack initiation and oxidation, they agreed that oxidation affects the life of these TBCs by altering the stress state in the TBC as previously reported by Miller et al [45]. Bartlett and Manshio [46] attributed the crack propagation in the TBC to a relatively low fracture energy of the coating in planes parallel to the

interface. The presence of a rough interface was mentioned as a possible source for crack initiation by causing stress concentration at asperity tips. The authors also showed that stresses generated during oxidation are not required for crack growth. In a recent study by Rabiei and Evans [50], the effects of oxidation on the failure of APS TBCs were observed to become important after a critical thickness of the TGO is reached. Once this critical TGO thickness was reached (5.5 μm), new cracks were observed to initiate at large undulations in the interface and they propagated in the TBC as well as through the TGO and along the interfaces.

Failure mechanisms of TBC systems also differ, depending on the underlying bond coats. Different failure mechanisms have been reported even for the same type of bond coats due to pronounced effects of different fabrication procedures and composition on their properties.

Mumm and Evans [51] investigated the failure mechanism of a TBC system with an MCrAlY bond coat and reported that the failure occurs by the coalescence of interface separations around imperfections such as embedded oxides associated with $\text{Y}_2\text{O}_3/\text{YAG}$ precipitate phases. Large oxide protrusions rich in reactive element precipitates have also been reported by other investigators [31, 32] to cause failure due to localized high levels of stress concentration at the oxide-bond coat interface. However, the effects of these reactive element rich oxide protrusions on the failure of MCrAlY bond coats were questioned and the failure of these TBC systems was attributed to the delaminations nucleated in the vicinity of the vertical separations in the TBC [52].

There is also substantial evidence that the formation of oxides other than alumina either by transient oxidation effects or by aluminum depletion in the bond coat during exposure results in failure of the TBC systems. However, the mechanisms by which they cause failure is not clear. Wu et al [53] proposed that the transient oxides that have formed at the TGO/TBC

interface might accelerate spalling of the TBC by causing crack initiation at these sites. In another study [54], these authors stated that the CTE mismatch stresses cannot be relieved due to the presence of oxides other than alumina that protruded into the microcracks of the TBC and, therefore, these stresses cause spallation of the TBC. Mutasim et al [2] have also observed detrimental effects of spinels and other oxides in the failure of TBC systems and attributed this effect to the lower mechanical strengths of these mixed oxides compared to alumina. In a study by Anton et al [55], the contribution of the transient oxides to the failure of TBC systems was related to the volumetric changes associated with the transformation of transient oxides to more thermodynamically stable phases with continued exposure. Lih et al studied the effects of preoxidation [56], prealuminization [57] and duplex treatment of prealuminization and preoxidation [58] on the oxidation behavior of TBC systems with MCrAlY bond coats. For each case, they observed an improvement in oxidation resistance and cyclic life of TBC systems. The main reason for this improvement was attributed to the formation of purer alumina scales with less transient oxidation. Shillington and Clarke [59] suggested that the TBC/spinel and TBC/ α -Cr₂O₃ interfaces have lower interfacial fracture resistance compared to TBC/ α -Al₂O₃ interface and conversion of α -Al₂O₃ into other mixed oxides as a result of aluminum depletion in the bond coat causes failure of these systems. They explained the stages in the conversion of α -Al₂O₃ into other oxides as follows: Cracking occurs in the alumina on the highly convoluted surfaces with the combined effect of the thermal expansion mismatch and the stresses generated due to high local curvatures. When the bond coat becomes depleted in aluminum such that it cannot reform alumina anymore, the oxygen diffusing through these cracks react with other elements in the bond coat leading to formation of other oxides. Volumetric change associated with the formation of other oxides causes further cracking in the TGO, accelerating the conversion of α -Al₂O₃ into

other oxides. Formation of the non protective scale allows further diffusion of oxygen into the bond coat resulting in internal oxidation of aluminum.

Haynes et al [60] investigated the fracture behaviour of APS TBCs deposited on both VPS and APS NiCrAlY bond coats. The alumina scale that formed on a VPS NiCrAlY bond coat was highly damaged, exhibiting variations in thickness and cracking and buckling of the alumina, especially on the convex surfaces, even after 25% of TBC lifetime. On the other hand, the alumina scale formed on APS NiCrAlY bond coat was less damaged and more adherent. However, the life of the TBC on a APS NiCrAlY bond coat was shorter showing that the severe alumina damage observed on an VPS NiCrAlY bond coats did not cause rapid failure. Depending on these observations, it is proposed that the mechanical integrity of the TGO in plasma sprayed TBCs may not be the critical factor. The importance of some other factors such as thermal expansion coefficient and bond coat strength has been discussed.

Failure mechanisms reported for TBC systems with platinum aluminide bond coats are different than the ones reported for TBC systems with MCrAlY bond coats. In the case of the platinum aluminides, a ratcheting phenomenon was proposed by A.G Evans [42] to explain the origin of out of plane tensile strains in the TBC that induce failure. Ratcheting, which refers to formation of undulations at the interface between the TGO and the bond coat, was reported to occur at sites where initial interface imperfections are present. When the amplitude of these initial interface imperfections are above a critical value, they induce stresses higher than the cyclic yield strength of the bond coat resulting in distortion of the bond coat. On the other hand, the presence of soft orientations on some of the β -NiAl grains close to the TGO promotes ratcheting in these locations due to their susceptibility to plastic straining normal to the interface. The shear stresses formed during cooling and the growth strain at high temperatures result in

plastic flow of the bond coat from the base to the tip of the undulations causing further increase in the amplitude of these undulations with each thermal cycle. When their amplitudes become large enough, they induce tensile stresses normal to the interface, which then cause cracking at locations with the lowest toughness. TBC failure occurs when the separations resulting from the coalescence of these cracks become large enough to start either large scale buckling or edge delamination.

Tolpygo and Clarke [61] proposed a different mechanism for the development of undulations on the platinum aluminide bond coats that eventually lead to failure of these systems. They proposed that the phase transformation from β to γ' results in a significant volume reduction in the bond coat and they attributed the surface rumpling to the localized volume reductions in the bond coat due to localized phase transformations observed in platinum aluminide bond coats. Another study on Pt aluminide bond coats by Chen et al. [62] and Zhang et al. [63] indicated that a martensitic transformation may take place in the β phase during thermal cycling. The effects of this transformation on strain accumulation in TBC systems as well as on surface rumpling, via accompanied volume changes, were discussed.

In a more recent paper by Darzens et al. [64], β to γ' phase transformation as well as martensitic transformation in the β phase were both suggested to be contributing factors on the rumpling of Pt aluminide bond coats. This effect was attributed to local misfit between the growing γ' domains and the volume strain accompanying the martensite transformation.

Gell et al [65] proposed a different failure mechanism for a TBC system with a platinum aluminide bond coat. In this study, the bond coat was not grit blasted prior to TBC deposition and consequently ridges were present on the bond coat grain boundaries. They proposed that the out of plane tensile stresses formed at the peak of the ridges were large enough to cause cracking

in the TGO above the ridges. The rapid transport of oxygen through these cracks resulted in preferential oxidation at the grain boundaries. Plastic deformation of the bond coat and tensile stresses generated during cooling at the ridges caused widening of these cracks into cavities and further grain boundary oxidation. On the other hand, the strain energy increased due to thickening of the TGO and the bond strength along TGO/bond coat interface decreased by diffusion of elements from the substrate such as S. They concluded that the crack and cavity formation around the grain boundary ridges combined with the increase in strain energy and the reduction in bond strength along the TGO/bond coat interface resulted in failure of these systems.

Tawancy et al [66] studied the comparative performance of TBC systems with different bond coats including MCrAlY, straight aluminide and platinum aluminide bond coats. They observed that all TBC systems failed by void formation and coalescence along the TGO/bond coat interface. This type of behavior was associated with degradation of bond coats with interdiffusion and oxidation. They also mentioned the importance of the superalloy substrate composition in the oxidation behaviour of TBC systems by altering the elements diffusing from the substrate to the surface of the bond coat.

Metastable aluminas are known to form prior to stable α -alumina formation as mentioned previously. The transformation from metastable alumina to stable α -alumina results in a significant volume reduction and it has been observed by Schaeffer [67] and Clarke et al. [68] that this volume change results in the failure of TBC systems if the transformation occurs after the deposition of the TBC. The authors discussed the importance of the pretreatments that can be applied before deposition of the TBC in order to prevent this type of failure.

3.0 EXPERIMENTAL DETAILS

The specimens used in this study were circular discs, which were 25.4 mm in diameter and 3.2 mm in thickness. A sample schematic is shown in Figure 6a. They consisted of a single crystal Ni base superalloy Rene N5 (Ni-7.5Co-7.0Cr-1.5Mo-5.0W-3.0Re-6.5Ta-6.2Al-0.15Hf-0.05C-0.01Y in wt%) as the substrate and an 8wt% YSZ as the TBC. The TBCs were deposited by the EBPVD process using commercial coating equipment operated by Praxair, Howmet and GE. Pt Aluminide and NiCoCrAlY coatings were used as bond coats. Some of the specimens had only the bond coats without a TBC, whereas some had TBCs deposited directly on the superalloy substrates.

The state of the art Pt modified aluminide bond coats, which were obtained from 2 different companies, were prepared by using a high temperature low activity CVD process. The superalloy substrates were first electroplated with 5-7 μ m of Pt and then annealed to permit some interdiffusion between the superalloy substrate and the Pt layer. This process was followed by chemical vapor deposition of aluminum, usually leading to final coating thicknesses of around 40-50 μ m. These coatings typically contained 40-45 at% Al, 8-10 at% Pt with the remainder being Ni and small amounts of other elements from the substrate. They were given a heavy grit blasting prior to TBC deposition. Heavy grit blasting was done by using 8 grit (2mm) alumina at a pressure of 60-80 psi (Ra~2 μ m).

The modified Pt Aluminide bond coats had varying thickness of Pt and aluminide layers, nominal thickness of which were 0.25 mil Pt-1.5 mil aluminide, 0.25 mil Pt-3 mil aluminide, 0.5 mil Pt-1.5 mil aluminide and 0.5 mil Pt-3 mil aluminide. Moreover, the surface preparation techniques were different. Some of these specimens were given a light grit blasting, by using 220 grit (700 μ m) alumina at a pressure of 25 psi (Ra~1.3 μ m). Some were given media finishing, where the specimens were tumbled in a certain media (Ra~0.6 μ m). Some of them were polished with a final surface finish of 3 μ m (Ra~0.2 μ m).

The state of the art NiCoCrAlY bond coats were prepared by two different fabrication procedures; namely the argon shrouded plasma spray process (NiCoCrAlY-A), and the detonation gun process (NiCoCrAlY-B). The coating thicknesses were around 160 μ m. The compositions of these bond coats are given in Table 1. After deposition, the coatings were vacuum heat treated, peened with stainless steel shot and vibratory finished with alumina media. They were also heavy grit blasted prior to TBC deposition by using 8 grit (2mm) alumina at a pressure of 60-80 psi

The modified NiCoCrAlY bond coats had Pt layers applied as an overlayer as well as an underlayer. Some of the NiCoCrAlY bond coats were aluminized. Different surface preparation techniques (media finish, vibro finish and hand polish with 3 μ m surface finish) were also used for these coatings.

The specimens with and without a TBC were subjected to cyclic oxidation testing in a bottom-loading furnace in laboratory air. Most of the tests were performed at 1100°C, whereas some were performed also at 1000 and 1200°C. The cycles consisted of 10 minutes for heating up to temperature, 45 minutes at temperature and 10 minutes for forced air cooling (Figure 6b).

Some of the specimens were also subjected to isothermal testing in order to compare the failure mechanisms under cyclic and isothermal test conditions.

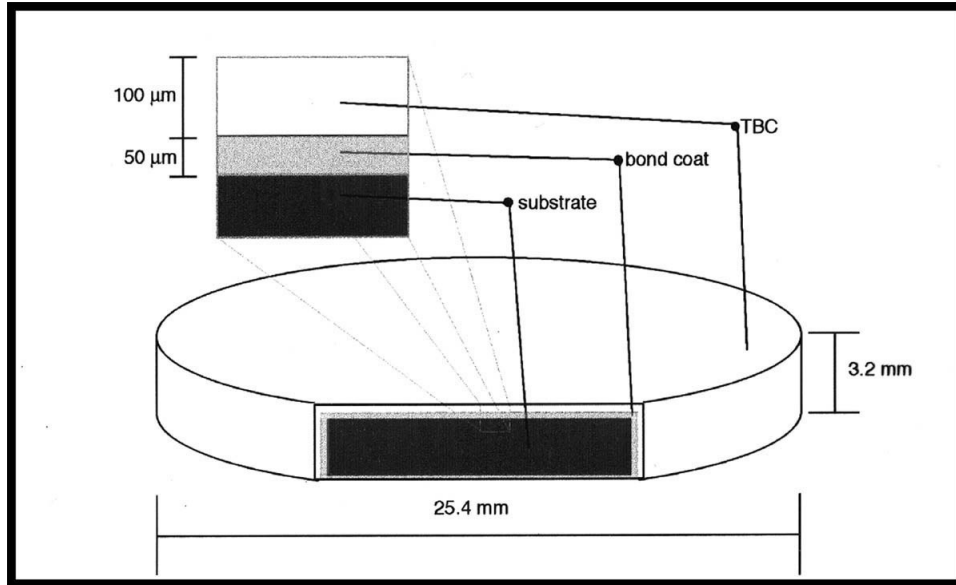
The specimens were taken out of the furnace after every 20 cycles and kept in a dessicator for several hours. During this time, they were examined by naked eye, if needed, by optical and/or stereo microscopy. They were removed from the test when a significant amount of TBC spallation was observed. Figures 7a and Figure 7b are two examples that show typical failures. Some of the specimens failed in the furnace either during the last cooling cycle, or before, whereas some failed in the dessicator.

Some of the specimens without a TBC were given a preoxidation heat treatment to investigate the effects of preoxidation on the characteristics of the oxides formed. The preoxidation was performed in a horizontal tube furnace by using an Ar/4%H₂ atmosphere at 1080°C.

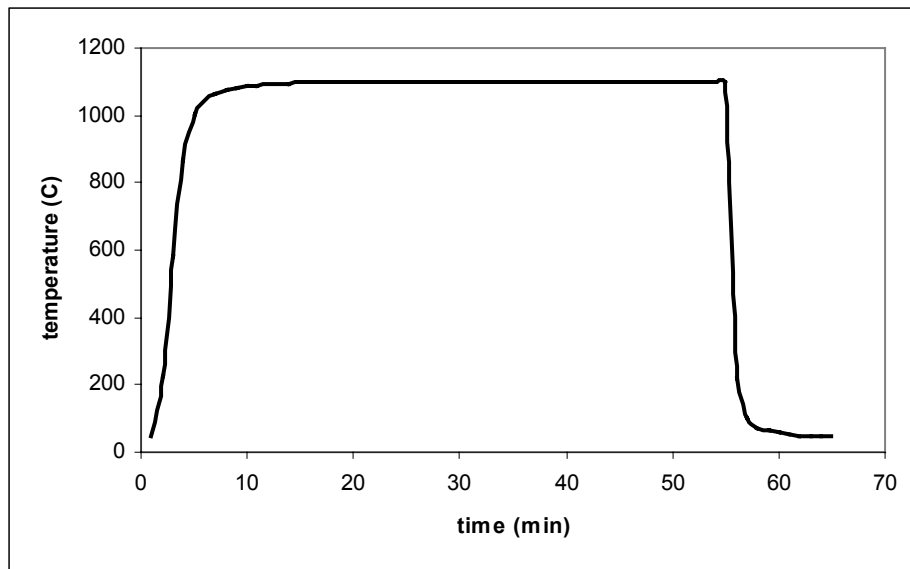
Optical and scanning electron microscopy (SEM) were used for characterization of the specimens. Some of the specimens were indented using a Rockwell C indenter under a load of 150 kg. The indentation testing, details of which can be found in reference [69], is usually used to calculate the interfacial toughness by using the debond radius after indentation. However, in this study, it was used just to determine the fracture paths as a function of exposure cycles by examining the delaminated areas.

Table 1 Compositions of NiCoCrAlY bond coats (wt %)

Coating	Ni	Co	Al	Cr	Y	O	C
NiCoCrAlY-A	48.0	21.78	12.58	16.45	0.43	0.16	-
NiCoCrAlY-B	44.4	22.95	13.82	16.59	0.57	0.9	0.58



(a)

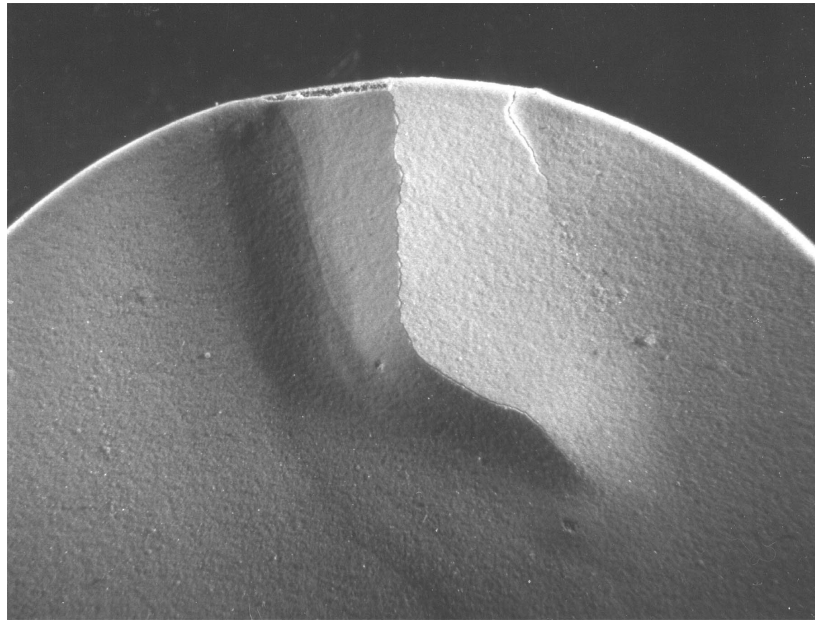


(b)

Figure 6 (a) Schematic to show the typical configuration of the specimens used in this study. (b) Temperature profile of the bottom loading furnace.



(a)



(b)

Figure 7 Macrographs showing the typical TBC failures, (a) and (b).

4.0 RESULTS AND DISCUSSION

4.1 STUDIES OF BOND COATS WITHOUT TBCS

The specimens without a TBC were thermal cycled until severe degradation of the bond coats was observed. These specimens were examined as a function of time in order to compare the sequence of degradation of the different types of bond coats.

4.1.1 NiCoCrAlY Bond Coats

The surfaces of the NiCoCrAlY bond coats deposited either by argon shrouded plasma spray (NiCoCrAlY-A) or detonation gun technique (NiCoCrAlY-B) were very irregular (Figure 8a) and the as-processed coatings exhibited some porosity and oxide inclusions as shown in Figure 8b. The microstructures consisted of γ (Ni solid solution), β (NiAl) and Cr rich phases as well as Y and/or Hf containing phases (Figure 8c). In the case of the NiCoCrAlY-B coatings, significant amount of yttrium containing oxides encapsulated with alumina were observed throughout the cross section (Figure 8d).

Photomicrographs showing the degradation of these coatings as a function of time at 1100 °C are presented in Figure 8 and Figure 9 for NiCoCrAlY-A and NiCoCrAlY-B coatings, respectively. After 209 cycles of exposure (Figure 9a and 10a) the β phase was depleted from both the surface and the substrate/bond coat interface as a result of oxidation and interdiffusion with the substrate, respectively. Oxide protrusions, which developed by rapid transport of

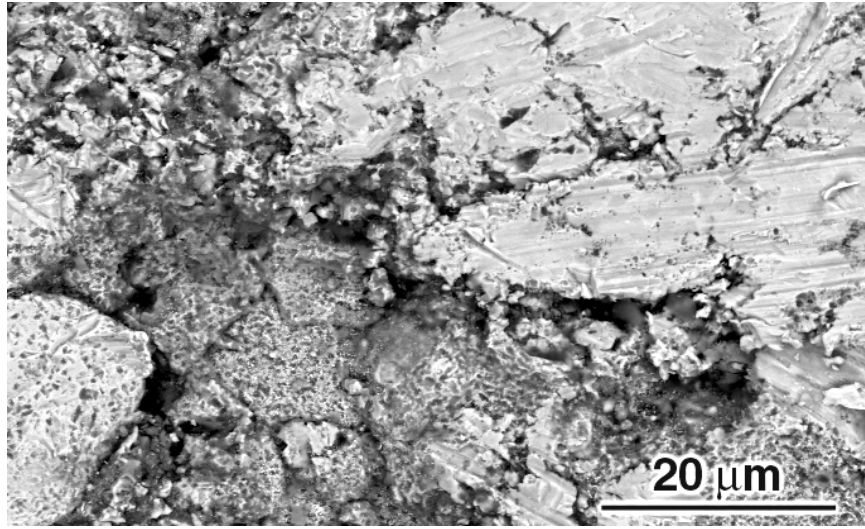
oxygen through the Y and Hf containing oxides and its reaction with aluminum in the alloy, were observed and they became more pronounced after 955 cycles of exposure (Figure 9b). This is shown in a high magnification micrograph of the alumina scale developed on these coatings (Figure 9c). However, these stringers of oxides protruding into the bond coat were very rare in the case of the NiCoCrAlY-B coatings. This is related to the yttrium being tied up as an oxide in the bond coat during processing (Figure 8d). Comparison of the microstructures of the NiCoCrAlY coatings after 955 cycles of exposure (Figure 9b and 10b) shows a difference in the amount of aluminum depletion between these two coatings. This difference may be related to the excessive oxidation in the NiCoCrAlY-A coatings due to formation of the reactive element rich oxides, which were rapid oxygen transport paths through the alumina scale. After 3031 cycles of exposure, the β phase was depleted completely from both of the coatings, leaving only the γ phase (Figure 9d and 10c) Penetration of oxidation through the thickness of the coating was observed in the NiCoCrAlY-A coatings in some localized areas and it propagated along the substrate-bond coat interface. Depletion of aluminum in the cyclic test will lead to development of less protective oxides and more rapid consumption of the coating. Penetration of the coating as in Figure 9d may be caused by the large amounts of reactive element oxides in the scale.

The surfaces of these coatings were observed to become wavy with exposure as evident by comparing Figure 11a, in the as-processed condition, with Figures 11b and 11c after 209 and 955 cycles of exposure at 1100°C, respectively. However, the surfaces became smoother after still longer exposure times (such as after 3031 cycles at 1100°C as in Figure 11d). The surfaces might have become rougher as a consequence of thicker oxide formation at localized areas due to reactive element rich oxides, followed by spallation along the oxide/bond coat interface at these sites. The smoothening of the surface at longer exposure times, then, can be explained by these

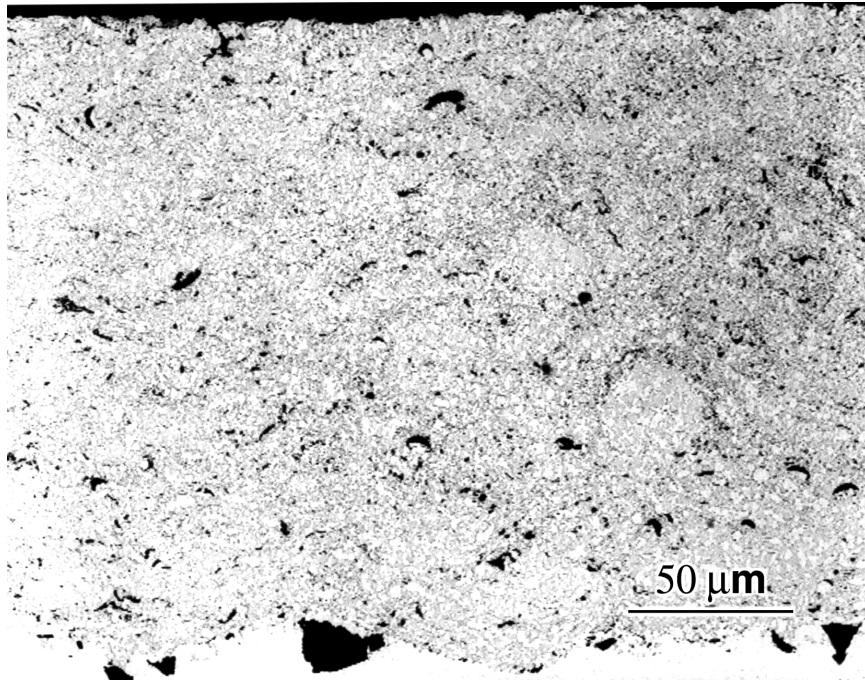
reactive element rich oxide protrusions which became more uniformly distributed over the surface with time as can be seen from the sequence of micrographs given in Figure 11. On the other hand, the plastic deformation of the bond coat in the presence of thermal and growth stresses is a possibility, but, in this case, it becomes difficult to explain the smoothing of the surface with longer exposure times. More work needs to be done to understand the surface roughening of the NiCoCrAlY bond coats which appears to be different than the surface roughening of the Pt aluminide bond coats, which will be shown later on.

Oxides other than alumina developed on the surfaces of these bond coats at the very early stages of oxidation due to transient oxidation effects. Figures 12a and Figure 13a show the transient oxides formed on the surfaces of NiCoCrAlY-A and NiCoCrAlY-B coatings after 2 hours of exposure at 1080 °C in air, respectively. Oxidation experiments were performed under low partial pressure of oxygen to prevent transient oxidation. The oxide scales formed on these preoxidized bond coats were purer which shows that the oxygen partial pressure obtained was lower than that required for the oxidation of other elements in the alloy such as Ni, Cr and Co. Moreover, the oxide scale was observed to spall from the specimens which were exposed in air, whereas it was still adherent on those which were preoxidized under a low partial pressure of oxygen and then exposed in air under the same conditions (Figures 12b and Figure 13b).

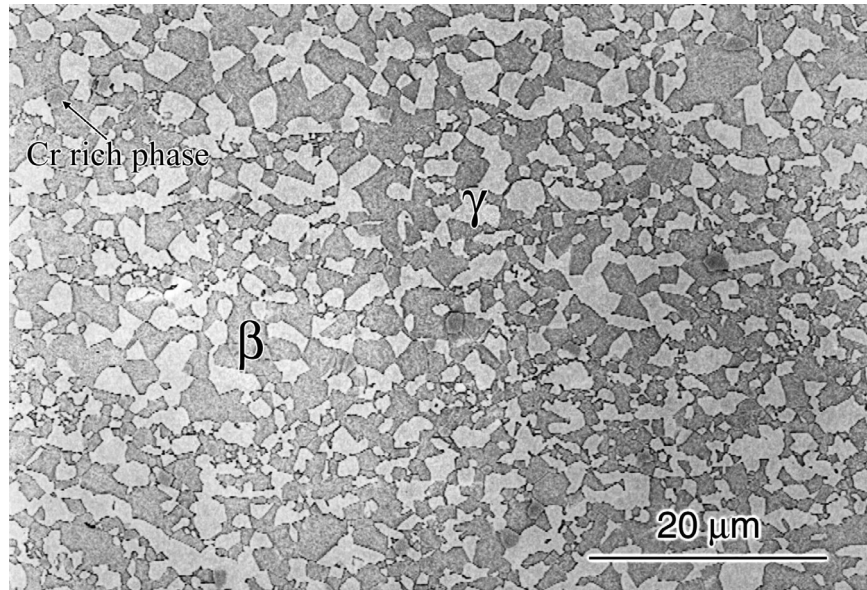
The adherence of the oxide scales on these bond coats were also affected by the surface condition. The alumina scales developed on hand polished NiCoCrAlY bond coats were more adherent (Figures 14a and 14b) compared to the alumina scales developed on heavy grit blasted NiCoCrAlY bond coats (Figures 15a and 15b). Moreover, the alumina scales had fewer transient oxides on hand polished specimens.



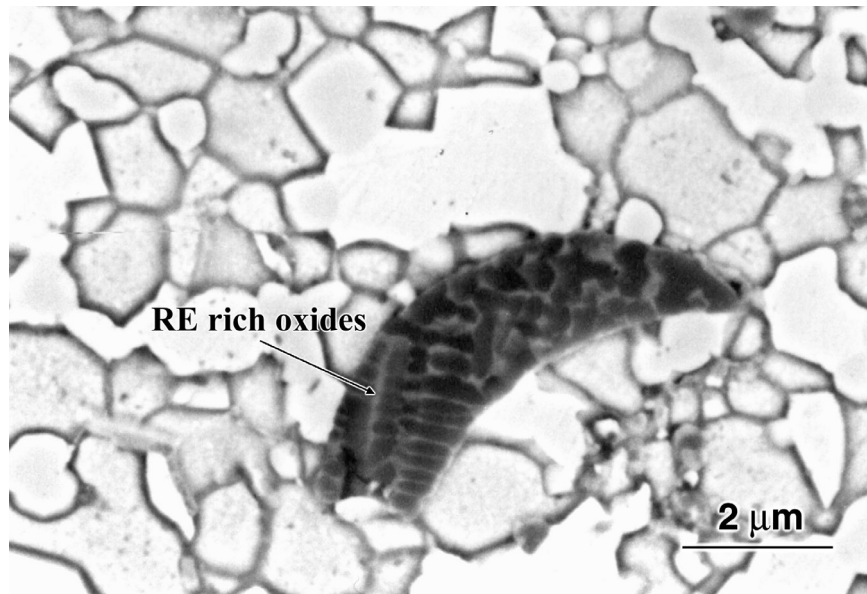
(a)



(b)

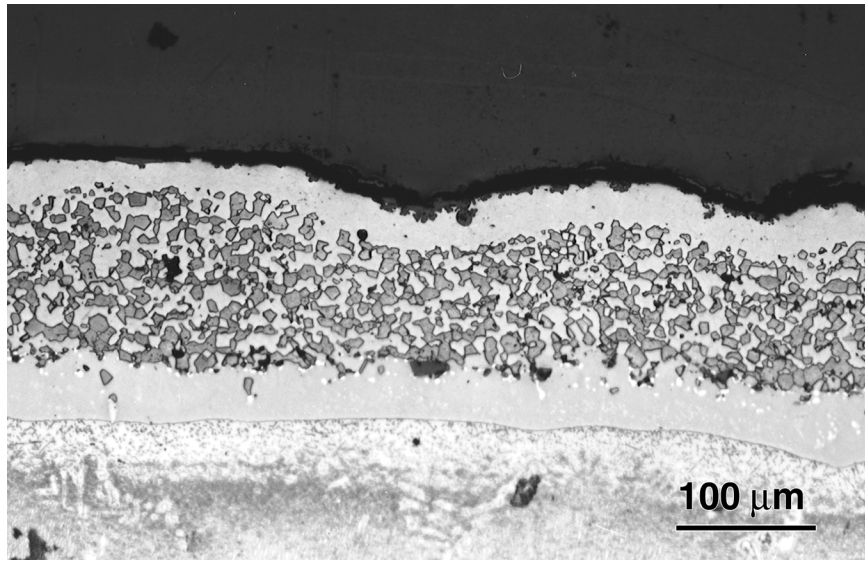


(c)

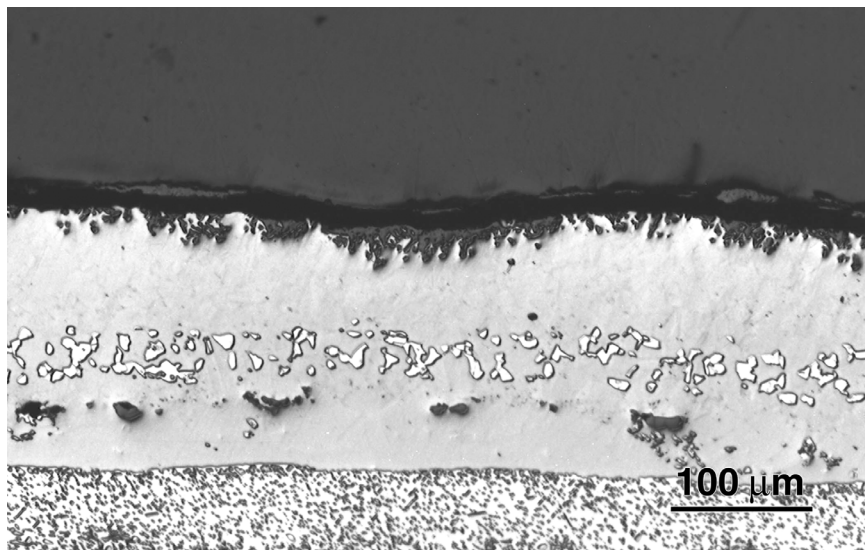


(d)

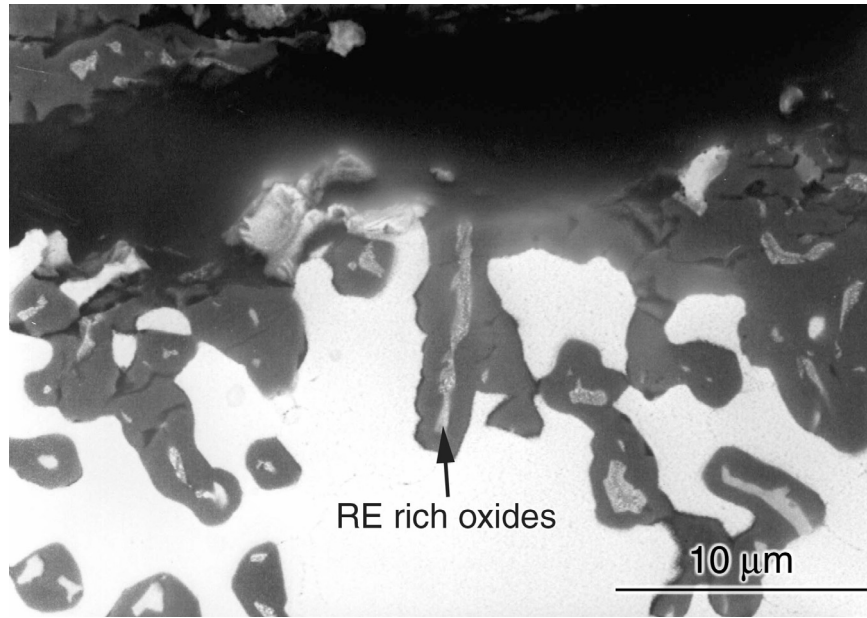
Figure 8 The surface, (a), and cross-sectional micrographs, (b), of NiCoCrAlY bond coats showing the presence of surface defects as well as porosity and oxide inclusions in the as processed condition. The phases present in NiCoCrAlY-A and NiCoCrAlY-B coatings are labeled in (c) and (d) respectively.



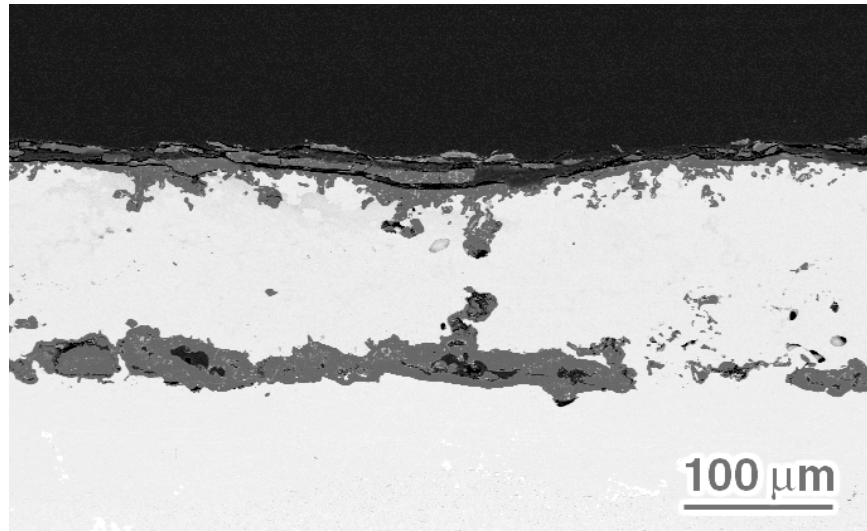
(a)



(b)

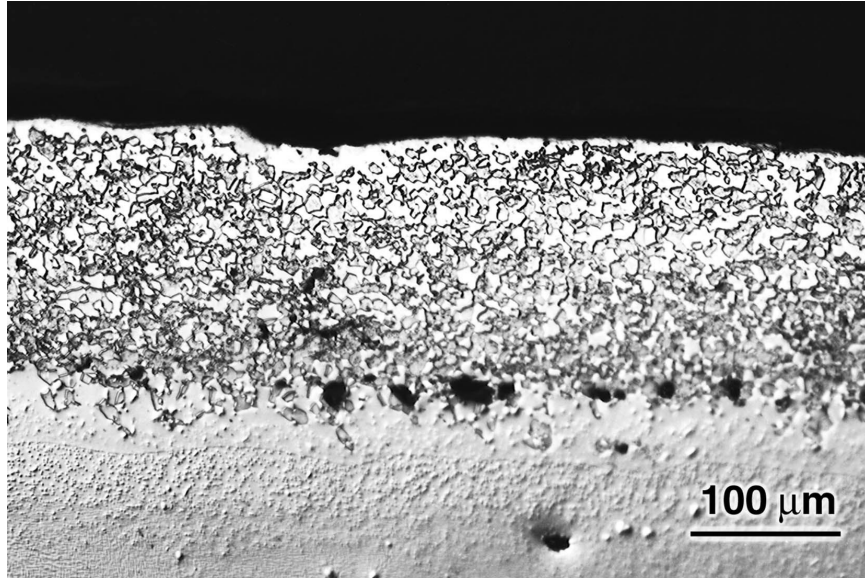


(c)

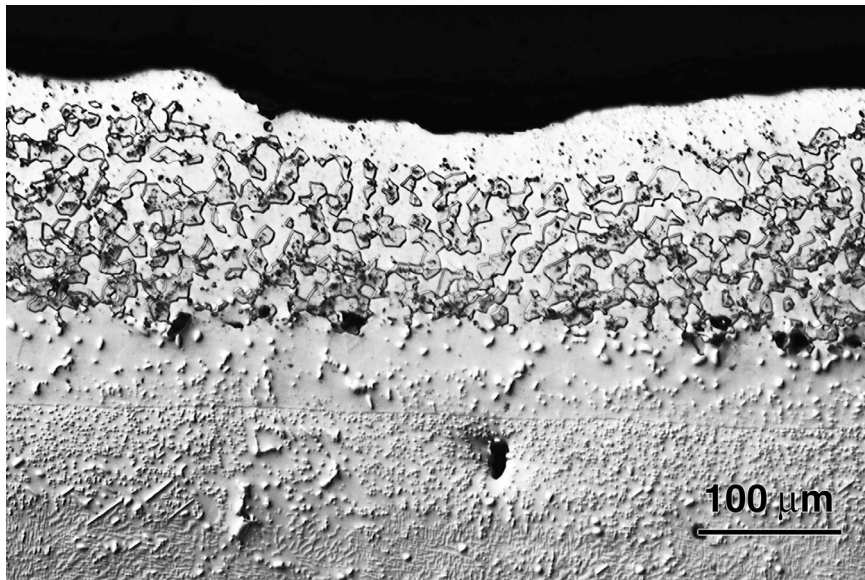


(d)

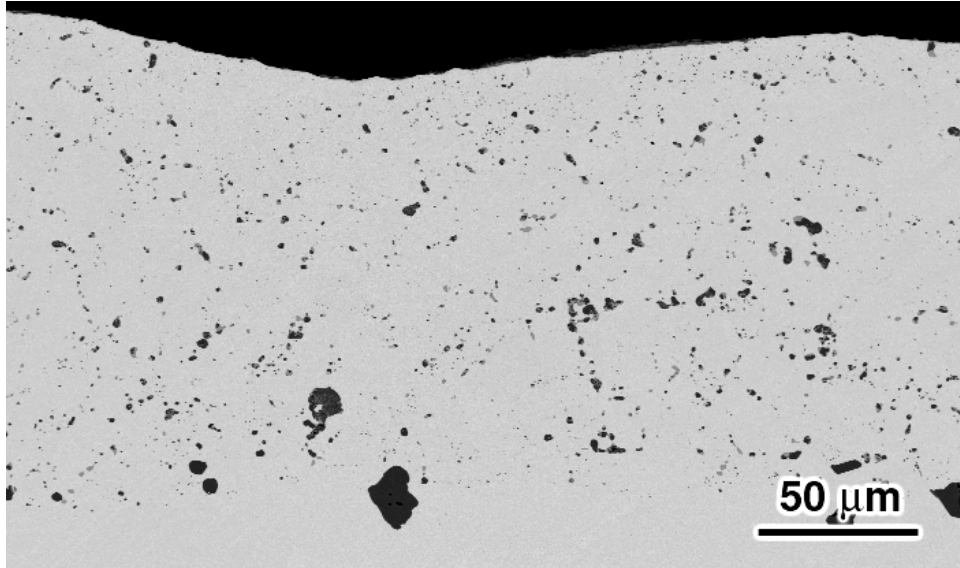
Figure 9 Scanning electron micrographs showing the degradation of NiCoCrAlY-A bond coats after 209, (a), 955, (b and c), and 3031, (d), cycles of exposure at 1100°C.



(a)

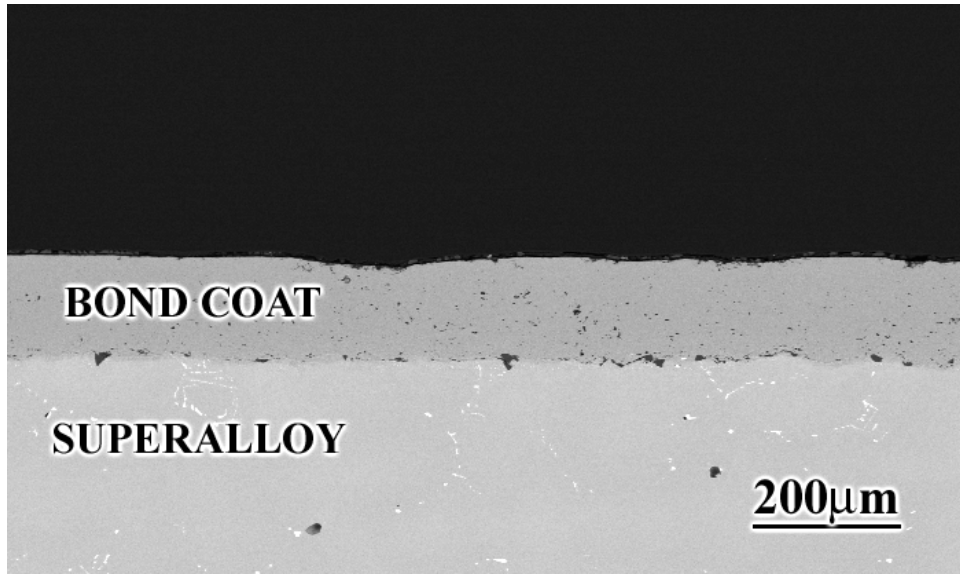


(b)

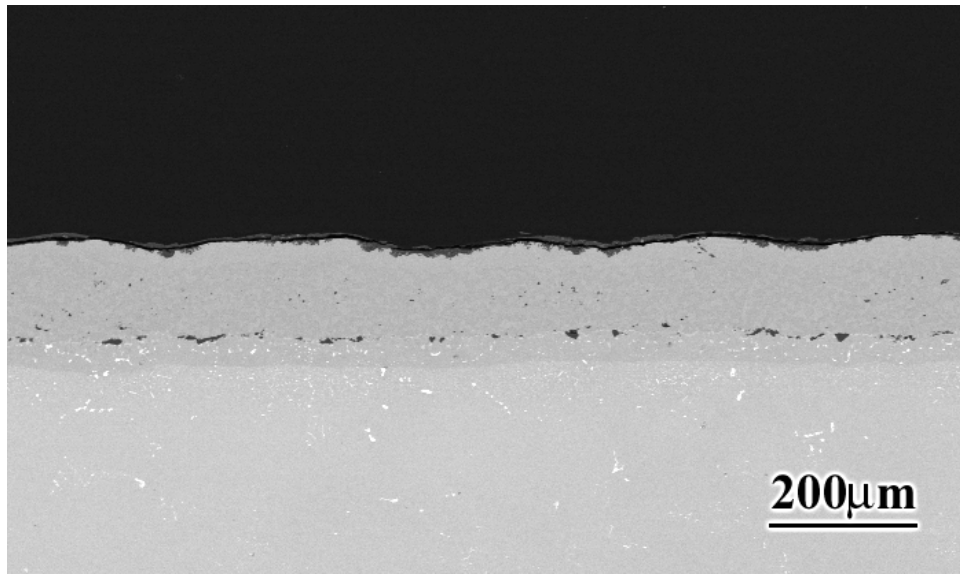


(c)

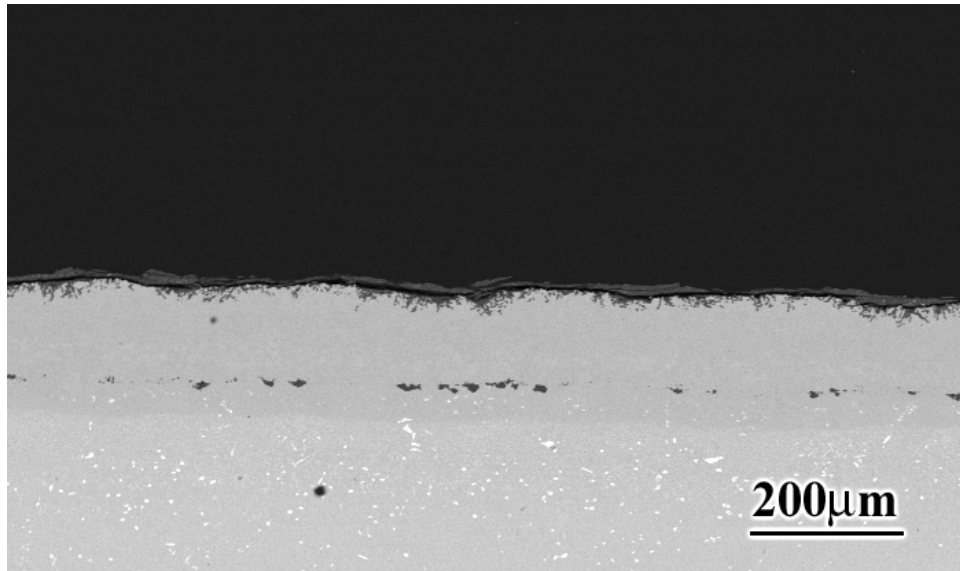
Figure 10 Scanning electron micrographs showing the degradation of NiCoCrAlY-B coatings after 209, (a), 955, (b), and 3031 cycles, (c), of exposure at 1100°C.



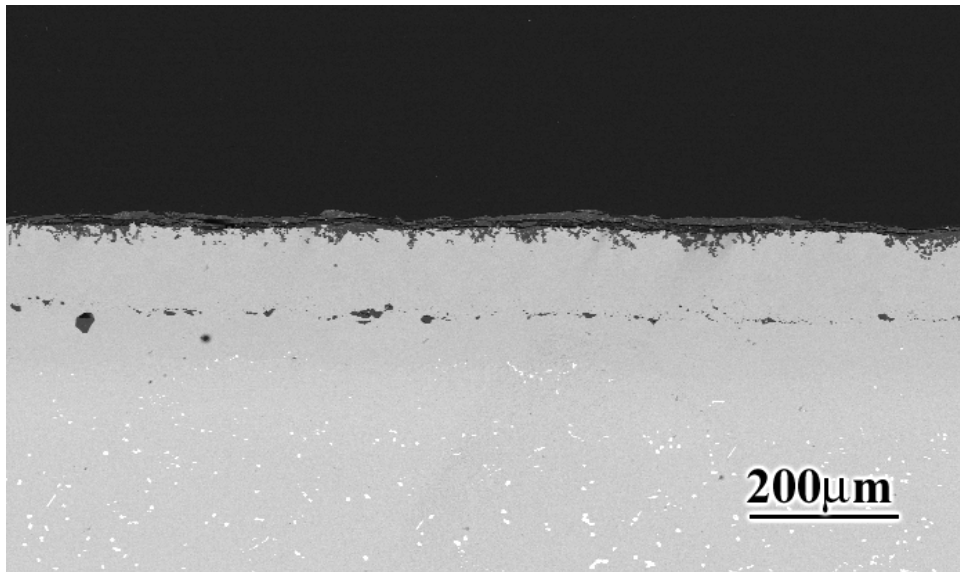
(a)



(b)

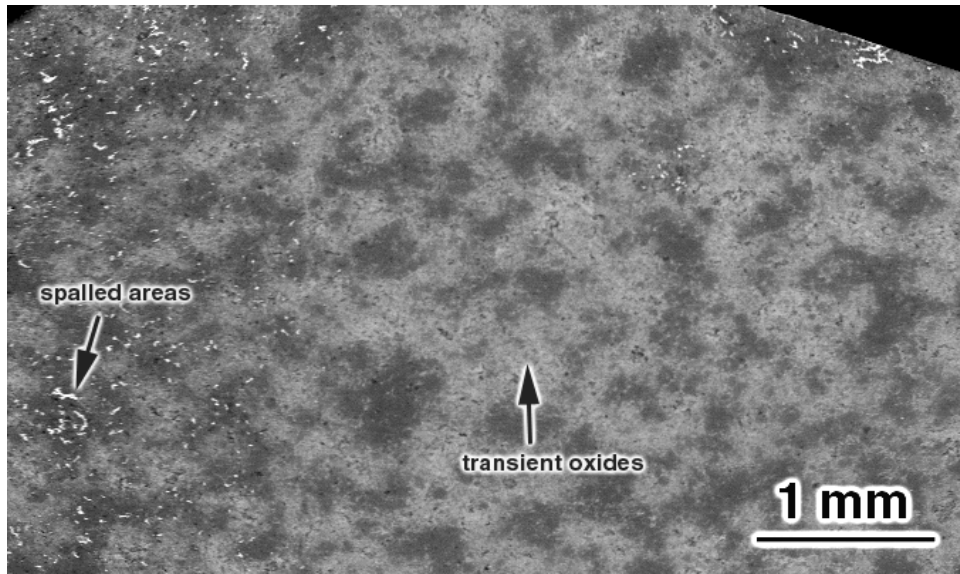


(c)

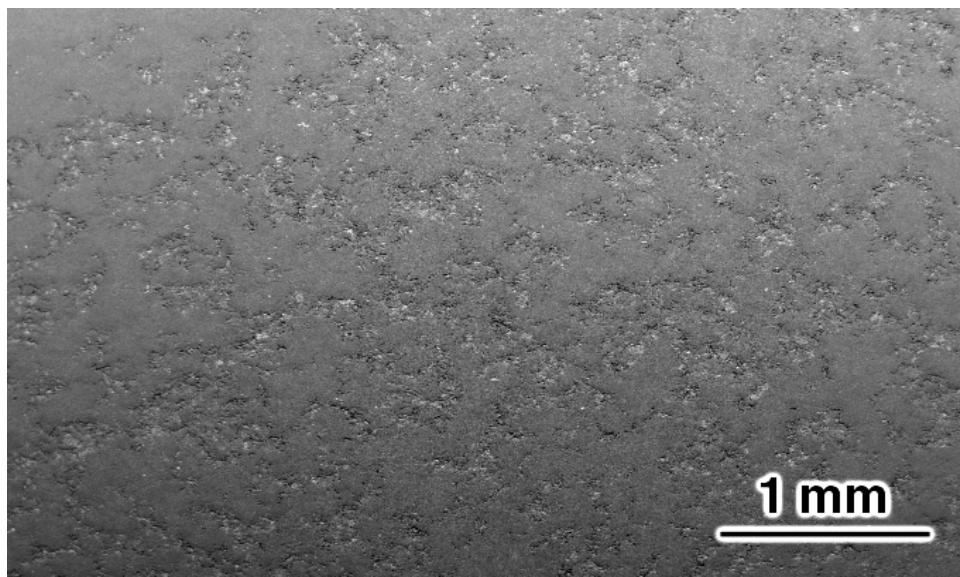


(d)

Figure 11 Cross sectional micrographs from a NiCoCrAlY-A bond coat in the as processed condition, (a), and after 209, (b), and 955, (c), cycles of exposure at 1100°C showing the roughening of the surface. The surface became smoother after 3031 cycles of exposure (d).

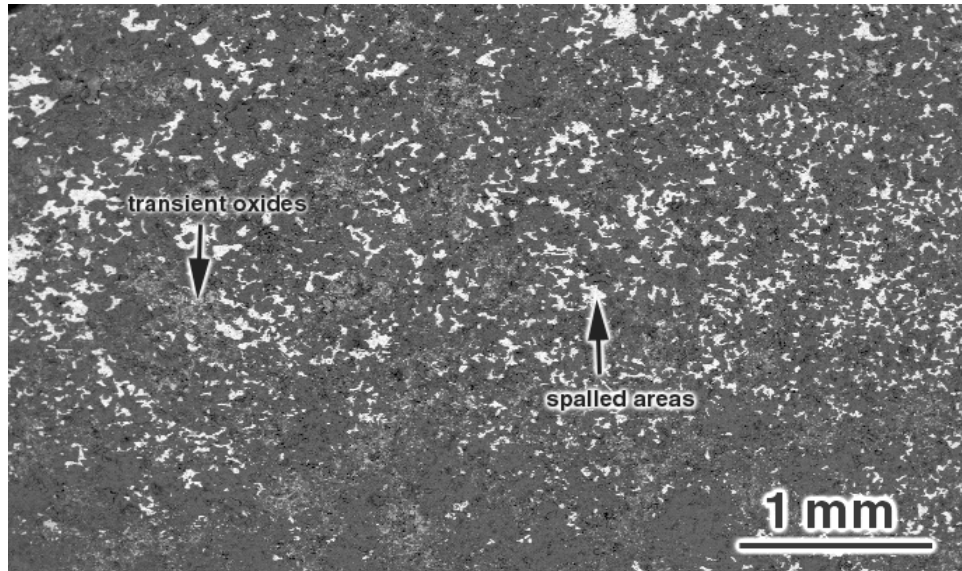


(a)

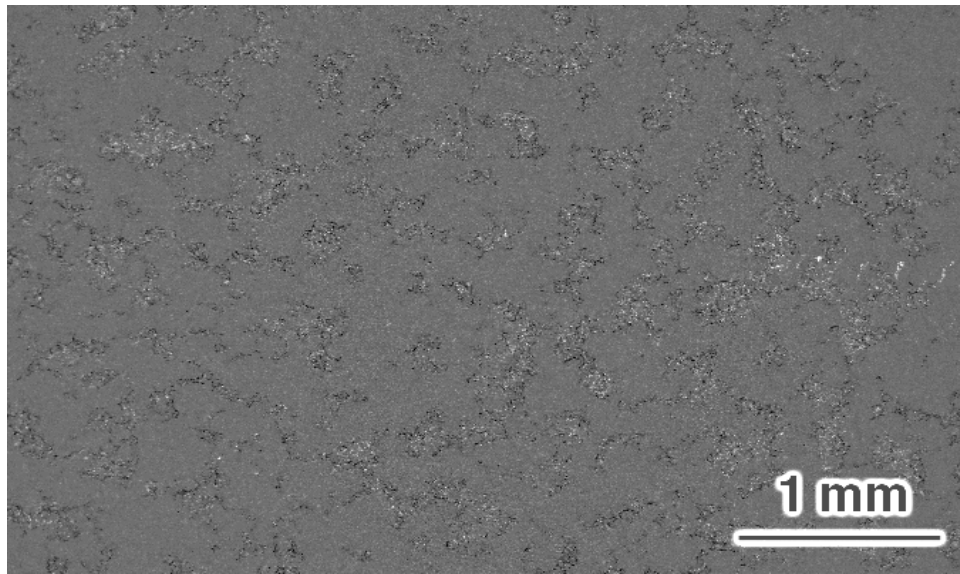


(b)

Figure 12 (a) Surface micrograph of the NiCoCrAlY-A bond coat after exposure at 1080°C for 2 hrs in air showing the transient oxides developed and the spallation of the oxide scale. (b) Surface micrograph showing the purer and more adherent alumina scale developed after the bond coat was preoxidized in an Ar-4% H_2 atmosphere at 1100°C for 100 hrs and then exposed in air under the same conditions as in (a).

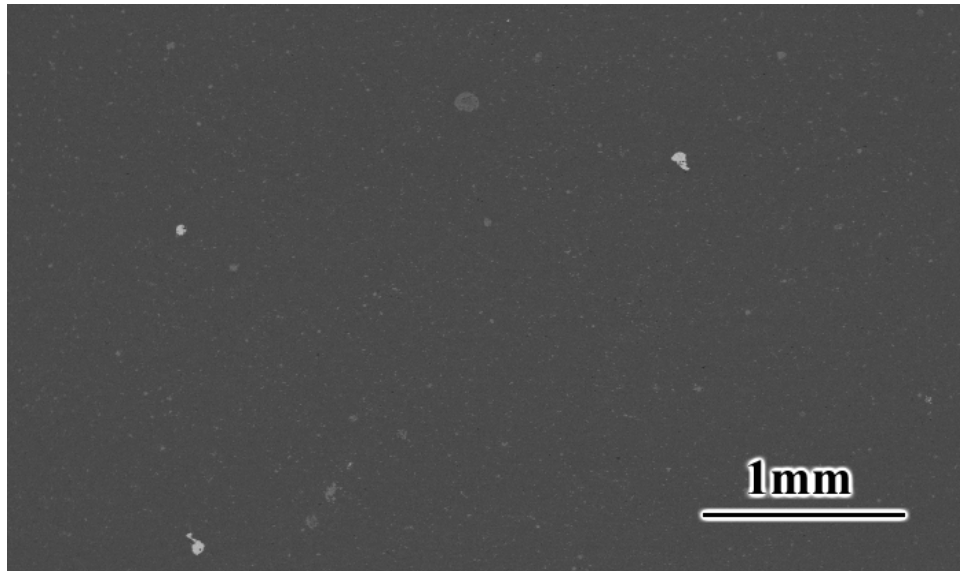


(a)

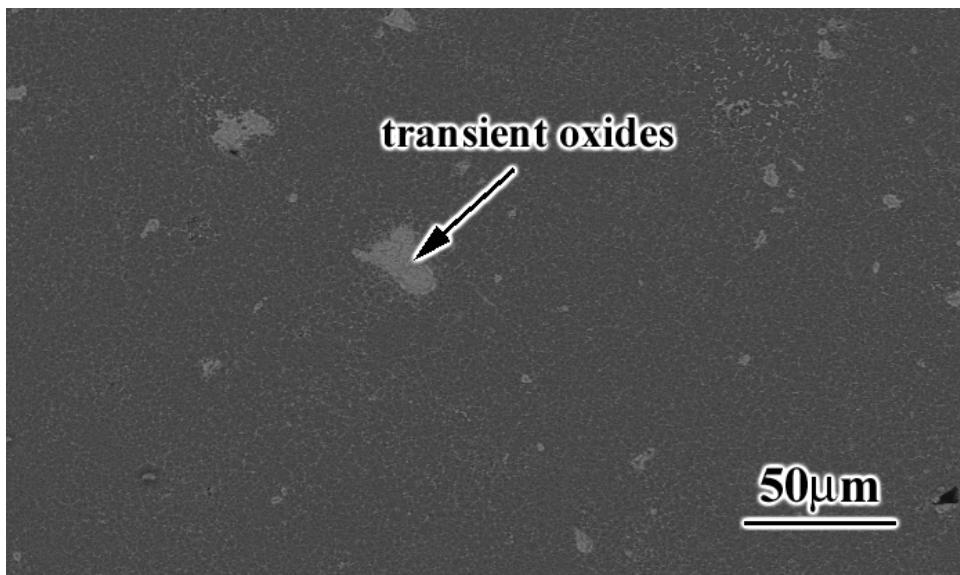


(b)

Figure 13 (a) Surface micrograph of the NiCoCrAlY-B bond coats after exposure at 1080°C for 2 hrs in air showing the transient oxides developed and the spallation of the oxide scale. (b) Surface micrograph showing the purer and more adherent alumina scale developed after the bond coat was preoxidized in an Ar-4% H_2 atmosphere at 1100°C for 100 hrs and then exposed in air under the same conditions as in (a).

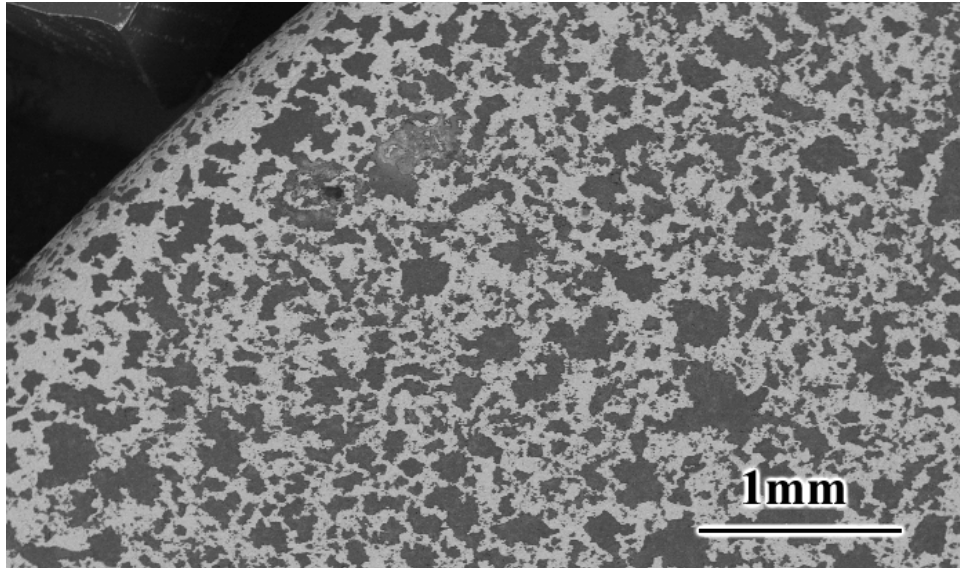


(a)

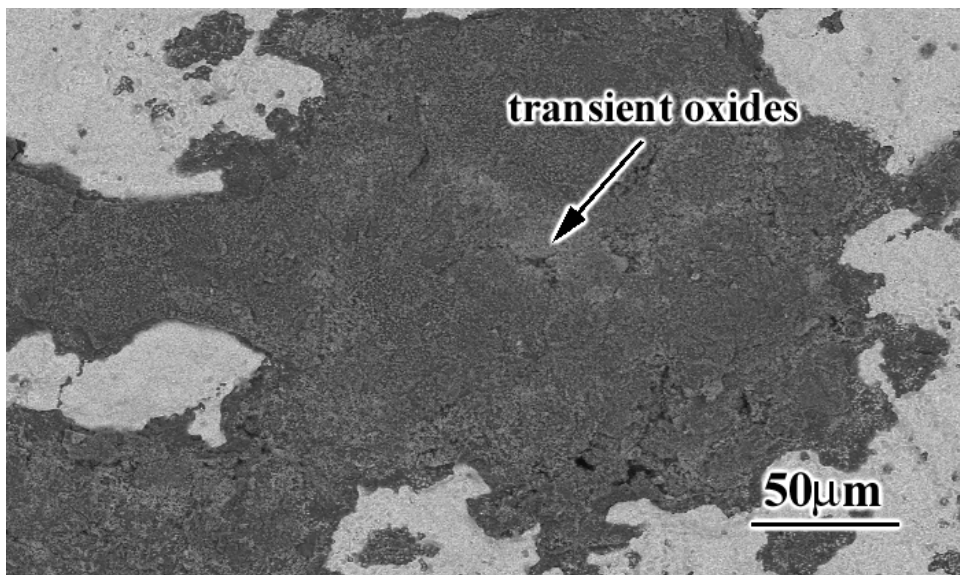


(b)

Figure 14 Scanning electron micrographs showing the surface of a hand polished NiCoCrAlY-A bond coat after exposure at 1100°C for 100 cycles at (a) low and (b) high magnifications.



(a)



(b)

Figure 15 Scanning electron micrographs showing the surface of a heavy grit blasted NiCoCrAlY-A bond coat after exposure at 1100°C for 100 cycles at (a) low and (b) high magnifications.

4.1.2 Platinum Aluminide Bond Coats

The microstructural evolution of Pt modified aluminide bond coats under cyclic oxidation conditions was examined as a function of time at both 1100 and 1200°C. In the as-processed condition, the coating microstructure consisted of β (NiAl) and Pt rich phases. Refractory metal rich precipitates, which form as a result of low solubility of certain substrate elements (W, Ta, Re...) in β (NiAl), were observed in the interdiffusion zone (Figure 16a).

After 20 cycles of exposure at 1200°C, the bond coat consisted of mainly β phase with some γ' (Ni₃Al) which nucleated preferentially at the grain boundaries of the β phase (Figure 16b). The grain boundaries of the bond coat are paths for the outward diffusion of refractory elements. Figure 16c shows a β phase grain boundary, which is enriched in refractory elements. The presence of these refractory elements may also be enhancing the nucleation of γ' at the grain boundaries. The grain size of the β phase just below the original alloy surface where refractory metal rich precipitates are pronounced, was found to be smaller and the nucleation of γ' at these grain boundaries resulted in the formation of a continuous layer of γ' in the β phase (Fig 16d)

The β phase retreated both from the bond coat/oxide interface and the bond coat/substrate interface with continued exposure. Figures 17a through 17f show the micrographs after exposure at 1200°C for 40, 60, 80, 100, 130 and 200 cycles, respectively. The last traces of β phase after a large number of cycles of exposure was close to the bond coat/TGO interface which shows that Al depletion of the bond coat due to interdiffusion with the substrate was more pronounced than the aluminum depletion at the bond coat/oxide interface (Figure 17f). This may be related to the

development of adherent alumina scales, which reduce the aluminum depletion due to oxidation at the bond coat/oxide interface.

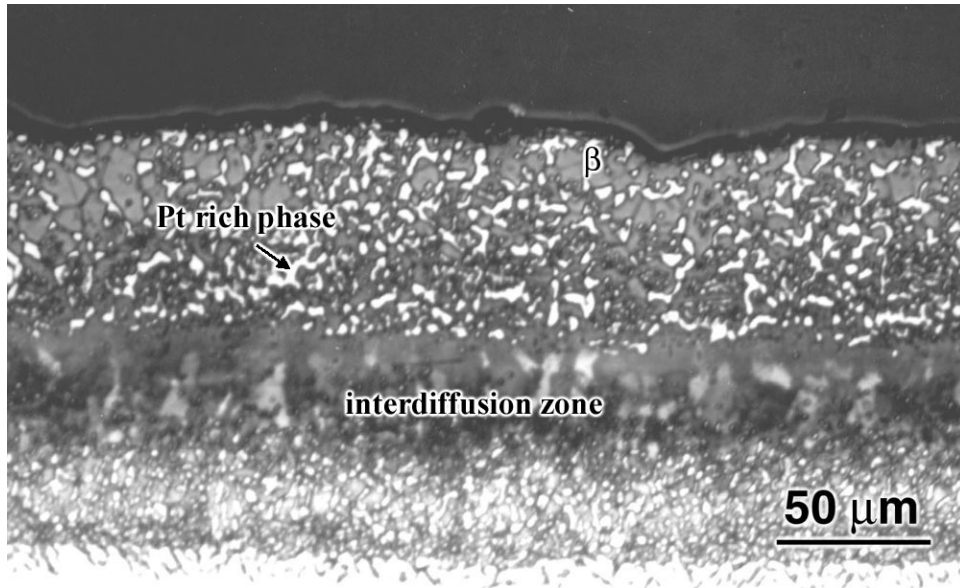
A surface micrograph of the as-processed Pt aluminide bond coat shows the ridges that developed at the grain boundaries of the bond coat (Fig 18a). After cyclic exposure, cracks were observed in the alumina scale on these grain boundary ridges (Figure 18b). The formation of these cracks is reported to be due to out of plane tensile stresses generated at the peaks of the ridges [65]. However, these grain boundary ridges are removed after grit blasting which is generally performed prior to TBC deposition (Fig 18c).

Metastable aluminas are known to form prior to stable α -alumina formation. The transformation from metastable alumina to stable α -alumina results in a volume reduction, which causes formation of cracks during the initial stages of oxidation. The surface micrograph of the Pt modified aluminide bond coat, which was exposed at 1200°C for 15 hours, showed the cracks and the oxide ridges developing at these cracks (Figures 19a and 19b). The development of the oxide ridges as a result of transformation from metastable to stable α -alumina is also reported elsewhere [35].

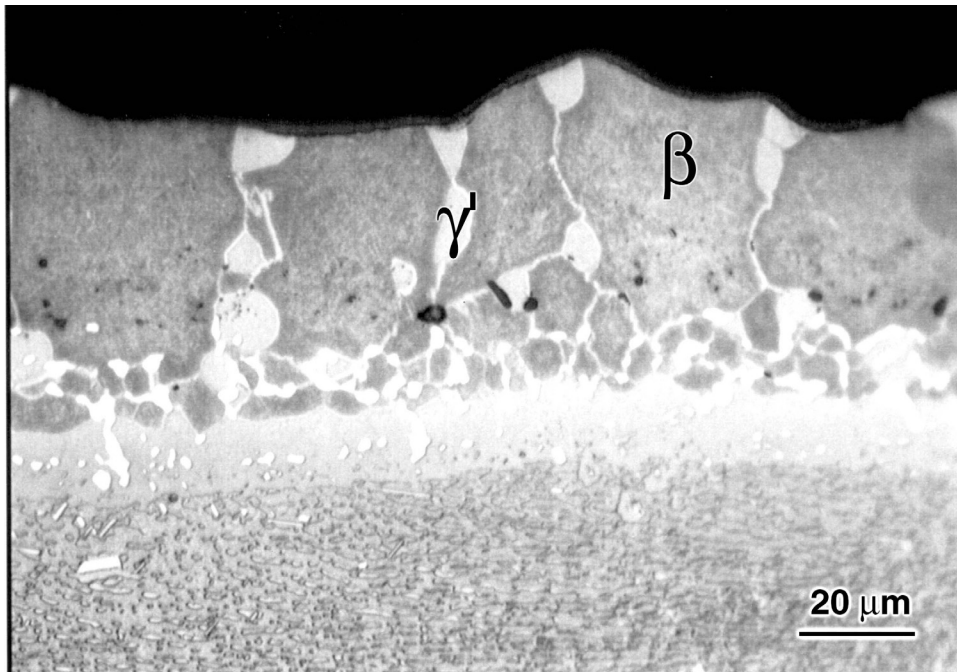
Surface rumpling is one of the basic features of the Pt aluminide bond coats. Figure 20a shows the surface of a Pt aluminide bond coat, which was highly rumpled after exposure at 1100 °C for 955 cycles. After large numbers of exposure cycles, large cavities formed in the bond coat (Fig 17e) and at the bond coat/oxide interface (Figure 20b). It appears that alumina formed on the surface of these cavities as a result of oxygen diffusion through the cracks present in the initially formed alumina (Figure 20c). In some places, spinel formation was observed on the alumina scales formed at these cavities (Figure 20d). The gamma phase observed in the bond

coat at places where spinel has formed shows that the spinel formation was related to aluminum depletion.

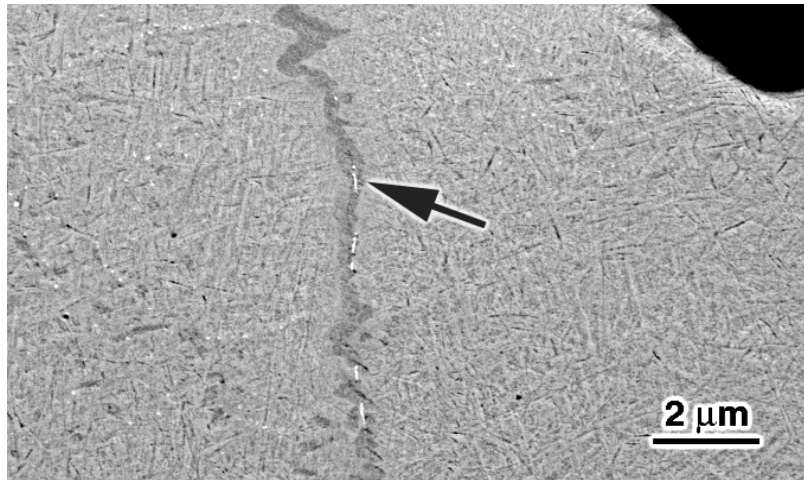
In summary, the initial oxidation of NiCoCrAlY bond coats was more severe with evidence of transient oxidation and spalling. On the other hand, the Pt aluminide bond coats developed purer and more adherent alumina scales initially. However, with long exposure times, the surfaces of Pt aluminide bond coats became highly irregular and large voids developed along the oxide/bond coat interface as well as along the initial superalloy/bond coat interface. Based on these observations, the total oxidation lives of NiCoCrAlY and Pt aluminide bond coats can be considered to be comparable.



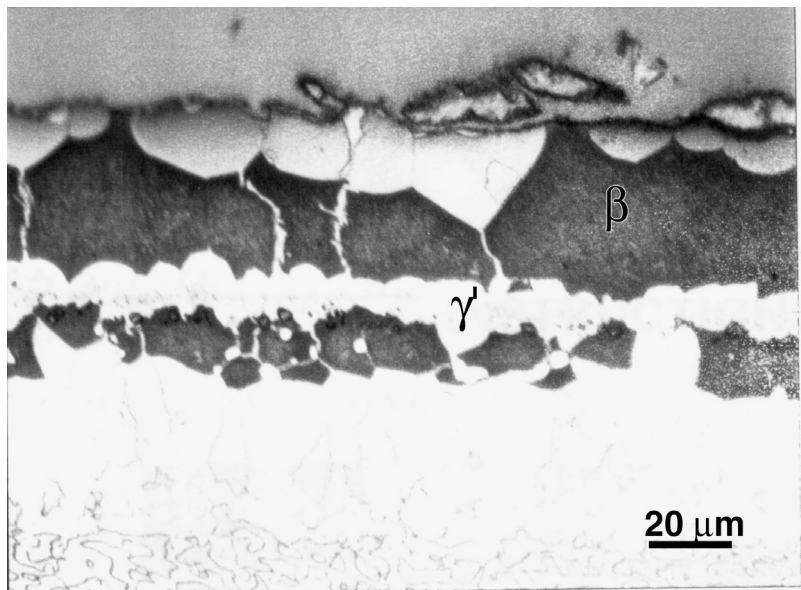
(a)



(b)

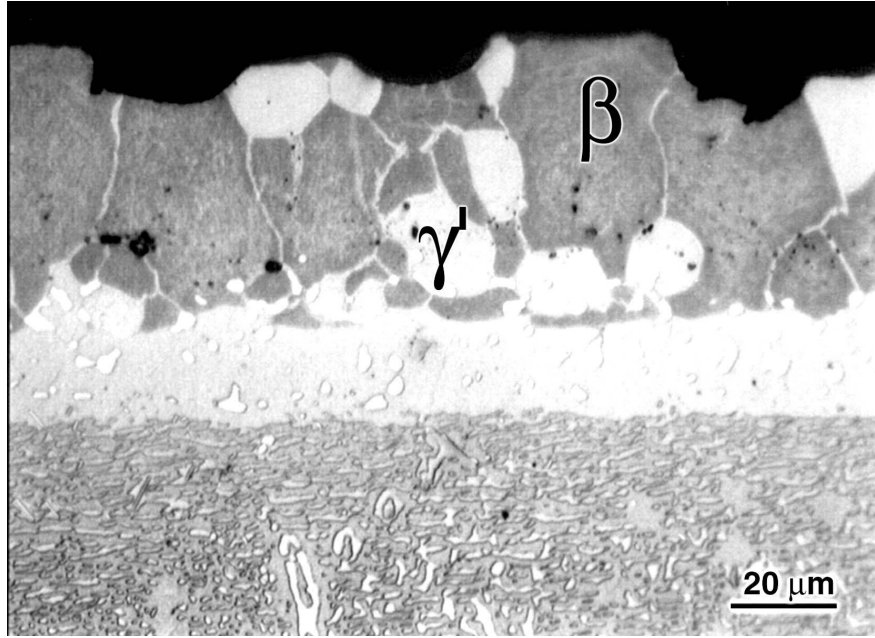


(c)

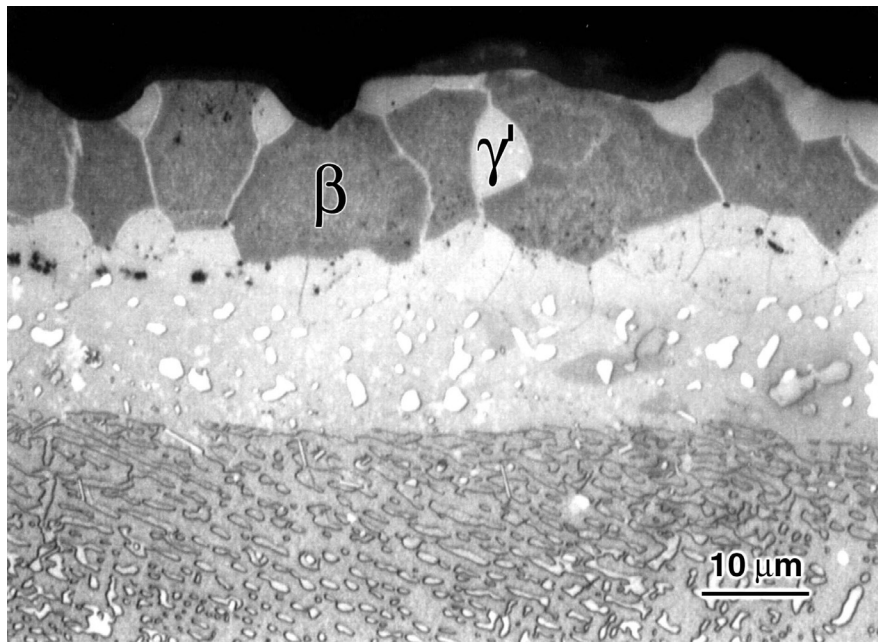


(d)

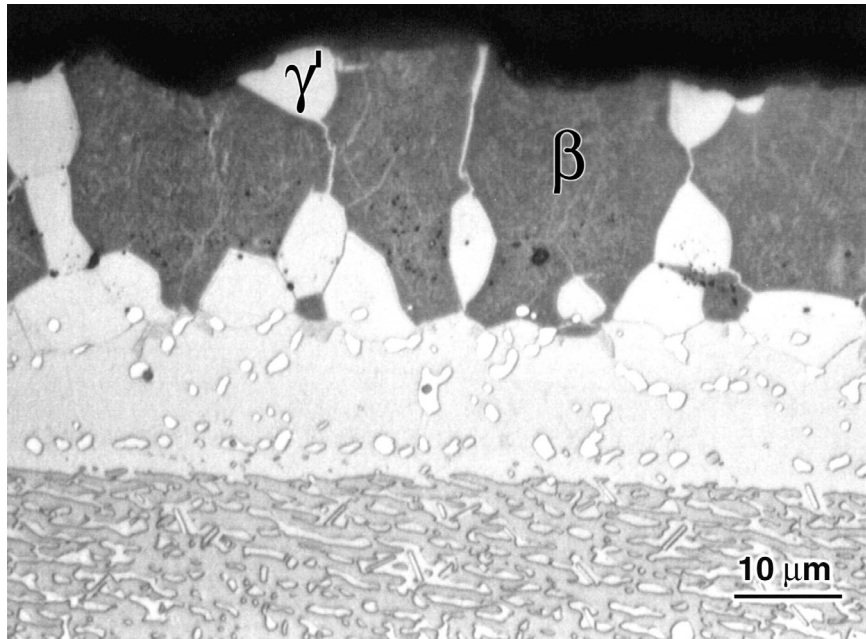
Figure 16 Optical micrographs of the Pt-Aluminide bond coat a) in the as processed condition, b) after exposure at 1200°C for 20 cycles showing the γ' that nucleated preferentially at the β phase grain boundaries, (c) Scanning electron micrograph showing a β phase grain boundary enriched in refractory metal rich particles, (d) optical micrograph of the TBC system with the Pt Aluminide bond coat, which failed at 1200°C after 132 cycles, showing the development of a continuous layer of γ' in β phase.



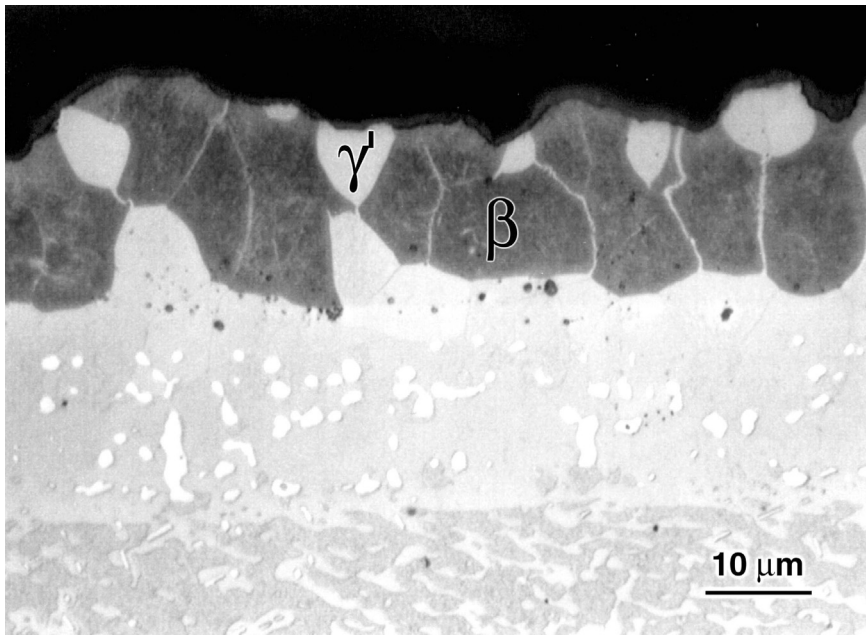
(a)



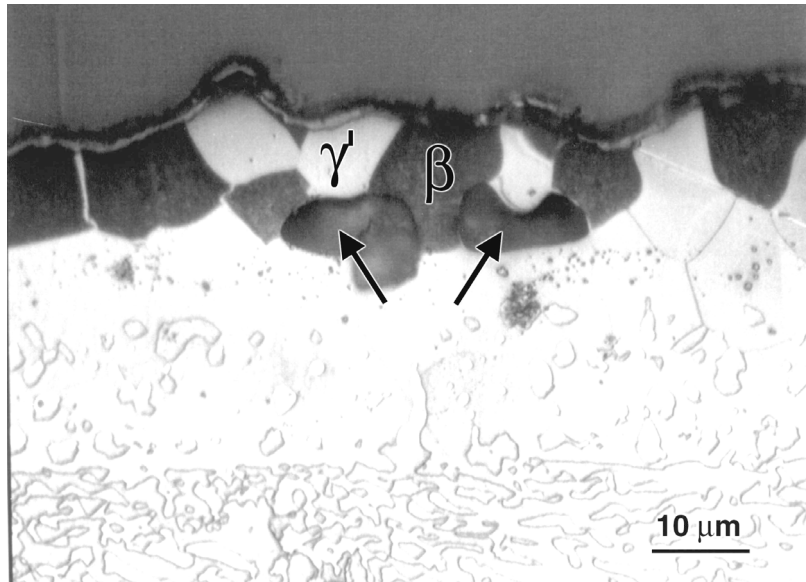
(b)



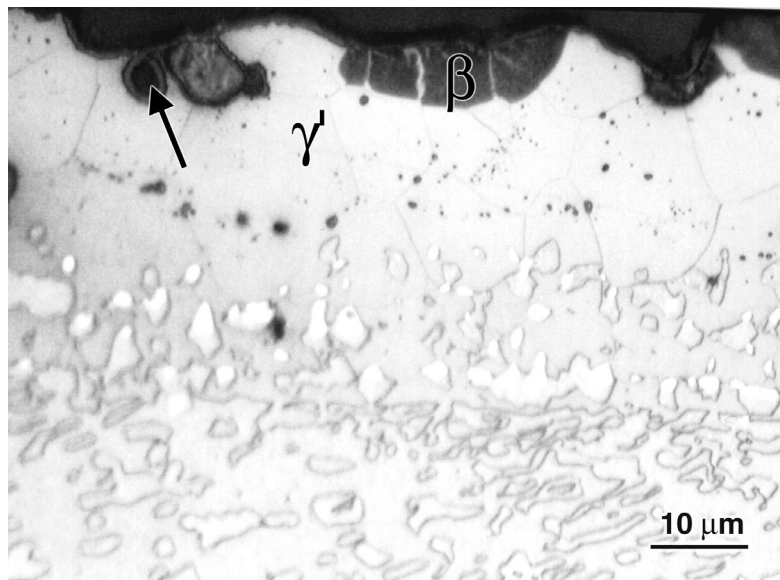
(c)



(d)

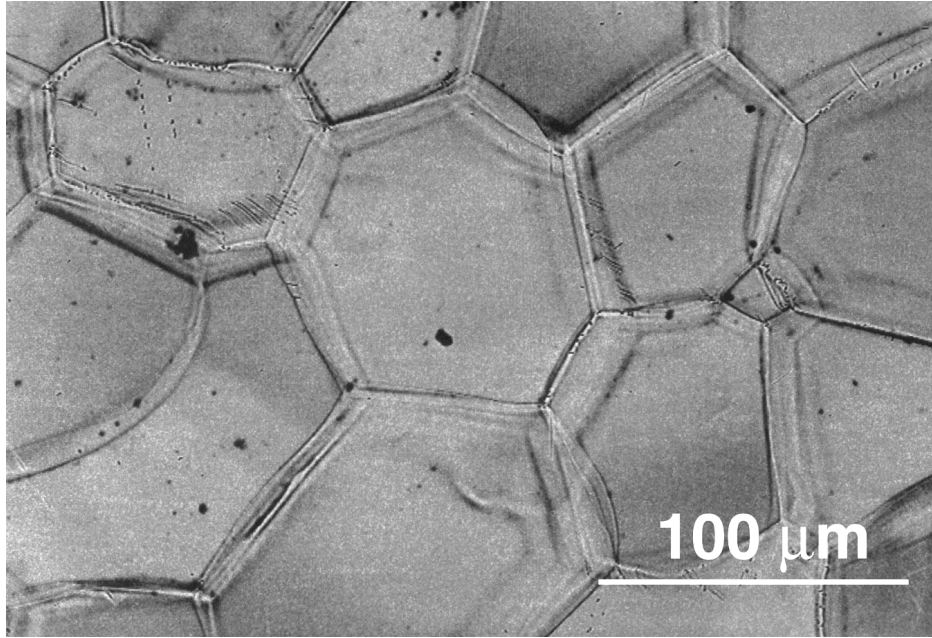


(e)

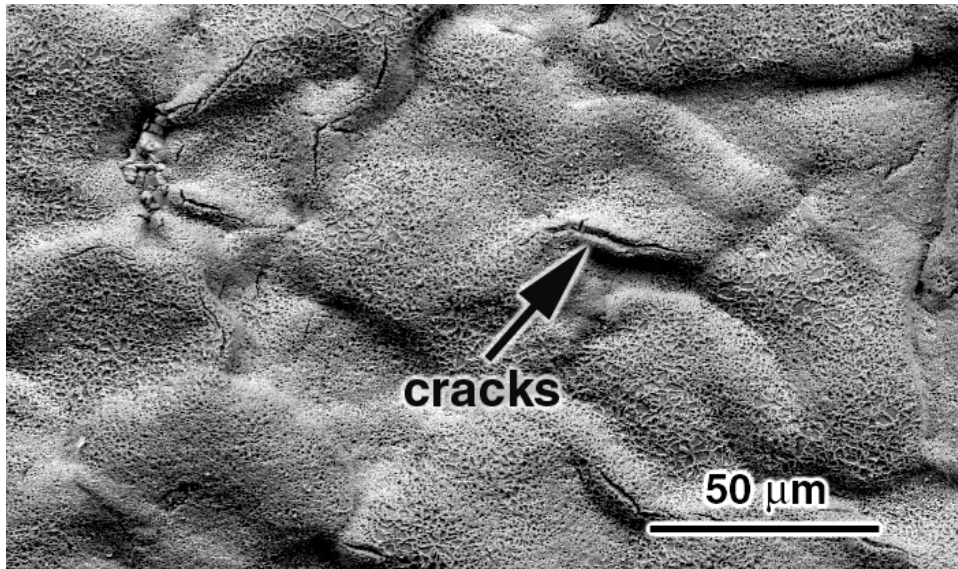


(f)

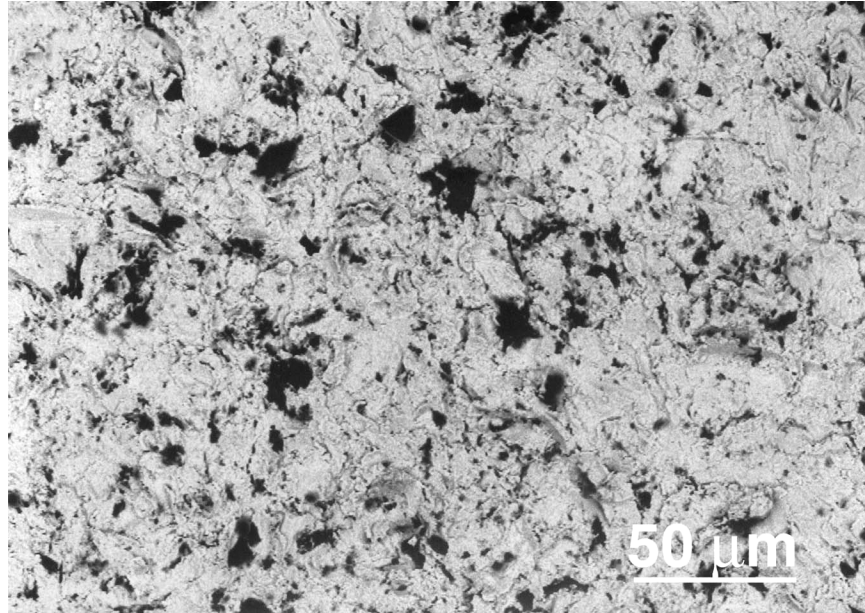
Figure 17 Cross-sectional micrographs showing the degradation of Pt aluminide bond coats after exposure at 1200°C for 40, (a), 60, (b), 80, (c), 100, (d), 130, (e), and 200 cycles, (f), respectively. The arrows point to the large cavities formed at the later stages of oxidation in the bond coat, (e), and at the bond coat/oxide interface, (f).



(a)

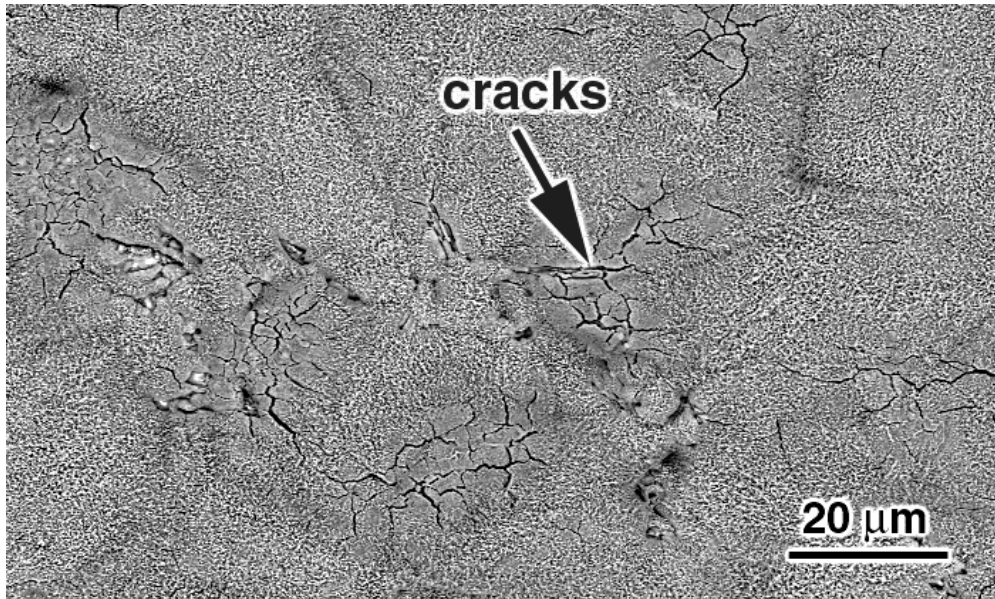


(b)

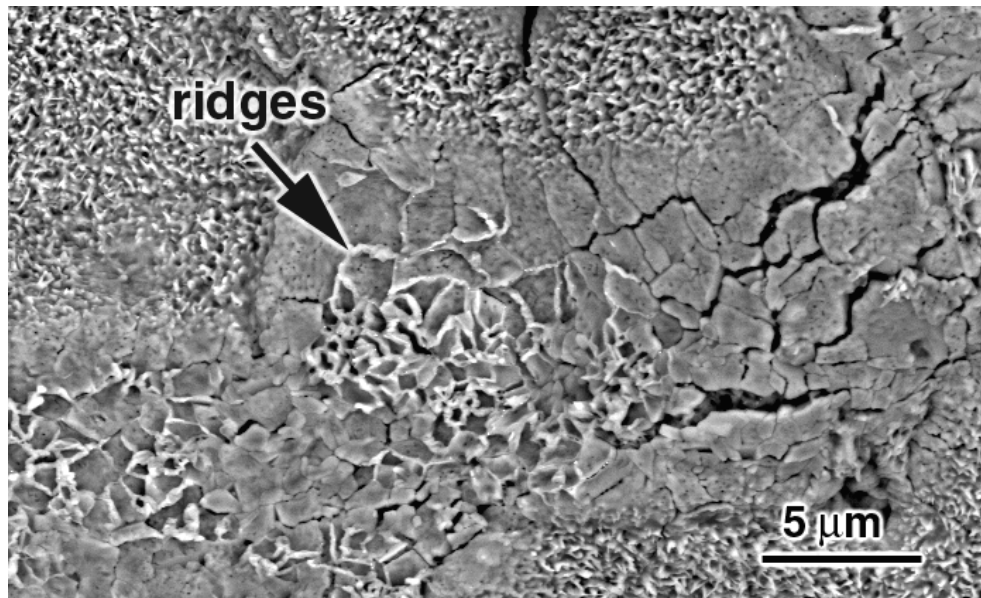


(c)

Figure 18 Scanning electron micrographs from the surface of Pt aluminide bond coats showing a) the ridges that developed at the grain boundaries of the bond coat , b) the cracks that formed on these grain boundary ridges after exposure at 1200°C for 40 cycles, c) the absence of ridges after grit blasting operation, which is generally applied prior to TBC deposition.

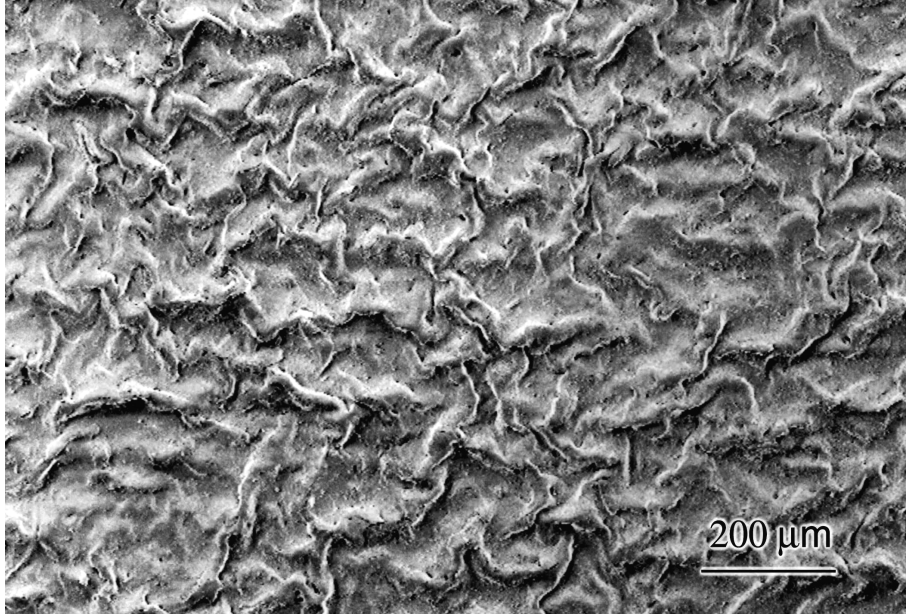


(a)

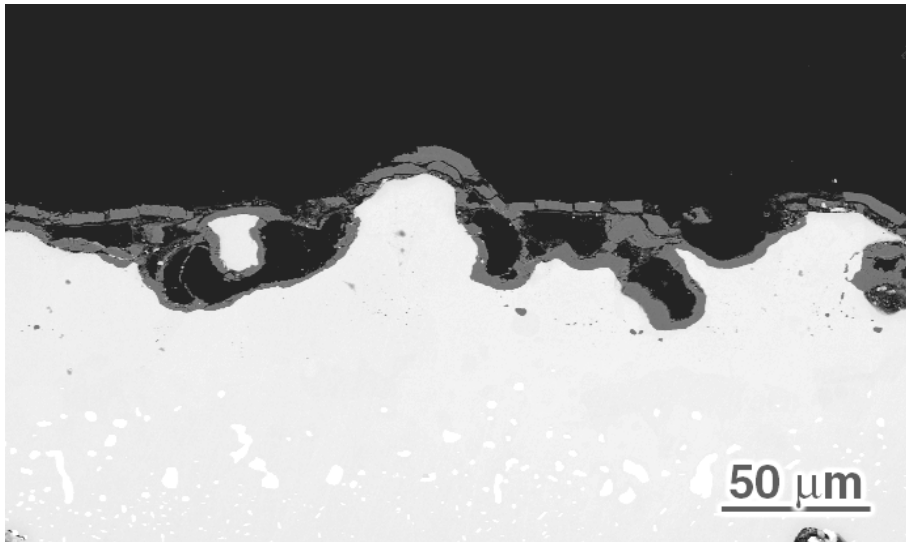


(b)

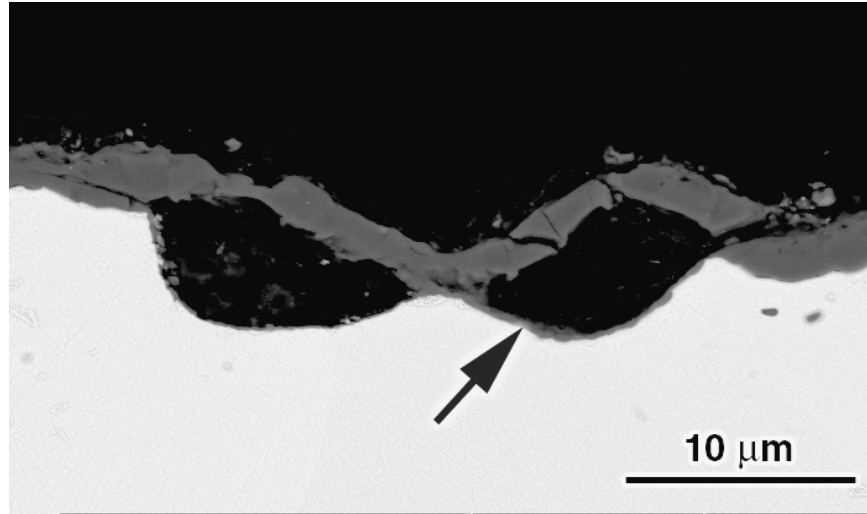
Figure 19 Scanning electron micrographs from the surface of the Pt aluminide bond coat, which was exposed at 1200°C for 15 hours, showing the cracks that developed due to volume reduction following the phase transformation from metastable to stable alumina, (a), and the oxide ridges developing at these cracks, (b).



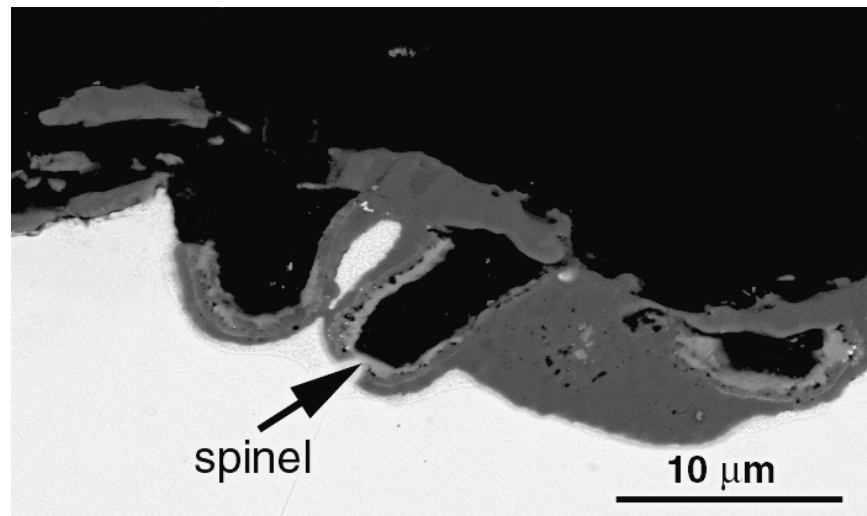
(a)



(b)



(c)



(d)

Figure 20 a) Scanning electron micrograph from the surface of the Pt-Aluminide bond coat, which was highly rumpled after exposure at 1100°C for 955 cycles. Cross sectional scanning electron micrographs showing (b) the large cavities formed at the bond coat/oxide interface after exposure at 1100°C for 3031 cycles. (c) the alumina formed on the surface of the large cavities, (arrow), as a result of oxygen diffusion through the cracks present at the initially formed alumina,(d) the spinel phase formed on the alumina scale in these cavities.

4.2 TBC INVESTIGATIONS

4.2.1 TBC Failure Premises

The specimens with TBCs were tested until a significant amount of TBC spallation was observed on the surfaces. Some of the specimens were also examined prior to failure. After a detailed examination of these specimens, various defects have been identified. Cracks were observed to initiate in the vicinity of most of these defects and then they propagated through the weak points in the system. The cracks either propagated separately or coalesced with others forming larger cracks. Failure eventually occurred when these cracks reached a critical size.

All of the defects that were identified in this study, are believed to contribute to the failure of these TBC systems. However, none of these defects were observed to cause failure by themselves unless they were very pronounced. The failure was usually a result of combination of weaknesses in the vicinity of several of these defects as well as other factors such as the stored strain energy and/or poor interfacial toughness.

The strain energy accumulates in the TGO with exposure as a result of growth and thermal stresses that develop during oxidation. This energy, which is referred to as “stored strain energy in the TGO”, is a strong function of TGO thickness and residual stresses in the TGO. The systems usually want to relieve this energy by separation along the TGO/bond coat interface since maximum strain energy is relieved this way. Thus, the TGO/bond coat interface becomes more susceptible to fracture with exposure time and it is expected to have more failure along the TGO/bond coat interface with longer exposure times unless there are weaker points elsewhere in the system. The plot of logarithms of the reciprocal of the failure times versus reciprocal of

temperature for the state of the art TBC systems with NiCoCrAlY and Pt Aluminide bond coats (Figure 21) shows a decrease of failure times of these systems by about an order of magnitude with 100 °C increase in exposure temperature. An Arrhenius relationship is followed with an activation energy of 356 kJ/mole which is close to that obtained from the parabolic rate constants for the growth of α -alumina scales on Pt-Al alloys [36]. These results suggest the role of TGO growth rate and accordingly, the stored strain energy in the TGO on the failure of these systems. However, relatively thick TGOs could be attained by minimizing the defects in these systems by various modifications. The data points of the failure times for some of these modified systems at 1100°C are also shown in Figure 21. It is believed that the defects were the crack initiation sites and the stored energy in the TGO was the driving force for the propagation of failure. Thus, the systems could withstand larger strain energies in the presence of fewer defects.

The stored energy in the TBC is usually considered negligible due to the open and porous structure of the YSZ. However, it has been observed that a relatively dense TBC can develop depending on the surface condition and/or the TBC deposition conditions. There is also the sintering factor, which results in densification in the TBC. In these situations, the stored energy in the TBC can also become a contributing factor in the failure. Separations can occur along or close to the TGO/TBC interface to release this energy (Figure 22a) or cracks that initiated elsewhere in the system can propagate in the dense TBC (Figure 22b).

Interfacial toughness is another property that is important for the failure of these TBC systems. Some of the improvements obtained by various modifications are believed to be a result of increased interfacial toughness, as will be shown later.

The mechanical properties of the constituents of the TBC systems, especially the strength of the bond coat, have a big influence on the failure behavior of these systems. It is believed that

having a stronger bond coat, which does not plastically deform during exposure, may improve the lives to some extent. However, it will also be shown that the TBC usually constrains the deformation of the bond coat as long as it is in good contact with the bond coat and free of defects which may result in areas of weaknesses in the TBC. Thus, under these conditions the strength of the bond coat may not be so critical.

A simple schematic summarizing the preceding discussion on TBC failures is given in Figure 23. In the following section, the defects in TBC systems will be described in general regardless of the system, followed by the failure characteristics of these TBC systems where the defects specific to each system will be given.

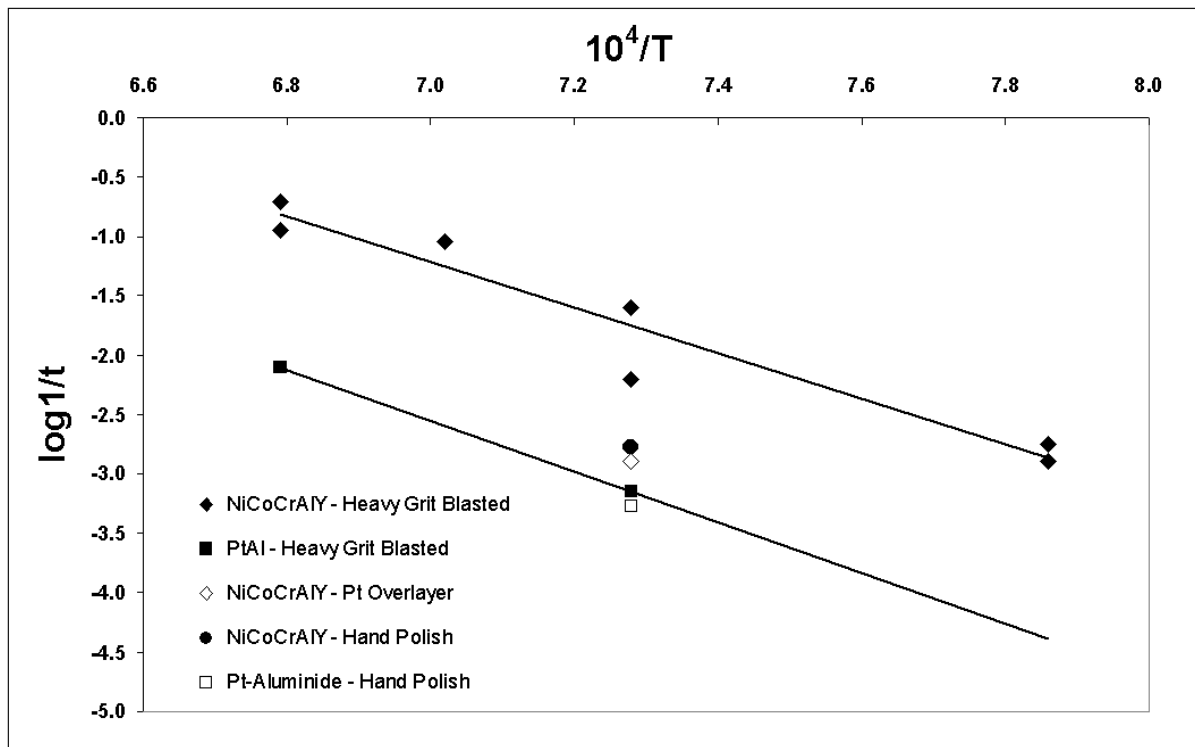
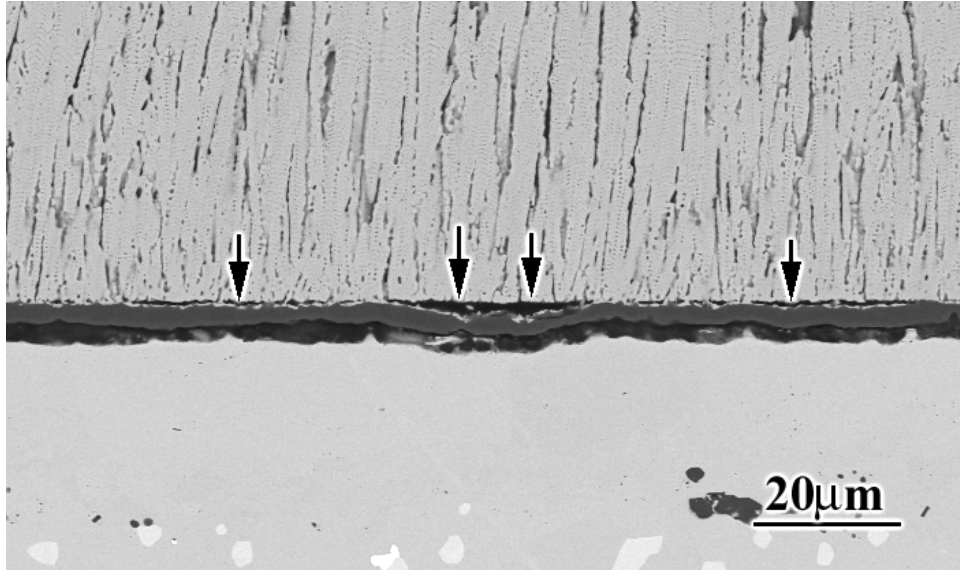
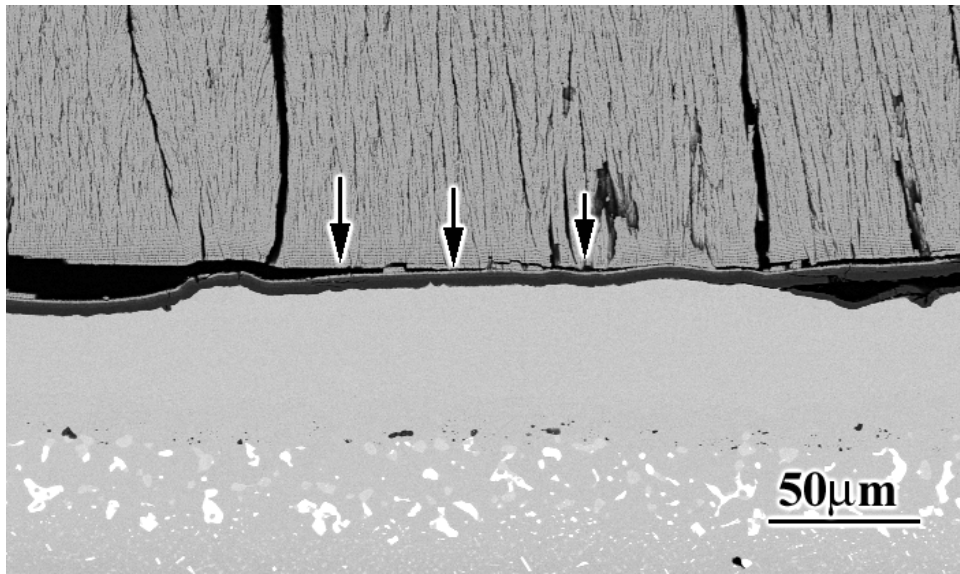


Figure 21 The plot of inverse of the failure times (t) versus reciprocal temperature (T) for the state of the art TBC systems with NiCoCrAlY and Pt aluminide bond coats.



(a)



(b)

Figure 22 Scanning electron micrographs showing that dense TBCs can be a source of crack initiation (a) and / or propagation sites (b), probably due to relatively high stored energy in the TBC.

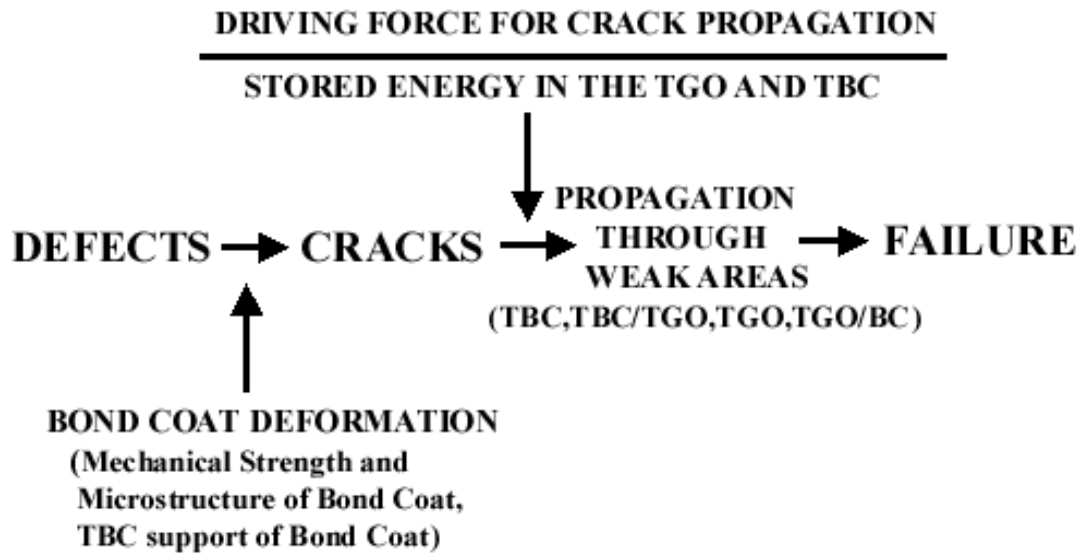


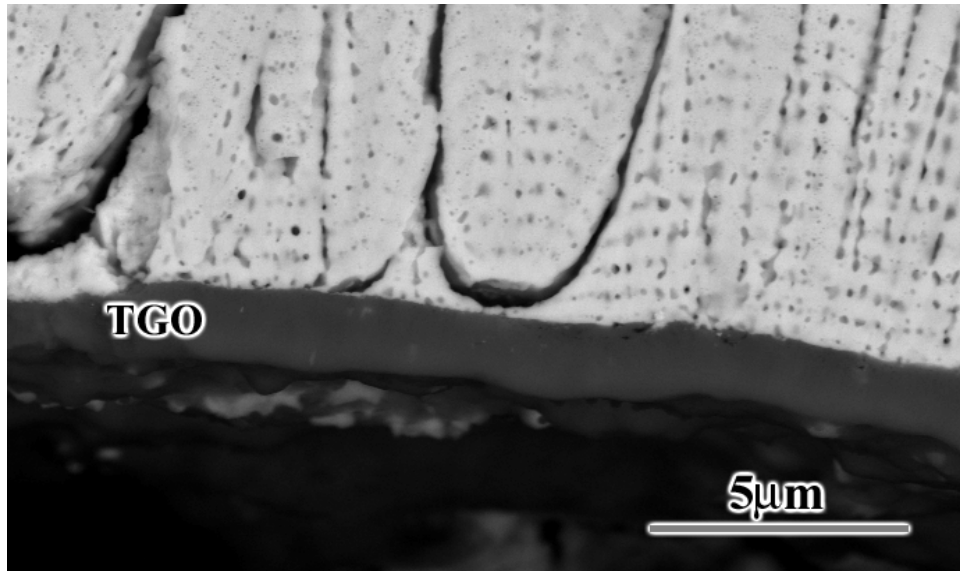
Figure 23 Schematic diagram summarizing the TBC failures based on experimental results.

4.2.2 Defects in TBC systems

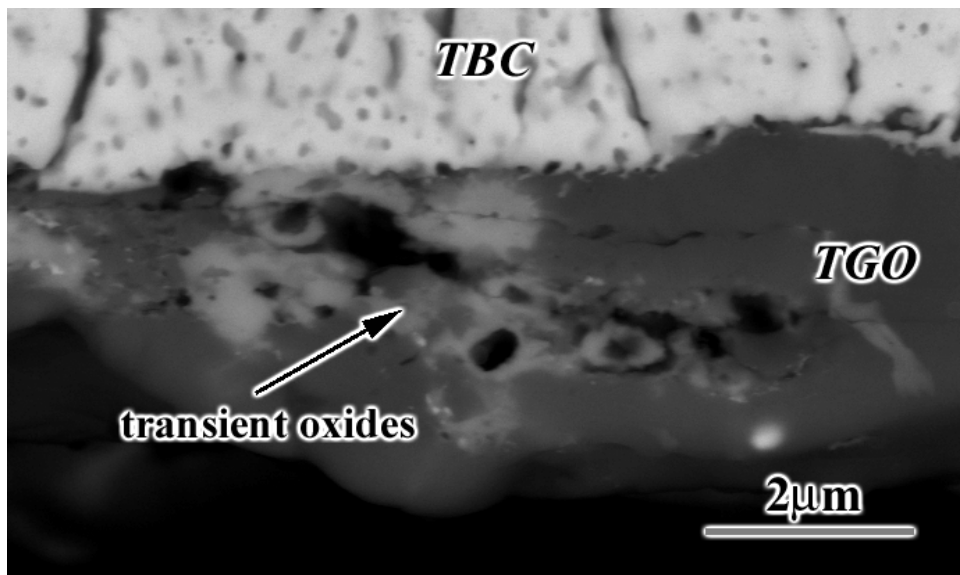
4.2.2.1 Transient Oxides When the TGO is pure alumina, it usually forms as a dense and continuous layer as in Figure 24a. However, when oxides other than alumina are present (e.g. Cr_2O_3 , NiAl_2O_4), the TGO is porous and non-uniform (Figure 24b). Moreover, the adherence between the transient oxides and the TBC, as well as the alumina, seems to be weaker (Figures 25a and 25b, respectively) compared to adherence between the alumina and the TBC. The arrow in Figure 25c points to a part of a TGO where it is pure alumina and in good contact with the TBC, in contrast to the neighboring parts with significant amounts of transient oxides. It has also been observed that the thickness of the transient oxide is important for adherence. The interface between the transient oxide and the TBC seemed to become weaker as the thickness of the transient oxide increased. The arrow in Figure 25d points to a relatively thin transient oxide,

which appears to have a better bond to the TBC, compared to the other areas with thicker transient oxides.

Formation of oxides other than alumina results in extra interfaces. Every interface can be a source of weakness in these TBC systems, especially if there is a CTE (coefficient of thermal expansion) difference between the layers, which may be the source of poor adherence in the presence of transient oxides in these systems. The porous and non-uniform morphology also makes them susceptible sites for crack initiation since the stress is concentrated in their vicinity.

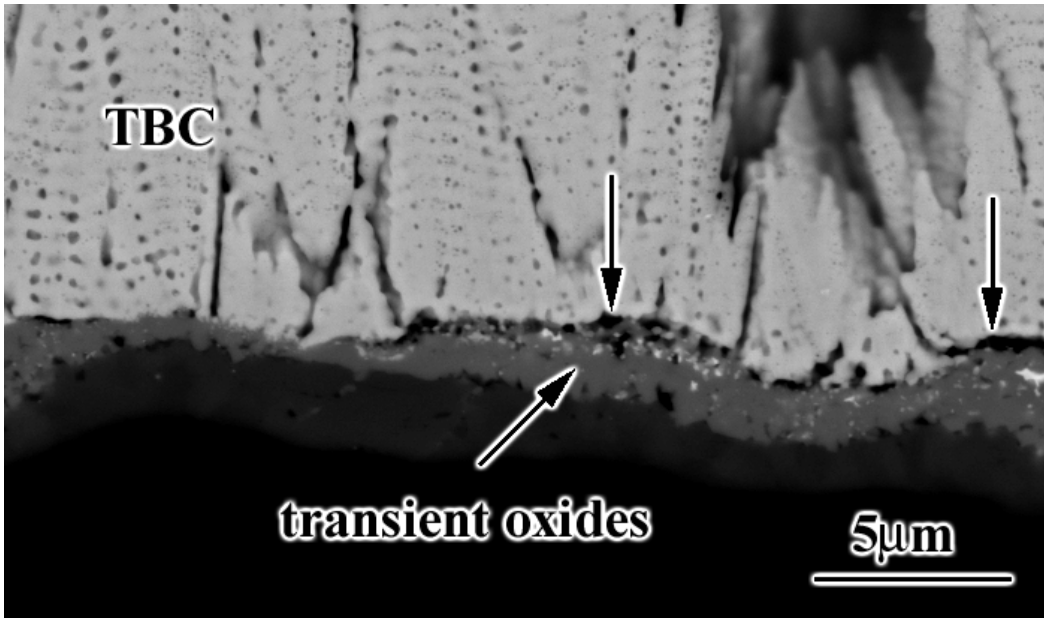


(a)

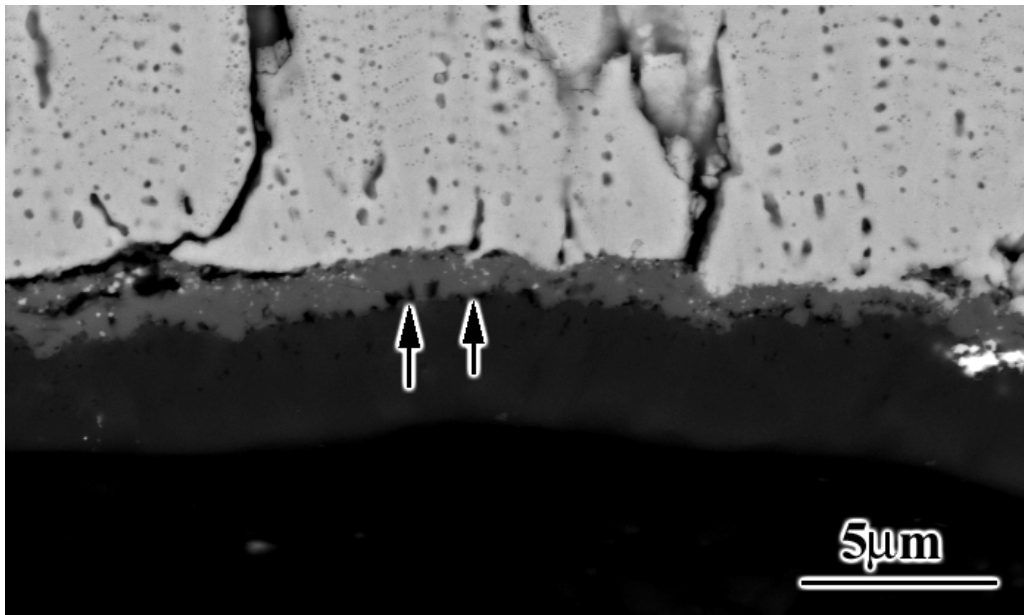


(b)

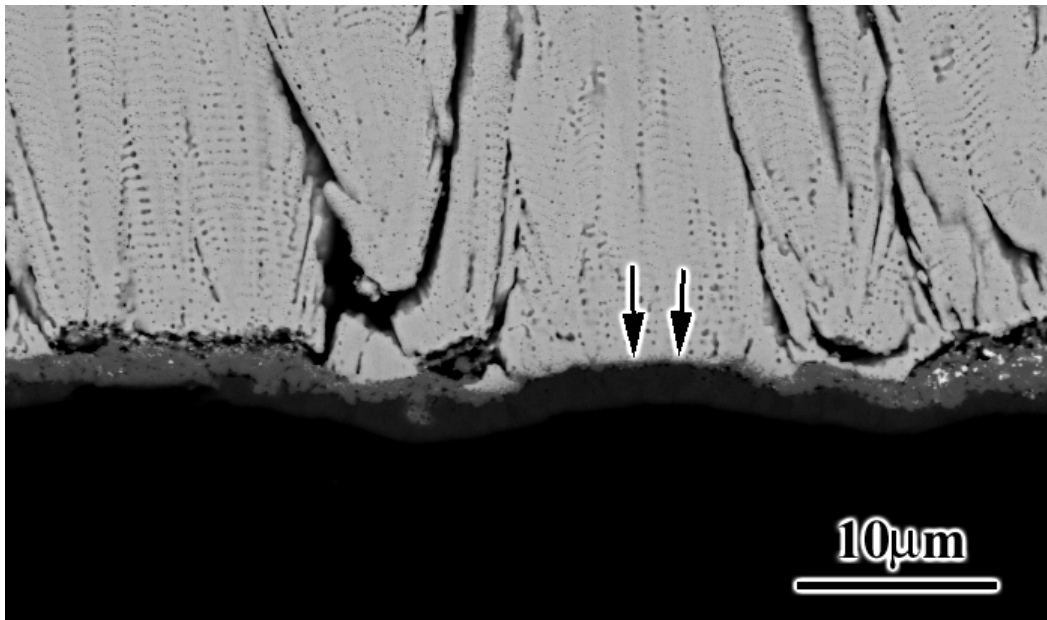
Figure 24 Scanning electron micrographs showing the presence of a dense and uniform TGO when it is pure alumina, (a), and the porous and non uniform TGO when oxides other than alumina are present, (b).



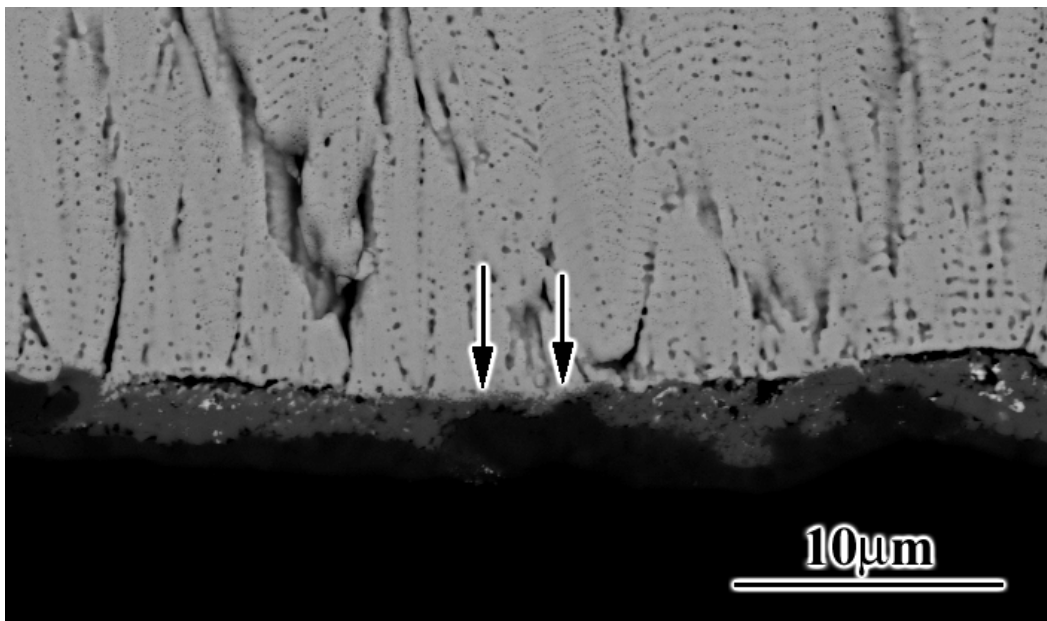
(a)



(b)



(c)



(d)

Figure 25 Scanning electron micrographs showing the poor adherence between the transient oxides and the TBC, arrow in (a), as well as between the transient oxides and the alumina, arrow in (b). The adherence between the TBC and the TGO is stronger when it is pure alumina, arrow in (c) and also when the transient oxide is relatively thin, arrow in (d).

4.2.2.2 TBC defects Various defects can be present in the TBC depending on the surface condition of the bond coat, as well as the TBC deposition conditions. Some of these defects which were identified in this study are :

- **regions of separation in the TBC** - This is a very general classification which refers to any kind of discontinuities in the TBC, especially close to the TGO/TBC interface. These type of defects can act as stress concentration sites in the TBC where cracks can nucleate (Figure 26). Corn Kernel defects are specific cases of regions of separation in the TBC which appear as conical shaped TBC segments close to the TGO (Figure 27) These conical shaped TBC segments are poorly bonded to the rest of the TBC, resulting in the development of points of weakness in the TBC.

Depending on the surface condition and/or TBC deposition conditions, regions of separation in the TBC can form so frequently that weaknesses, which are continuous over relatively long distances, develop in the TBC in the vicinity of these defects (Figure 28a) The failure can easily initiate and/or propagate in the vicinity of these defects (Figure 28b) In this case, the development of these defects seems to be a function of an initially very irregular interface. Figure 28c shows failure propagating along these weak points until a stronger TGO/TBC interface, which lacks these TBC defects, has been encountered. The failure, then, changed its direction towards the TGO/bond coat interface.

Figure 29a is another example showing similar TBC defects with a much finer scale, which developed on a smoother interface. Closer examination of this interface showed a significant amount of very small conical shaped TBC segments that seemed to be poorly bonded to the rest of the TBC. The TBC deposition conditions are believed to result in such a

morphology. This specimen also had a significant amount of failure along this weak interface as can be seen from the fracture surface as well as cross sectional micrographs given in Figures 29b and 29c.

- **vertical separations** - These defects usually form on initially irregular surfaces. Due to shadowing effects during TBC deposition, small openings develop between the columns above the surface irregularities (Figure 30a). Upon exposure at high temperatures, these openings can enlarge resulting in the formation of so called “vertical separations” (Figure 30b) The sintering between the columns, which are already in contact, as well as the sintering within columns appear to be responsible for the enlargement of the openings that were already present between the columns in the as-processed condition.

The reasons that lead to formation of vertical separations for some systems but not for the others with similar initial surface roughness have been investigated and it has been found that the TBC morphology also plays a role in their formation. The TBCs that did not develop vertical separations, had well defined, dense and relatively larger columns in the as-processed condition (Figure 31a) compared to the ones that developed vertical separations (Figure 31b). On the other hand, the column width increased with distance away from the interface. Figures 32a through 32c show high magnification micrographs from areas close to the interface, middle and then the top of the TBC, respectively. For systems which developed vertical separations, the column width did not change much with distance away from the interface as can be seen from Figures 33a through 33c. The widening of the columns away from the interface seems to fill in the gaps preventing the formation of openings that go all the way through the TBC in the as-processed condition as observed for the TBCs that developed vertical separations (Figure 30a)

The marked difference in the morphology of these TBCs can also be seen by comparing the top views of the TBCs. Figure 34a and Figure 34b show the TBCs in the as-processed condition for the specimens which developed vertical separations and which did not, respectively. The columns that had a fine morphology sintered during exposure whereas the ones with denser columns remained almost the same (Figures 34c and 34d respectively). This is believed to be one of the reasons which leads to formation of vertical separations for the TBCs with a finer structure. The already present openings enlarge as the columns get sintered with exposure. The vertical separations being more well developed with exposure at higher temperatures (compare Figures 35a and 35b after exposure at 1000°C and 1150°C, respectively) is also consistent with sintering being an important factor for their formation.

These vertical separations may also contribute to the failure of TBC systems by acting as crack initiation sites (Figures 36a and 36b) The importance of these vertical separations on the failure was also explained by Evans [52]. However, it is also worth mentioning that long lives were obtained despite a large number of vertical separations for some TBC systems (Figure 37) which shows that the presence of these defects alone is not sufficient to cause failure of these systems. More work is required to better define the role of these defects on the failure of TBC systems.

- **spits** - This is another type of TBC defect that may form during TBC processing (Figure 38a). In some cases, cracks have been observed to initiate in the vicinity of these spits as in Figure 38b.

- **holes in the TBC** - These defects were observed during examination of the top surface of some TBCs. However, they could not be observed by cross sectional examination. Accordingly, the depth of these holes is not known. Observation of the top surfaces of the TBCs with this type

of defect almost always showed cracks passing through the holes as in Figure 39. These observations may suggest the role of these defects also as crack initiation and/or propagation sites.

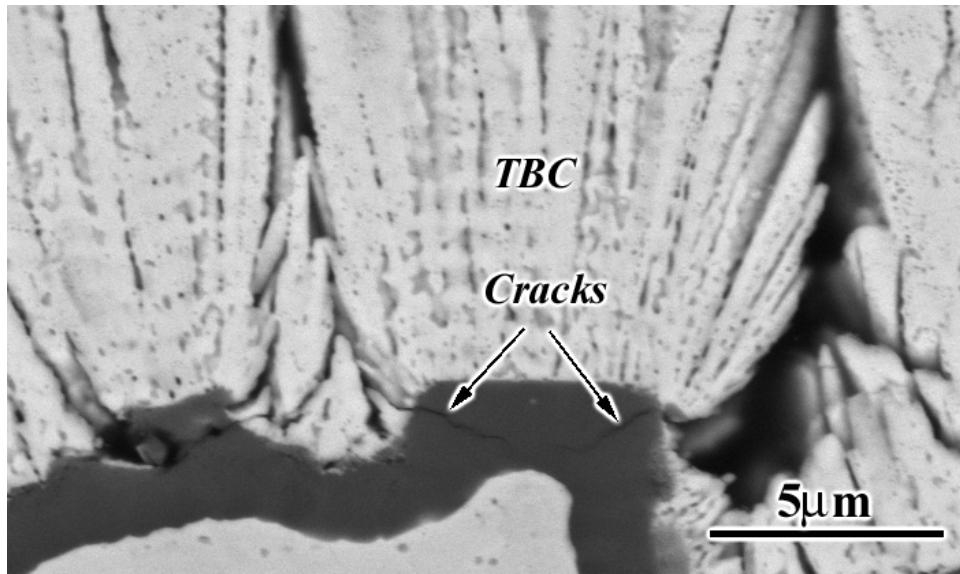


Figure 26 Scanning electron micrograph showing cracks initiated in the vicinity of defects, which were referred to as “points of separation in the TBC”.

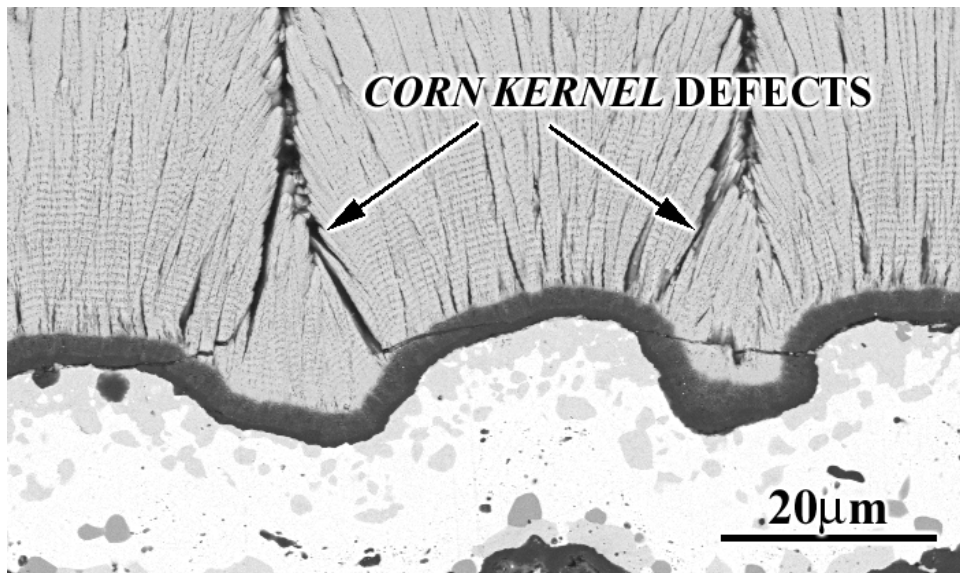
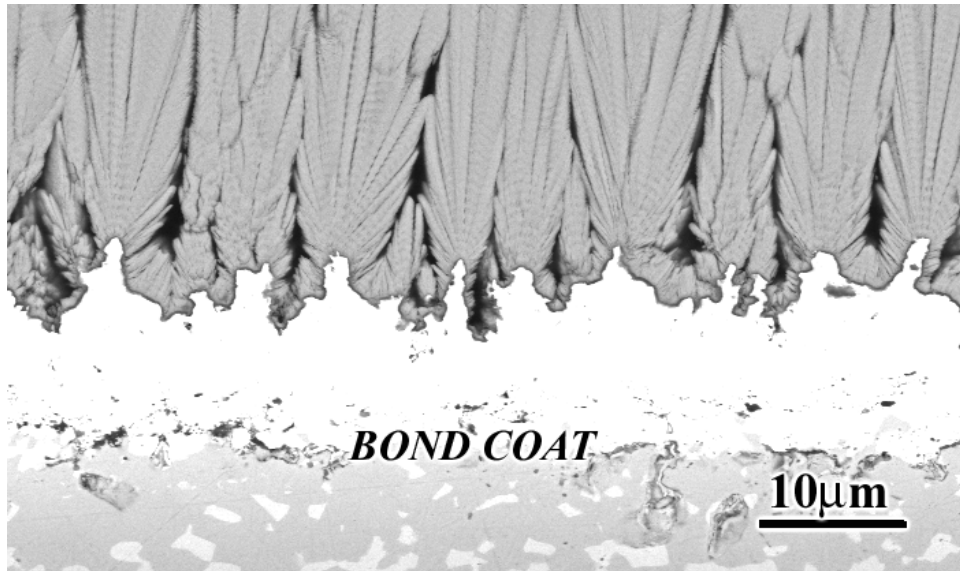
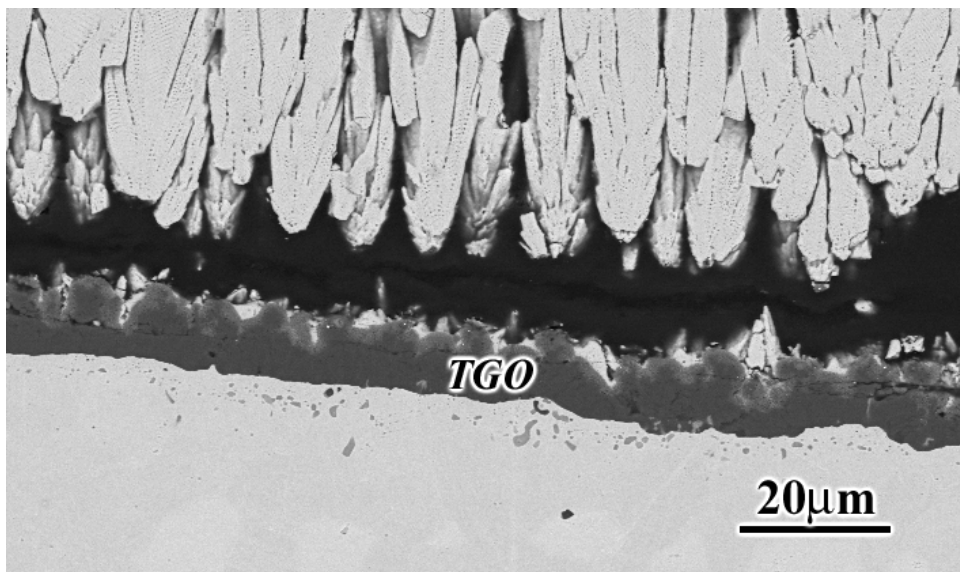


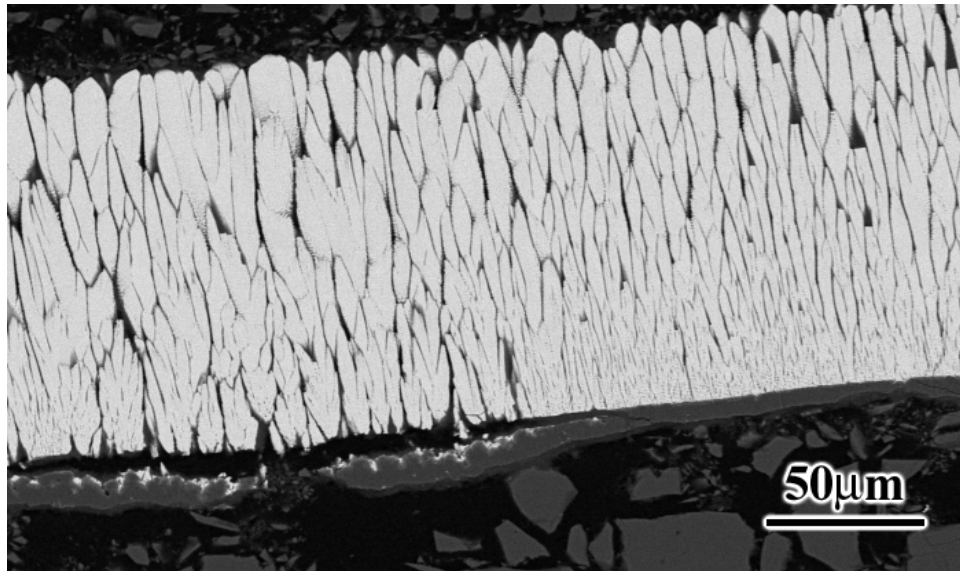
Figure 27 Scanning electron micrograph showing a corn kernel type of defect in the TBC.



(a)

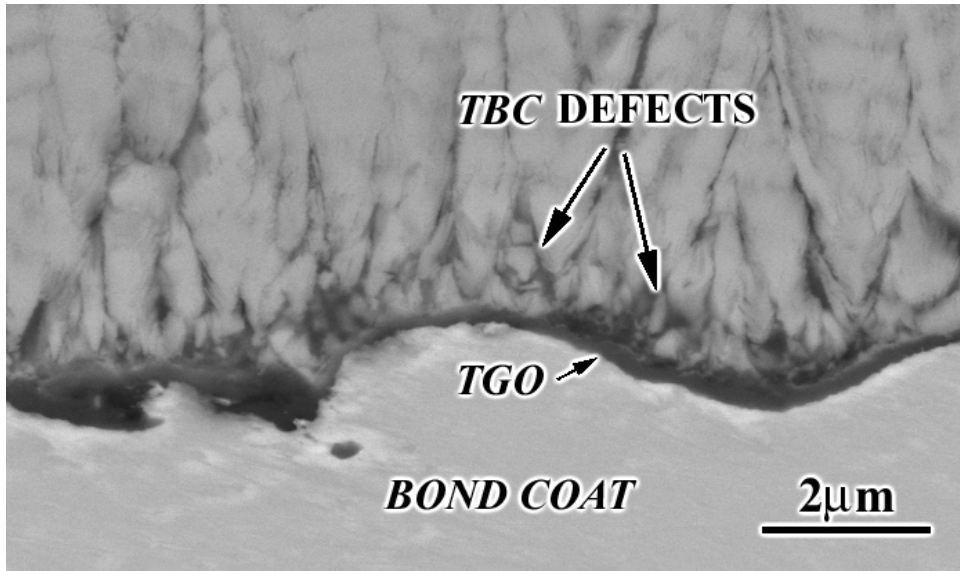


(b)

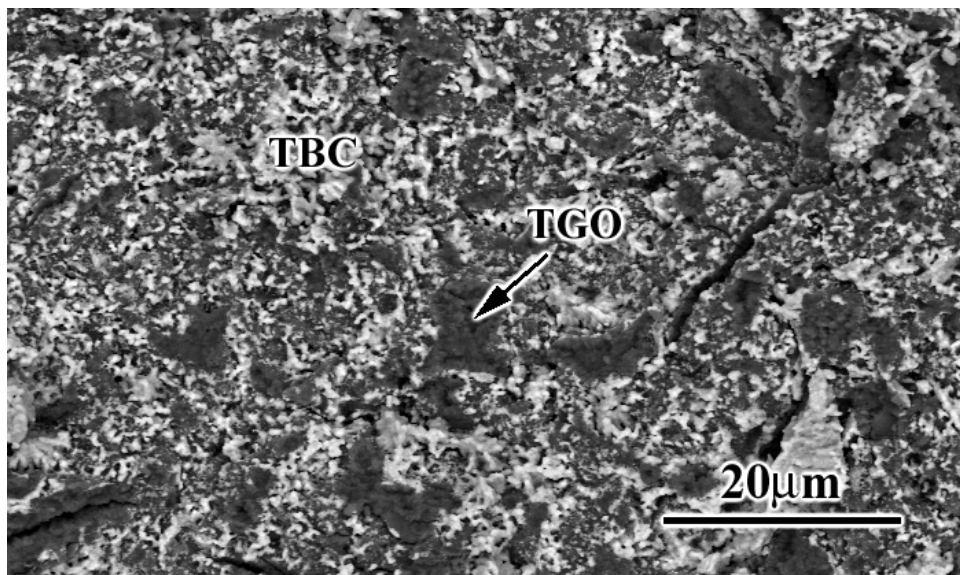


(c)

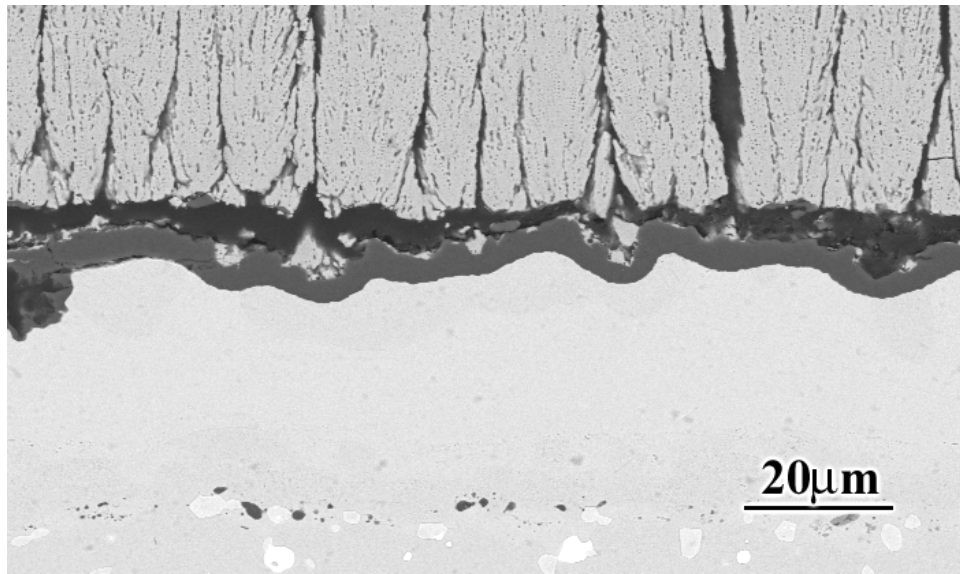
Figure 28 Scanning electron micrographs of a specimen with many TBC defects, which were referred to as “points of separation in the TBC”, in the as processed condition, (a), and after the failure, (b) and (c).



(a)

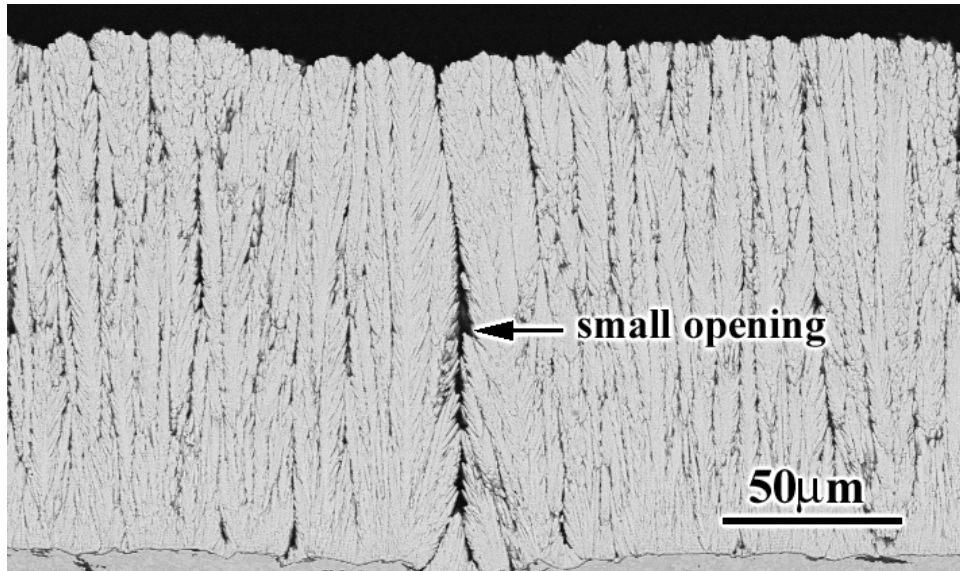


(b)

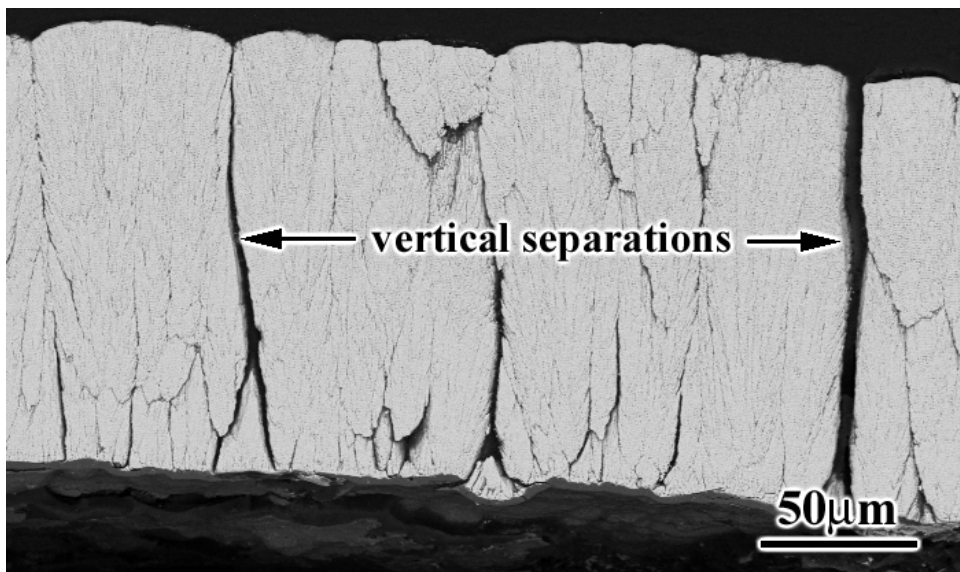


(c)

Figure 29 Scanning electron micrograph showing another example to “points of separation in the TBC” in the as processed condition (a). The failure propagated mainly in the TBC in the vicinity of these defects as can be seen from the fracture surface (b), and the cross section (c) of the failed specimens.

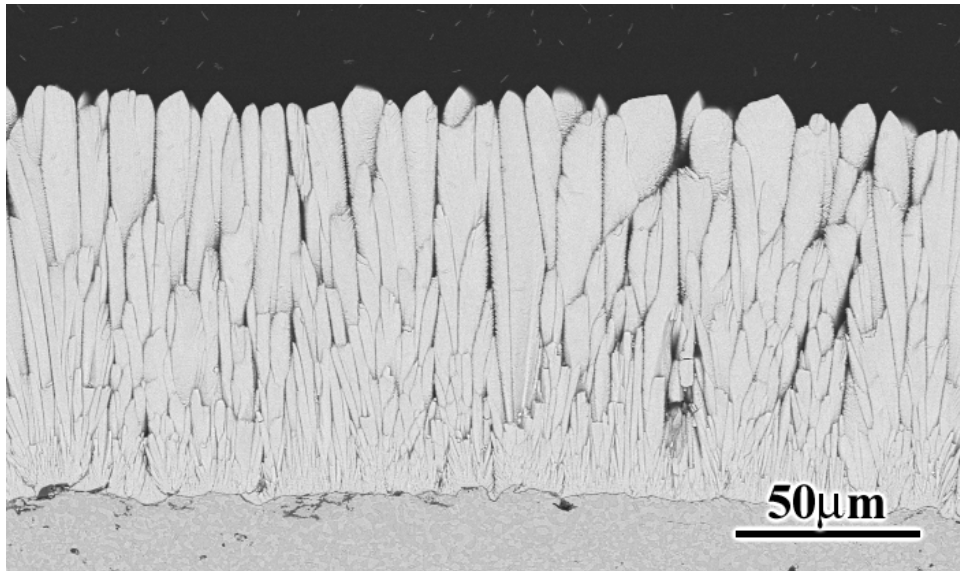


(a)

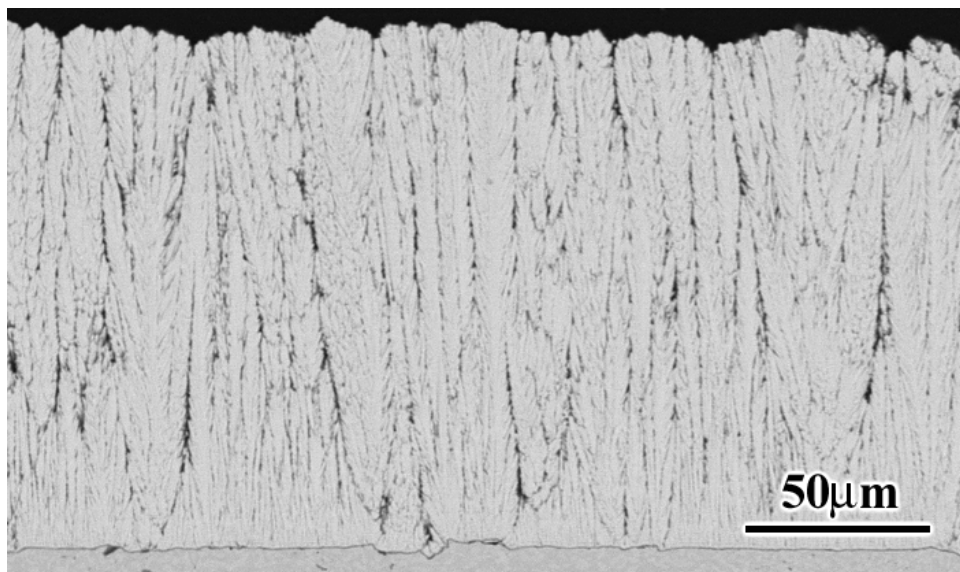


(b)

Figure 30 Scanning electron micrograph of a specimen with small openings in the TBC in the as processed condition, (a). These openings enlarged with exposure resulting in the formation of so-called “vertical separations” in the TBC, (b).

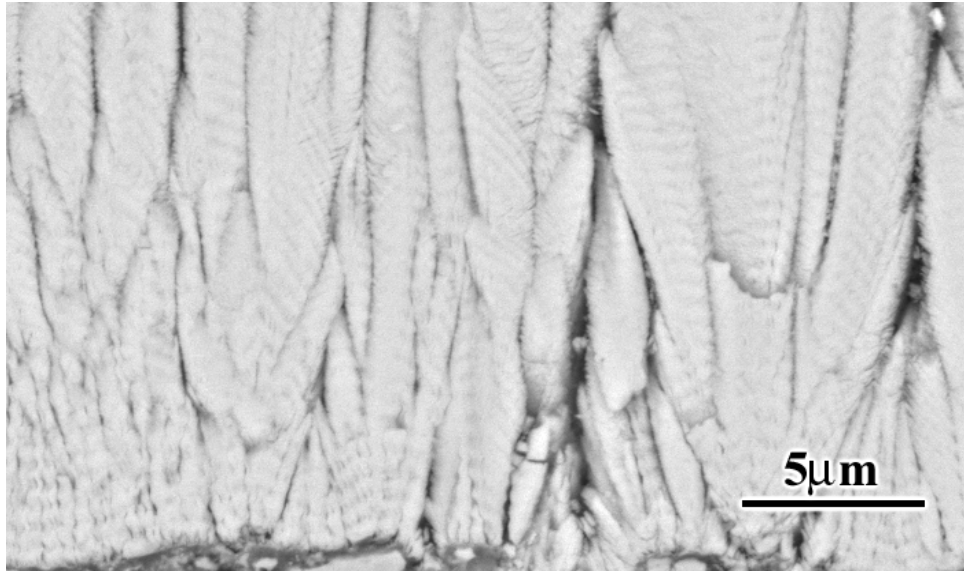


(a)

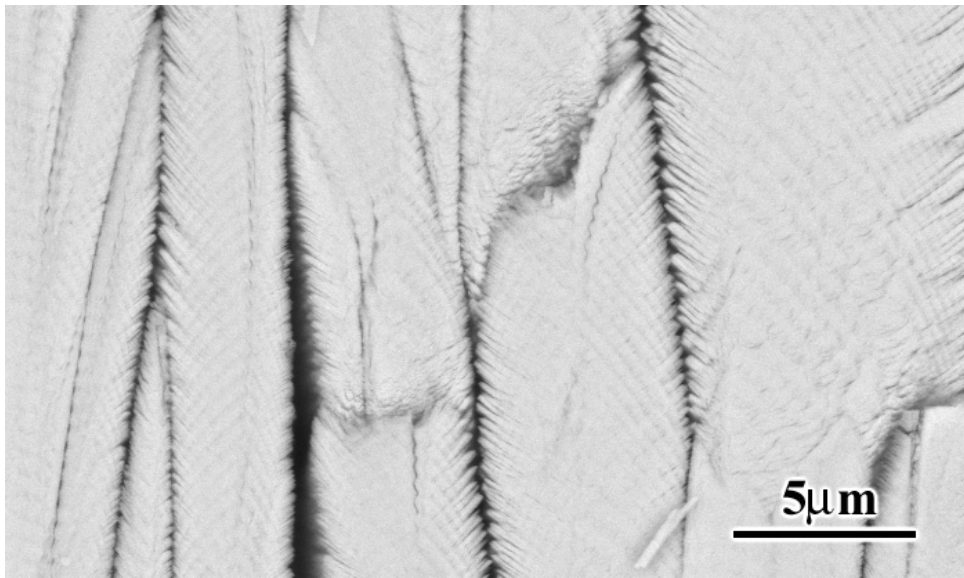


(b)

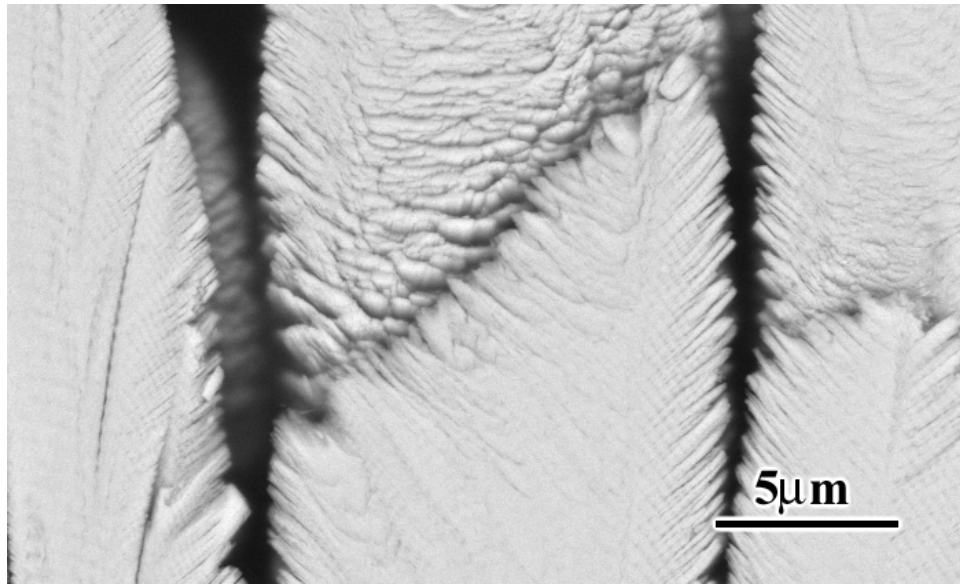
Figure 31 Scanning electron micrographs showing the morphology of the TBC in the as-processed condition for the specimens that did not (a) and that did develop vertical separations in the TBC with exposure (b).



(a)

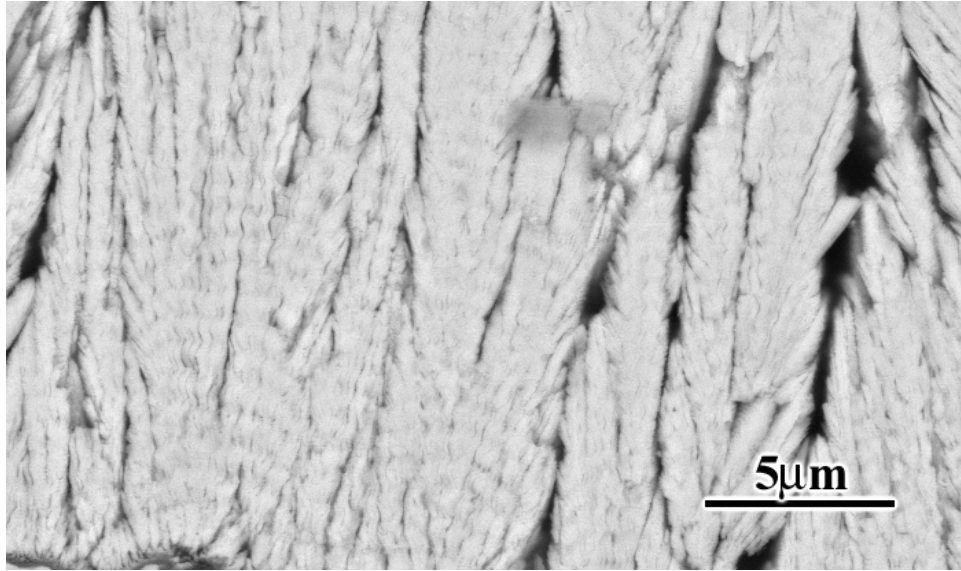


(b)

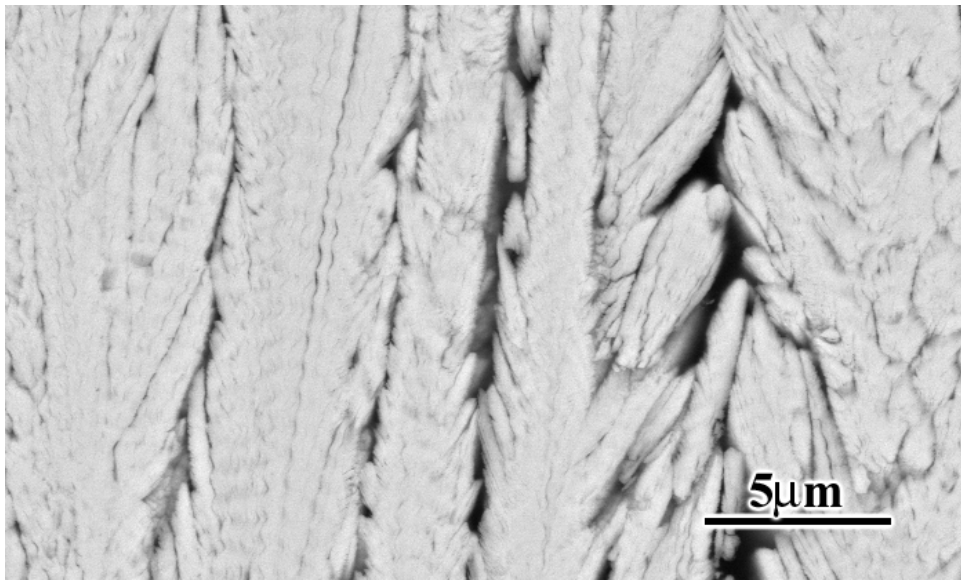


(c)

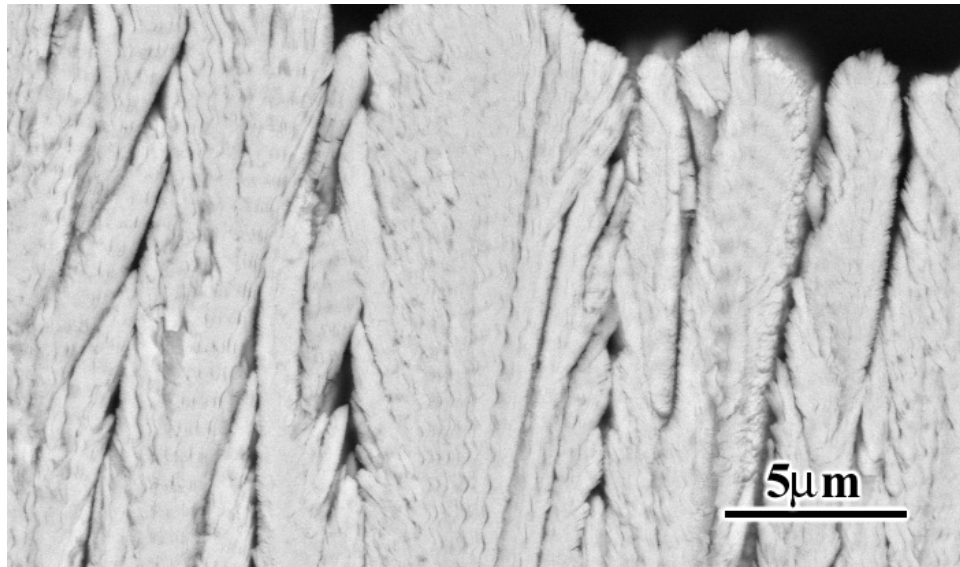
Figure 32 High magnification scanning electron micrographs from areas (a) close to the interface, (b) middle and (c) the top of the TBC of an as processed TBC system which did not develop vertical separations in the TBC.



(a)

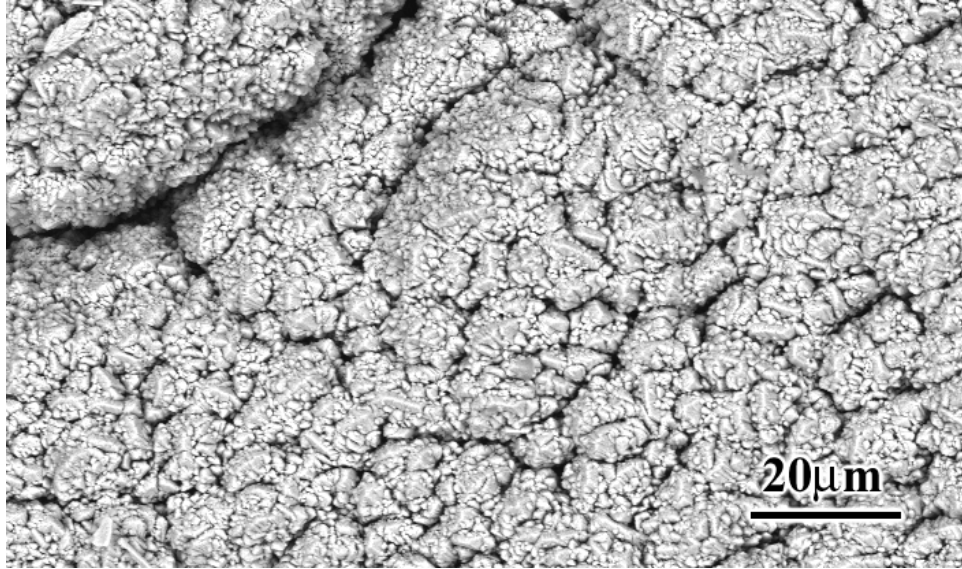


(b)



(c)

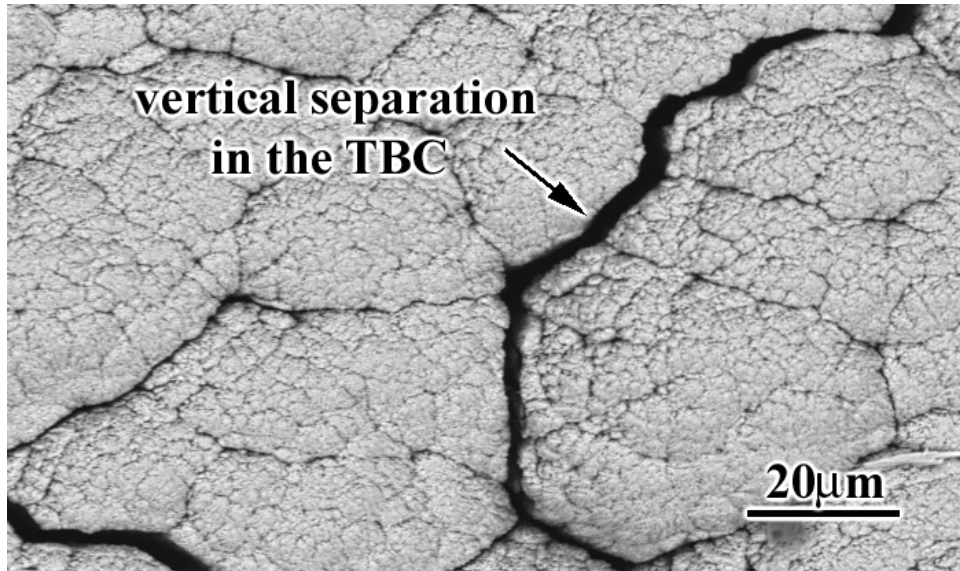
Figure 33 High magnification micrographs from areas (a) close to the interface, (b) middle and (c) the top of the TBC of an as processed TBC system which developed vertical separations in the TBC.



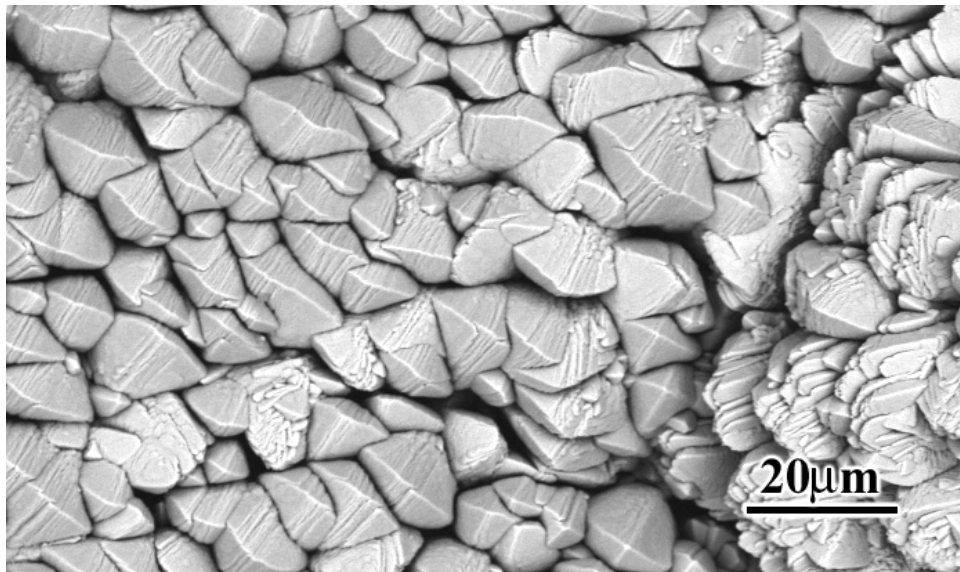
(a)



(b)

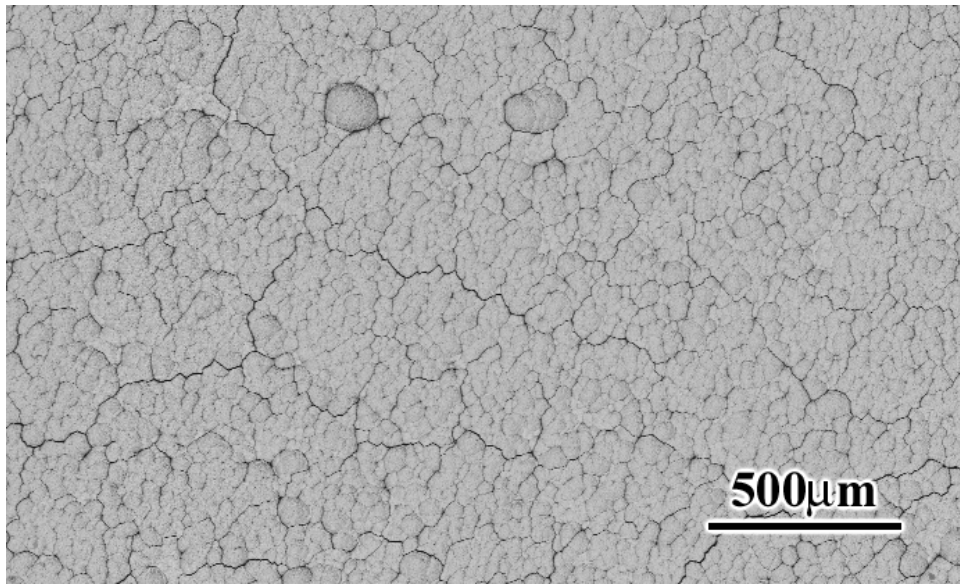


(c)

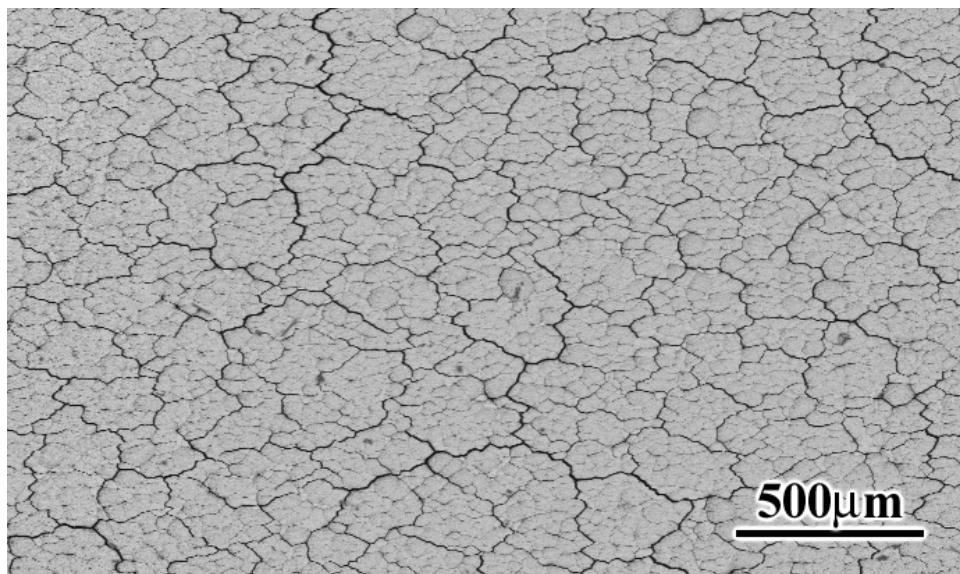


(d)

Figure 34 Top views of TBCs in the as-processed condition for the specimens (a) which developed vertical separations in the TBC and (b) which did not. The columns in (a), which had a fine morphology, got sintered during exposure resulting in the formation of vertical separations (c), whereas the denser columns, (b), remained almost the same (d).

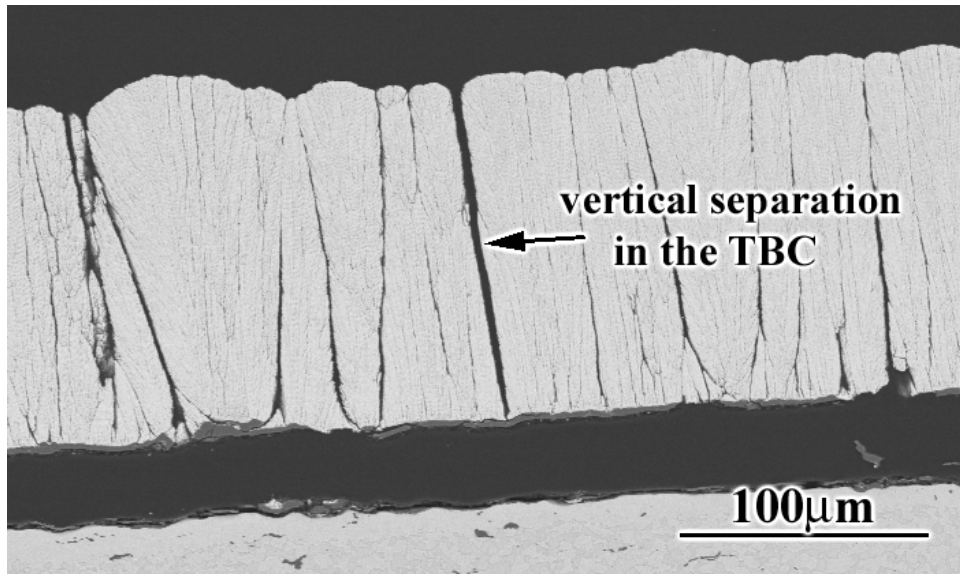


(a)

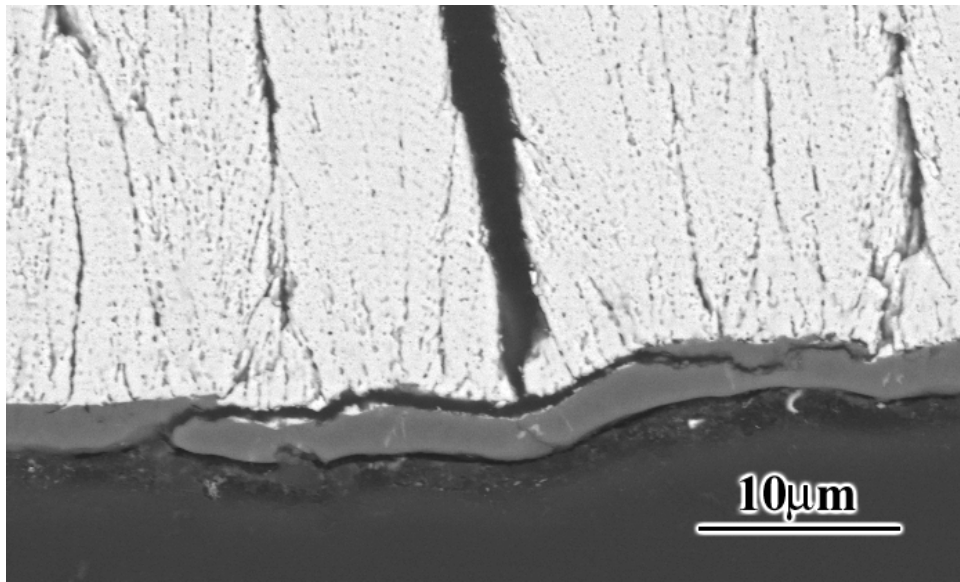


(b)

Figure 35 Top views of TBCs for specimens that developed vertical separations after exposure at (a) 1000°C for 780 cycles and (b) 1150°C for 15 cycles. The vertical separations were more well developed after exposure at 1150°C.



(a)



(b)

Figure 36 Cross sectional micrographs showing vertical separations and cracks in their vicinity at (a) low and (b) high magnifications.

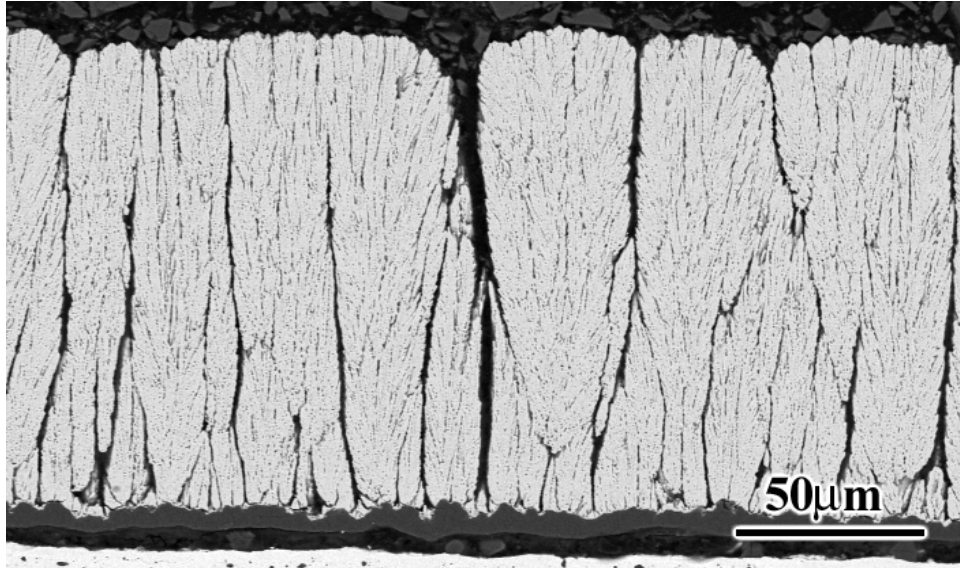
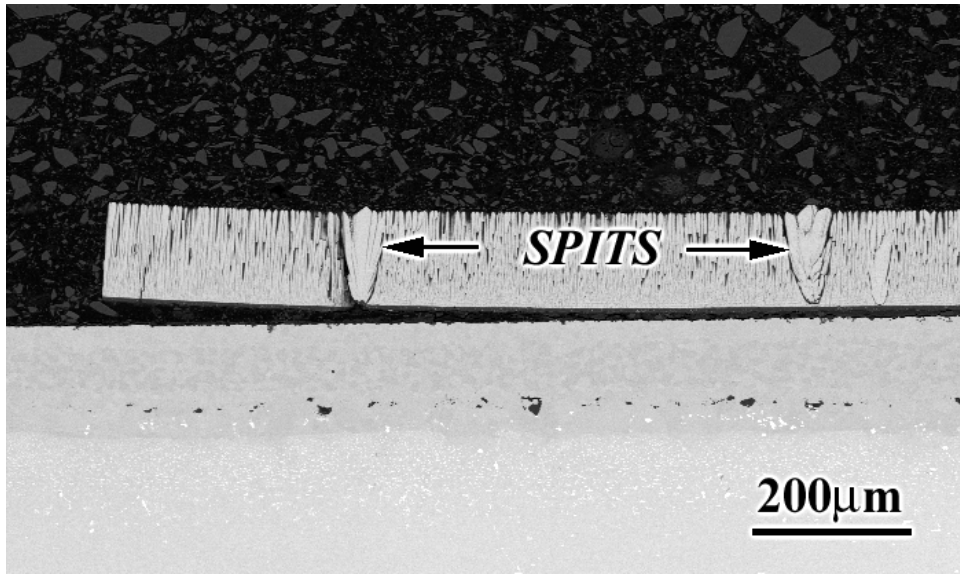
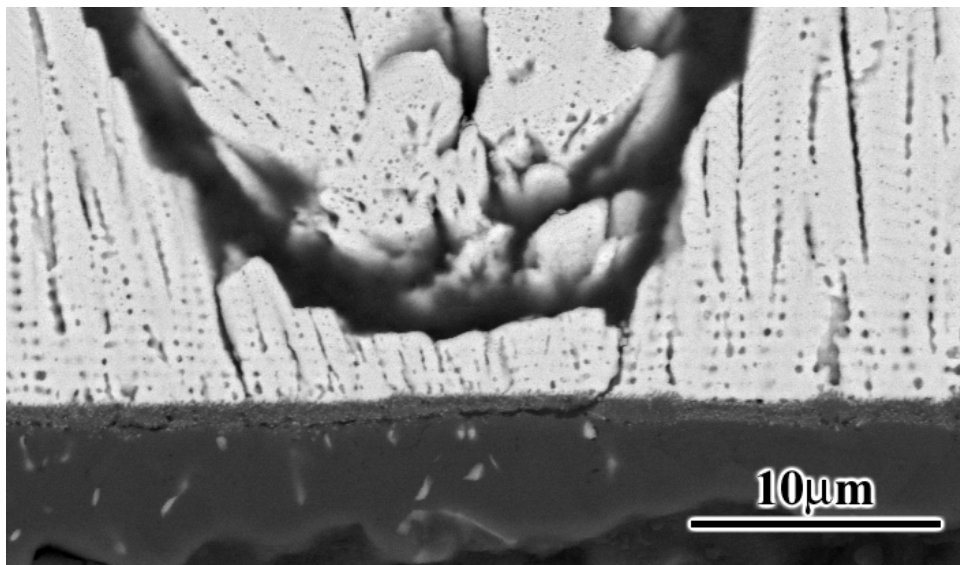


Figure 37 Scanning electron micrograph showing a large number of vertical separations in a TBC system which had a significantly long life.



(a)



(b)

Figure 38 Scanning electron micrographs showing (a) spits in the TBC and (b) cracks initiating in the vicinity of a spit.

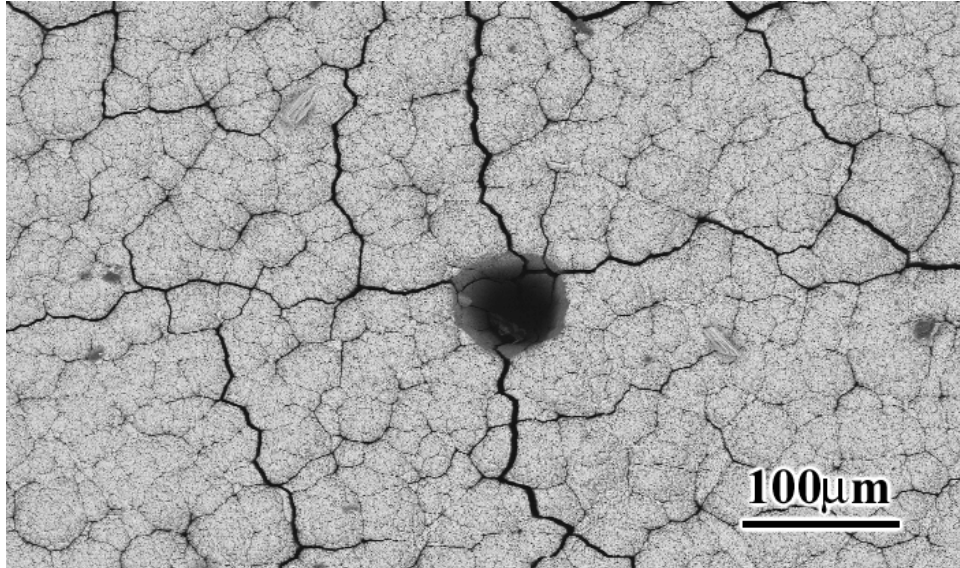
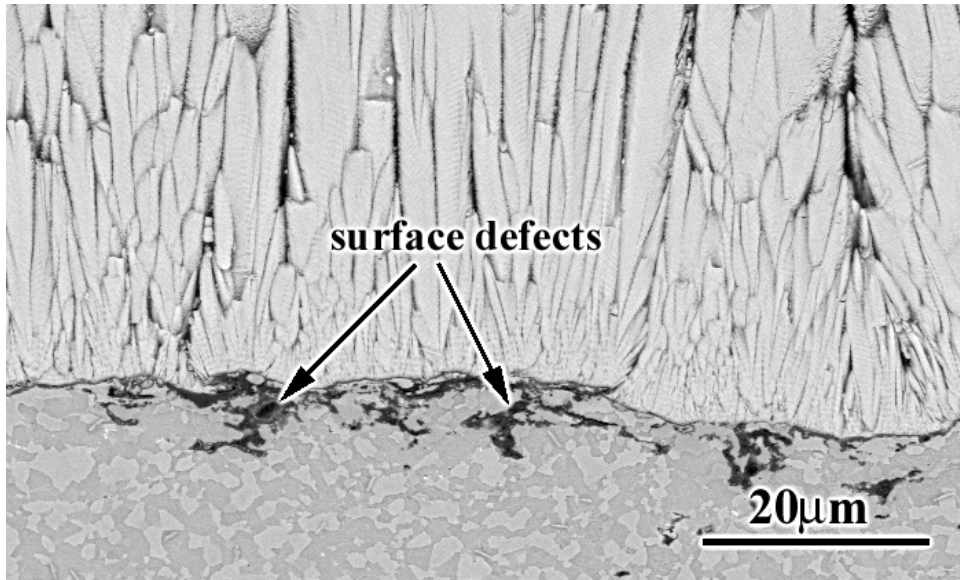


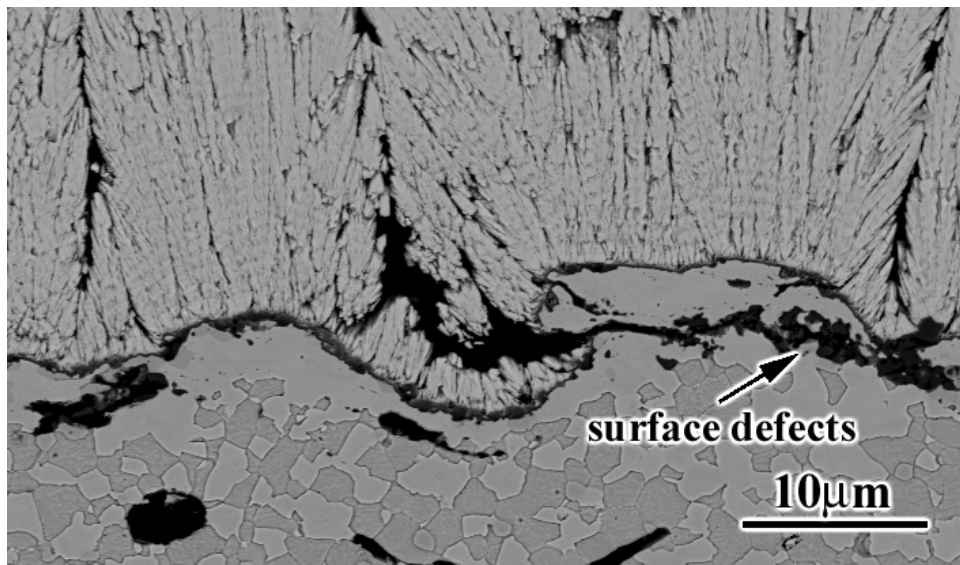
Figure 39 Top view of a TBC showing a hole and cracks passing through it.

4.2.2.3 Surface defects The features that are referred to as surface defects in this study are the embedded grit blast particles and oxide inclusions, that cut the surface at various angles (Figure 40a). These oxide inclusions may have formed by cracking of the bond coat during surface preparation and then oxidation during subsequent heat treatment or TBC deposition. In some areas, the alloy was undercut by these surface defects (Figure 40b), which is believed to cause formation of oxides other than alumina with subsequent exposure.

The presence of oxide particles on the surface makes it more difficult to form an adherent TGO. Figure 41a is from a fracture surface, which was reoxidized after TBC spallation. The arrow points to these oxide inclusions and the discontinuous oxide that formed around these oxide inclusions. In some cases, voids were also observed to develop around these oxide inclusions (Figure 41b)

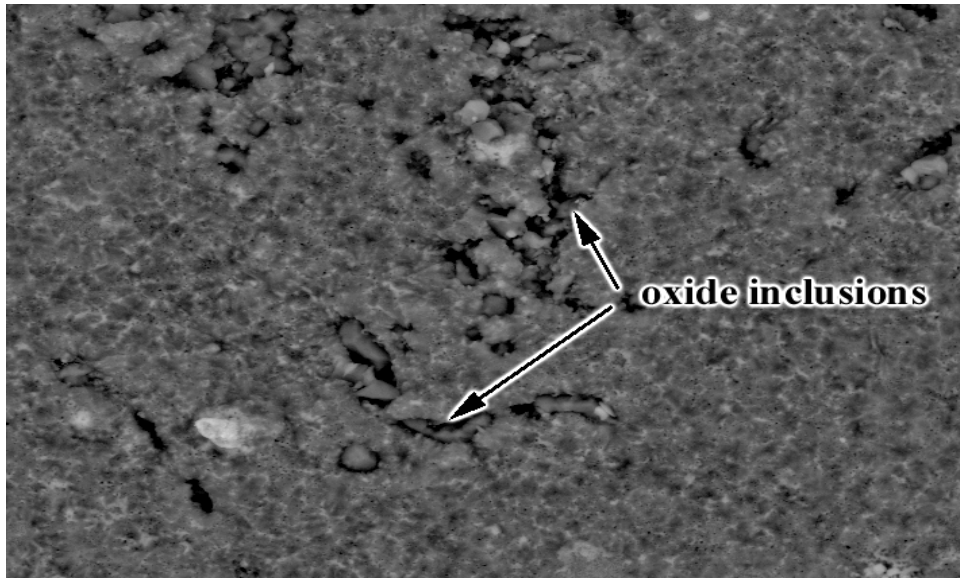


(a)

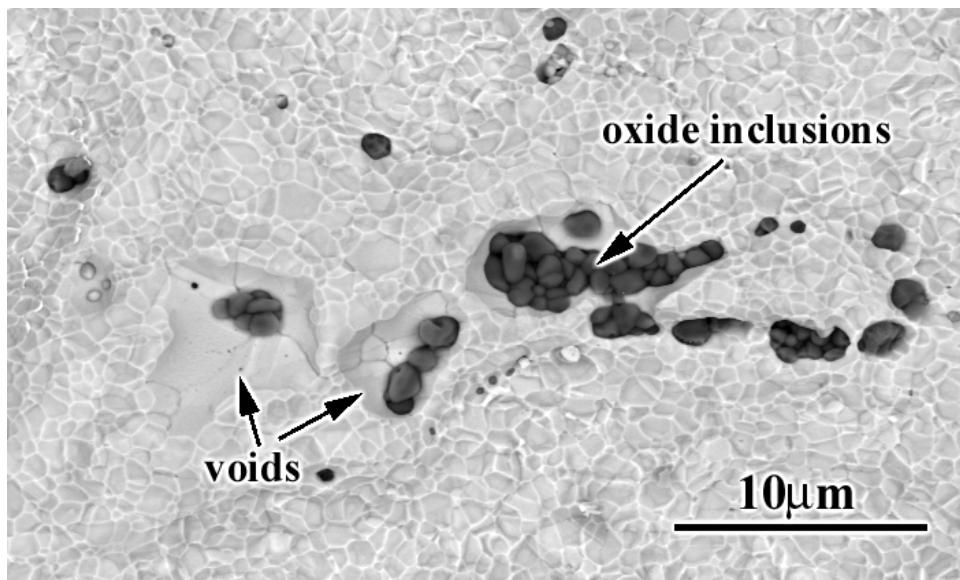


(b)

Figure 40 (a) Scanning electron micrographs showing oxide inclusions that cut the surface at various angles. In some areas, the alloy was undercut by these oxide inclusions, (b).



(a)



(b)

Figure 41 Scanning electron micrographs from the fracture surfaces of specimens with surface defects showing the development of a discontinuous oxide in the vicinity of oxide inclusions, (a) and voids around some of these oxide inclusions , (b).

4.2.2.4 Reactive Element Oxide Protrusions Rapid transport of oxygen through reactive element rich oxides and its reaction with aluminum in the alloy results in formation of stringers of reactive element rich oxides encapsulated in alumina (Figure 42) The amount and distribution of these oxides vary depending on the composition of the alloy and deposition technique, as well as the preoxidation conditions.

When TBC systems with NiCoCrAlY bond coats fail, a significant amount of failure usually propagates along the TGO/bond coat interface, cutting through RE rich oxide protrusions (Figure 43a). Even though clear evidence that suggests crack initiation in the vicinity of these oxide protrusions could not be found, the presence of cracks in the TGO where excessive amounts of these oxide protrusions are present (Figure 43b), is believed to be partly due to stress concentration in the vicinity of these oxide protrusions. The importance of these reactive element rich oxide protrusions for the failure of TBC systems was also discussed by other investigators [31, 32, 51].

Incorporation of these reactive element rich oxides into the TGO is also believed to result in the formation of thick TGOs by acting as fast diffusion paths for oxygen (Figure 44) Therefore, these reactive elements can also contribute to failure this way by increasing the stored strain energy in the TGO, which is a strong function of TGO thickness.

4.2.2.5 Intermixed zone The intermixed zone is usually a mixture of alumina and zirconia plus yttria [70] which forms along the TGO/TBC interface. It may form discontinuously at localized areas (Figure 45a) as well as a uniform continuous layer (Figure 45b) Examination of one set of specimens as a function of exposure time at 1100°C showed that a continuous layer of intermixed zone increased in thickness with exposure time after TBC deposition and it stopped growing after a short amount of time. Figures 46a through 46e show the SEM micrographs from

these specimens in the as-processed condition as well as after exposure at 1100°C for 10, 60, 100 and 880cycles, respectively. The formation of this intermixed zone seems to involve outward transport of Al as proposed by Stiger et al. [70]. Figures 47a and 47b are high magnification micrographs from the fracture surface of a specimen that developed a continuous intermixed zone. As can be seen from these tapered sections from the TGO/TBC interface, the TBC consists of nanosized equiaxed grains as well as porosity close to TGO/TBC interface and the alumina seems to incorporate these grains and porosity by outward diffusion. In some cases, the intermixed zone consisted of whiskers of alumina penetrating into the zirconia (Figure 47c). Metastable aluminas, which are known to grow by outward aluminum diffusion, also have a whisker like morphology, which looks similar to whiskers of alumina observed to penetrate into the TBC for some of these systems. Therefore, it is possible that the intermixed zone in these specimens formed as a result of formation of outward growing metastable aluminas. However, the TEM study of a specific system by Stiger et al. [70] did not show any evidence of metastable aluminas in the intermixed zone. In some specimens, the intermixed zone was observed to consist of zirconia and transient oxides (Figure 47d).

All these results suggest that there may be various ways for the formation of intermixed zones, all of which involve outward diffusion into the TBC. One possibility may be the development of outward growing metastable aluminas as well as transient oxides. Another possibility may be the outward growth component of α -alumina, especially when the TGO is thin.

Table 2 is a summary of the development of this intermixed zone for various TBC systems. Based on these observations, preoxidation, TBC deposition conditions and composition appear to affect the development of the intermixed zone. These effects are believed to be a

consequence of a change in the initial oxidation characteristics. However, there is still a need for more detailed studies on this intermixed zone issue to be able to reach conclusive results.

Examination of some specimens which developed a continuous layer of intermixed zone showed small buckles along the TGO/intermixed zone interface (Figure 48a) and cracks emanating from these buckles (Figure 48b) In some areas a significant amount of failure was observed to propagate along this interface (Figure 48c). These observations indicate that the intermixed zone can also contribute to failure through acting as crack initiation and/or propagation sites.

Table 2 Summary of the development of intermixed zone for various TBC systems

BOND COAT- PREPARATION	Continuous Intermixed Zone	Discontinuous Intermixed Zone	None / very few Intermixed Zone
NiCoCrAlY- HGB		√	
NiCoCrAlY- MF		√	
NiCoCrAlY- VF		√	
NiCoCrAlY- Pt underlayer		√	
NiCoCrAlY- Aluminized		√	
NiCoCrAlY- Hand polish	√		
NiCoCrAlY- Hand polish-preoxidation			√
NiCoCrAlY- Pt Overlayer	√		
NiCoCrAlY- MF-Pt Overlayer	√		
NiCoCrAlY- MF-Pt Overlayer-MF	√		
NiCoCrAlY- MF-Pt Overlayer-MF-preoxidation	√		
Pt Aluminide- As Aluminized	√		√
Pt Aluminide- HGB		√	
Pt Aluminide- Hand polish			√
Pt Aluminide- LGB-preoxidation			√
Pt Aluminide- MF-preoxidation			√

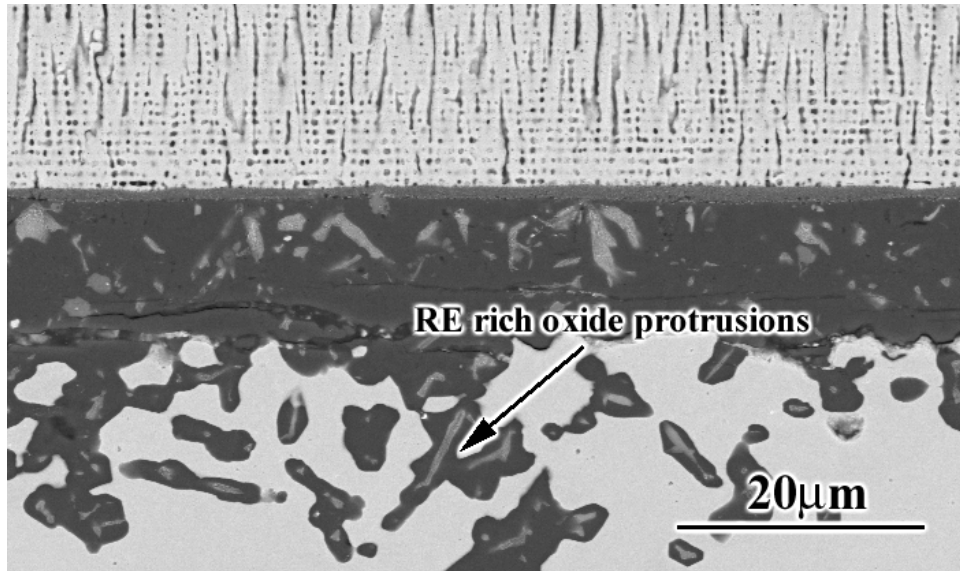
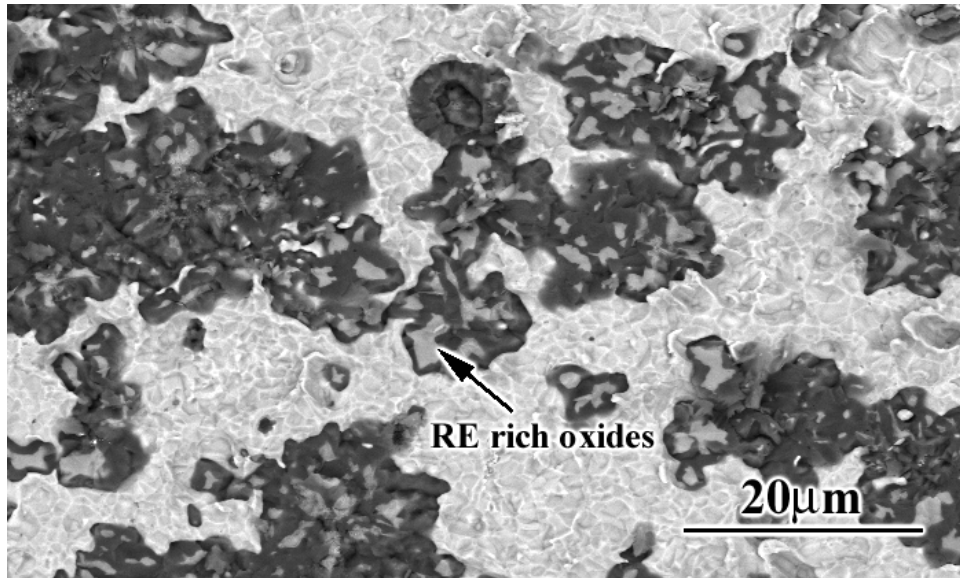
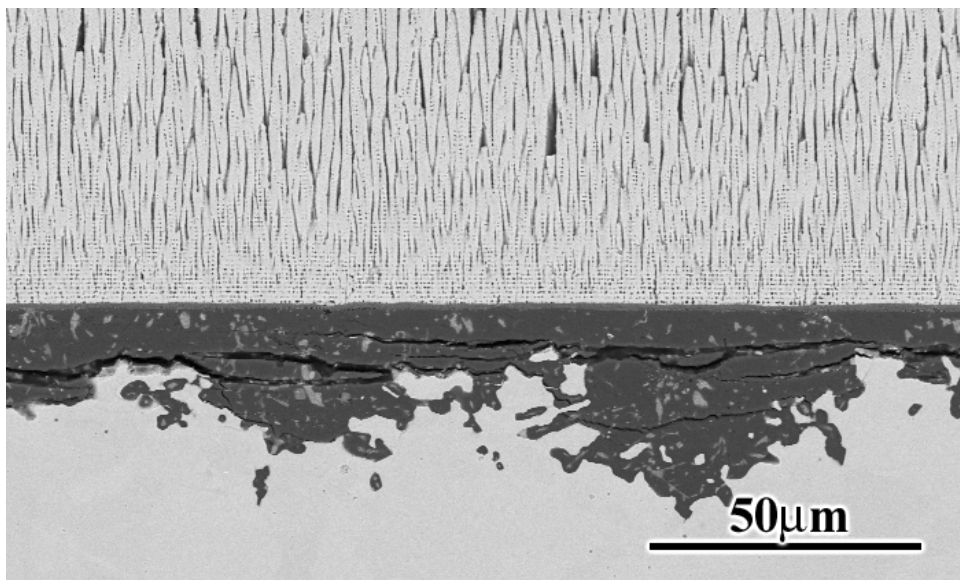


Figure 42 Scanning electron micrograph showing stringers of reactive element rich oxides encapsulated in alumina.



(a)



(b)

Figure 43 (a) Scanning electron micrograph showing the fracture surface of a specimen where the failure cut through RE rich oxide protrusions. (b) Cross sectional examination showed the presence of cracks in the vicinity of these oxide protrusions.

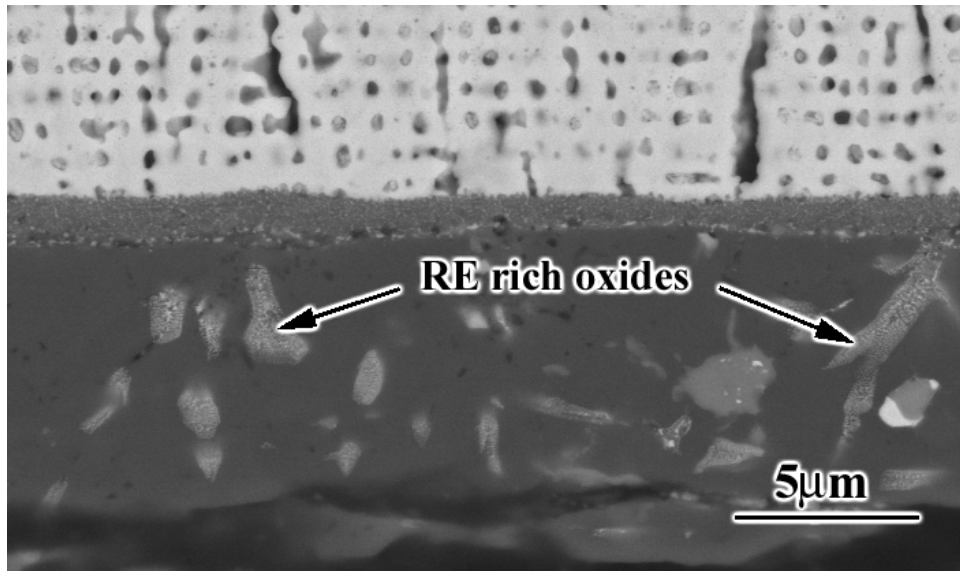
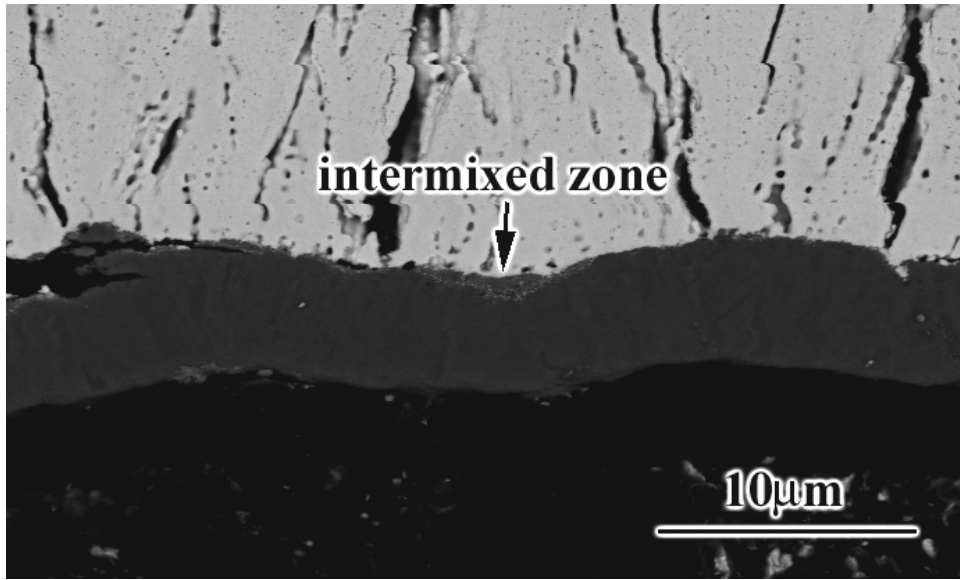
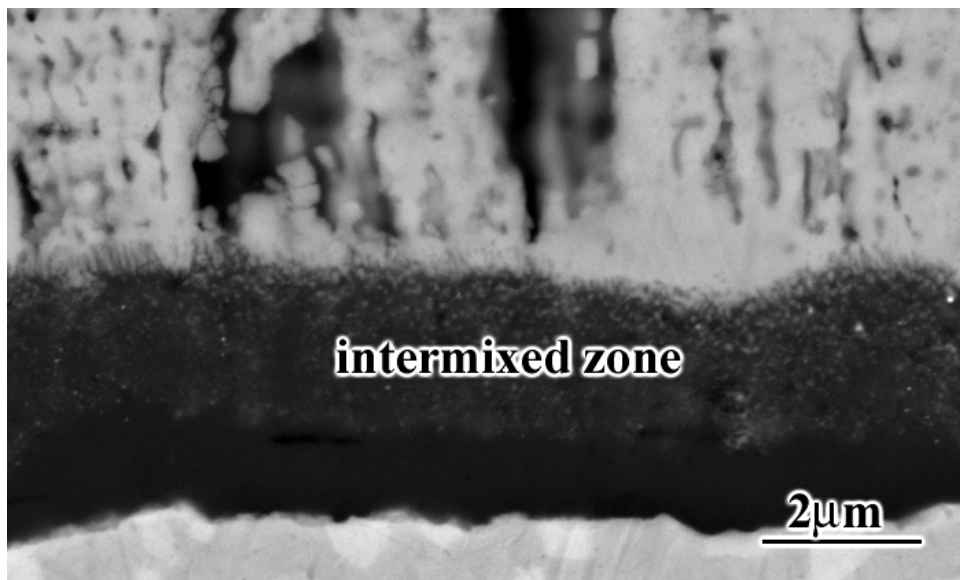


Figure 44 Scanning electron micrograph showing the presence of a thick TGO which had incorporated RE rich oxides

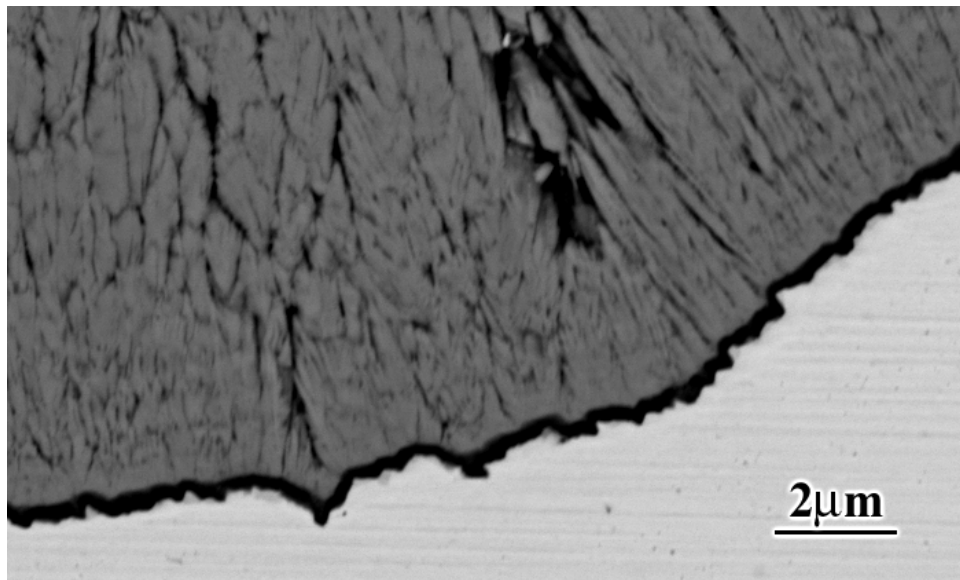


(a)

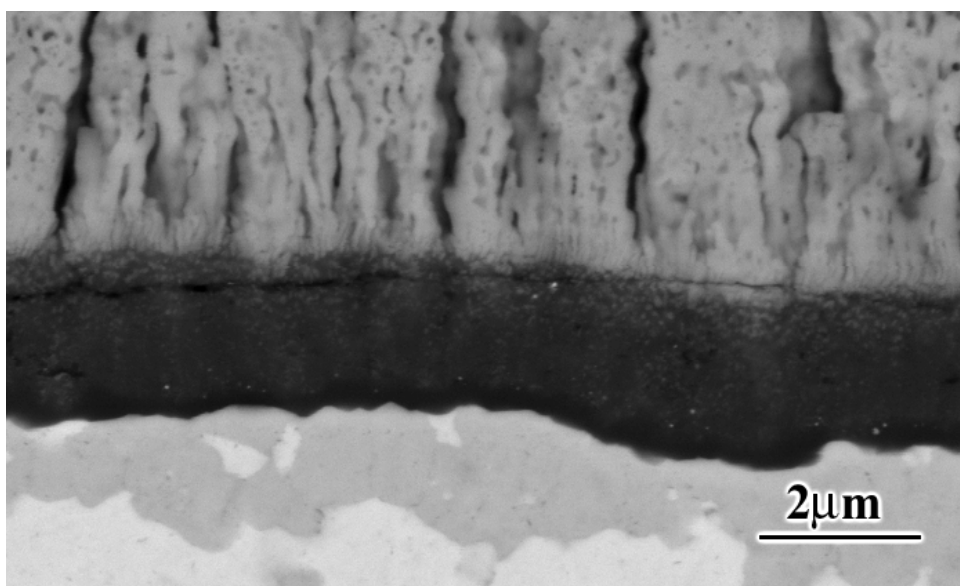


(b)

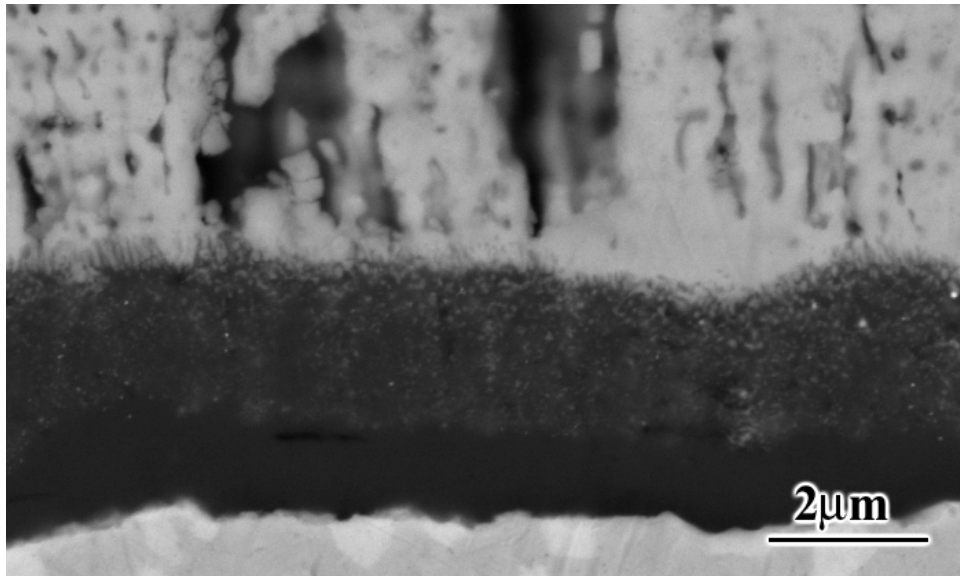
Figure 45 Scanning electron micrographs showing a discontinuous, (a), and a continuous layer of intermixed zone, (b).



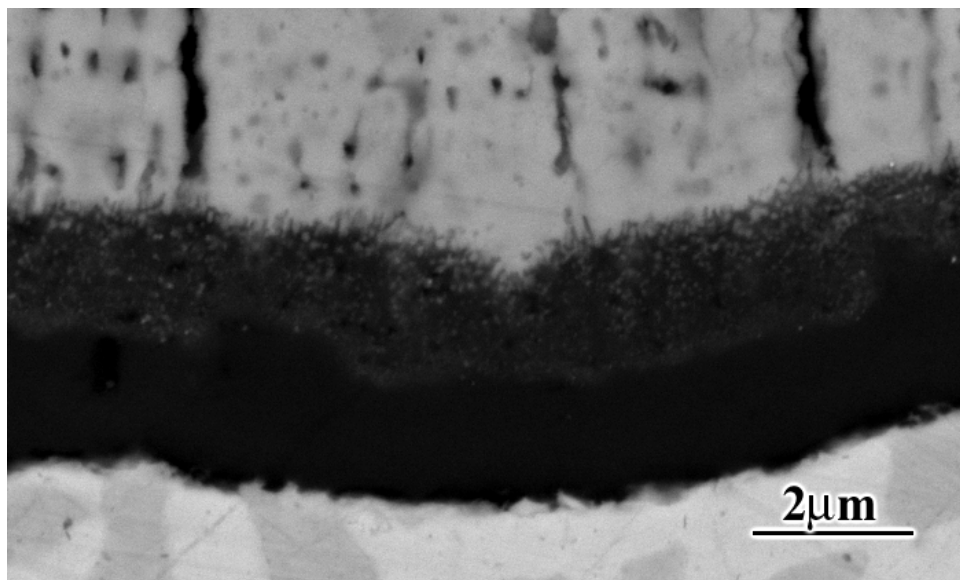
(a)



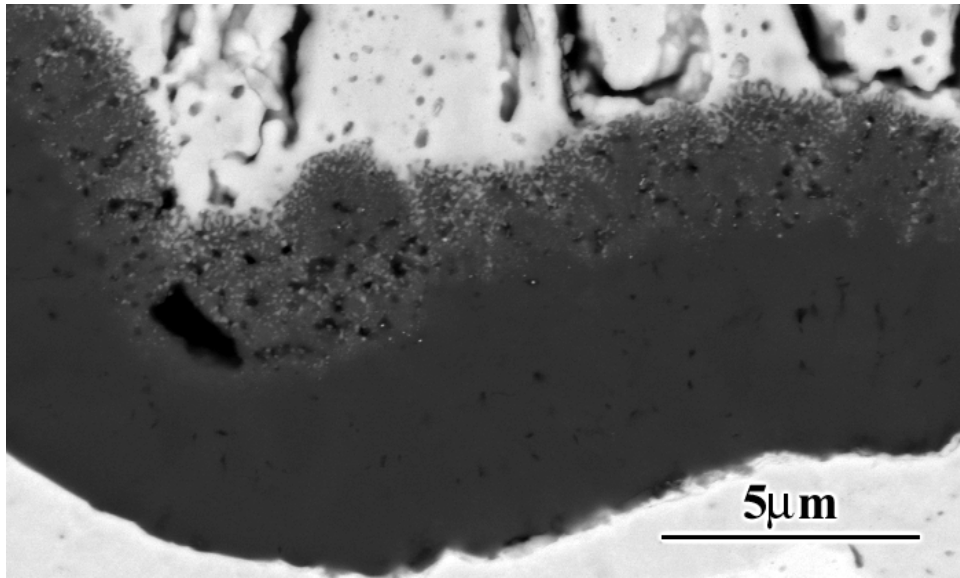
(b)



(c)

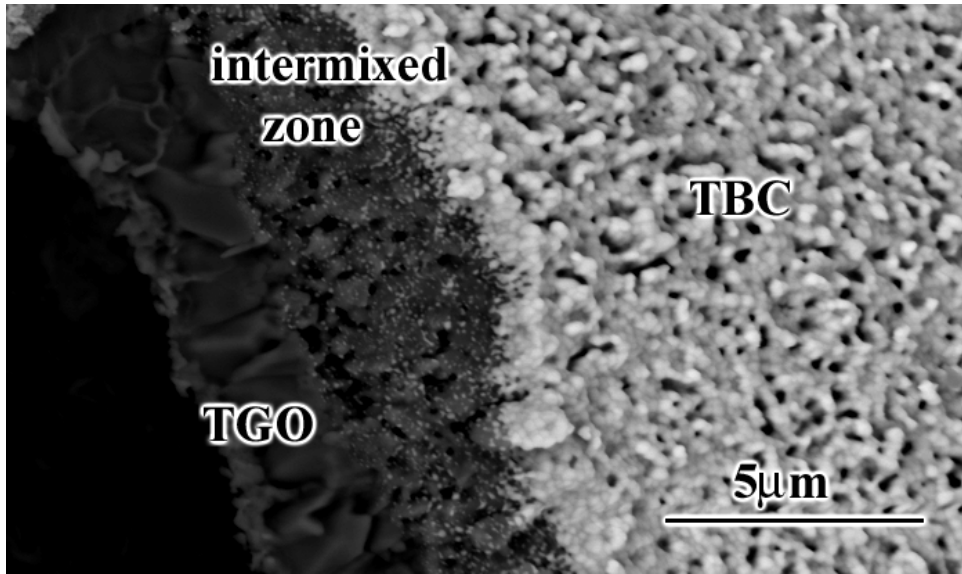


(d)

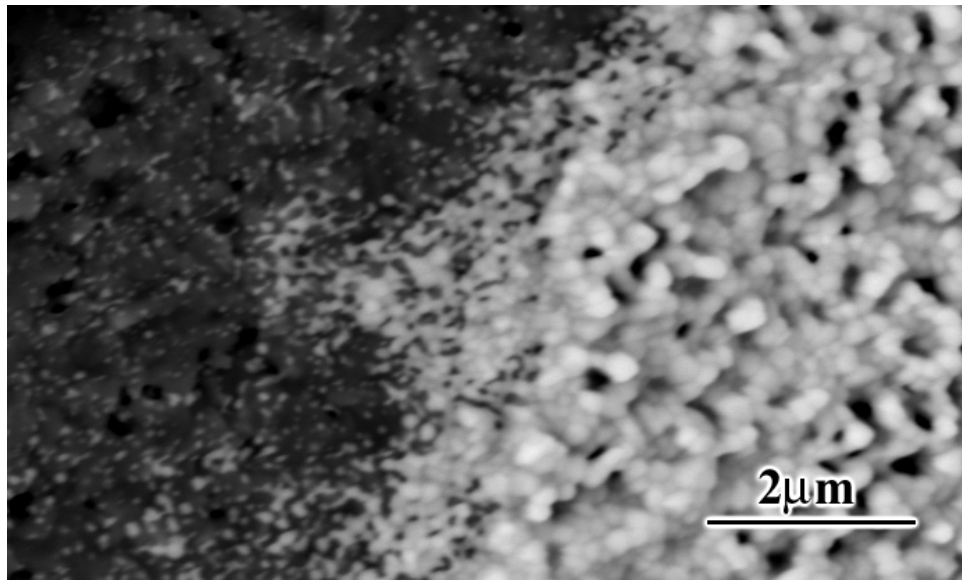


(e)

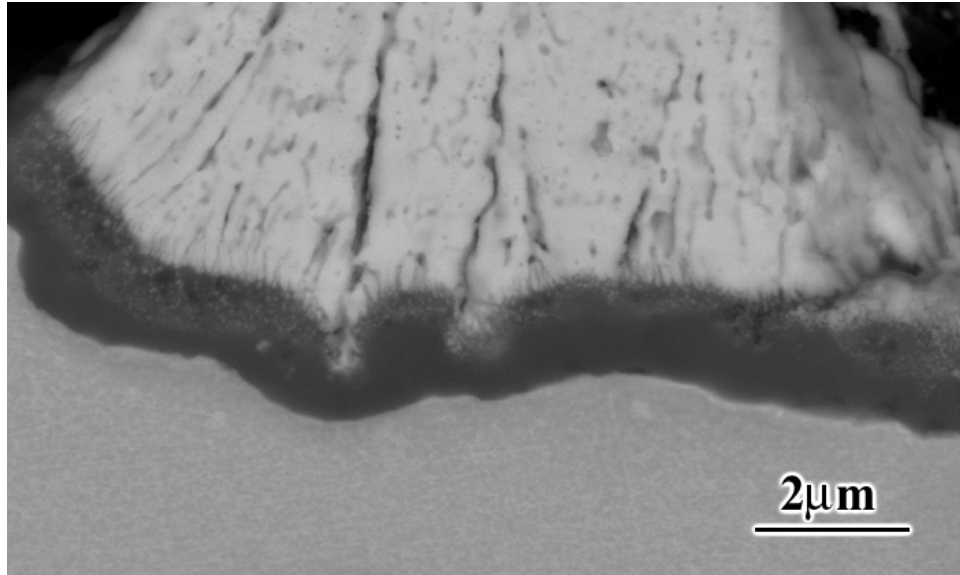
Figure 46 Scanning electron micrographs from a specimen in the as-processed condition (a), as well as after exposure at 1100°C for 10, (b), 60 (c), 100 , (d), and 880 cycles, (e), showing the development of the intermixed zone with time.



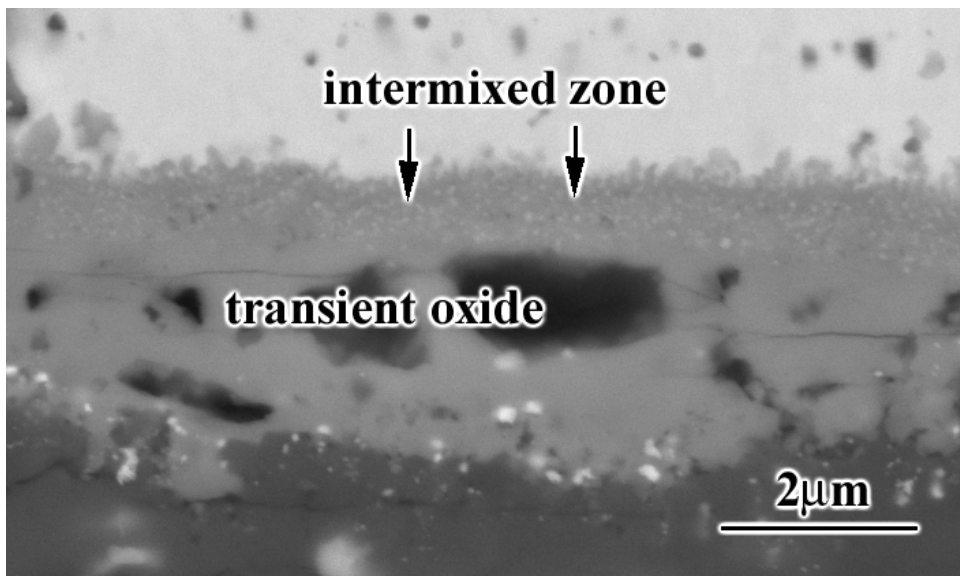
(a)



(b)

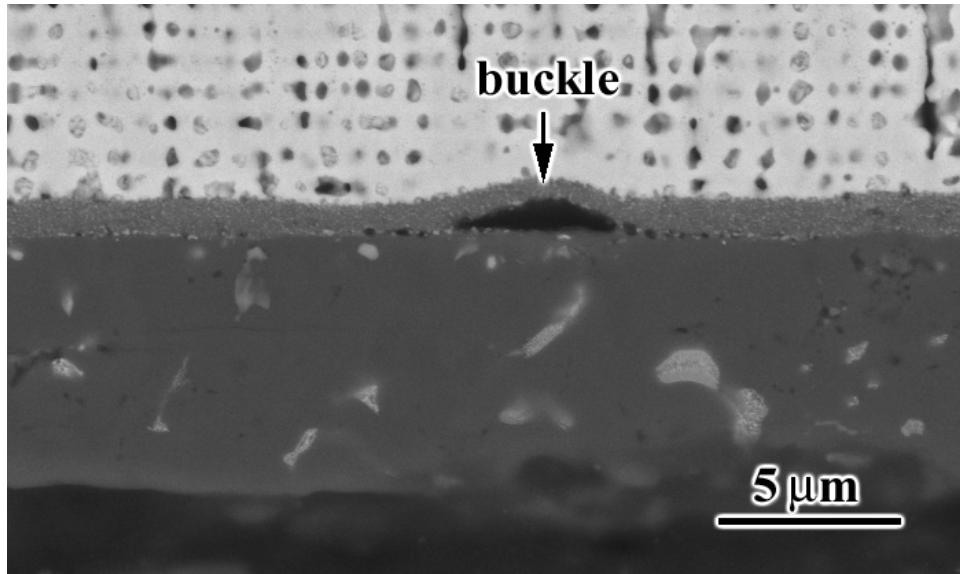


(c)

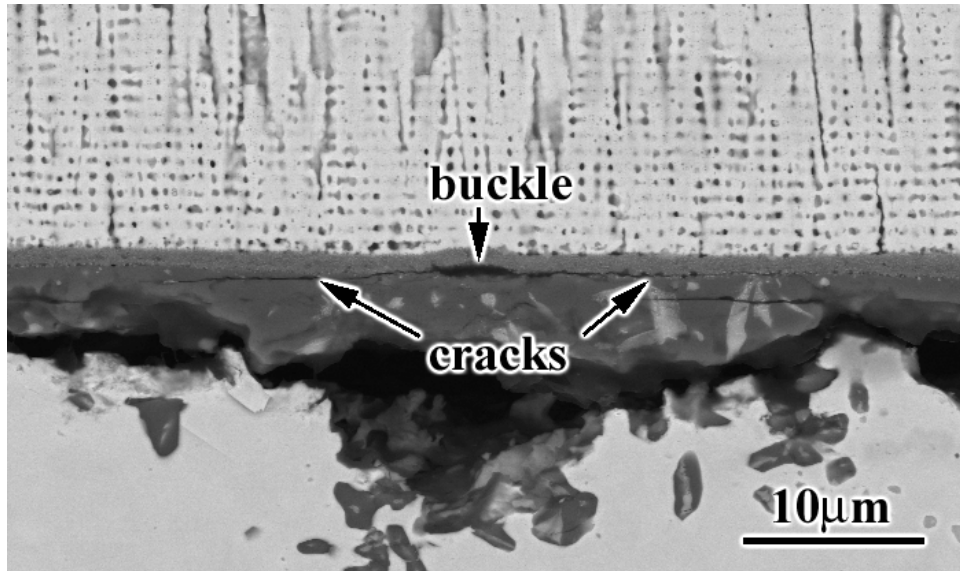


(d)

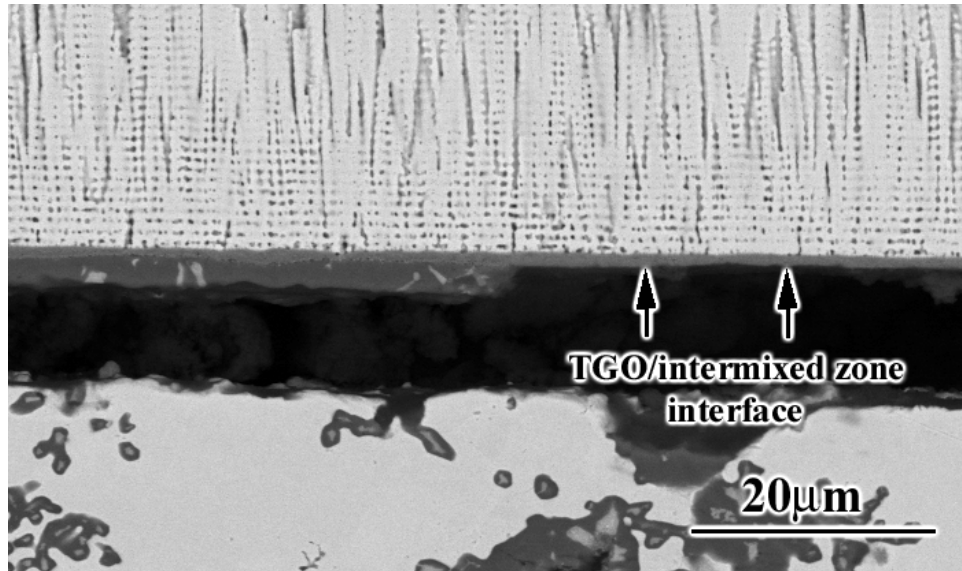
Figure 47 Scanning electron micrographs of the fracture surfaces, (a) and (b) , and cross sections, (c) and (d) , of specimens that developed intermixed zones. See text for details.



(a)



(b)



(c)

Figure 48 Scanning electron micrographs showing a buckle, (a), and cracking in the vicinity of a buckle along the TGO/intermixed zone interface, (b). Significant amount of failure was sometimes observed to propagate along this TGO/intermixed zone interface, (c).

4.2.2.6 Contamination Contamination during processing of the TBC, especially with Fe, provides another area where cracks can initiate. Figure 49a shows a large Fe rich oxide contamination close to the center of a region where the specimen failed. It is possible to determine whether the alumina was in contact with the TBC during exposure or it separated and reformed before final failure by examining the morphology of the TGO as will be explained later on in the microstructural observations section. This is important because it gives clues about where the separations occurred before final failure. In Figure 49b, the light gray areas are where the bond coat surface was reoxidized after failure whereas the dark gray areas around the contamination correspond to thicker alumina where the bond coat was reoxidized before final failure. Cross sectional examination of this specimen showed accelerated oxidation and penetration of the bond coat in the vicinity of these defects (Figure 49c). Figures 49d and 49e are

from different specimens also showing reoxidized areas and accelerated oxidation in the vicinity of contamination sites, respectively. All these results indicate that separations occurred in the vicinity of these defects followed by accelerated oxidation.

Contamination is believed to be responsible for some of the early failures. However, there are some long lived specimens which were also contaminated. Thus, it is believed that the size of the separation in the vicinity of the contamination as well as its interaction with the other weaknesses in the system determines its effect on the final failure.

4.2.2.7 Voids Voids were observed to develop in some TBC systems along the TGO/bond coat interface (Figure 50a) and/or along the initial bond coat / superalloy interface (Figure 50b). Most of these voids are believed to form as a function of exposure time and diffusion in the bond coat seems to be responsible for their development. They were usually associated with the grain boundaries in the bond coat (Figure 50c), which are known to be fast diffusion paths as well as sinks for vacancies. On the other hand, fewer voids were observed to develop in the Pt aluminide specimens with thicker Pt as well as aluminide layers. This change in void density seems to be related to diffusion kinetics, which are affected by the presence of different thicknesses of Pt and aluminide layers. However, systematic diffusion studies are needed to be able to give a detailed description of diffusion phenomena for these systems.

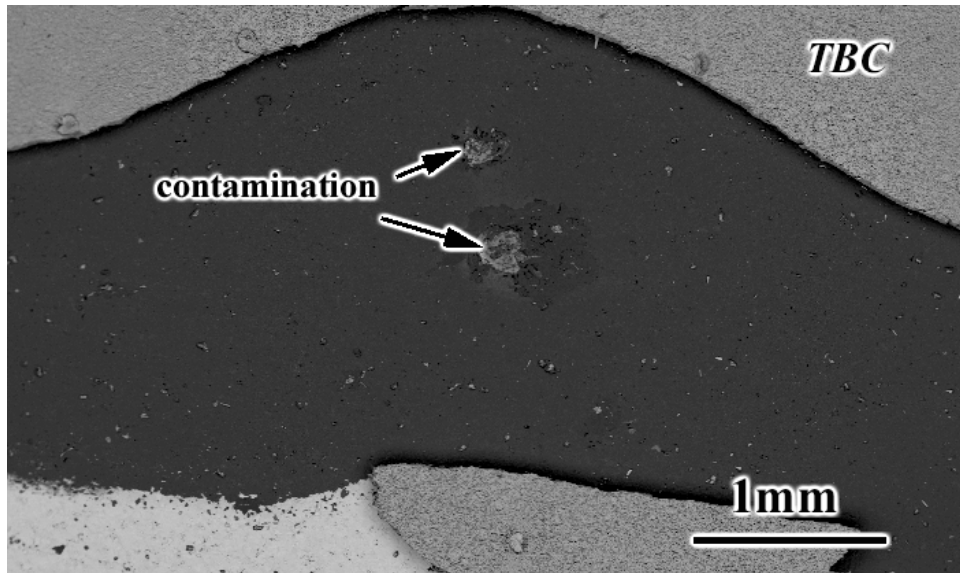
Areas of reoxidation before final failure were also observed around some of these voids, which are indications of separations in the vicinity of voids prior to final failure (Figure 50d) as explained previously. Therefore, they are believed to act as stress concentration sites as in the case of many other defects, causing cracks to initiate in their vicinity. They also reduce the area of contact between the TGO and the bond coat, which is believed to be another important undesirable effect of having too many voids.

4.2.2.8 Grain boundary ridges Ridges develop on Pt aluminide bond coats at locations where the grain boundaries intersect the outer surface of the bond coat. These so called “grain boundary ridges” develop as a result of faster diffusion along grain boundaries during the aluminizing process. Figure 51a is from the top surface of a Pt aluminide bond coat without a TBC, whereas Figure 51b is from the cross section of a Pt aluminide bond coat with a TBC, showing the grain boundary ridges in both cases

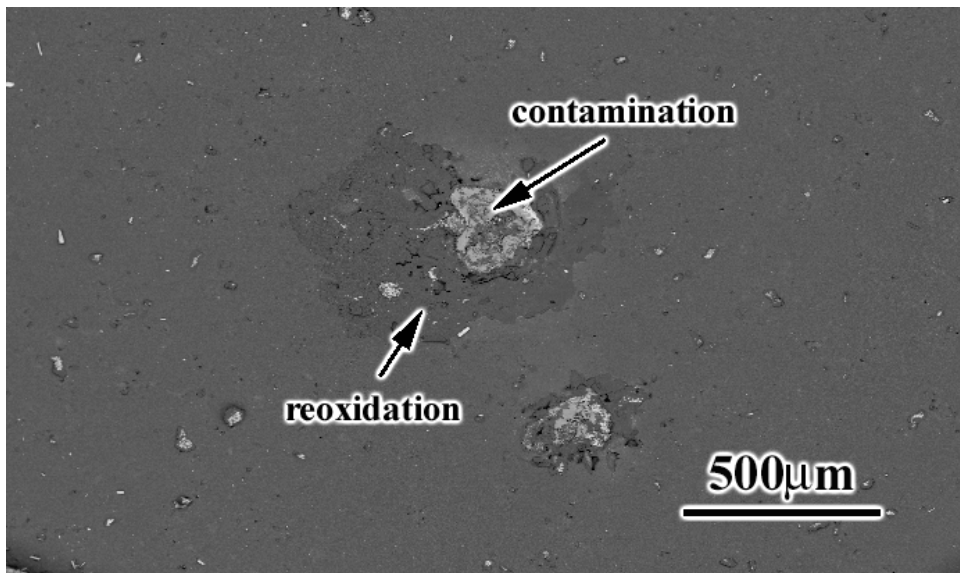
It has been reported earlier that cracks initiate in the vicinity of these ridges due to tensile stresses generated at the peak of these ridges [65]. The results obtained in this study with as aluminized Pt aluminide bond coats with and without TBCs also confirmed crack initiation at these sites (Figures 51c and 51d, respectively)

4.2.2.9 Abnormal Defects These are defects of undetermined origin, which are believed to cause premature failures (failures that occur earlier compared to systems that are all prepared under the same conditions). Figure 52a is an example of such a defect. Numerous voids along the bond coat/superalloy interface as well as some voids along the TGO/bond coat interface were present in a localized area only where a buckle has formed.

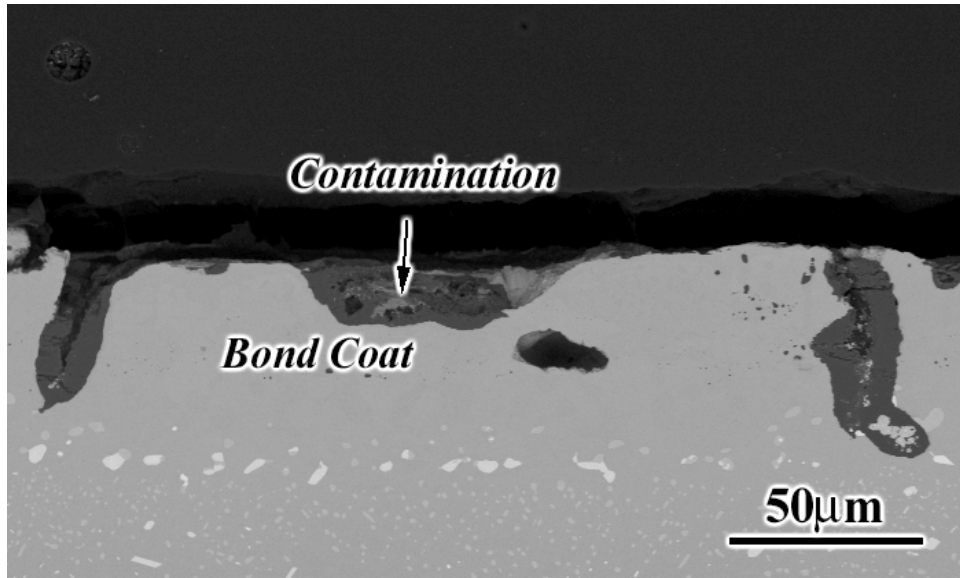
Figure 52b is from a different specimen that also developed a buckle above a localized defective area. In this case, the TBC had a strange morphology in a localized area (Figure 52c), which is believed to be present in the as-processed condition. These types of defective areas may have developed as a result of some processing defects that remain to be identified. Upon exposure, accelerated oxidation might have occurred in these areas followed by buckling and premature failure. Whatever the causes of these abnormal defects are, it is very important to minimize these kinds of defects in order to establish the durability and reliability of these systems.



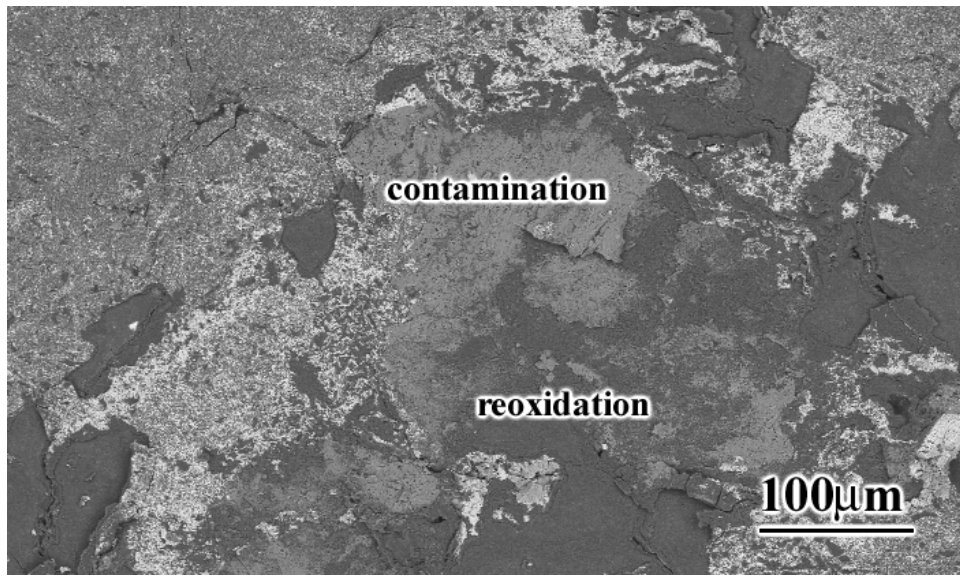
(a)



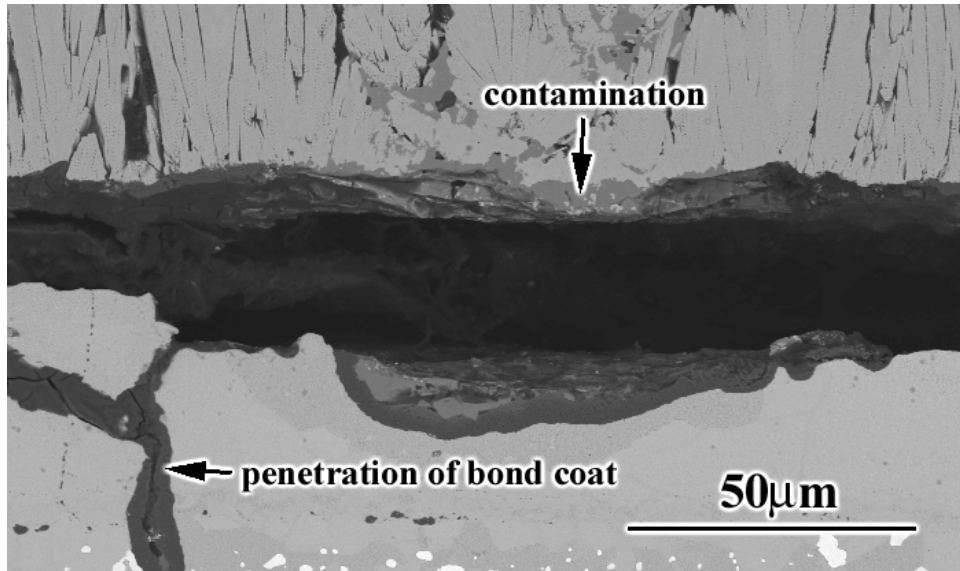
(b)



(c)

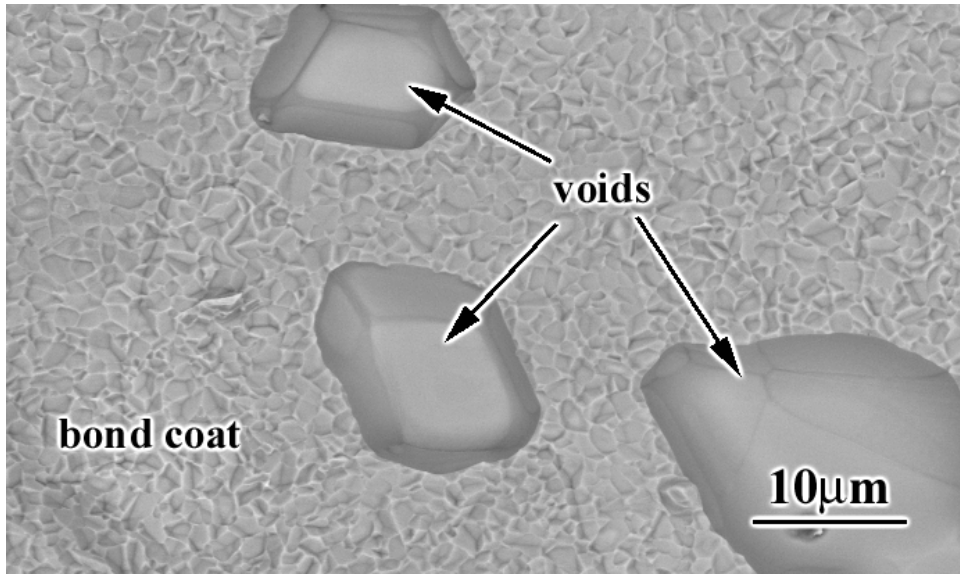


(d)

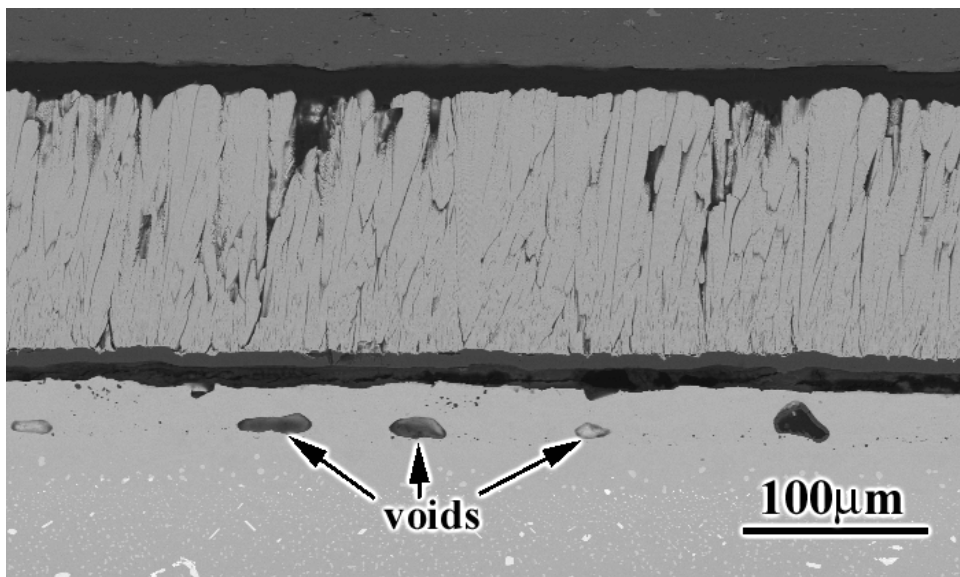


(e)

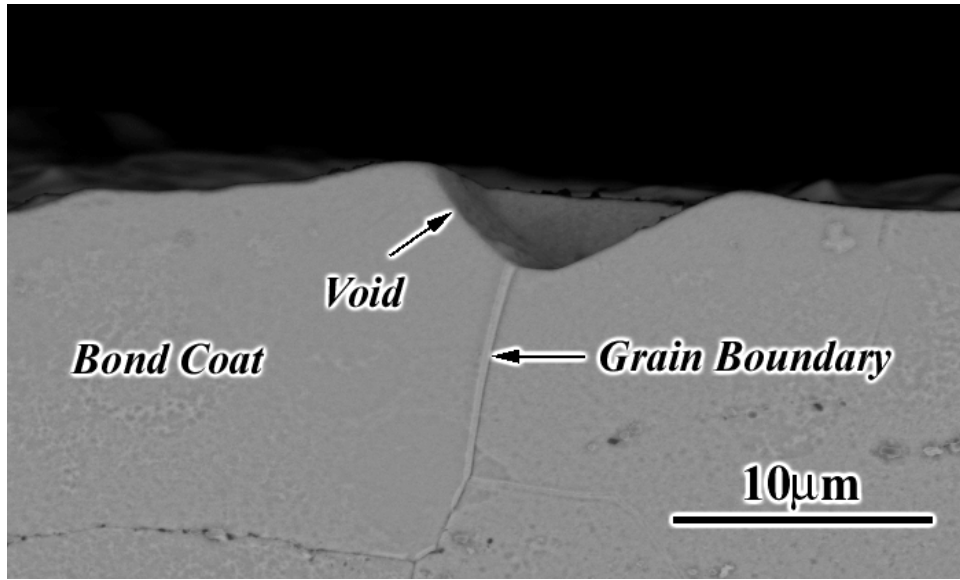
Figure 49 Scanning electron micrographs of the fracture surface of a specimen showing an Fe rich contamination and re-oxidation around it at (a) low and (b) high magnifications. Accelerated oxidation and penetration of the bond coat was evident in the vicinity of a contamination site, (c). Other examples of reoxidation and accelerated oxidation for different specimens in the vicinity of contamination sites are given in (d) and (e), respectively.



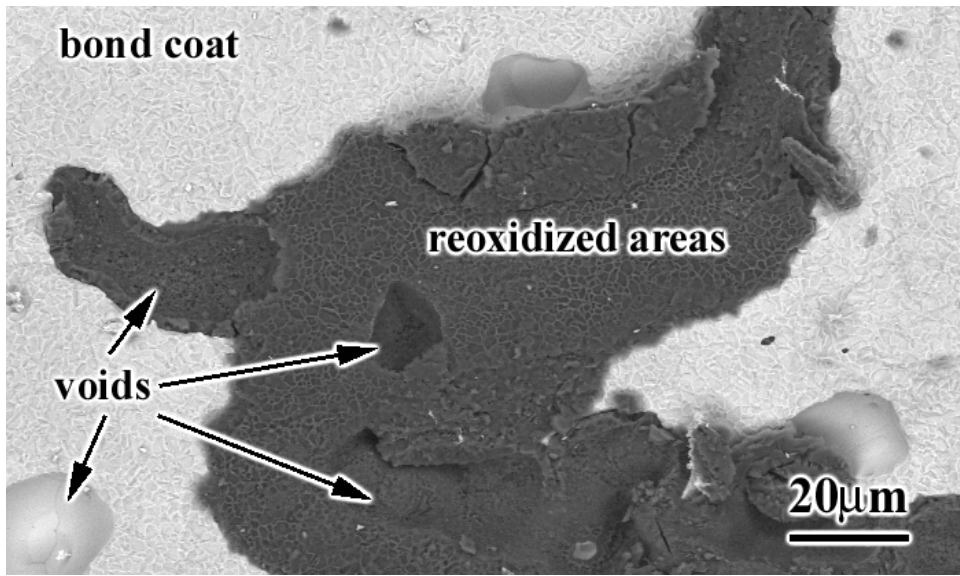
(a)



(b)

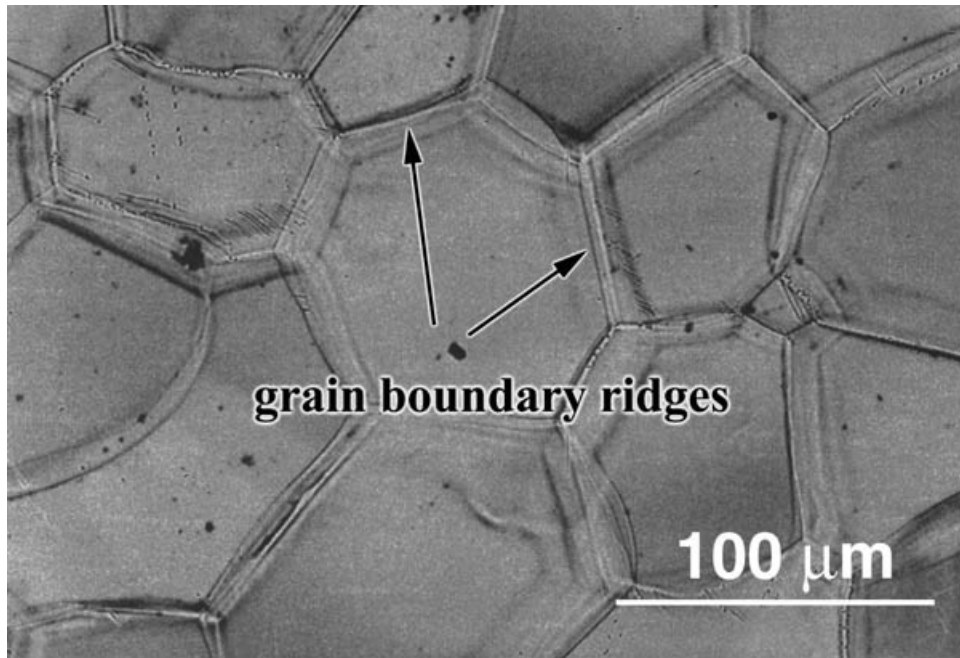


(c)

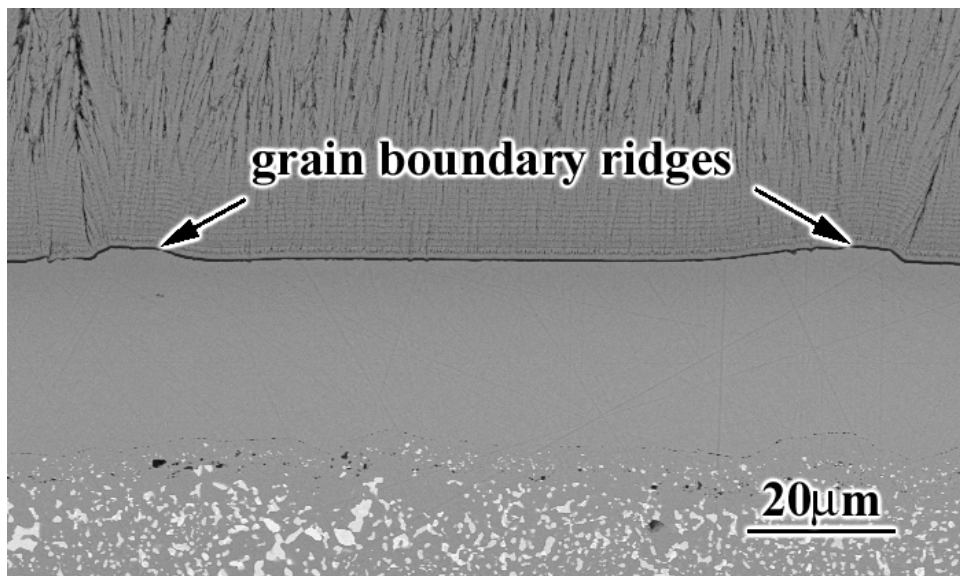


(d)

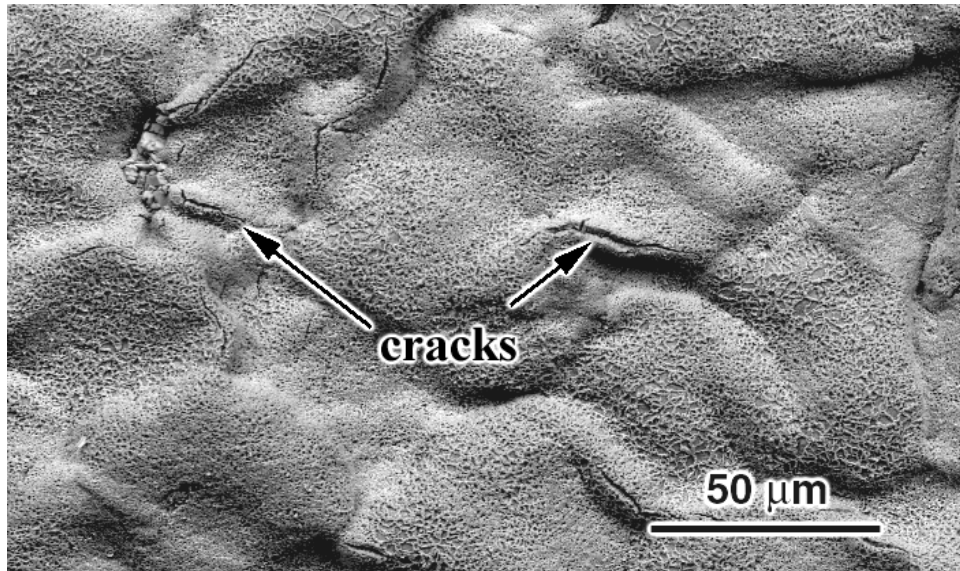
Figure 50 Scanning electron micrographs (a) from the fracture surface and (b) the cross sections of the specimens that developed voids along the TGO/BC and BC/superalloy interface, respectively. These voids were usually associated with the grain boundaries, (c), and reoxidized areas were present around some of these voids, (d).



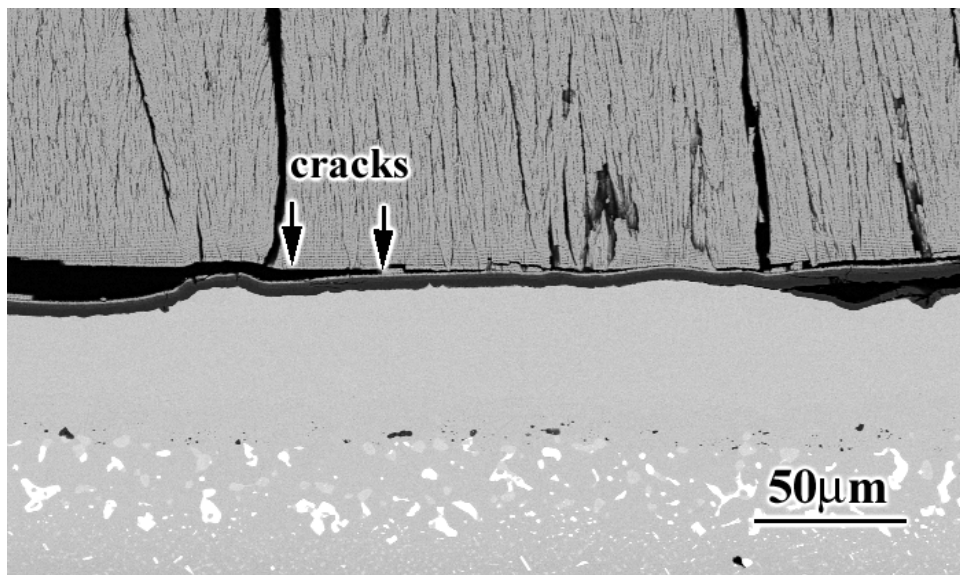
(a)



(b)

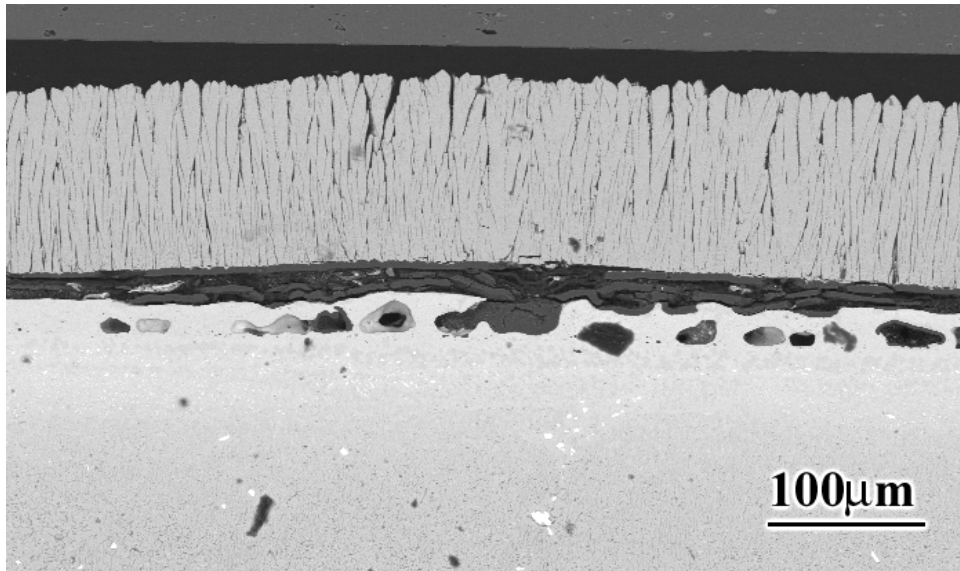


(c)

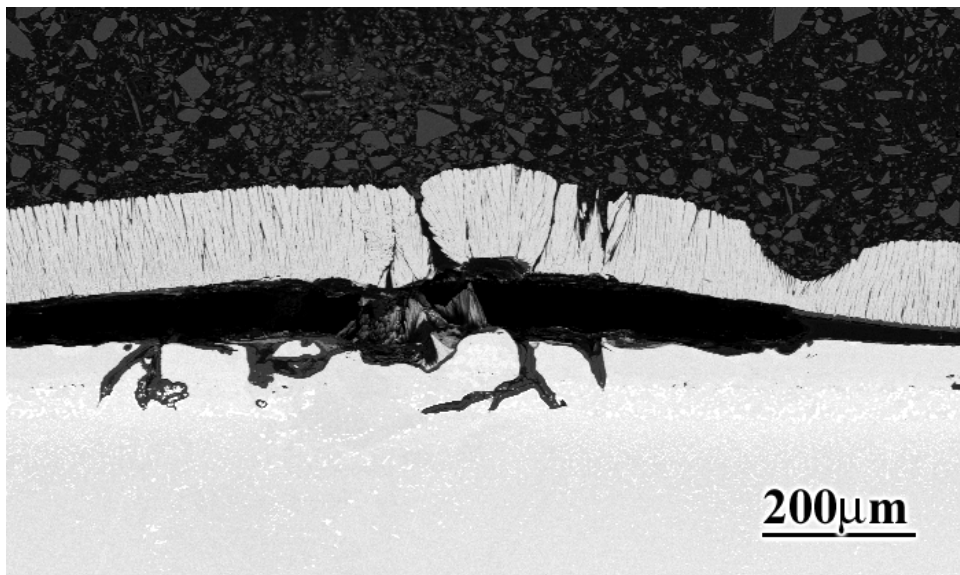


(d)

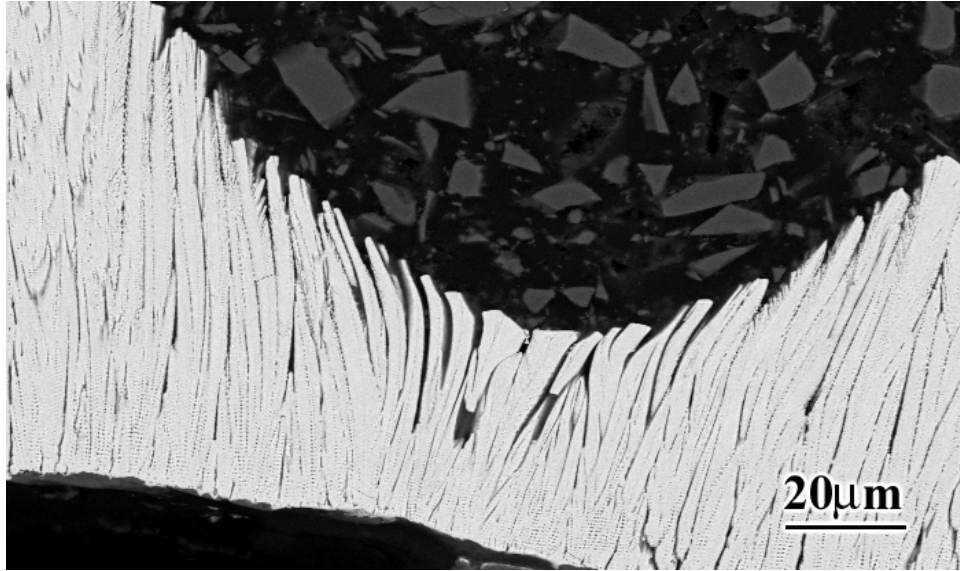
Figure 51 Scanning electron micrographs showing the grain boundary ridges on the surface of a Pt aluminide bond coat without a TBC, (a) and Pt aluminide bond coat with a TBC, (b). Upon exposure, the surface of a Pt aluminide bond coat without a TBC, (c), and cross section of a TBC system, (d), showed cracks in the vicinity of grain boundary ridges.



(a)



(b)



(c)

Figure 52 Scanning electron micrographs showing examples of abnormal defects, above which buckles developed.

4.2.3 Failure of Current State-of-the-Art TBC Systems

In Table 3 a summary of the failure times of the current state-of-the-art TBCs with different bond coats, which were given heavy grit blasting prior to TBC deposition, is presented. It is clear from the failure times that the specimens with platinum aluminide bond coats outperformed those with NiCoCrAlY bond coats. However, it should also be mentioned here that the relative performance of these systems was reversed in rapid cycling [71]. In this section, the general failure behavior of these TBC systems during 1 hour cycles will be given.

Table 3 Failure Times for the current state of the art TBC systems

BOND COAT	Failure Time at 1100°C (# of 1 hr cycles to failure)
Pt Aluminide	840, 1005, 1040, 1100, 1120, 1220, 1280
NiCoCrAlY	40, 40, 40, 60, 60, 60, 76, 102, 102, 139

4.2.3.1 NiCoCrAlY Bond Coats The NiCoCrAlY bond coats were deposited by two different fabrication procedures as mentioned in the experimental details section. The general failure characteristics of TBC systems with these two different NiCoCrAlY bond coats were similar, even though there were some microstructural differences. Therefore, the failure characteristics for these systems will be given in general regardless of the fabrication procedure.

Figure 53a shows a typical cross sectional micrograph from a NiCoCrAlY bond coat with a TBC in the as-processed condition. As can be seen from this low magnification micrograph, some oxide inclusions as well as porosity, which are common for the plasma sprayed coatings, were present throughout the coating. The microstructure of the bond coat consisted of γ (Ni solid solution), β (NiAl) and Cr rich phases as well as Y and/or Hf rich phases (Figure 53b).

The TGO was not uniform, exhibiting variations in thickness and also it was not always pure alumina. The interface was highly irregular. Surface defects (Figure 53c) as well as TBC defects (Figure 53d), which were referred to as “regions of separation in the TBC”, were present as described before.

These specimens were subjected to cyclic oxidation testing at 1100°C and they failed after significantly shorter times compared to TBC systems with platinum aluminide bond coats as mentioned previously. The failure occurred mainly along the TGO/bond coat interface with numerous excursions into the TGO and TBC (Figure 54a). Examination of the fracture surfaces of these coatings after spalling of the TBC showed the presence of Y and sometimes Hf rich oxides encapsulated in alumina (Figure 54b), oxide inclusions (Figure 54c), oxides other than alumina (Figure 54d) and TBC segments (Figure 54e). It should be mentioned here that the proportions of these features observed on the fracture surfaces varied from batch to batch. However, the failure times did not change much. Figure 55 is an example showing a buckle formed following a significant amount of separation along the TGO/TBC interface in contrast to some other samples where the failure was more along the TGO/bond coat interface. Moreover, some batches of specimens developed vertical separations in the TBC, whereas some did not. This difference seems to be a consequence of different TBC morphologies, as mentioned previously.

Cross sectional examination of the failed specimens showed that the Al depletion was not the cause of failure since there was still a significant amount of Al rich β phase left at the time of failure (Figure 56).

An indentation test was performed on the as-processed specimens as well as on specimens exposed to cyclic oxidation conditions and the fracture surfaces have been examined as a function of exposure cycle. In the as-processed condition, the failure was along the TGO/TBC interface with some excursions into the TGO and TBC (Figure 57a). After 10 cycles of exposure at 1100°C, the failure was still mainly along the TGO/TBC interface and in the TGO and TBC with some spallation along the TGO/bond coat interface (Figure 57b). With continued

exposure (after 25 cycles and failure) , the dominant fracture path changed from the TGO/TBC interface to the TGO/bond coat interface (Figures 57c and 57d).

Significant amounts of failure taking place along or close to TGO/TBC interface after indentation for the as-processed specimen and the one subjected to 10 cycles show that this interface was weak, however, the stored energy in the TBC was not large enough to cause failure. The weakness of this interface at short exposure times can be explained by the presence of defects along and/or close to this interface such as TBC defects and transient oxides. With continued exposure, strain energy accumulated in the TGO. The change in the dominant fracture path with time seems to be a result of weakening of the TGO/bond coat interface due to stored strain energy in the TGO as well as weaknesses in the vicinity of defects along this interface which were identified as reactive element rich oxide protrusions and surface defects. All these defects and their role in the failures of TBC systems were described previously in the section “Defects in TBC systems”.

Based on these observations, a tentative failure mechanism for the state of the art TBC systems with NiCoCrAlY bond coats can be summarized with the help of a very simple schematic diagram given in Figure 58 as follows:

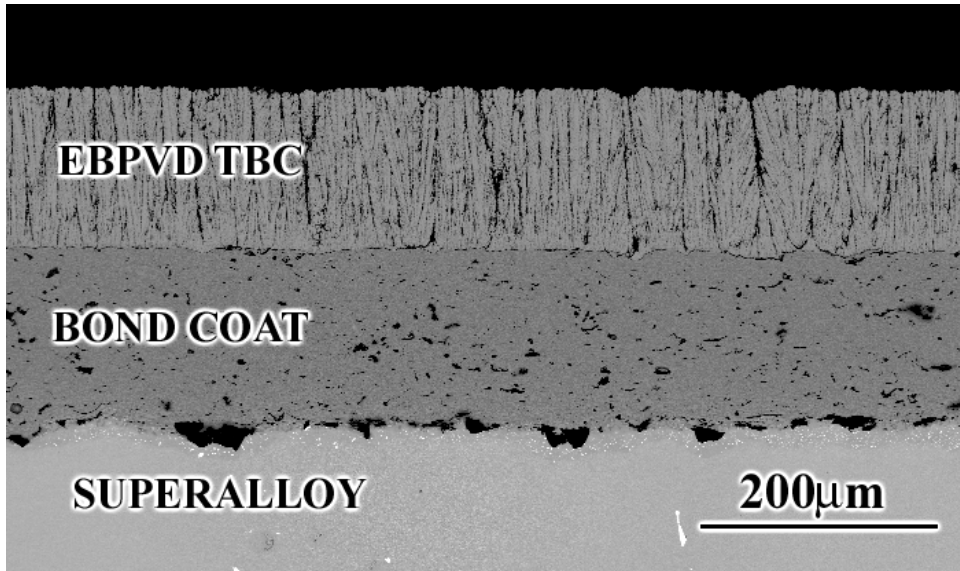
-Certain “defects” are present in these TBC systems, some of which are present in the as-processed condition, whereas some develop with time. The ones that are present along and/or close to the TGO/TBC interface can be described as oxides other than alumina and TBC defects usually associated with the initially irregular interface whereas the ones along the TGO/bond coat interface are reactive element rich oxide protrusions as well as initially-present surface defects (Figure58a). Depending on the concentration and frequency of these defects, the following failure processes can take place:

- When the defects along and/or close to the TGO/TBC interface are frequent, the cracks that initiated in the vicinity of these defects may link up causing failure mainly along or close to TGO/TBC interface as shown in Figure 58b.

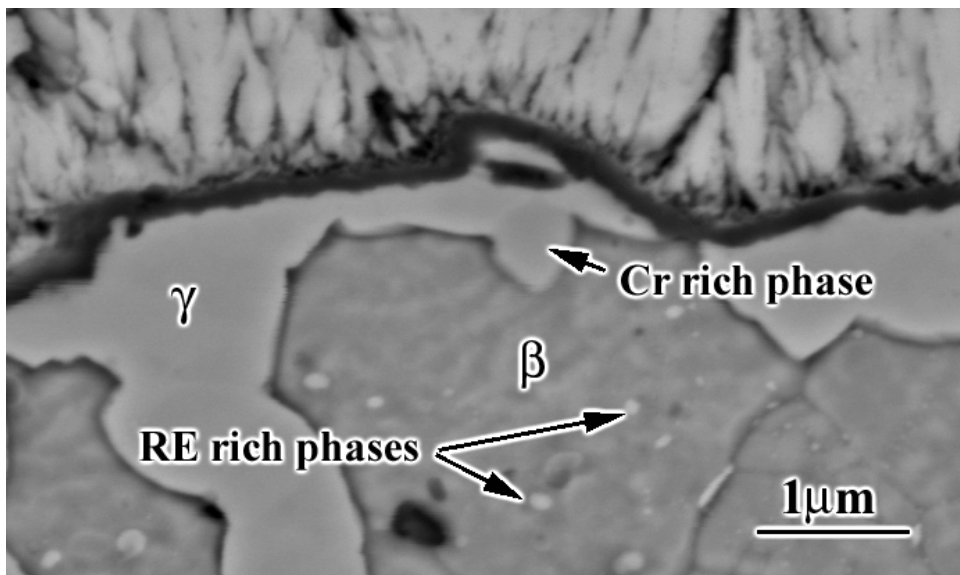
-When the defects along the TGO/TBC interface are not so frequent, the cracks that initiate in their vicinity propagate through the TGO and then along the TGO/bond coat interface as the stored energy in the TGO increases (Figure 58c)

-The cracks can also initiate in the vicinity of the defects along the TGO/bond coat interface. These cracks, once initiated, can propagate along the TGO/bond coat interface (Figure 58d)

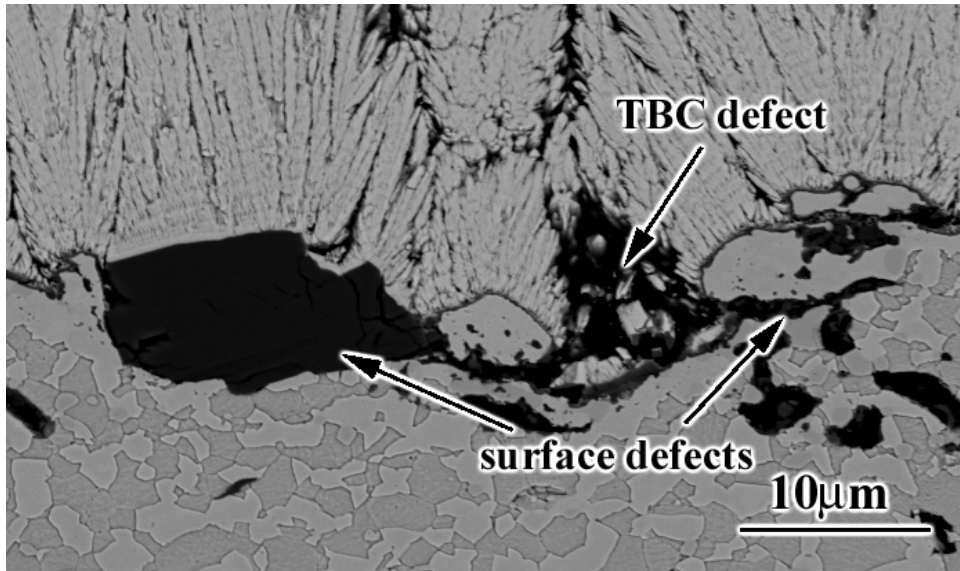
-The failure can occur by a mixture of the above-mentioned failure processes, which is usually the case for the specimens used in this study.



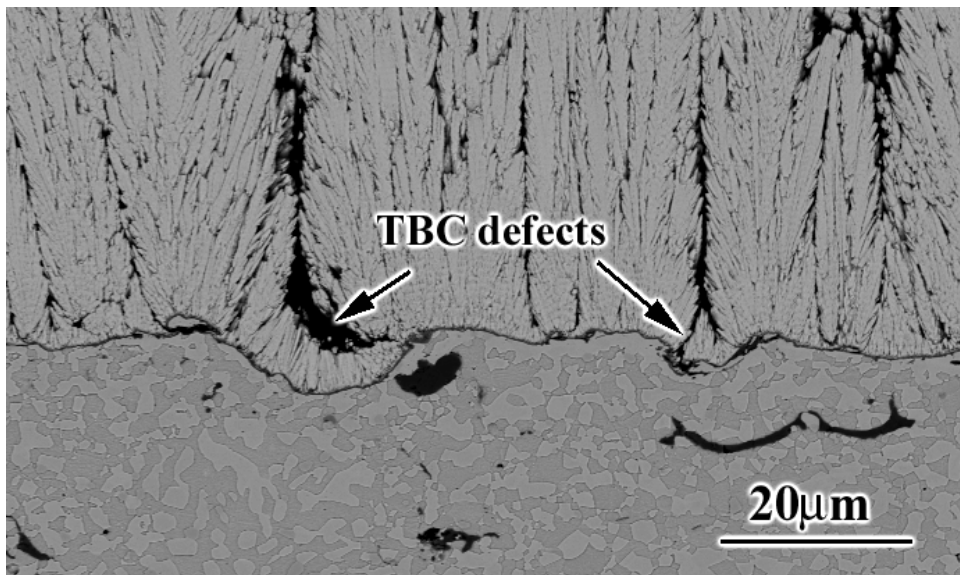
(a)



(b)

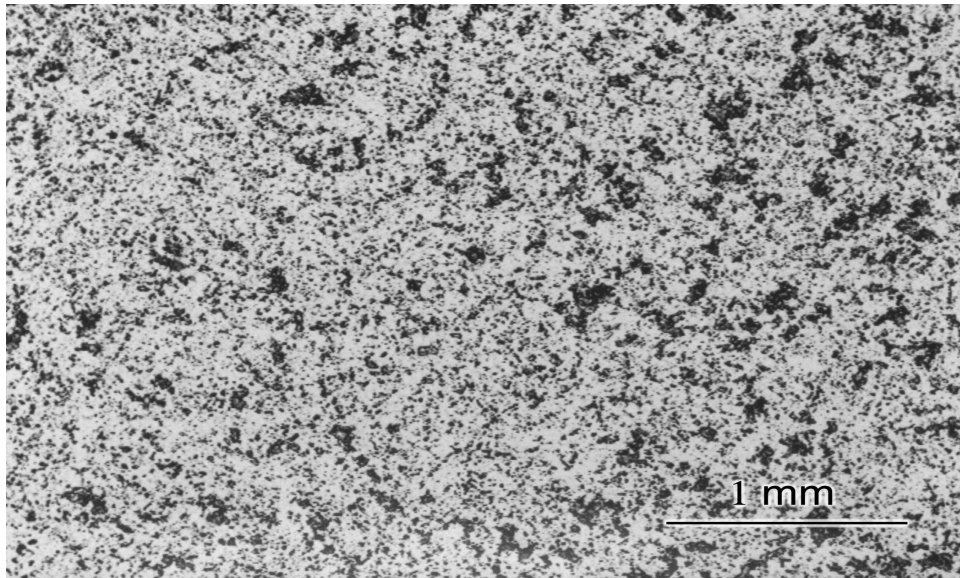


(c)

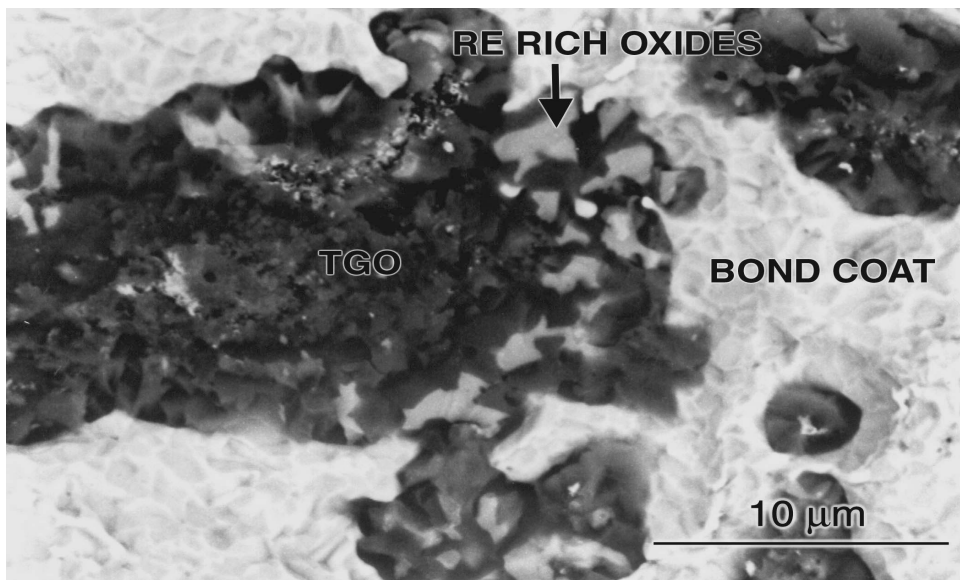


(d)

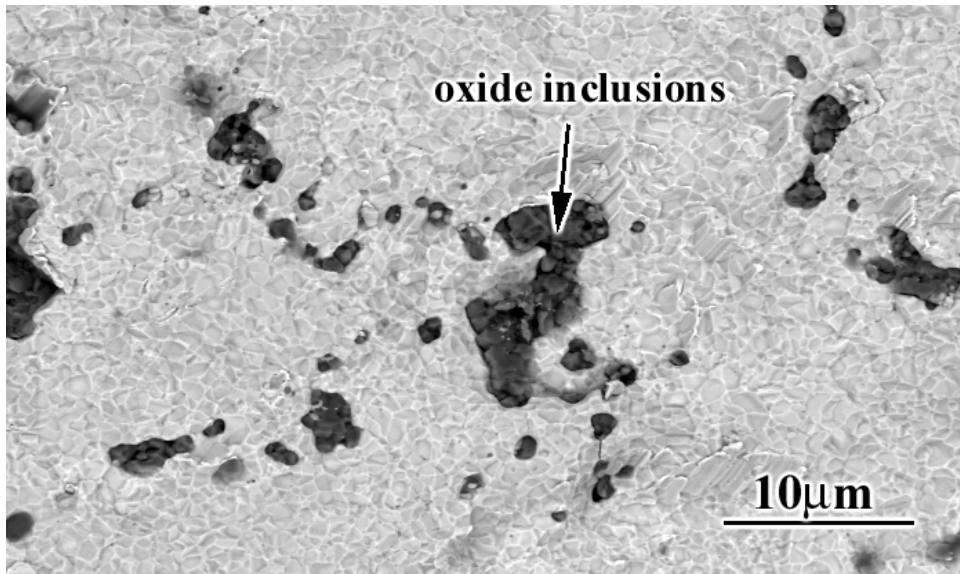
Figure 53 Scanning electron micrographs showing the typical state of the art TBC systems with NiCoCrAlY bond coats in the as processed condition. The bond coat consisted of porosity and oxide inclusions throughout the coating, (a), and β , γ as well as Cr and RE rich phases, (b). Surface defects (c), as well as TBC defects (d), were present.



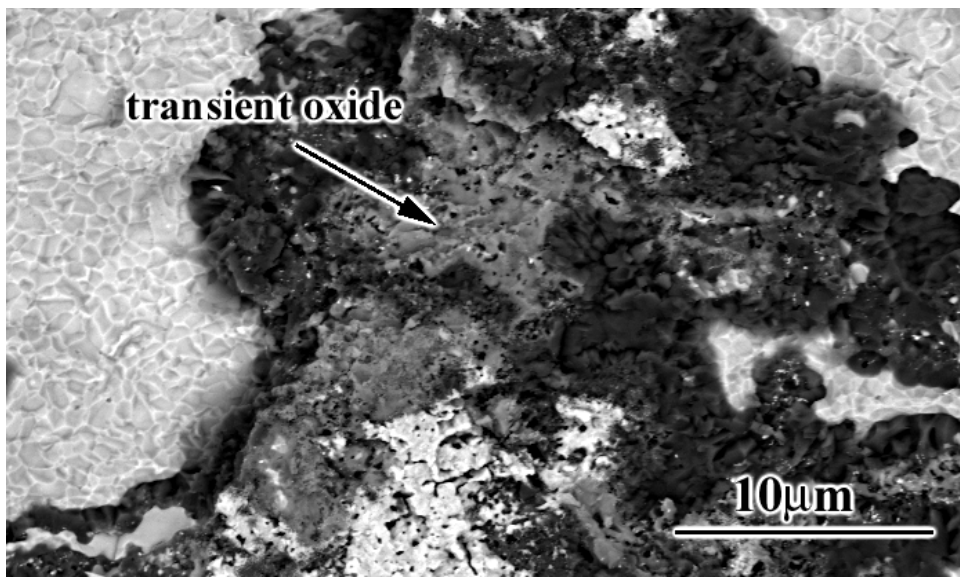
(a)



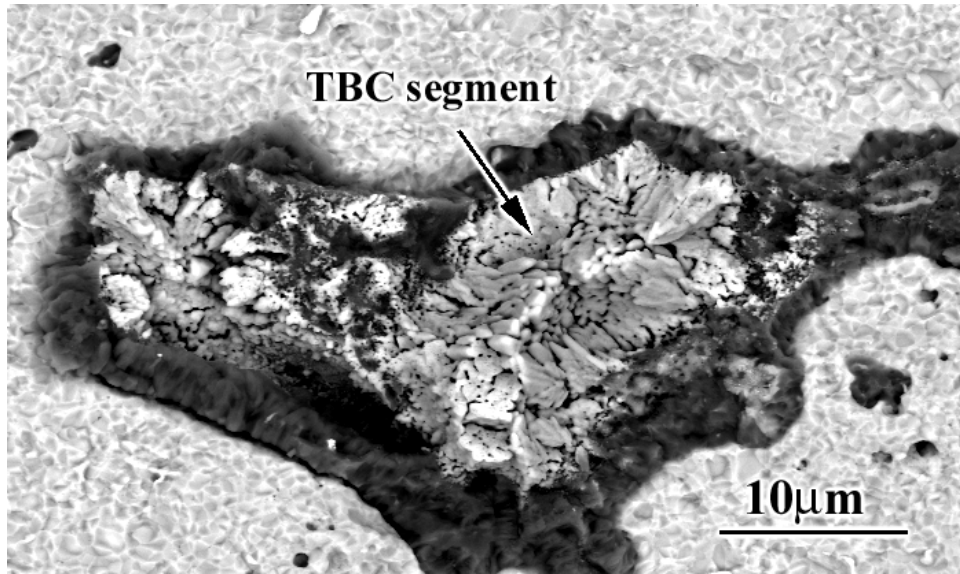
(b)



(c)



(d)



(e)

Figure 54 Scanning electron micrographs showing the fracture surfaces of state of the art NiCoCrAlY bond coats. The failure was mainly along the TGO/BC interface with numerous excursions into the TGO and TBCs (a). The typical features observed on the fracture surfaces were RE rich oxide protrusions (b), oxide inclusions (c), transient oxides (d), and TBC segments (e).

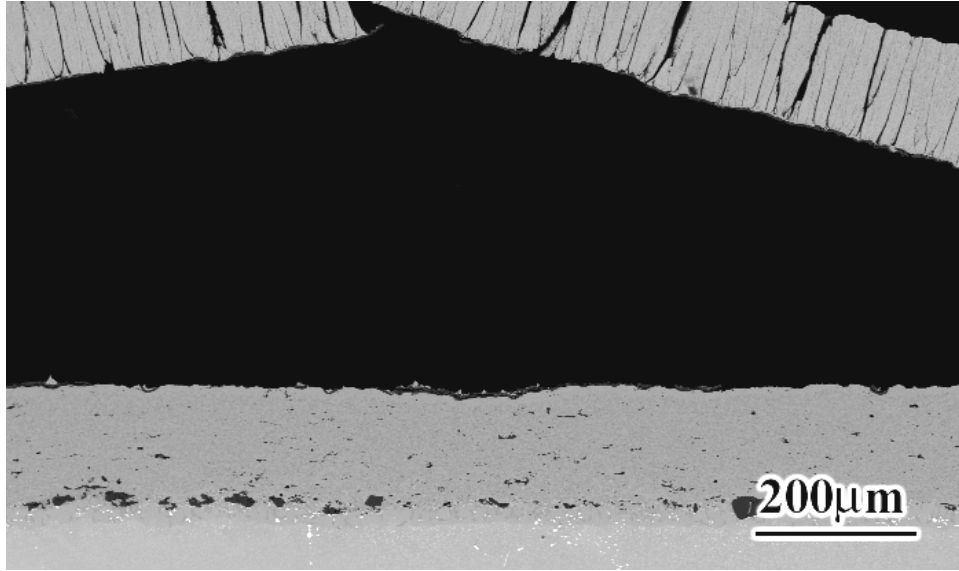


Figure 55 Scanning electron micrograph of a TBC system with state of the art NiCoCrAlY bond coat showing a significant amount of separation along the TGO/TBC interface followed by buckling

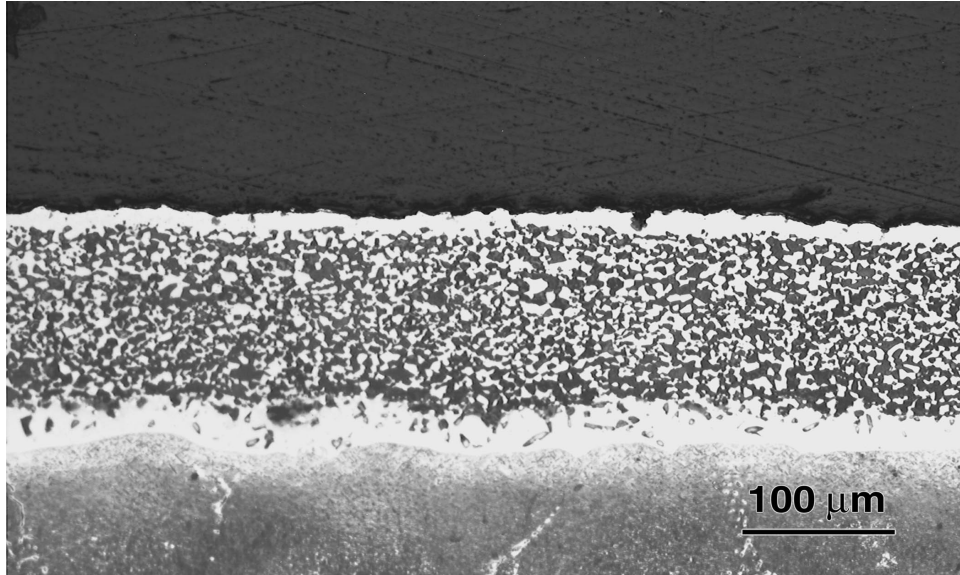
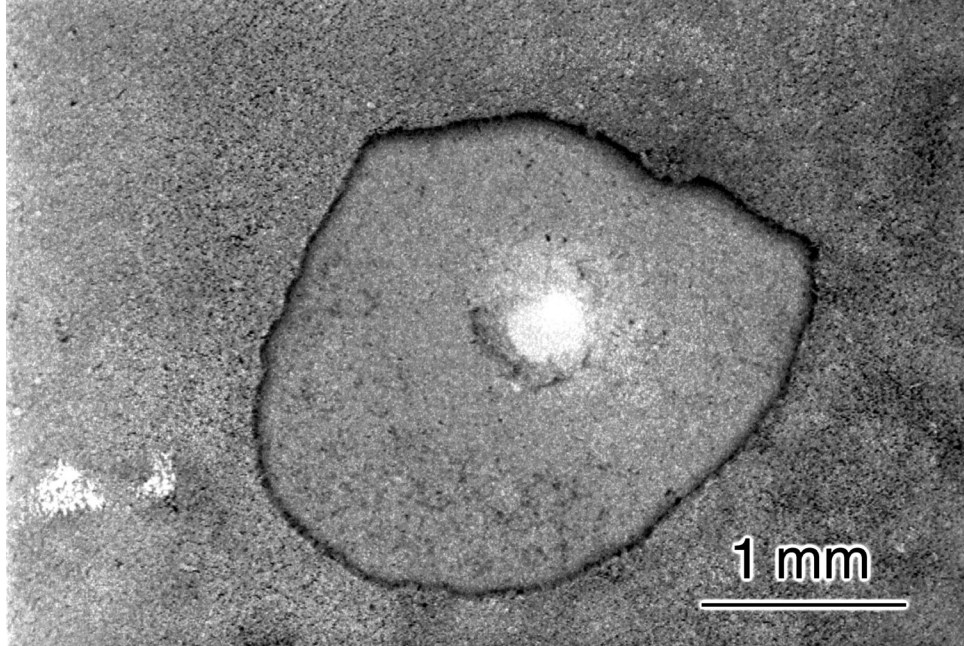
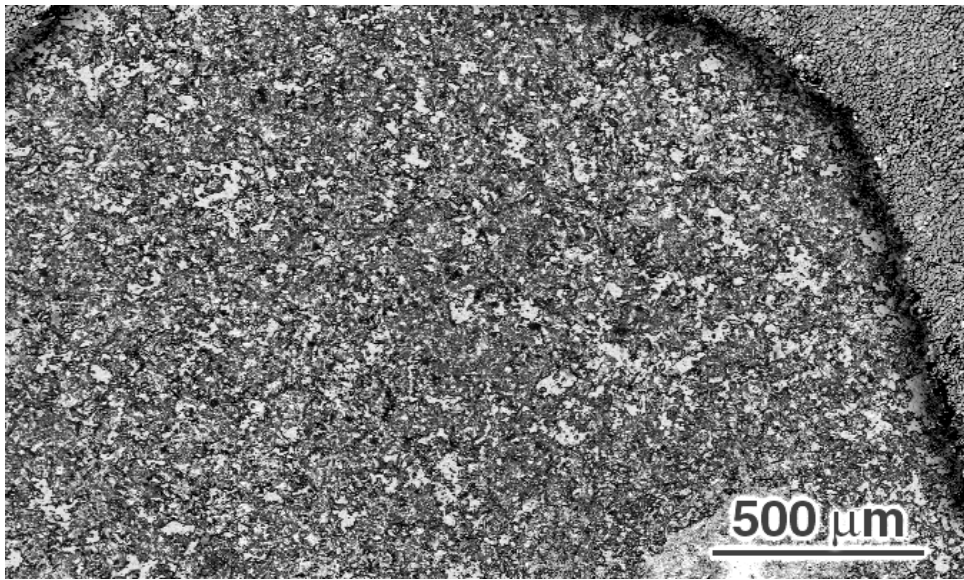


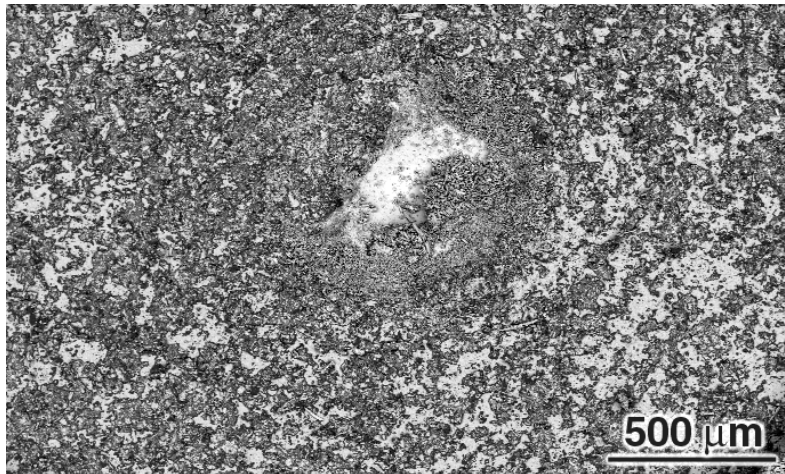
Figure 56 Optical micrograph of a TBC system with state of the art NiCoCrAlY bond coat after failure showing that a significant amount of Al-rich β phase was present at the time of failure.



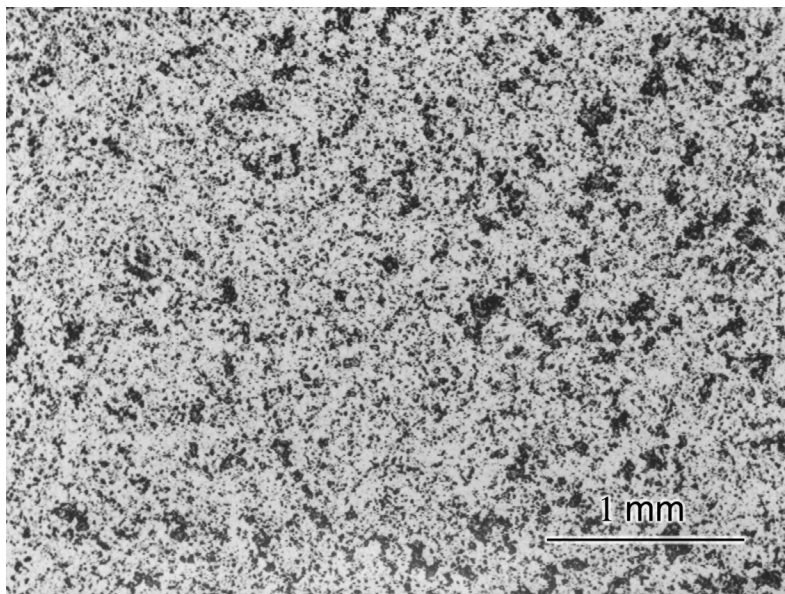
(a)



(b)



(c)



(d)

Figure 57 Scanning electron micrographs from the fracture surfaces of the TBC systems with the state of the art NiCoCrAlY bond coats after an indentation test has been performed on the as-processed specimens (a), as well as on the ones which were exposed at 1100°C for 10 (b), and 25 cycles (c). The fracture surfaces of the specimens, which failed after 102 cycles of exposure is also shown in (d). Dark areas correspond to the TGO and the TBC while white areas correspond to the bare bond coat.

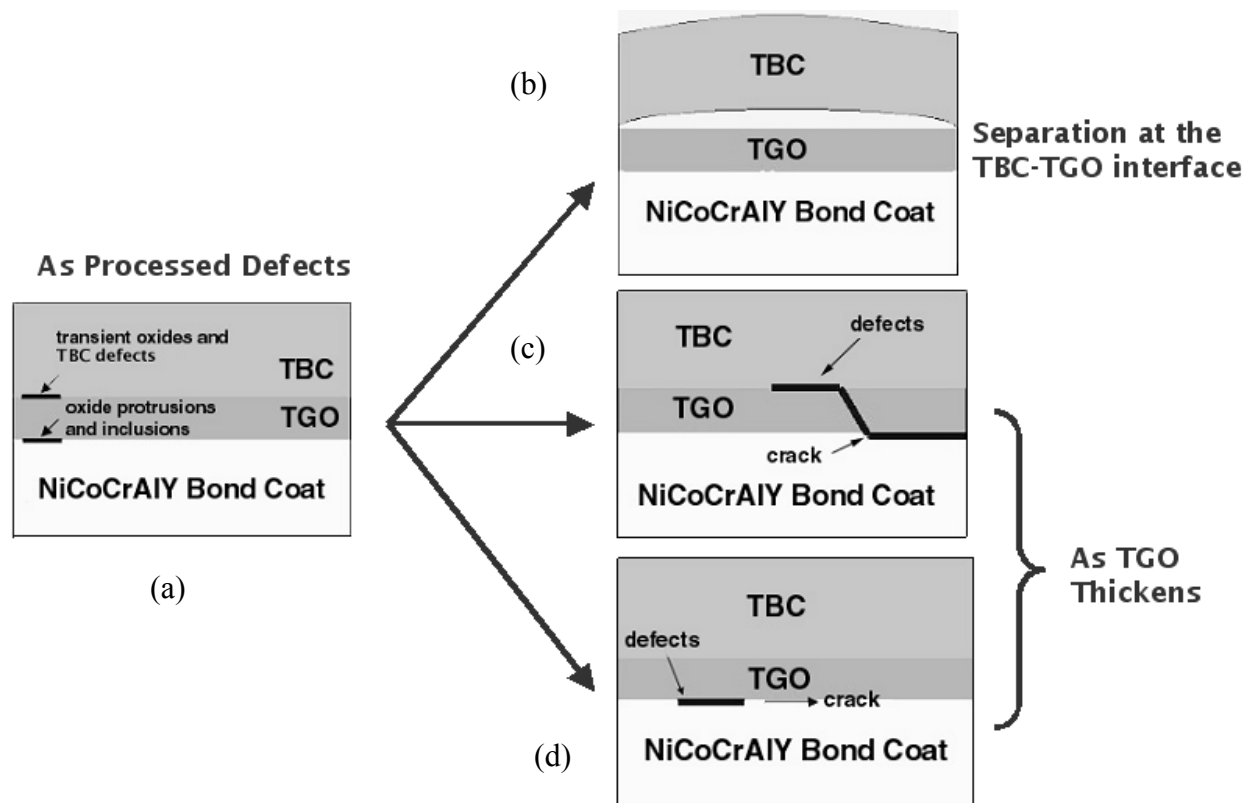


Figure 58 A simple schematic summarizing the failure behavior of the state of the art TBC systems with NiCoCrAlY bond coats. See text for details

4.2.3.2 Platinum Modified Aluminide Bond Coats The platinum modified aluminide bond coats were prepared by 2 different companies and some minor differences were present in terms of composition and thickness of the bond coats. There was also a difference in the grain size of the bond coats. However, the general failure behavior of these systems was similar. As in the case of TBC systems with NiCoCrAlY bond coats, the general failure behavior will be given for these systems first, regardless of the processing differences. The early failure of one set of specimens which had TBCs deposited by a different company will be discussed next, followed by the effects of grain size and thermal cycles on the failure of these systems. A tentative failure mechanism will be given at the end based on these observations.

The microstructure of the platinum modified aluminide bond coats with a TBC in the as-processed condition consisted of only β (NiAl) phase with Pt, Cr and Co in solid solution (Figure 59a). The interface was irregular due to heavy grit blasting and corn kernel type TBC defects, which were discussed previously, were present in the TBC (Figure 59b) above the surface irregularities. This type of defect is believed to make a big contribution to the failure of these TBC systems as will be explained in the following paragraphs.

The failures have been observed to be mainly along the TGO/TBC interface and in the TBC and TGO. However, there was also spallation along the TGO/bond coat interface (Figures 60a and 60b). Examination of cross sections of these TBC systems before and after failure indicated that the bond coat surfaces deformed resulting in an increase in the initial surface roughness. (Figures 61a and 61b, respectively) Cracks were observed to develop in the TBC in the vicinity of these deformed areas (Figure 61c). This is known as a ratcheting mechanism, which was explained in detail in the background section, and it dominates the failure of the state of the art Pt aluminide systems.

In the following sections, it will be shown that the TBC constrains the deformation of the bond coat. Based on this observation, it is believed that the ratcheting occurred first at areas that were referred to as corn kernel TBC defects. The reason behind this idea is the weaker TBC constraint to deformation of the bond coat in the vicinity of these defects. Accordingly, the bond coat could deform more easily with less constraint given by the TBC (Figure 62a). The stresses are also higher at these initial interface imperfections, which drives the deformation of the bond coat at these sites as proposed by Evans et al. [42] Figure 62b is from the fracture surface showing a TBC segment that was pulled from the TBC due to ratcheting at a corn kernel type TBC defect. In other areas, where the interface was initially smoother, the TBC constraint to deformation of the bond coat was larger as a result of a more well-developed columnar TBC morphology. Thus, the resistance to ratcheting was stronger in these areas and the interface remained relatively smooth (Figure 62c).

As the amplitude of the ratchets increases by the deformation of the bond coat, the cracks that initiated in the vicinity of these ratchets propagate away from the ratchets. This results in new separations along the TGO/TBC interface and accordingly, weak areas where there is no more TBC constraint to deformation of the bond coat. New ratchets, then, may form at these sites resulting in additional crack formation and propagation. This process continues until these cracks in the vicinity of ratchets link up reaching a critical size, causing final failure. If the ratcheting is not pronounced enough, which is determined by the frequency, size and amplitude of the ratchets, the cracks initiated in the vicinity of the ratchets can propagate through the TGO and then along the TGO/bond coat interface as the stored strain energy in the TGO increases. However, if the ratcheting is severe, the cracks initiated in the vicinity of these ratchets link up before the failure can propagate through the TGO, causing more failure along the TGO/TBC

interface. Some variation in the fracture paths was also observed in this study for specimens from different batches.

A different batch of TBC systems with heavy grit blasted Pt aluminides, which had TBCs deposited by a different company, failed at relatively shorter times at 1100°C after 500 and 760 cycles of exposure. Cross sectional examination of this specimen showed very significant amounts of ratcheting even after a fewer number of cycles to failure compared to other batches (Figure 63a). Examination of the as-processed specimen indicated the presence of a different TBC morphology close to the TGO even though the surface roughnesses were similar. The TBC close to the TGO consisted of small corn kernel type TBC defects lined up side by side in the as-processed condition (Figure 63b) and it also developed vertical separations with time (Figure 63c). This different type of morphology is believed to be a function of TBC deposition conditions. Based on the argument given previously, the TBC constraint to deformation of the bond coat must be less for these specimens, which can explain the early failure and the significant amount of ratcheting for these specimens. The vertical separations may also be a contributing factor in their early failure. These results show that the TBC deposition conditions also can have an effect on the TBC morphology, and accordingly on the failure, besides the surface condition.

There are various proposed mechanisms for ratcheting as mentioned in the background section. Plastic deformation of the bond coat, as well as the volume reductions as a result of phase transformations in the bond coat may be all playing a role in the ratcheting type of failure. Our results also indicate the importance of grain boundaries for ratcheting. Specimens obtained from one of the companies had comparatively smaller grain size. Cross sectional examination of this specimen showed more pronounced ratcheting (Figures 64a and 64b) compared to other

specimens with larger grain size (Figures 64c and 64d). The failure was more along the TGO/TBC interface as a result of this significant amount of ratcheting. Also, the ratchets were usually associated with the grain boundaries (Figure 64b). These observations may suggest the importance of grain boundaries in ratcheting. One explanation may be the role of grain boundary sliding in the plastic deformation of the bond coat. However, more work has to be done to make this argument stronger.

Thermal cycling also has a significant effect on the amount of ratcheting and accordingly on the fracture path. Examination of specimens after cyclic (Figure 65a) and isothermal tests (Figure 65b) showed smaller amounts of ratcheting for the isothermally tested specimen. This observation indicates the role of thermal stresses on the ratcheting type of failure.

Based on these observations, a tentative failure mechanism for these TBC systems can be summarized as follows with the help a simple schematic diagram given in Figure 66:

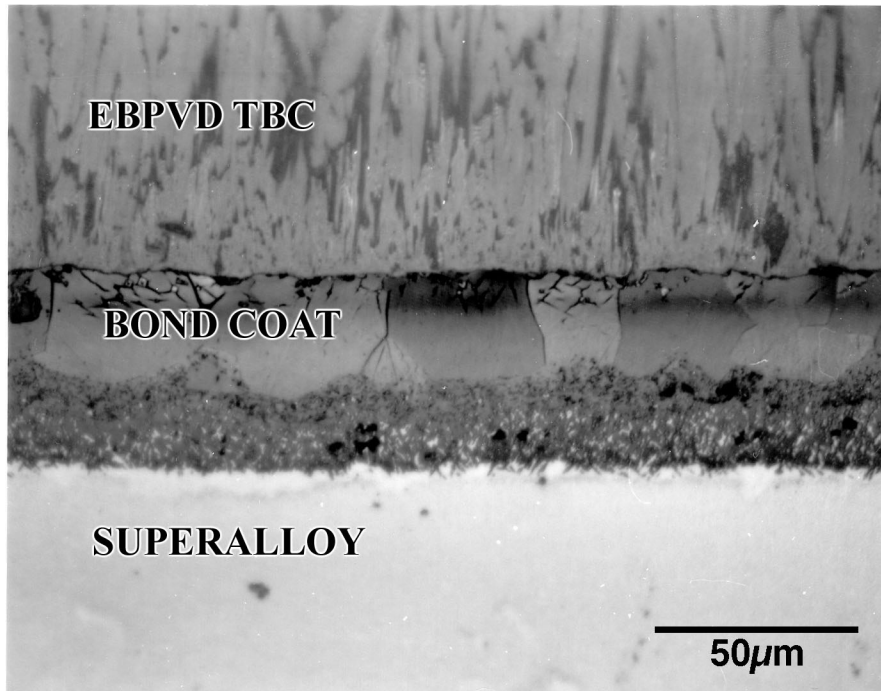
- The state of the art Pt Aluminide bond coats have irregular interfaces in the as-processed condition due to heavy grit blasting (Figure 66a). TBC defects, which are referred to as “Corn Kernel TBC defects”, develop at these surface irregularities, most probably due to shadowing effects during TBC deposition. The TBC constraint to deformation of the bond coat is weaker in the areas where these defects are present due to poorer bonding of the TBC segments to the rest of the TBC.

- With thermal exposure, the bond coat deforms plastically by the well known ratcheting mechanism. The ratcheting originates at the initial interface irregularities, which were usually associated with TBC defects, due to the combined effects of high stresses and the weaker TBC constraint at these sites (Figure 66b). The cracks, which initiated at these sites, propagate away

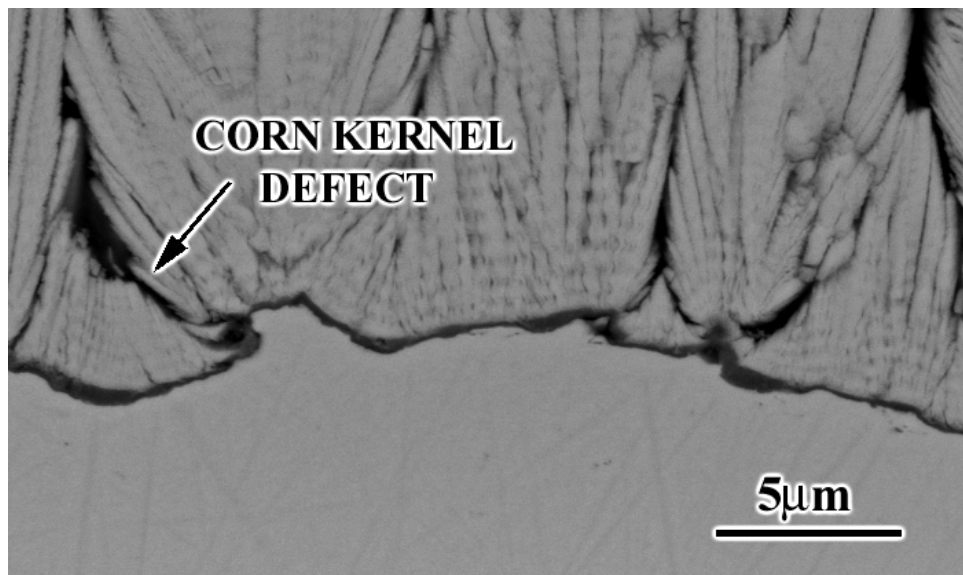
from these ratchets causing separations along the TGO/TBC interface. The TBC constraint also becomes weaker at these separated areas, which may lead to formation of new ratchets (Figure 66c).

-The failure occurs when these cracks in the vicinity of the ratcheted areas link up reaching a critical size. In this case, the failure is more along or close to the TGO/TBC interface (Figure 66d).

-On the other hand, the TGO/bond coat interface also becomes more susceptible to fracture due to stored strain energy in the TGO. If the amount of ratcheting is not very significant, the cracks that initiated in the vicinity of the ratchets can propagate through the TGO and then along the TGO/bond coat interface as the stored energy in the TGO increases (Figure 66e).

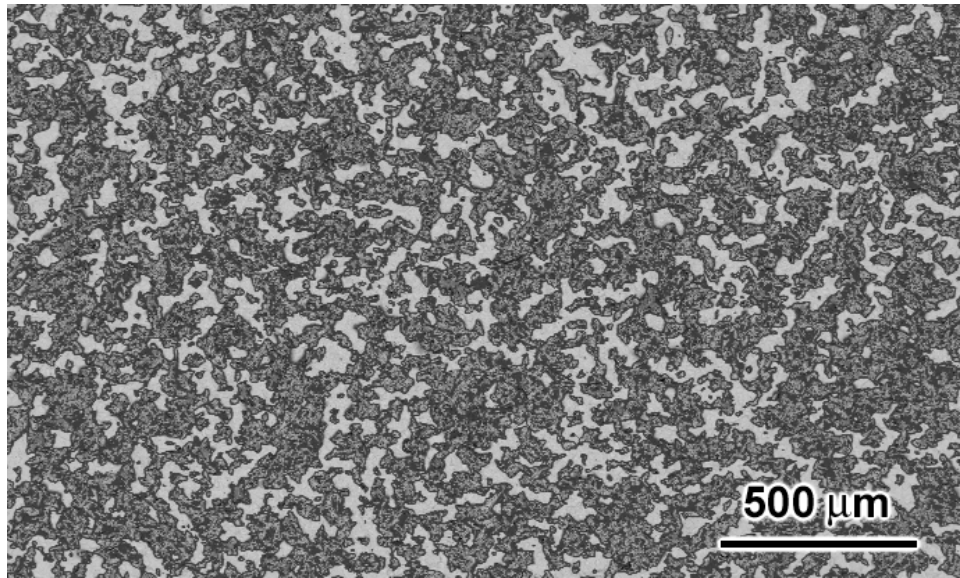


(a)

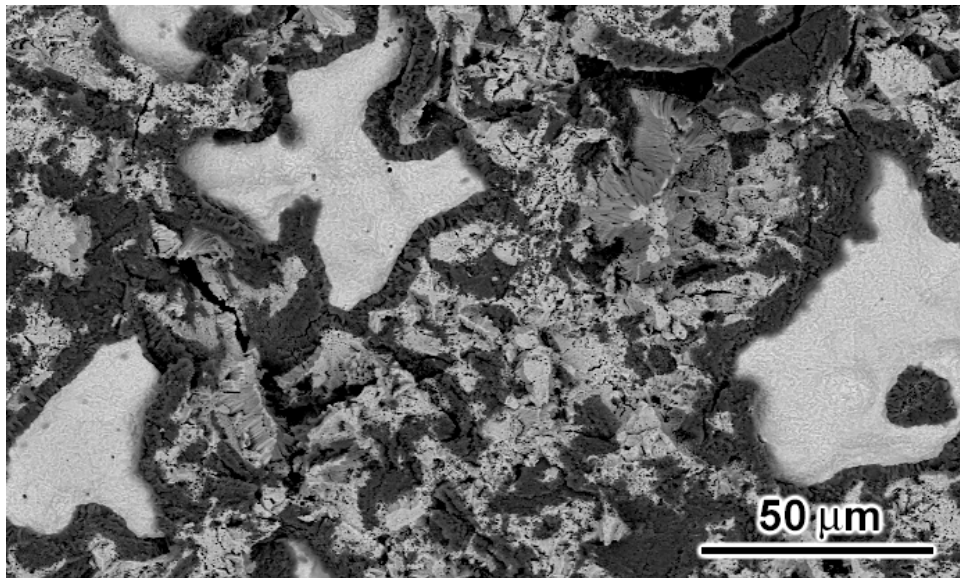


(b)

Figure 59 Scanning electron micrographs of typical state of the art TBC systems with Pt aluminide bond coats in the as processed condition. The microstructure consisted of only β phase with Pt, Cr and Co in solid solution (a). Corn Kernel TBC defects were present (b).

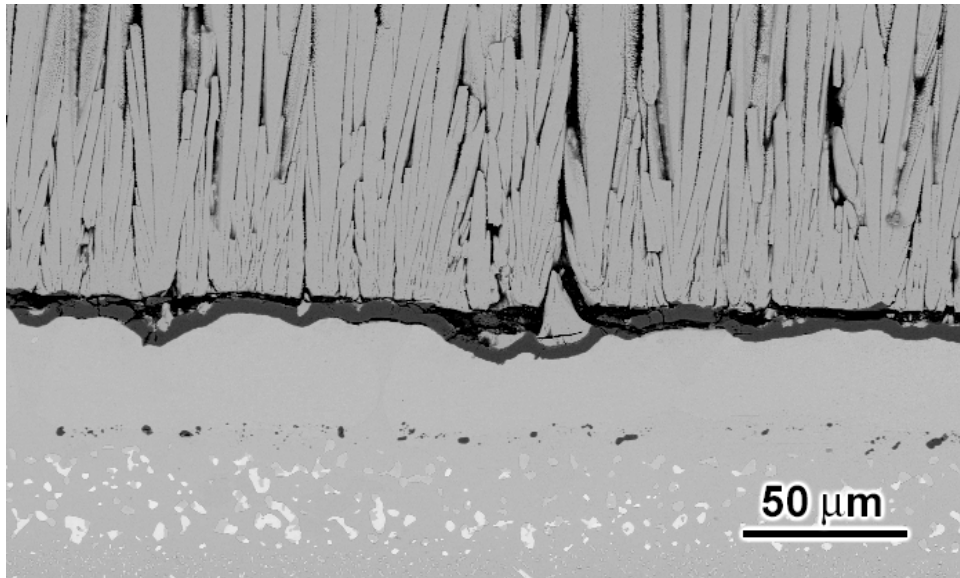


(a)

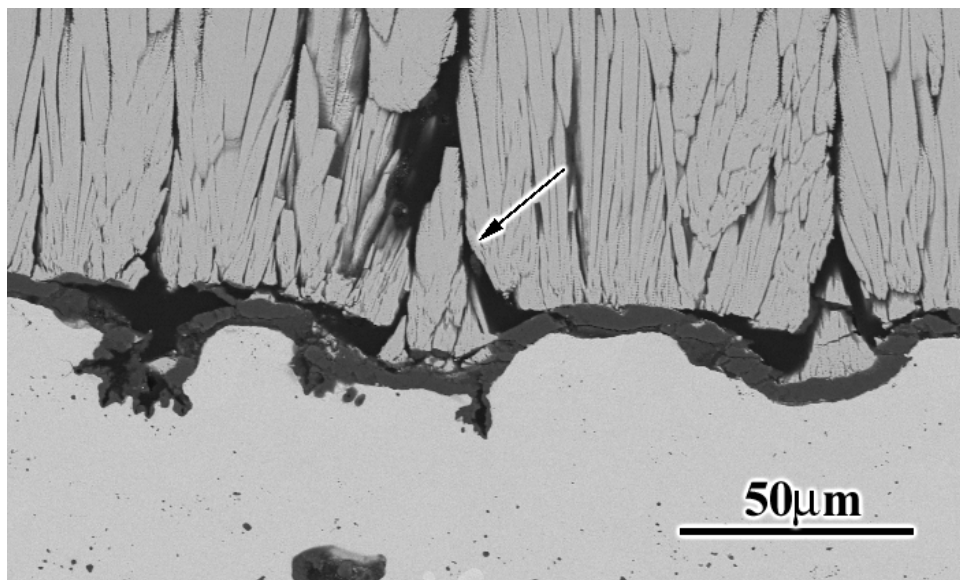


(b)

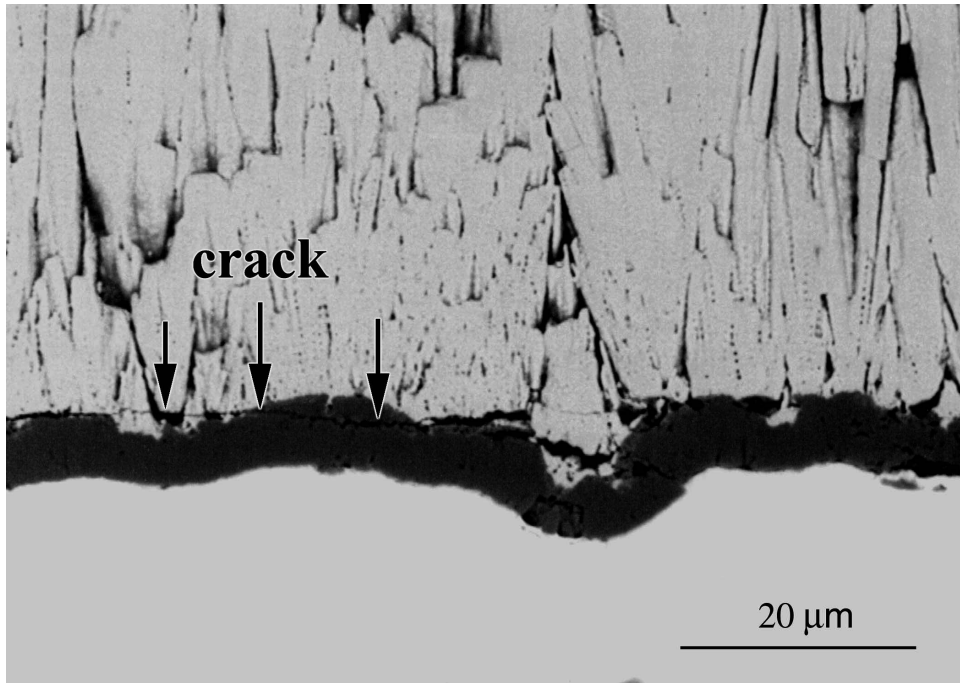
Figure 60 Scanning electron micrographs from the fracture surface of a state of the art TBC system with Pt Aluminide bond coat at (a) low and (b) high magnifications. A significant amount of failure was above the TGO/BC interface.



(a)

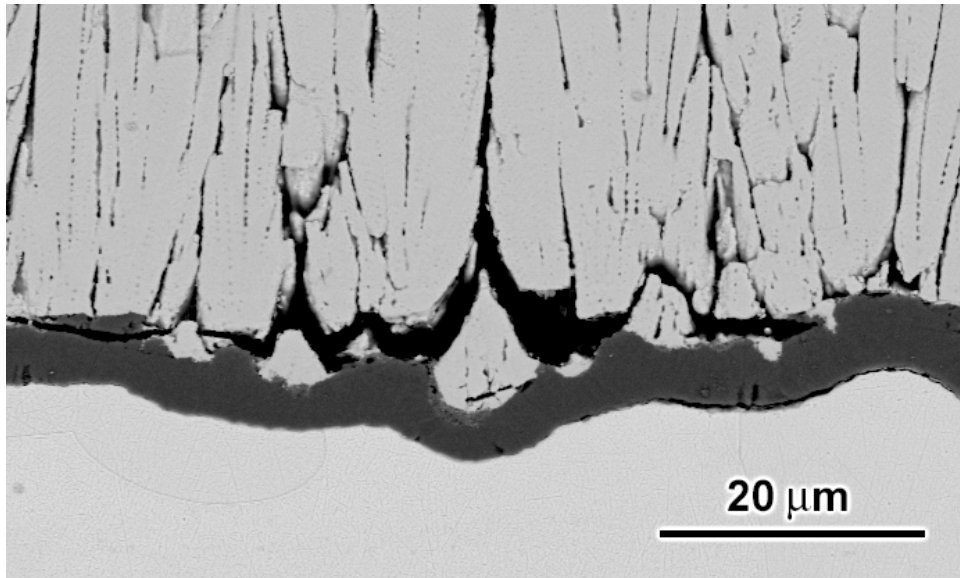


(b)

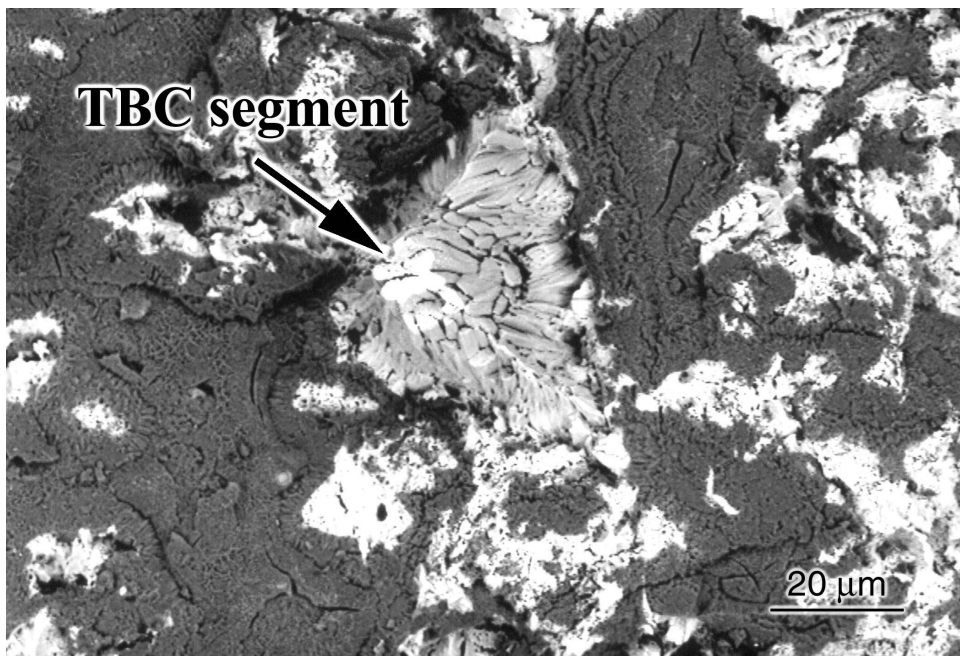


(c)

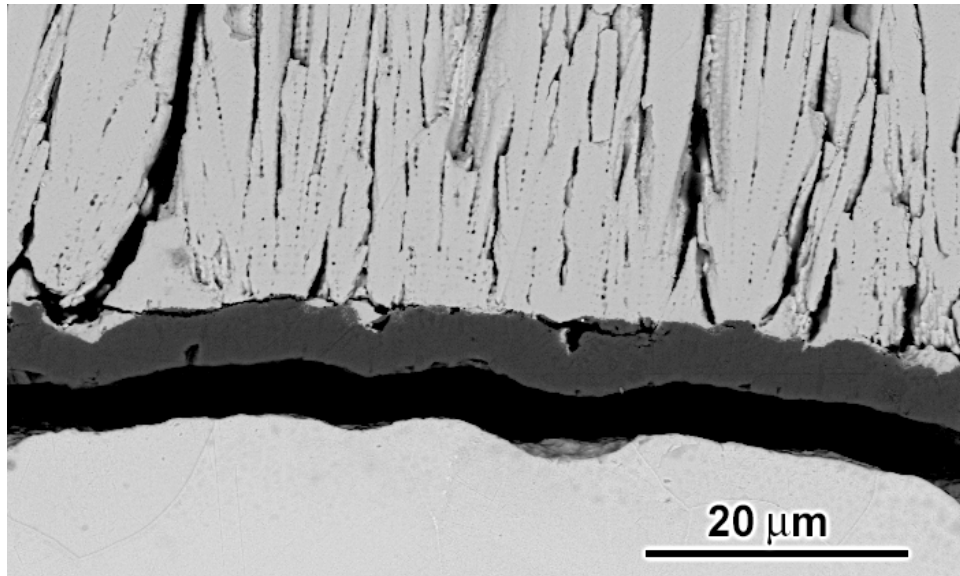
Figure 61 Scanning electron micrographs of TBC systems with state of the art Pt aluminide bond coats before (a), and after failure (b), both of which give examples to deformation of the bond coat with thermal exposure. Cracks initiate in the vicinity of the deformed areas (c).



(a)

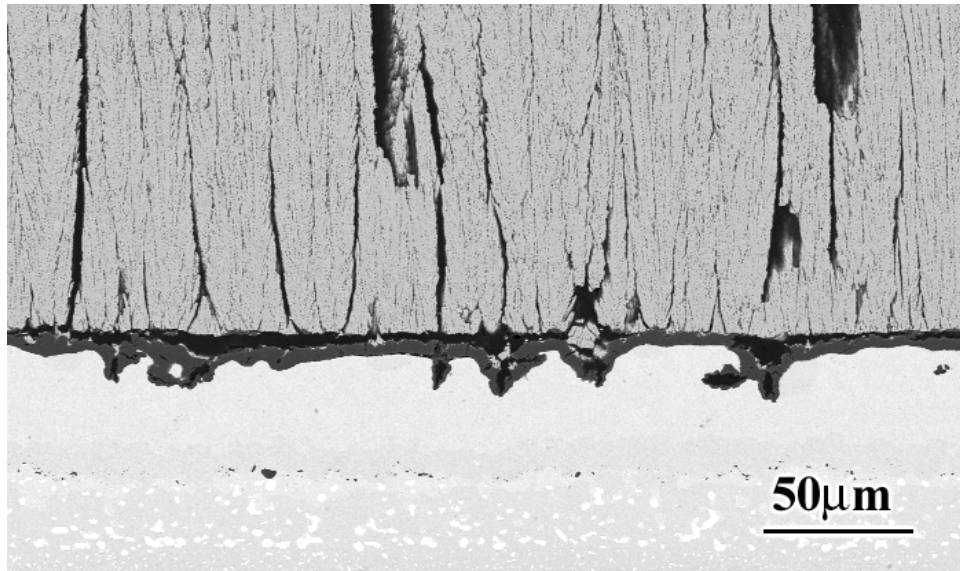


(b)

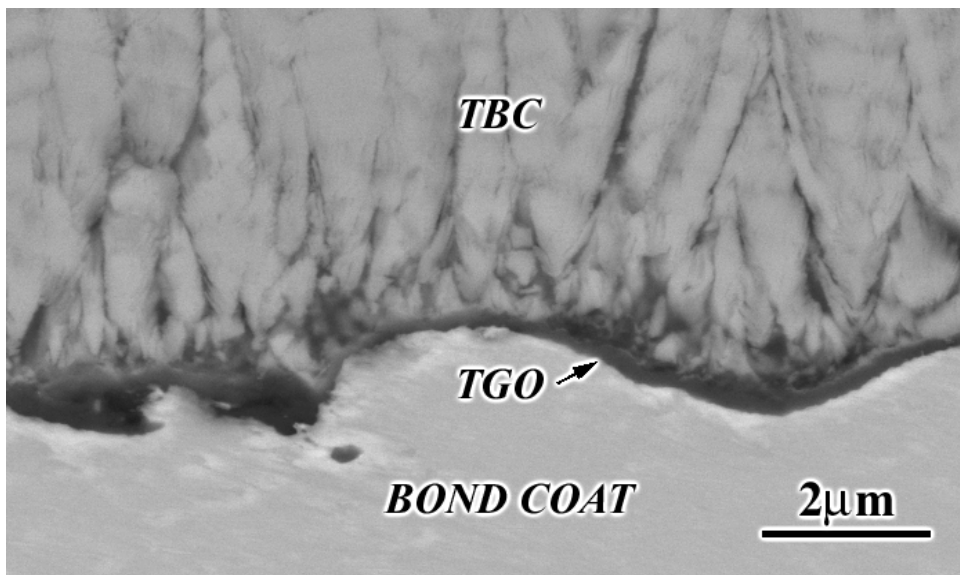


(c)

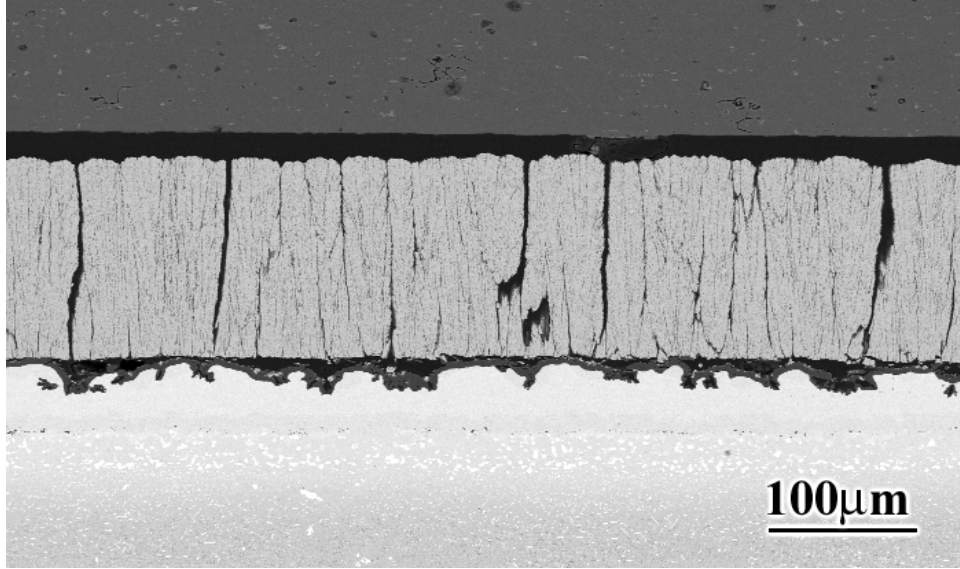
Figure 62 Scanning electron micrographs of state of the art TBC systems with Pt aluminide bond coats showing (a) ratcheting in the vicinity of corn kernel defects, (b) a TBC segment that was pulled from the TBC due to ratcheting at a corn kernel defect, (c) presence of a smooth interface in the absence of corn kernel defects.



(a)

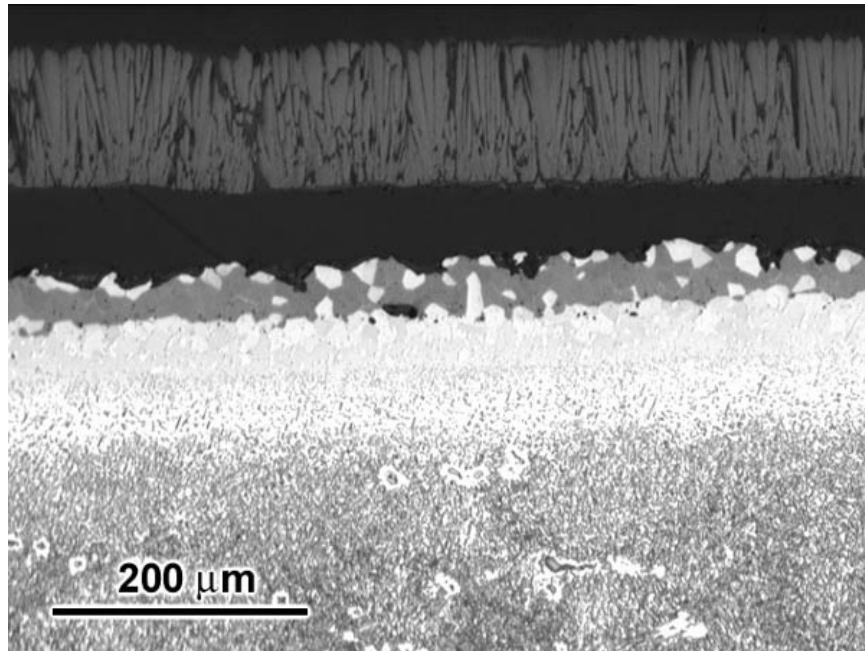


(b)

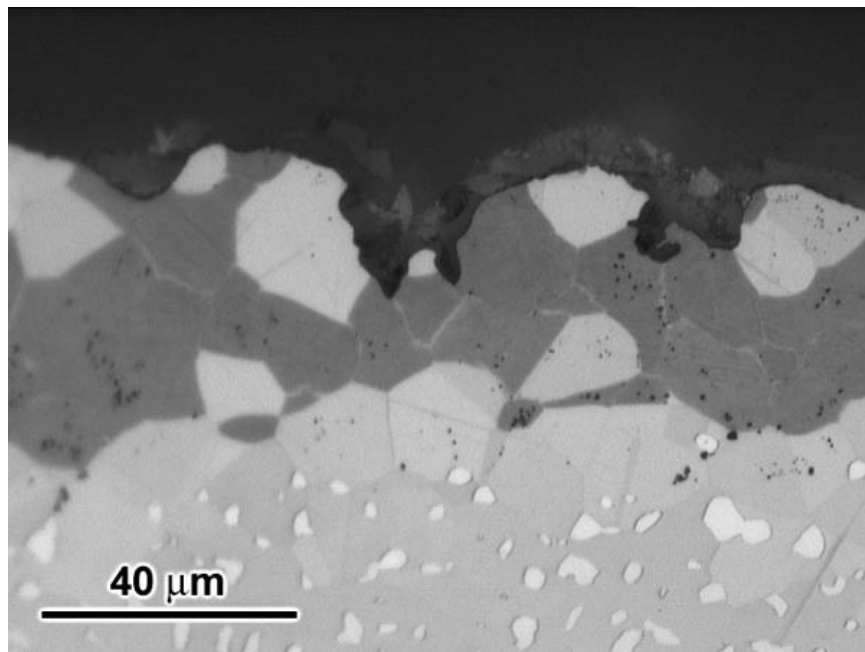


(c)

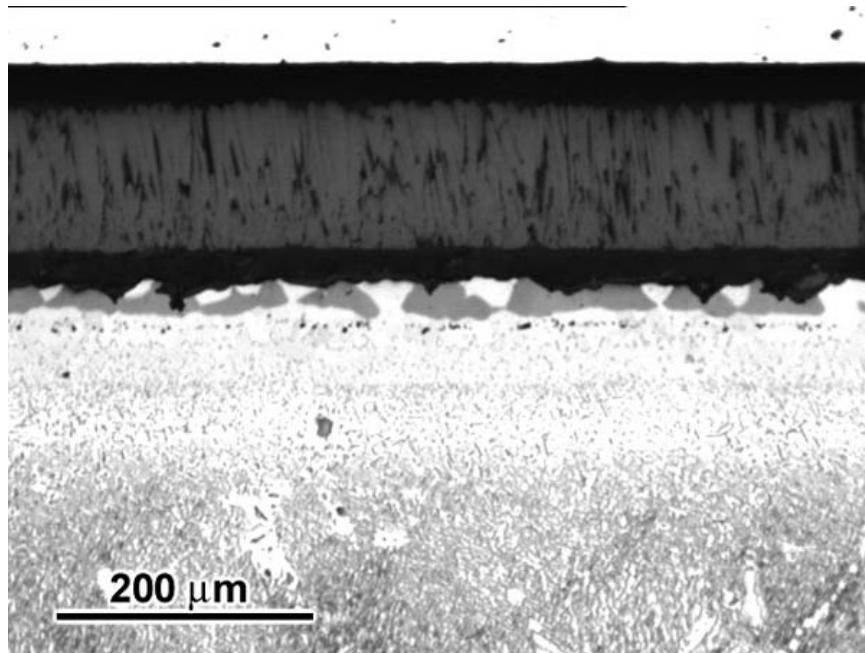
Figure 63 Scanning electron micrographs of a state of the art TBC system with Pt aluminide bond coat, which failed relatively early compared to its counterparts. There were significant amounts of ratcheting, (a), which were believed to be associated with the different TBC morphologies in the as processed condition, (b). This specimen also developed vertical separations in the TBC, (c).



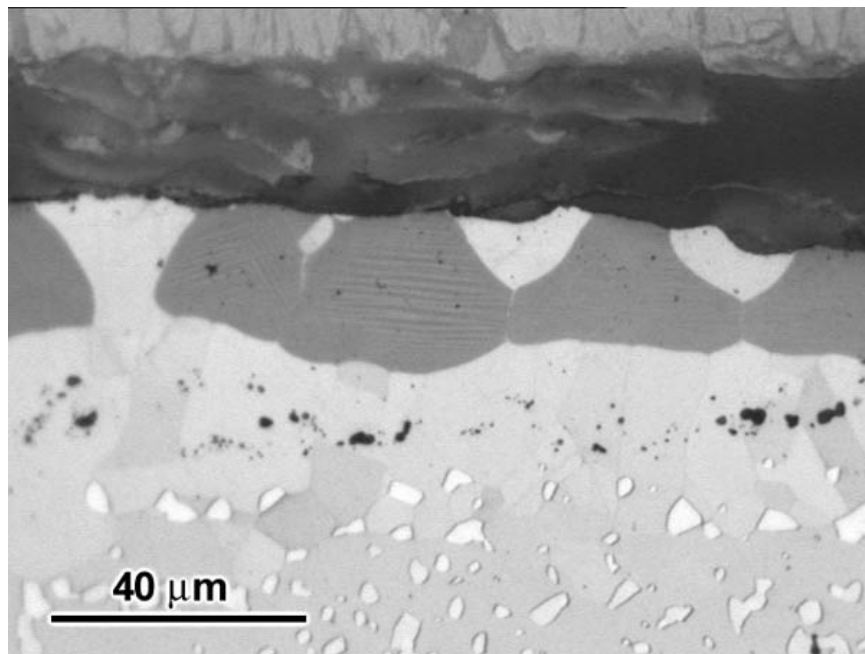
(a)



(b)

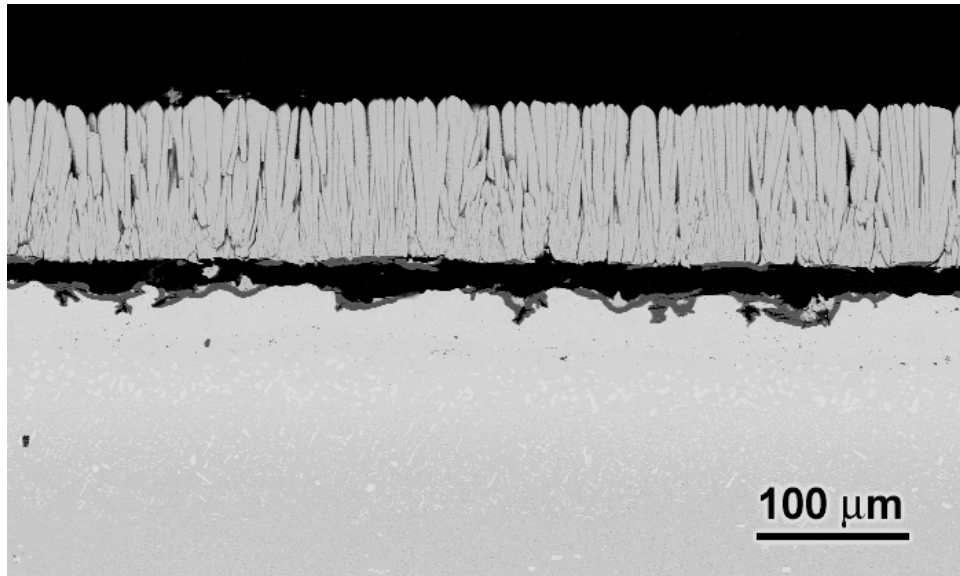


(c)

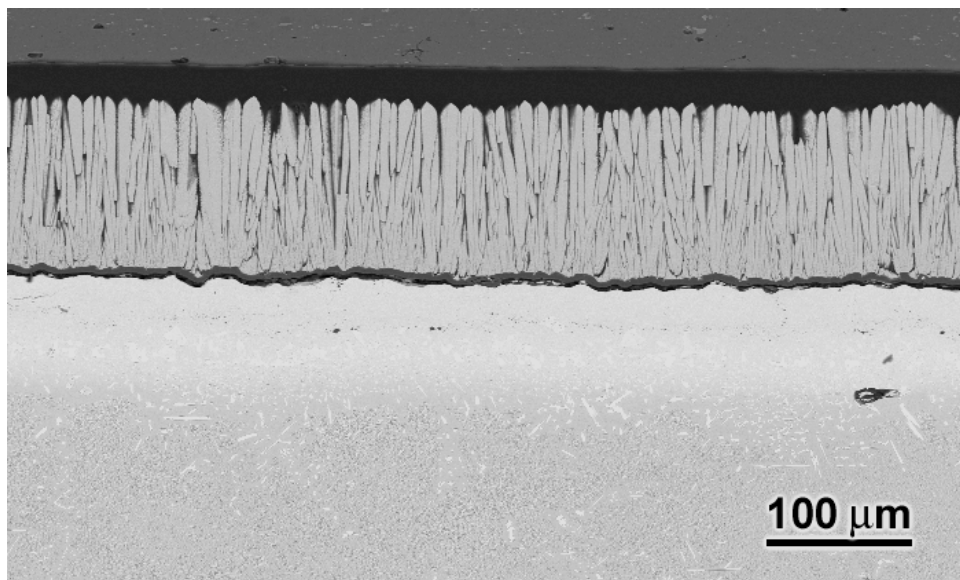


(d)

Figure 64 Optical micrographs of state of the art TBC systems with Pt aluminide bond coats with fine (a, b) and coarser grain size (c, d) at low and high magnifications. The amount of ratcheting was more pronounced for the specimens with finer grain size.



(a)



(b)

Figure 65 Scanning electron micrographs of state of the art TBC systems with Pt aluminide bond coats showing a marked difference in the amount of ratcheting for specimens which were subjected to cyclic, (a) and isothermal test, (b).

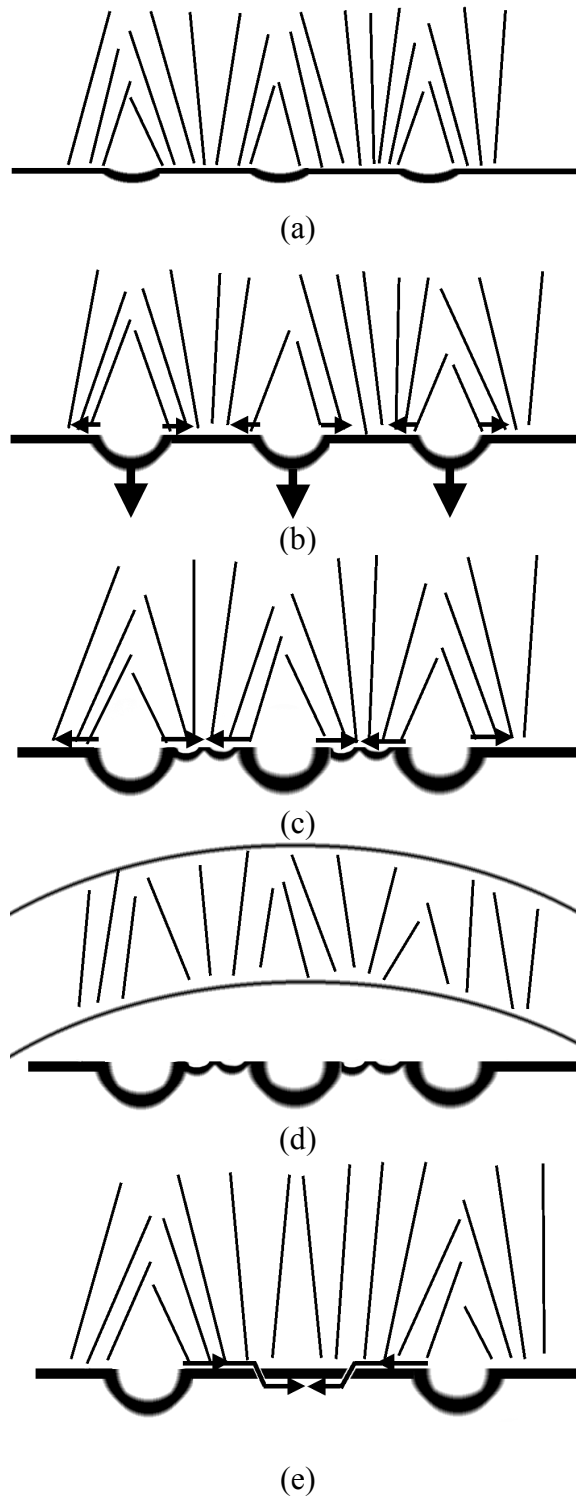


Figure 66 schematic diagram summarizing the failure behaviour of state of the art Pt Aluminide bond coats. See text for details

4.2.4 Modified TBC Systems

Based upon the tentative failure mechanisms formulated for the current state of the art TBC systems, some modifications were made to attempt to improve their lives. The failure characteristics of the modified TBC systems as well as the effects of modifications on their failure will be discussed in this section.

4.2.4.1 NiCoCrAlY Bond Coats TBC systems with NiCoCrAlY bond coats had various defects that contributed to their failures, as mentioned previously. Most of the modifications performed on these TBC systems minimized the defects to a certain degree, resulting in improvements. These modifications included: deposition of a Pt layer on the bond coat (Pt overlayer) and also on the superalloy substrate surface prior to deposition of the NiCoCrAlY bond coat (Pt underlayer), aluminizing the bond coat surface and performing different surface preparation techniques on the bond coats. Failure times for the modified TBC systems are given in Table 4. Again, the general characteristics of these modified systems will be given regardless of the different techniques used for the deposition of NiCoCrAlY bond coats.

Table 4 Failure times for the TBC systems with modified NiCoCrAlY Bond Coats

	Failure Time at 1100°C (# of 1 hr cycles to failure)
NiCoCrAlY- state of the art	40, 40, 40, 60, 60, 60, 76, 102, 102, 139
NiCoCrAlY Pt Underlayer	160, 160, 160, 560
NiCoCrAlY Aluminized	160, 220, 280, 380, 460
NiCoCrAlY Pt Overlayer	600, 880, 980, 1240, 1700
NiCoCrAlY MF-Pt Overlayer	520, 540
NiCoCrAlY MF-Pt Overlayer-MF	500, 620
NiCoCrAlY MF-Pt Overlayer-MF-preoxidation	500, 600
NiCoCrAlY Vibro Finish	40, 80
NiCoCrAlY Media Finish	80, 80
NiCoCrAlY Hand Polish	220, 720, 740, 1520+

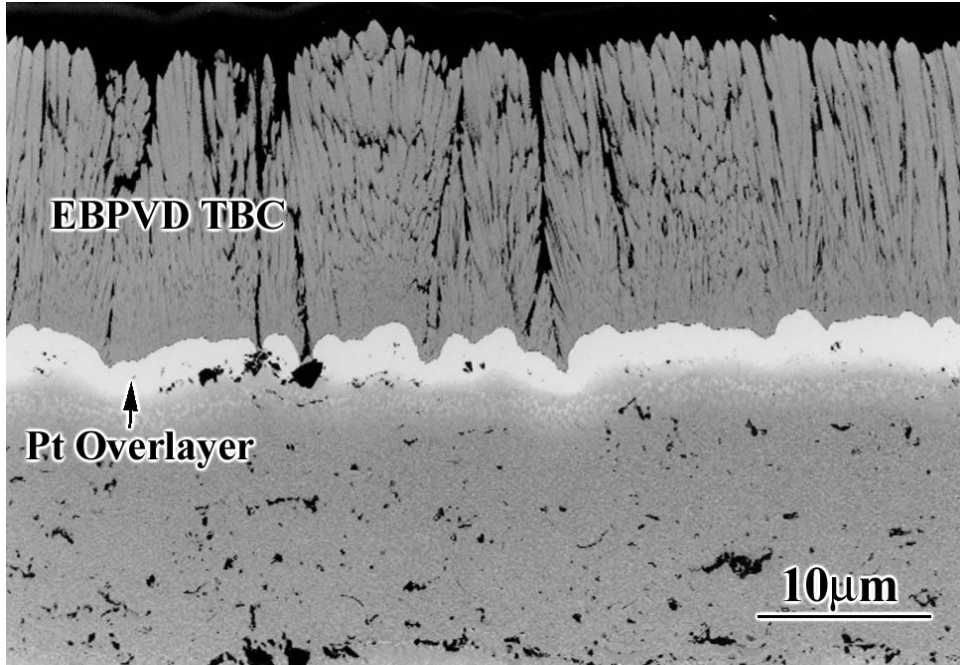
• **NiCoCrAlY Bond Coats with Pt Overlayer** - The surfaces of the as-processed TBC systems with Pt overlayers on NiCoCrAlY bond coats were highly irregular and numerous defects in the TBC were present as a result of this irregular interface (Figure 67a). In some localized areas, where large pieces of grit blast particles were embedded on the surface, the Pt layer did not develop continuity resulting in a defective area such as is evident in Figure 67b. On the other hand, a very uniform, continuous TGO, which was pure alumina, developed on the surface (Figure 67c). Moreover, the interface was free of the oxide inclusions, which were referred to as surface defects previously. Figure 68 gives the composition profile away from the interface. As can be seen from this profile, the bright layer is rich in Pt with small amounts of other elements (Ni, Al, Cr, Co), which diffused into the Pt layer during subsequent heat treatment as well as TBC deposition. An attempt was made to identify the platinum rich phase from Pt-Al-Ni ternary phase diagram [72]. However, the presence of Cr and Co complicated the identification. Therefore, transmission electron microscopy (TEM) and/or X-ray diffraction (XRD) analyses are required to determine this phase.

These specimens were also subjected to cyclic oxidation testing at 1100°C. Significant improvements in the lives of these TBC systems have been obtained in the presence of platinum overlayers as can be seen from Table 4. The failure was observed to be along the TGO/TBC interface as well as in the TGO and TBC (Figure 69a and 69b). Examination of these specimens prior to failure showed cracks initiating in the vicinity of the TBC defects (Figure 70a) and then they usually propagated in the TBC laterally, cutting through the TGO where the surface had a convex shape. These cracks, while they were propagating through the TGO, either linked-up (Figure 70b) or missed each other (Figure 70c) resulting in a fractured, layered alumina scale (Figure 70d). These cracks almost never propagated along the TGO/Pt overlayer interface, which

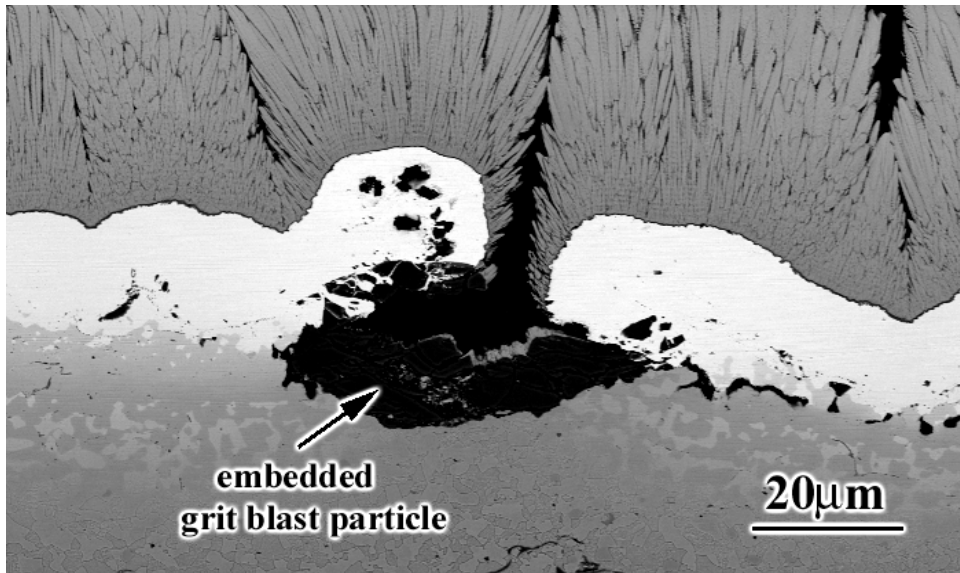
suggests a high interfacial toughness. A substantial amount of oxidation was also observed at the initial bond coat/Pt overlayer interface (Figure 71). This may be the combined result of rapid oxygen transport through the large surface defects present in the as-processed condition (Figure 67b) and the lack of adequate adhesion at the initial bond coat/ Pt overlayer interface due to surface defects present in the bond coats. All these results led to the idea of even greater improvements that might be obtained by applying proper surface preparation techniques before and after the deposition of the Pt overlayers. On the other hand, the initially irregular interface might have had beneficial effects due to reduced strain energy in the presence of parallel cracks that run in the TGO. This possibility was also considered. To clarify these uncertainties, new samples with surface modifications were prepared. These modifications included: deposition of Pt overlayers onto media finished NiCoCrAlY bond coats, media finishing the Pt overlayers that were deposited onto media finished NiCoCrAlY bond coats and preoxidizing the media finished Pt overlayers deposited onto media finished NiCoCrAlY bond coats. The failure times for these specimens were relatively short compared to the first batch of NiCoCrAlYs with Pt overlayers (Table 4). Unfortunately, these specimens had even more irregular interfaces with many associated defects in the TBC (Figure 72a) from which significant amounts of failure were observed to propagate (Figure 72b). These results showed that the surface irregularities might also develop during electro-plating of Pt itself, probably due to the dendritic growth of Pt. Media finishing performed after the deposition of the Pt layer was not very effective for smoothing the surface (Figure 72c), resulting in similar failure behavior.

The alumina scales developed on these systems were rather pure in contrast to the alumina scales developed on the state of the art NiCoCrAlY systems. It seems that the presence of a platinum overlayer on the surface promoted the selective oxidation of aluminum preventing

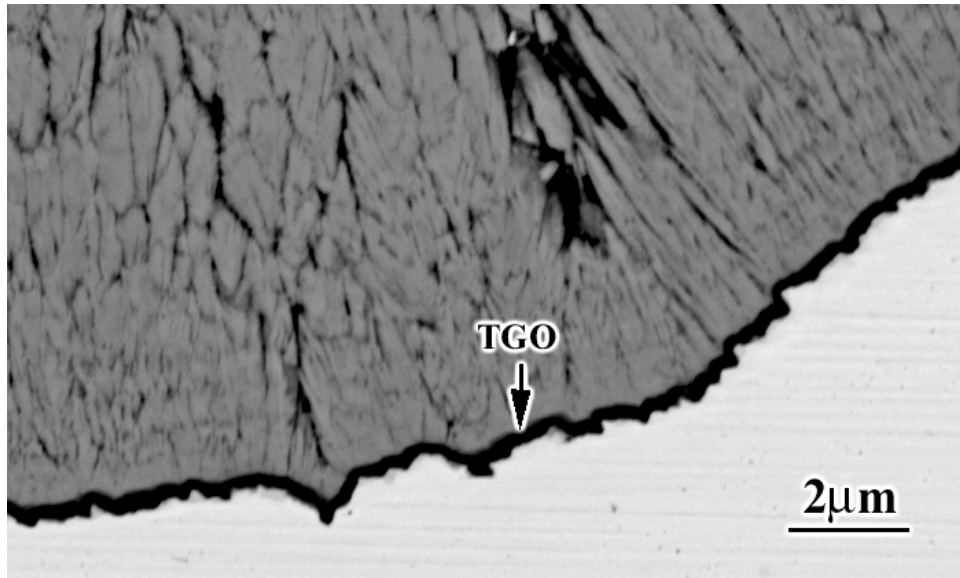
the formation of transient oxides. Moreover, the alumina scale was still adherent to the bond coat in most places even after much longer exposure times compared to the failure times of the state of the art NiCoCrAlY systems. The strong adherence of the TGO on these bond coats may be a result of improved inherent interfacial toughness in the presence of Pt as well as the lack of defects along the TGO/bond coat interface that were identified for the state of the art TBC systems. In summary, the improved performance of TBC systems with Pt overlayers seems to result from the development of pure and adherent alumina scales. If we disregard the thickness of the continuous layer of intermixed zone that developed at the early stages of oxidation, the growth rate of the pure alumina underneath was slower compared to the growth rate of the aluminas that developed on the state of the art NiCoCrAlY systems as can be seen from the diagram given in Figure 73. Therefore, the slower TGO growth rate can also be another contributing factor in their improved performance. On the other hand, the effects of smooth interfaces with Pt overlayers still need to be examined to see whether more significant improvements can be obtained by minimizing the TBC defects.



(a)



(b)



(c)

Figure 67 Scanning electron micrographs of a TBC system with a Pt overlayer on NiCoCrAlY bond coat in the as processed condition showing (a) highly irregular interface with associated TBC defects, (b) defective areas in the vicinity of large embedded grit blast particles, (c) very uniform and continuous TGO.

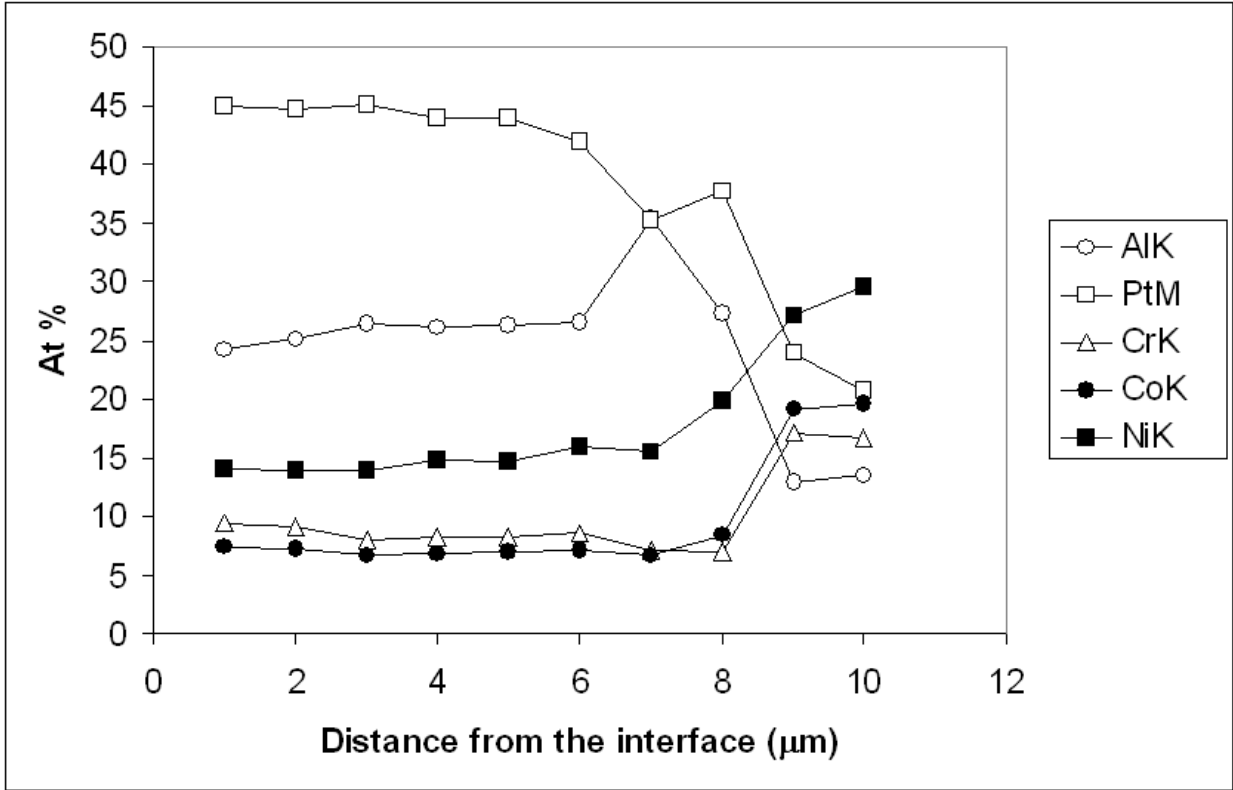
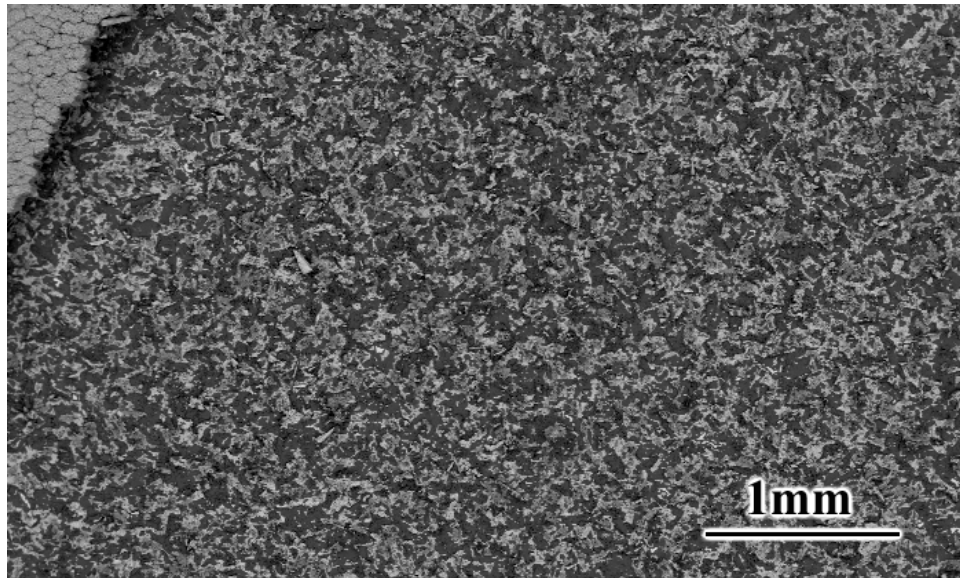
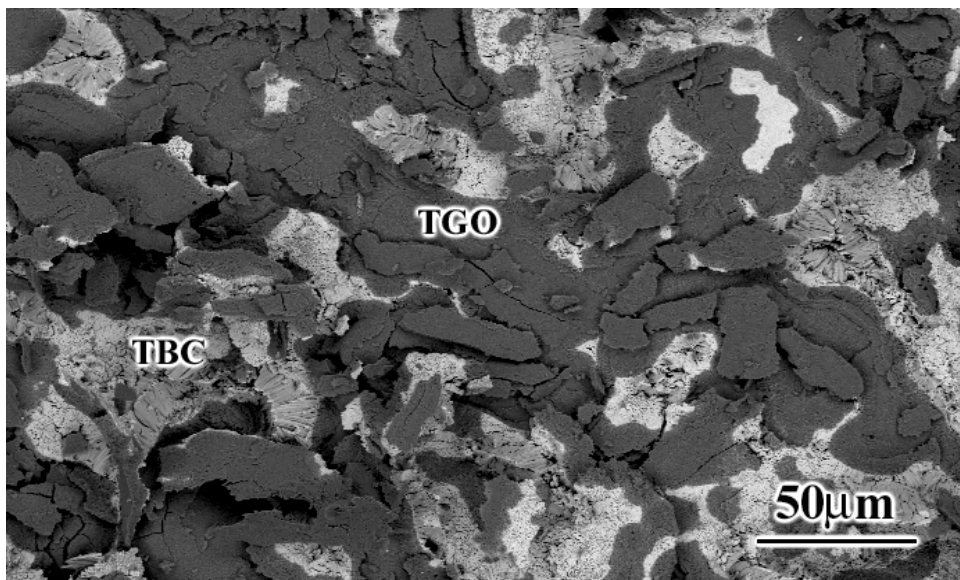


Figure 68 Composition profile away from the TGO/TBC interface for an as processed TBC system with Pt overlayer on NiCoCrAlY bond coat

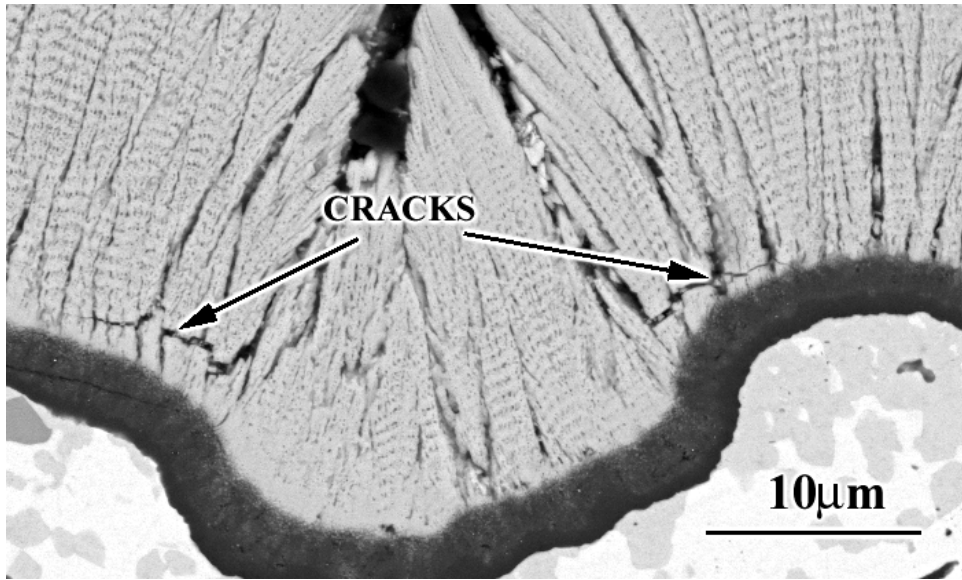


(a)

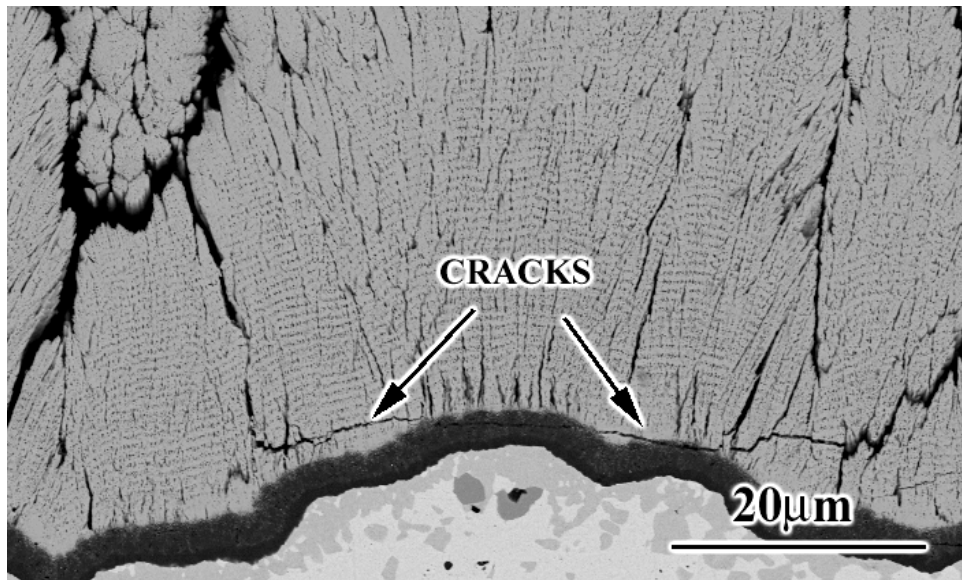


(b)

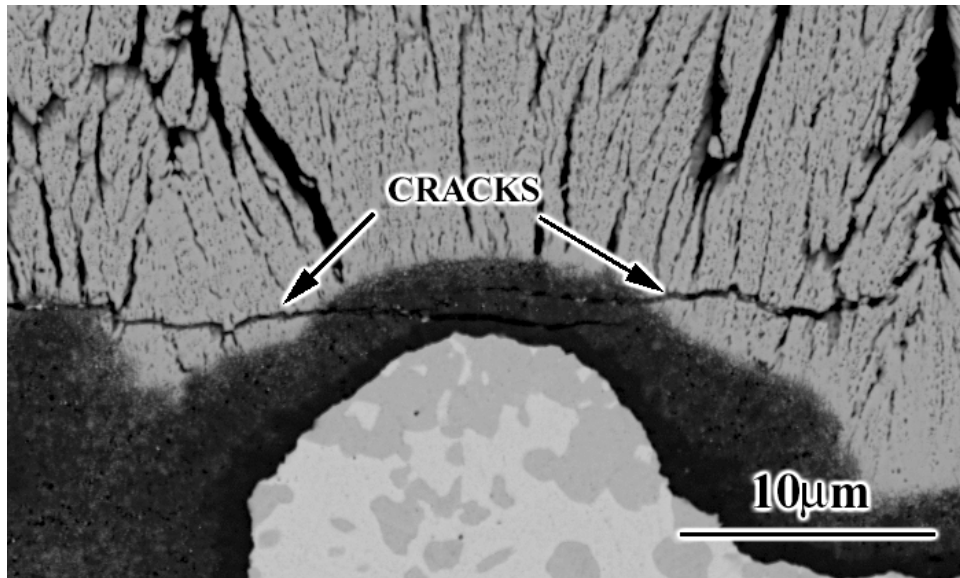
Figure 69 Fracture surface of the TBC system with Pt overlayer on the NiCoCrAlY bond coat showing that the failure was mainly along the TGO/TBC interface, as well as in the TBC and in the TGO (a). A higher magnification micrograph from the fracture surface is presented in (b).



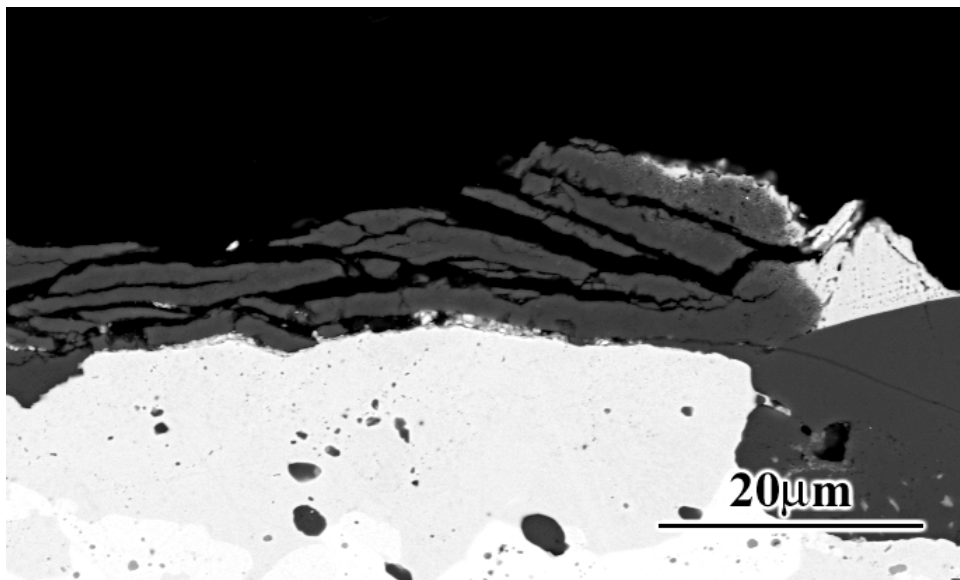
(a)



(b)



(c)



(d)

Figure 70 Scanning electron micrographs of the TBC system with Pt overlayer on the NiCoCrAlY bond coat after exposure at 1100 °C for 40 cycles showing that the cracks that initiated at TBC defects, (a), either linked up, (b), or missed each other, (c), causing a layered alumina scale, (d).

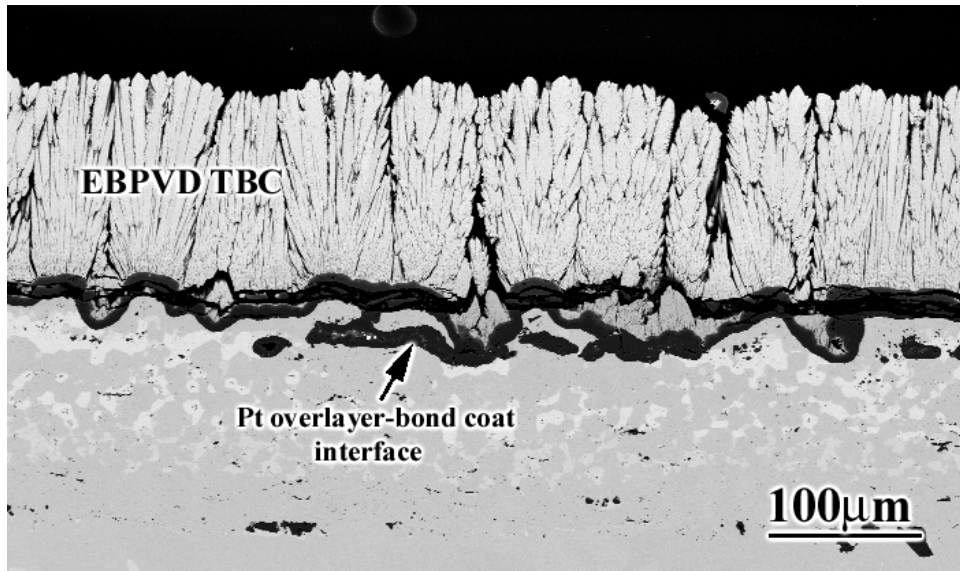
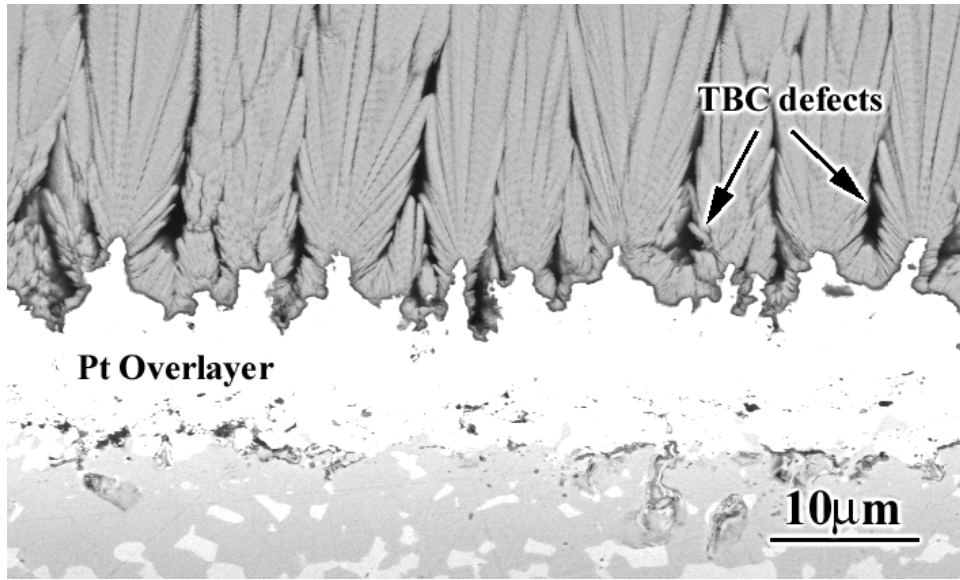
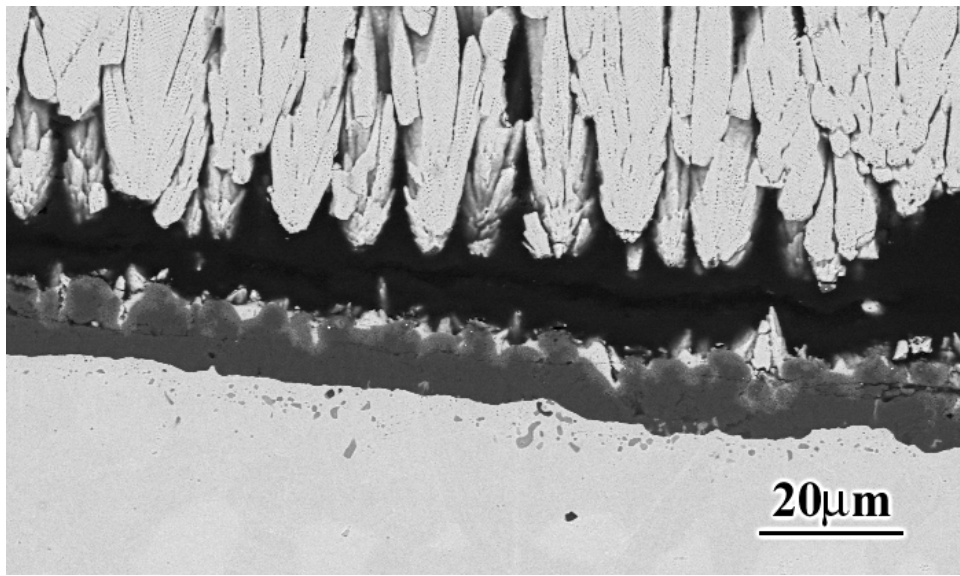


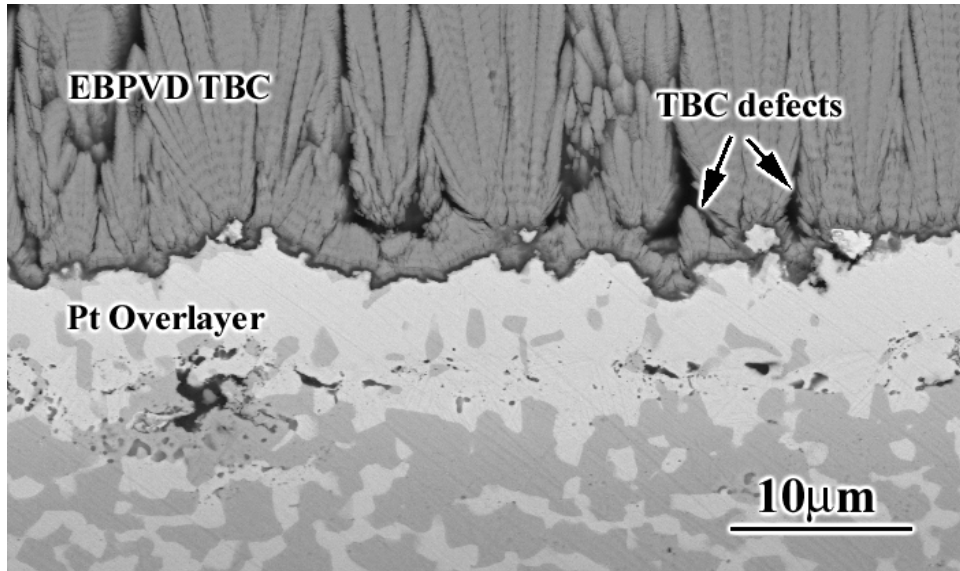
Figure 71 Scanning electron micrograph of the TBC system with Pt overlayer on the NiCoCrAlY bond coat after it failed, showing the extensive amount of oxidation along the initial bond coat/ Pt overlayer interface



(a)



(b)



(c)

Figure 72 Scanning electron micrographs of the TBC systems with Pt overlayer on the media finished NiCoCrAlY bond coats. The interface was highly irregular with associated TBC defects, (a), from which significant amounts of failure were observed to propagate, (b). The interface of the specimen that was given media finish after Pt deposition was still irregular, (c).

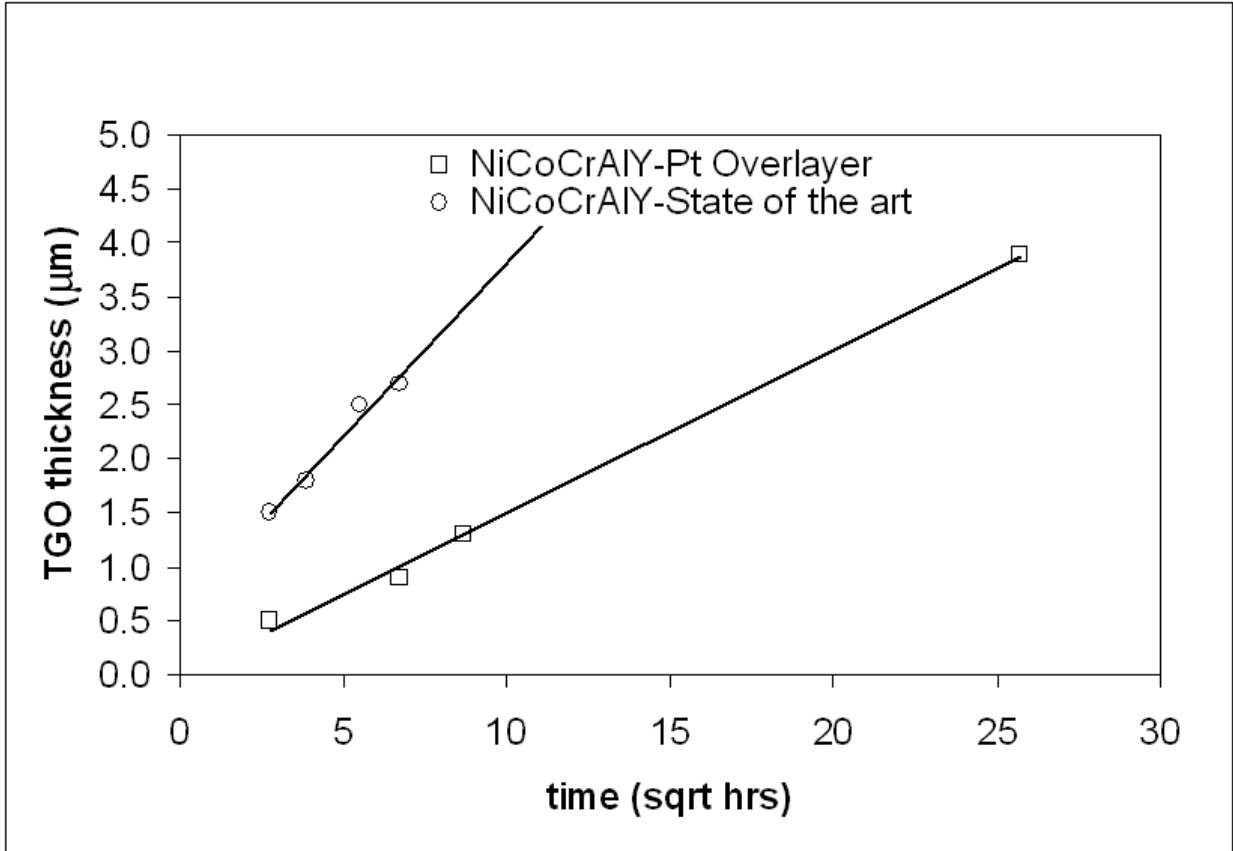


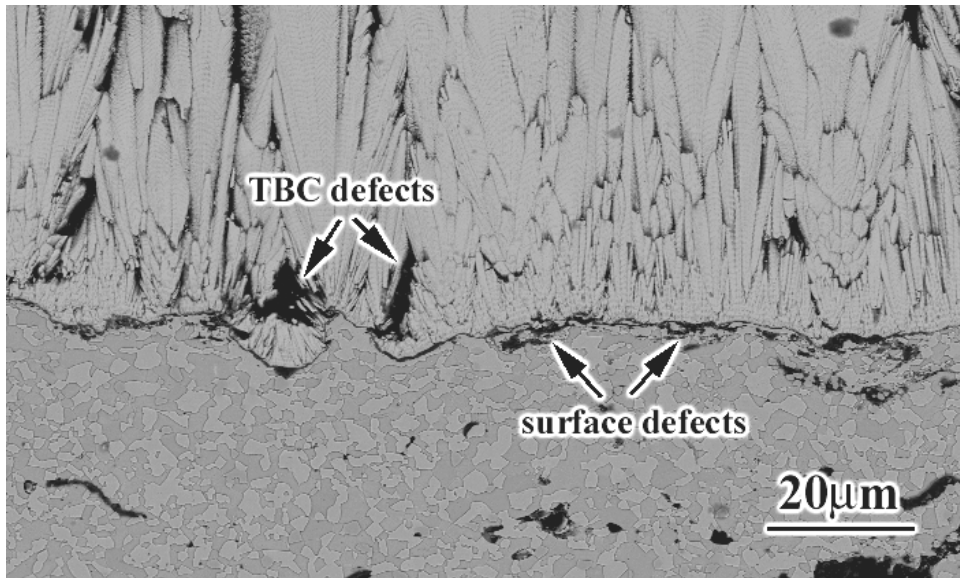
Figure 73 The TGO thickness vs square root of time for the TBC systems with Pt overlayer on NiCoCrAlY bond coat and state of the art NiCoCrAlY bond coat at 1100°C showing that the growth of the pure alumina underneath the intermixed zone for specimens with Pt overlayers was slower compared to the growth of the TGO on the state of the art NiCoCrAlY systems.

- **NiCoCrAlY Bond Coats with Pt Underlayer** - Pt has been known to inhibit the outward diffusion of substrate elements to the surface in the case of Pt aluminide diffusion coatings [73]. The fact that substrate elements have also been observed close to the TGO-NiCoCrAlY bond coat interface led to the idea of performing this modification for these TBC systems also. The objective was to see whether these elements contributed to the failure of these TBC systems.

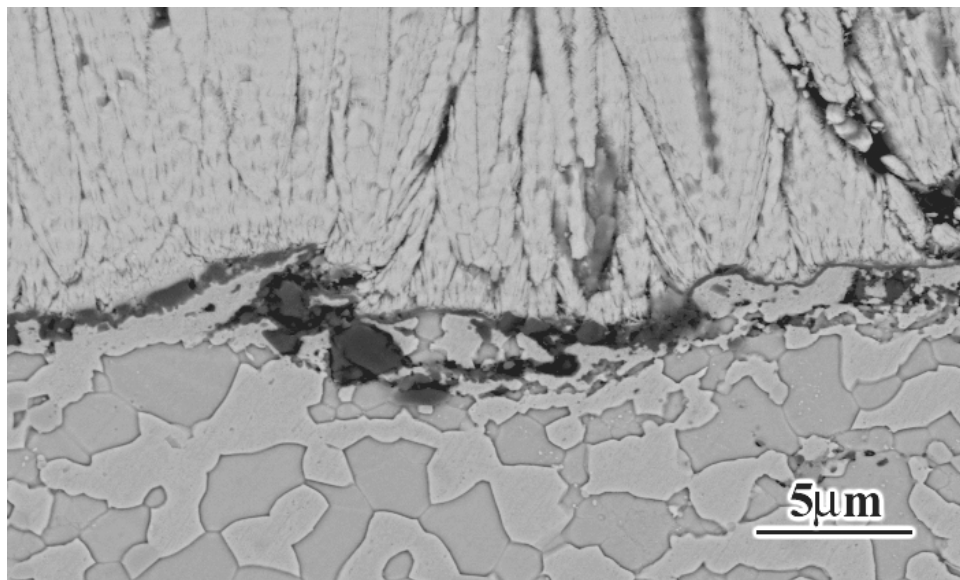
Even though there was some improvement in the lives of NiCoCrAlY systems in the presence of Pt underlayers, it was not significant compared to improvements achieved with other modifications. Cross sectional examination of these TBC systems in the as-processed condition did not show any difference in terms of the as-processed defects observed for the current state of the art TBCs. Figure 74a shows the surface defects and the highly irregular interface with associated TBC defects whereas Figure 74b shows the very non-uniform TGO, which is not always pure alumina.

The general failure behaviour of these systems was also very similar to those without any modification. The failure was mainly along the TGO/bond coat interface with numerous excursions into the TGO and TBC (Figure 75a). The typical features observed on the fracture surfaces were reactive element rich oxide protrusions (Figure 75b), oxide inclusions (Figure 75c), transient oxides and TBC segments (Figure 75d). Figure 75e is a cross sectional micrograph from the failed specimen showing damage in the vicinity of transient oxides and TBC defects. Some localized separation along the initial Pt underlayer / superalloy interface was also observed (Figure 75f), which is not believed to have contributed to failure in this case. However, this observation shows the likelihood of separations along this interface, which may result in complete detachment of the bond coat.

Substrate elements in solid solution were observed close to the TGO/bond coat interface for these systems. This observation rules out the role of substrate elements in the slight improvement obtained with a Pt underlayer. TGO growth rate can also be ruled out since a difference in the TGO thickness could not be observed (Figure 76). Pt was found in solid solution near the interface. One possible explanation for the longer lives of these systems may be the effect of Pt in improved adherence along the TGO/bond coat interface. Figures 77a and 77b are cross sectional micrographs from the state of the art NiCoCrAlY systems and the NiCoCrAlY systems with Pt underlayer, respectively, after 20 cycles of exposure at 1100°C and before failure. There was separation along the TGO/bond coat interface for the state of the art NiCoCrAlY systems due to metallographic preparation whereas it was still adherent for the ones with a Pt underlayer. If the separation during metallographic preparation can be considered as a simple adhesion test, assuming that every single step in sample preparation is the same, the lack of separation in the presence of the Pt underlayer shows improvement in adherence. In summary, the slight improvement obtained by using Pt underlayers is believed to be a result of improved inherent interfacial toughness. However, more work is required to fully understand the Pt effect on the improved interfacial toughness in these systems.

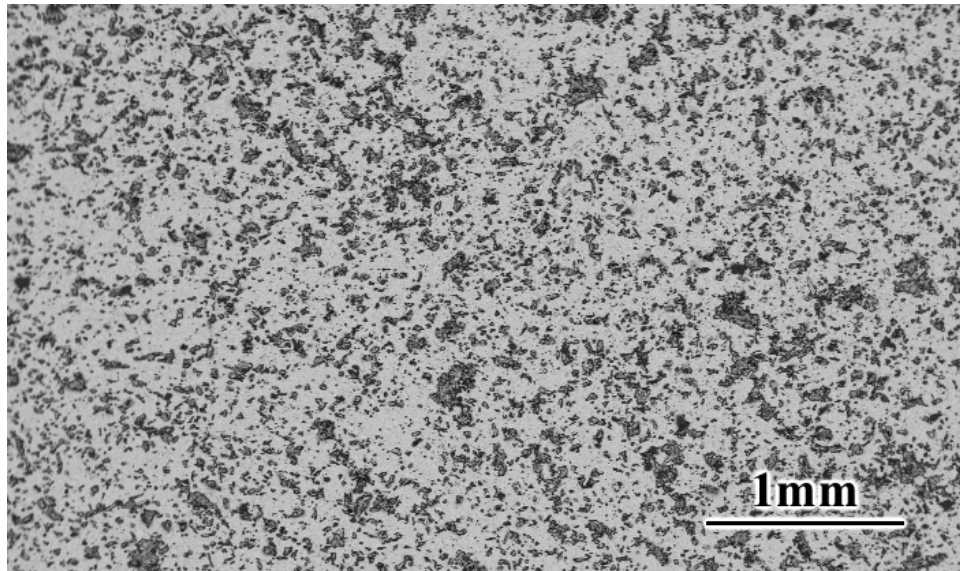


(a)

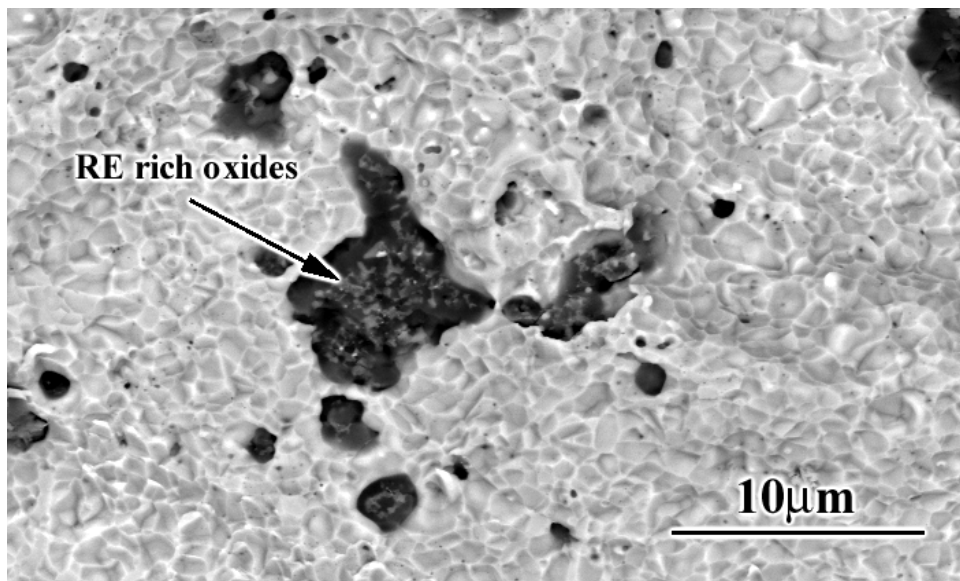


(b)

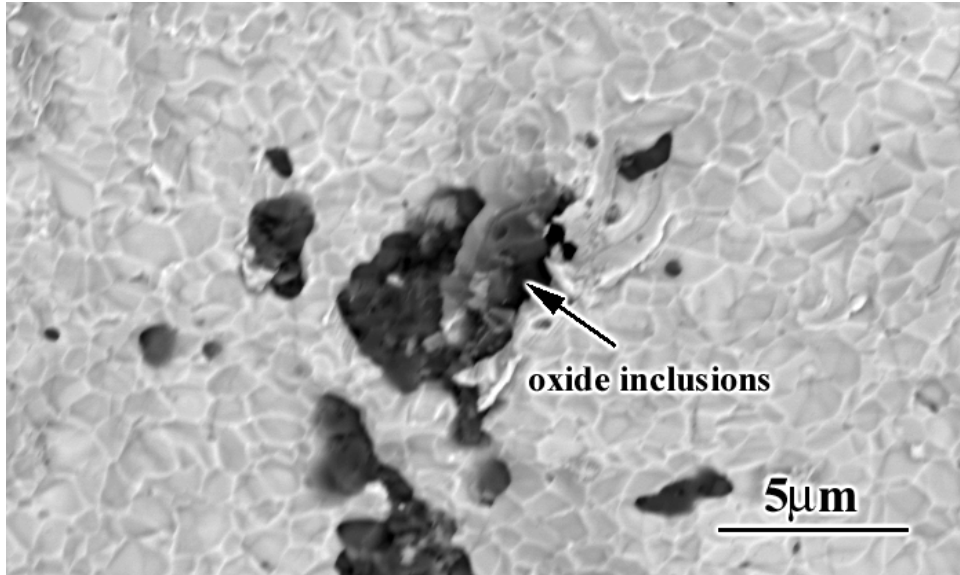
Figure 74 Scanning electron micrographs of the TBC systems on NiCoCrAlY bond coats with Pt underlayers in the as processed condition. Surface as well as TBC defects were evident, (a). The TGO was very non-uniform, (b).



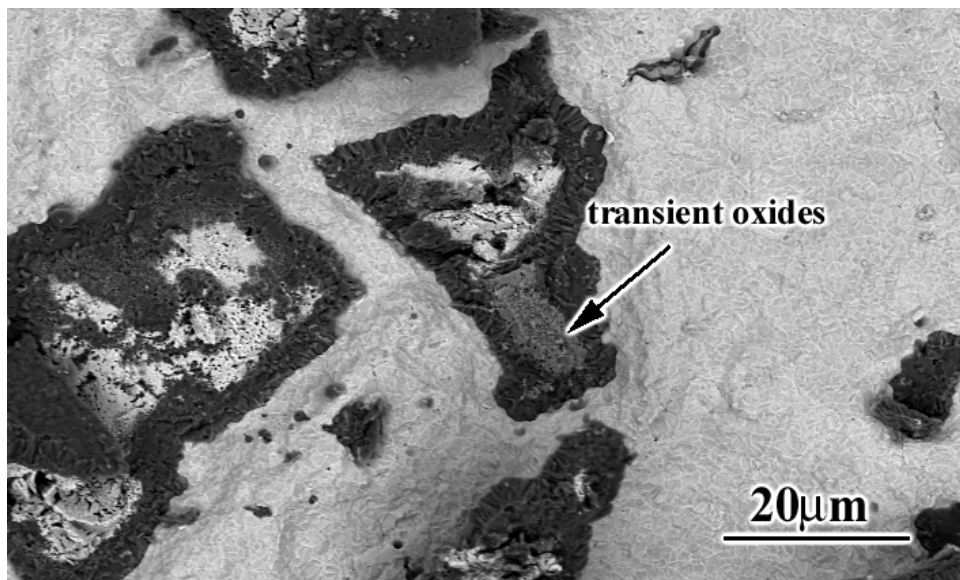
(a)



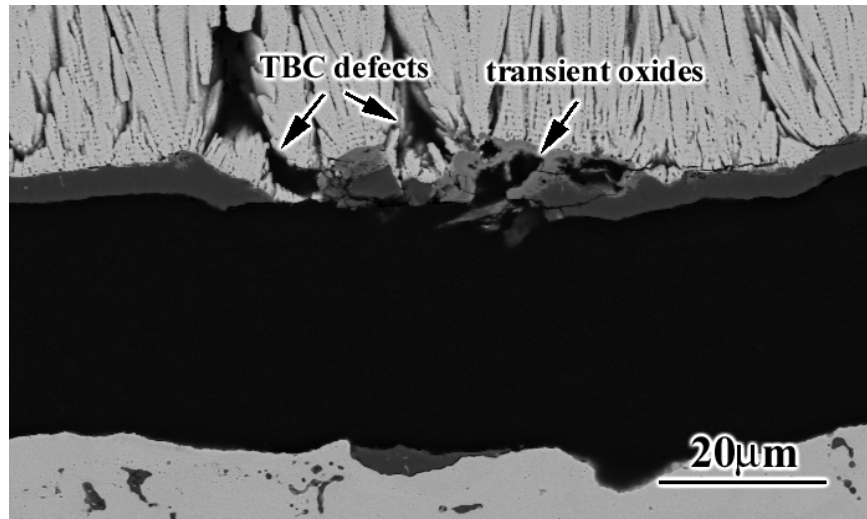
(b)



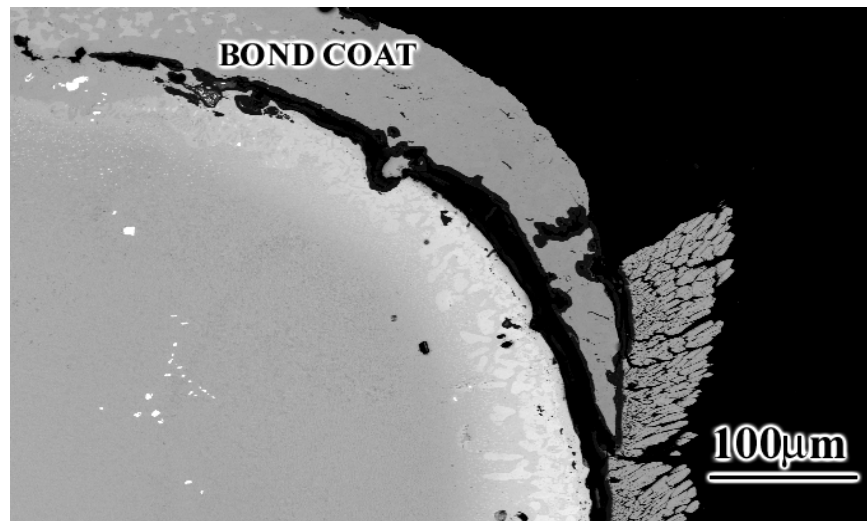
(c)



(d)



(e)



(f)

Figure 75 Scanning electron micrographs of TBC systems on NiCoCrAlY bond coats with Pt underlayers after failure showing the fracture path (a), as well as typical features observed on the fracture surfaces such as RE rich oxides, (b), oxide inclusions, (c), transient oxides and TBC segments, (d). A cross sectional micrograph indicating damage in the vicinity of transient oxides and TBC defects is presented in (e). It is also possible to get separation along the Pt underlayer- superalloy interface (f).

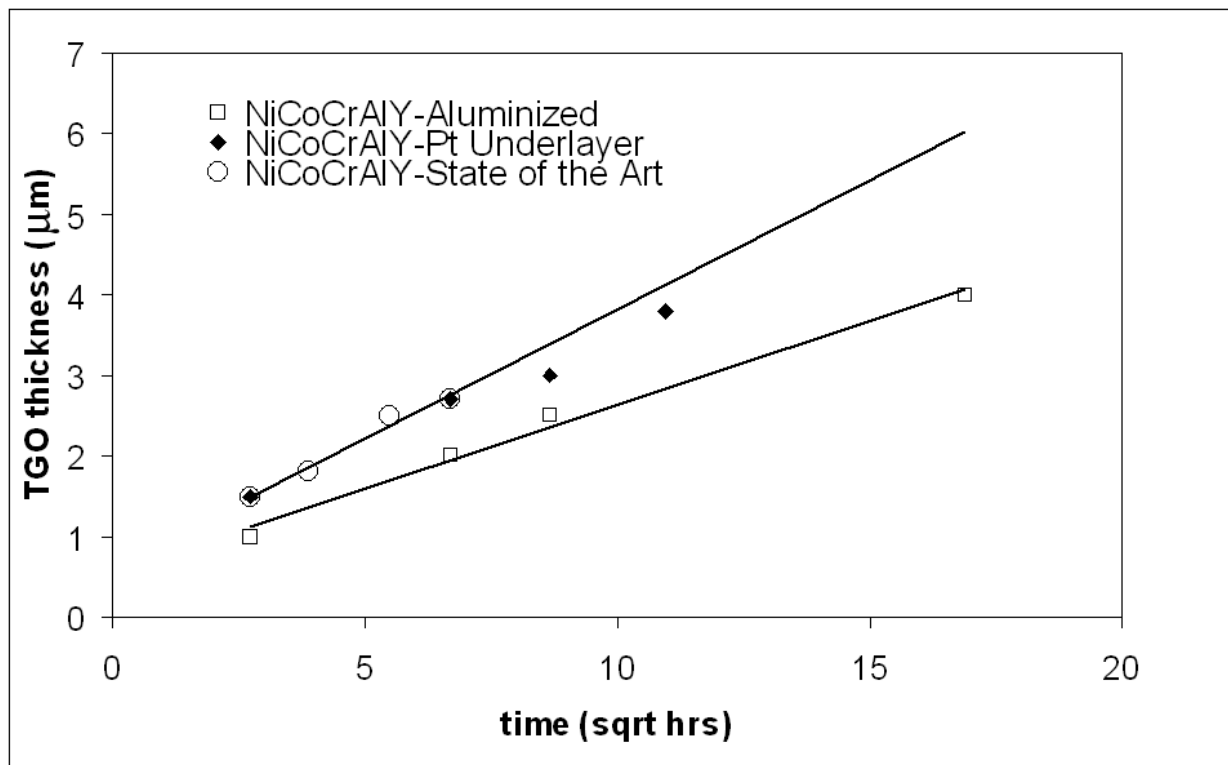
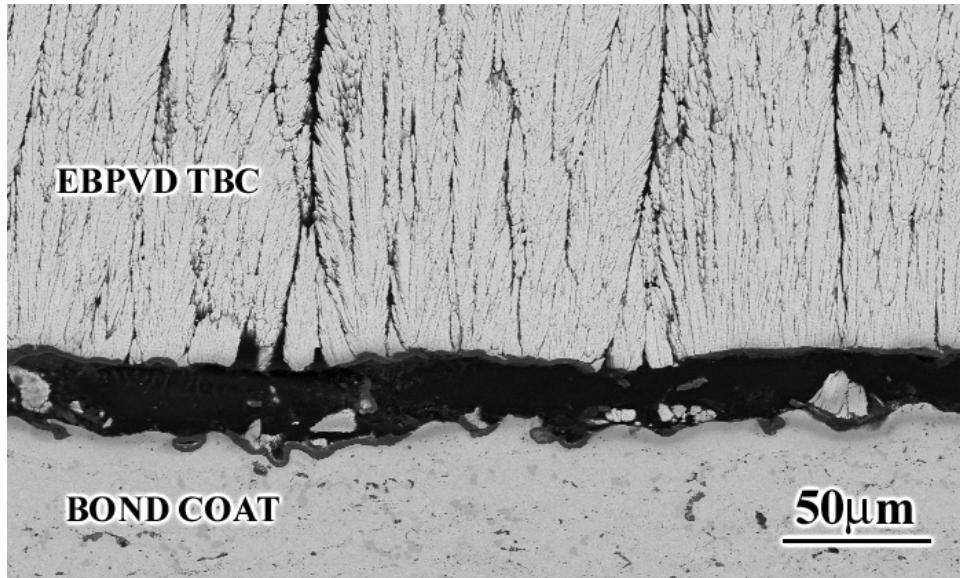
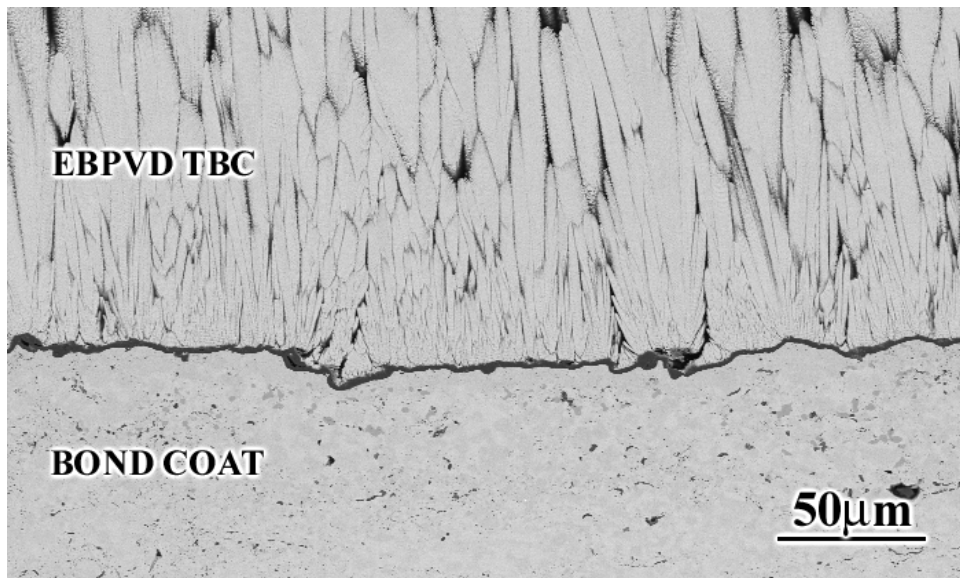


Figure 76 TGO thickness vs square root of time at 1100°C. The TGO growth rate on the state of the art TBC systems with NiCoCrAlY bond coats and the ones with Pt underlayers were similar, whereas the TGO growth on TBC systems with aluminized NiCoCrAlY bond coats were slower.



(a)



(b)

Figure 77 Scanning electron micrographs from TBC systems with state of the art NiCoCrAlY bond coats, (a), and the NiCoCrAlY bond coats with Pt underlayers, (b), after 20 cycles of exposure at 1100°C before failure. The absence of separation during metallographic preparation for the specimen with Pt underlayer suggests improved interfacial toughness.

- **Aluminized NiCoCrAlY Bond Coats** - Aluminizing the NiCoCrAlY bond coats also improved the lives, but not to the extent obtained by Pt overlayers and surface polishing. In the as-processed condition, fewer defects were present along the interfaces compared to the ones identified for the state of the art NiCoCrAlY systems. The TGO was pure and more uniform and the interface was free of the surface defects. However, the interface was still irregular with associated TBC defects (Figure 78).

Examination of these specimens as a function of exposure cycle showed that the interface became more irregular with time, similar to the behavior of the state of the art Pt aluminides (Figure 79a). The failure was more along or close to the TGO/TBC interface with some spallation also along the TGO/bond coat interface (Figure 79b). There were indications of separations along the TGO/bond coat interface prior to failure (Figure 79c). Al-rich nitrides were observed in these areas, which appear to have formed following the interface separation (Figure 79d).

The failure of the aluminized NiCoCrAlY systems are believed to be similar to the failure of the state of the art Pt aluminides which failed by the ratcheting mechanism. However, in addition to the ratcheting type of failure, aluminized bond coats also developed vertical separations in the TBC (Figure 80a) as well as voids along the TGO/bond coat interface (Figure 80b), both of which are also believed to contribute to the failure. These observations explain the relatively shorter lives of these systems compared to the state of the art Pt aluminides. The absence of Pt in the aluminized coatings is another factor that is believed to be important also in the performance difference.

Comparison of the TGO thickness with state of the art NiCoCrAlY systems and the ones with a Pt underlayer showed that the TGO growth rate was slower for the aluminized

NiCoCrAlY systems (Figure 76). Thus, the presence of fewer defects as well as the slower TGO growth seems to be responsible for the improvement in the lives of these systems compared to the state of the art NiCoCrAlYs.

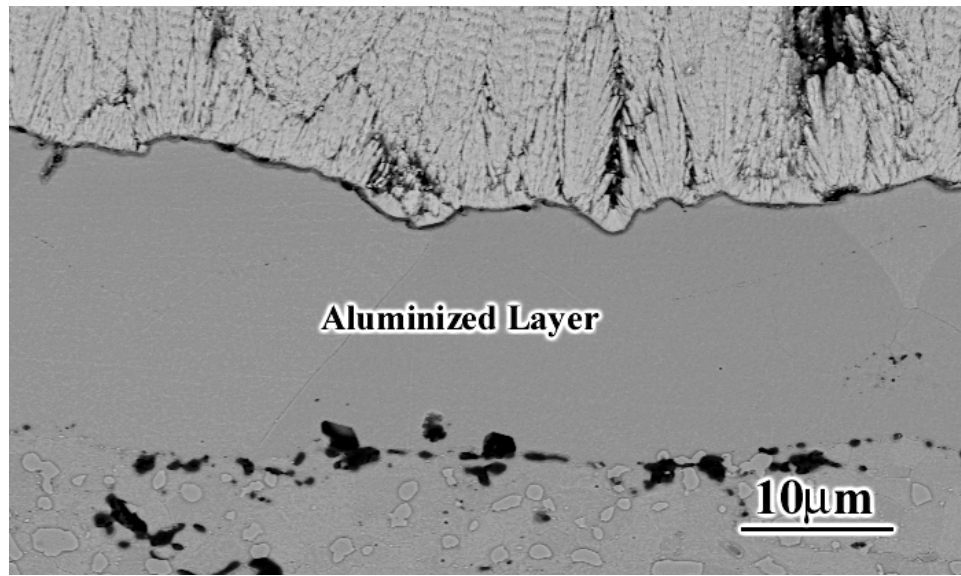
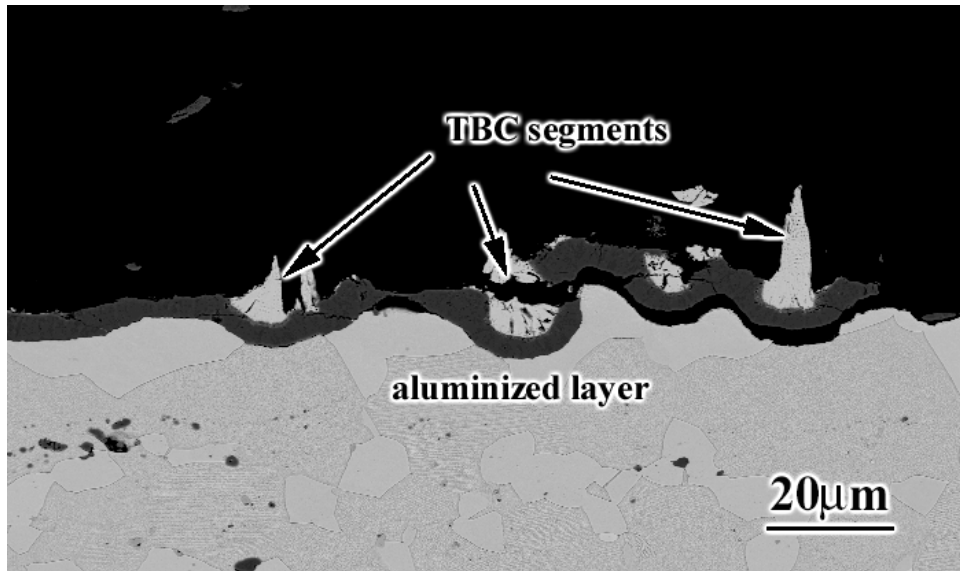
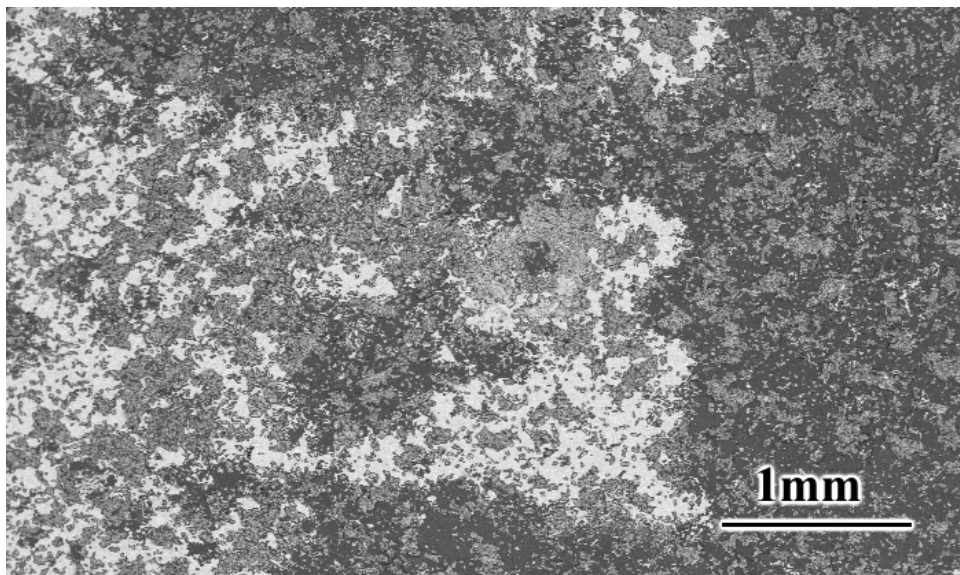


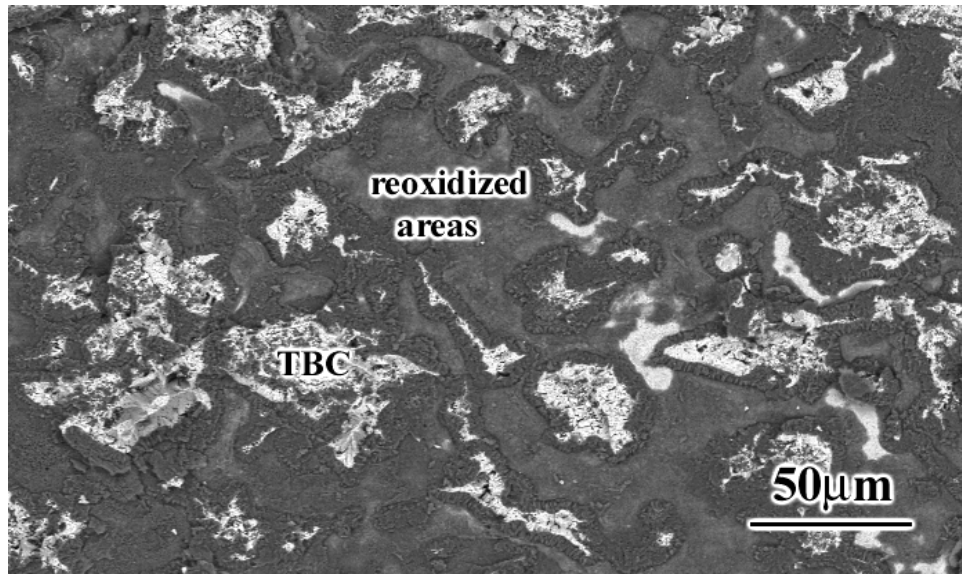
Figure 78 Scanning electron micrograph of a TBC system with aluminized NiCoCrAlY bond coat in the as processed condition showing the presence of a relatively defect free interface with more uniform TGO compared to the state of the art TBC systems. However, the interface was still irregular.



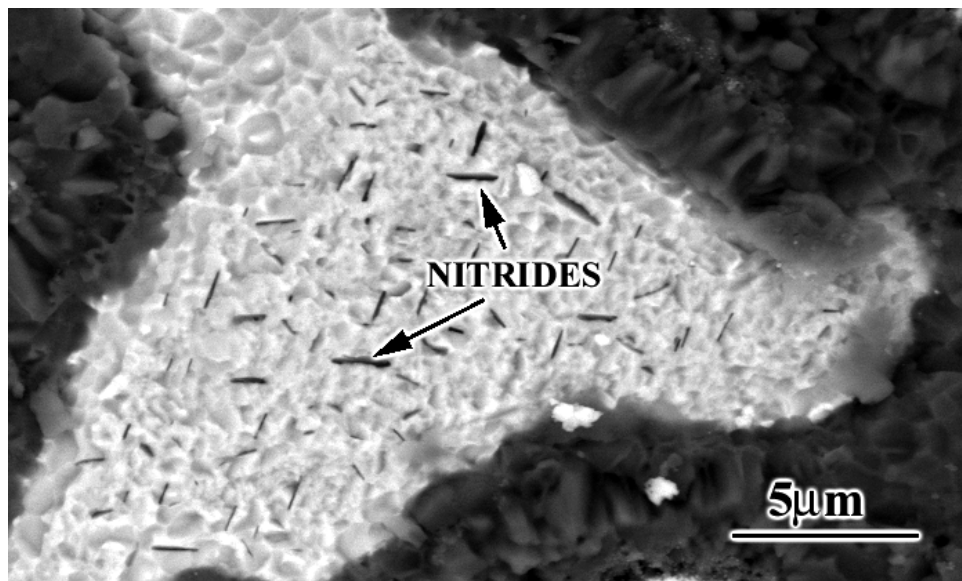
(a)



(b)

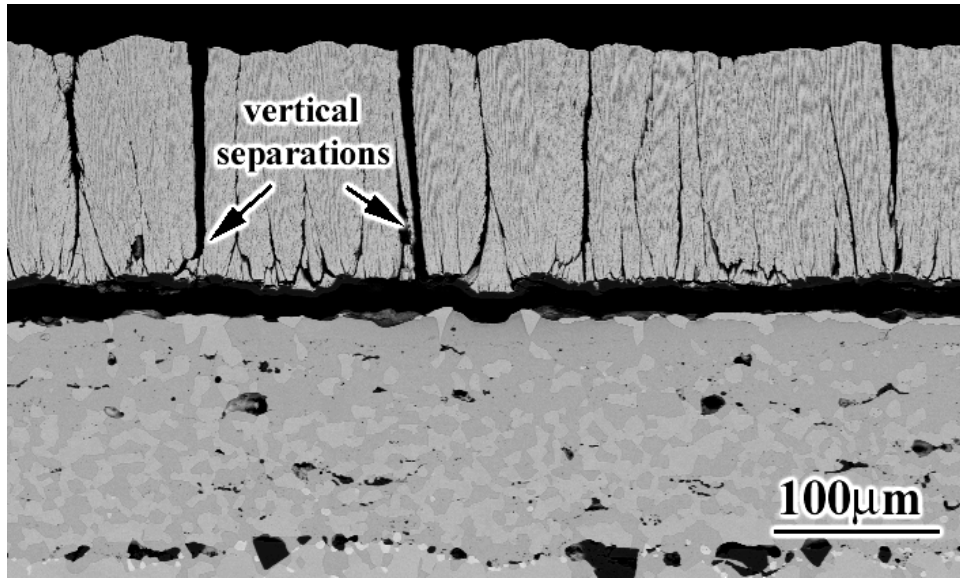


(c)

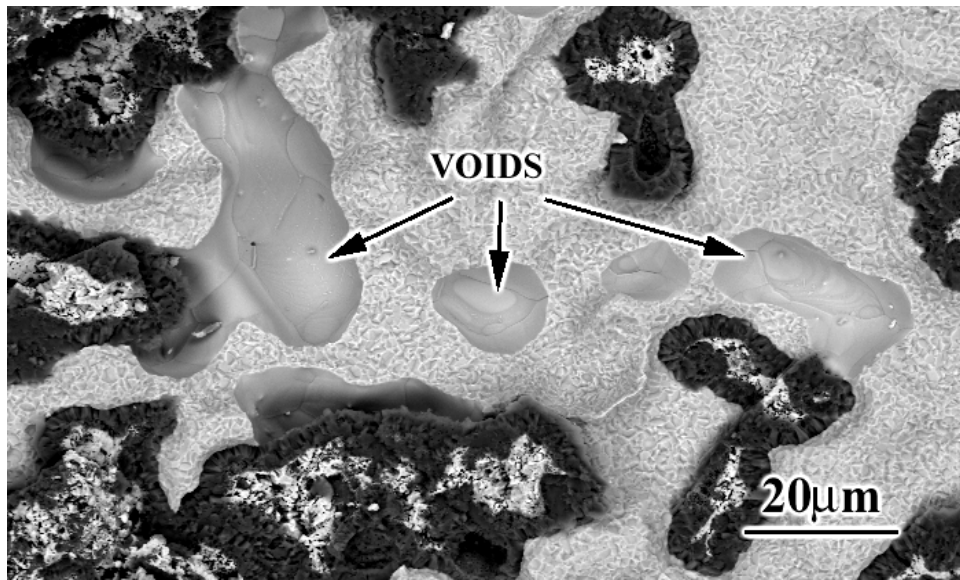


(d)

Figure 79 Scanning electron micrographs of TBC systems with aluminized NiCoCrAlY bond coats after failure. (a) The interface became more irregular with time, (b) Significant amount of failure was along or close to TGO/TBC interface, (c) There were indications of separation and reformation of the alumina prior to failure, (d) Al rich nitrides were observed at these sites where separation occurred prior to failure



(a)



(b)

Figure 80 Scanning electron micrographs of TBC systems with aluminized NiCoCrAlY bond coats after failure showing the development of (a) vertical separations in the TBC, (b) voids in the bond coat.

- **Surface Modified NiCoCrAlY Bond Coats** - Vibro finishing, media finishing and hand polishing are the 3 surface preparation techniques that have been applied to NiCoCrAlY bond coats. The failure times of these systems with different surface preparation techniques are given in Table 4. Hand polishing resulted in significant improvements whereas media finishing and vibrofinishing did not improve the lives at all.

Hand polished NiCoCrAlY Bond Coats: These specimens were hand polished resulting in a surface finish with an approximate Ra value of 0.2 μ m. The cross sectional examination of these specimens in the as-processed condition showed that the interface was very smooth and free of the surface defects as well as the TBC defects (Figure 81a). Closer examination of the interface area showed the presence of a very uniform and continuous TGO (Figure 81b) except in some localized areas where the continuity of the TGO was interrupted above Cr rich phases along the interface (Figure 81c). A few TBC defects were also observed above the areas where the porosity in the bond coat intersected the surface (Figure 81d).

These specimens were also subjected to cyclic oxidation testing at 1100°C. One of the specimens did not fail even after 1520 cycles, which is a significantly long time compared to failure times of the state of the art NiCoCrAlY systems. Cross sectional examination of this specimen showed that a very thick TGO with significant amounts of RE rich oxide protrusions developed during exposure (Figure 82a) Closer examination of the interface area showed the presence of an almost defect free TGO/TBC interface (Figure 82b). Nevertheless, in some localized areas, there were still some transient oxides as well as cracks initiating in their vicinity (Figure 82c). There were also some small, localized buckles along the TGO/intermixed zone interface (Figure 82d), which might have formed by linking up of small voids along this interface (Figure 82e). However, the amount of these types of defects was too small to cause early failure

of these TBC systems. Cracks were also present along and/or close to the original TGO/bond coat interface above the reactive element rich oxide protrusions (Figure 82f). This cracking may be due to the combined effect of stress concentration in the vicinity of these oxide protrusions as well as stored strain energy in the TGO. If this specimen had not been taken out of the furnace before failure, it could have been expected to fail along the TGO/bond coat interface as the cracking along this interface became more extensive. The long life of this specimen, even in the presence of a very thick TGO and significant amounts of RE rich oxide protrusions, both of which drive cracking along the TGO/bond coat interface, indicates the importance of defects along or close to the TGO/TBC interface for the early failure of the state of the art TBC systems.

Two other specimens failed mainly along the TGO/bond coat interface with some spallation also along the TGO/TBC interface after 720 and 740 cycles of exposure. These specimens were from different batches than the other two. Accordingly, there were some variations in the TBC morphologies as well as amounts of reactive element rich oxide protrusions. They had some TBC defects such as spits from which cracks were observed to initiate (Figure 83a). One of them was observed to have an abnormal defect where accelerated oxidation occurred (Figure 83b). Some transient oxides were also observed. The relatively early failure of these specimens compared to 1520 cycles may be related to these defects. One other specimen, which was also hand polished, failed after 220 cycles which was a very early failure time compared to the failure times of the other specimens with the same conditions. Examination of the fracture surface (Figure 84a and 84b) as well as the cross section of this specimen (Figure 84c and 84d) revealed significant amounts of failure along the TGO/intermixed zone interface in contrast to the failure of the other hand polished NiCoCrAlY bond coats. Transient oxides embedded in the intermixed zone were observed on the fracture surface (Figure 84e). Cracks

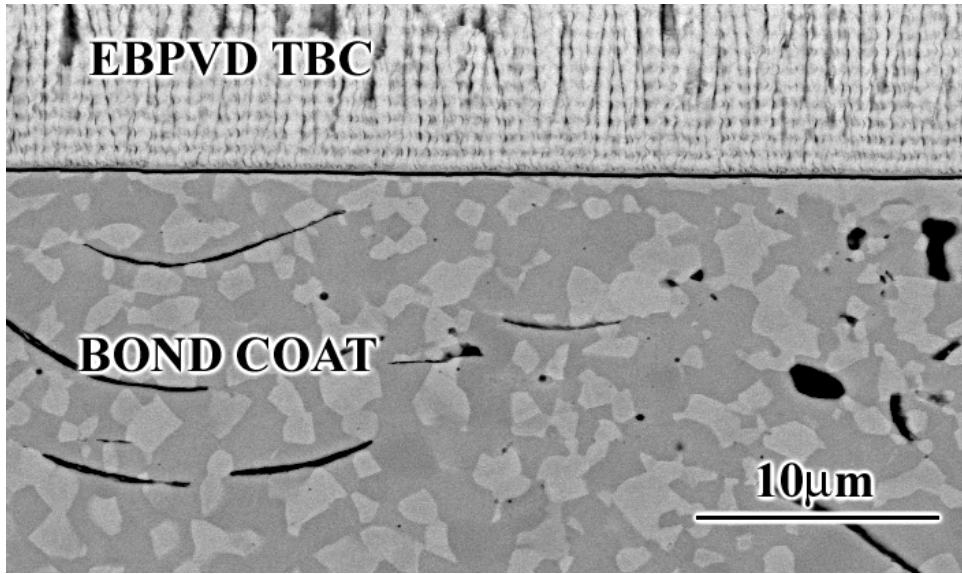
might have initiated in the vicinity of these transient oxides and/or voids along the TGO/intermixed zone interface and then might have propagated along this weak interface. Once cracks have initiated, their propagation may be relatively easy in the presence of very smooth interfaces due to lack of obstacles in their paths. This may result in premature failures in the presence of defects in more than a critical amount, which may be the case for the early failure of this specimen. However, more work is required to reach a conclusive result on this issue.

Vibro Finished NiCoCrAlY Bond Coats: Vibro finishing the surfaces of the NiCoCrAlY bond coats did not improve the lives at all. Cross sectional examination of the as-processed specimens showed that the interface was still highly irregular at localized areas with associated TBC defects (Figure 85a) These defects in the TBC were even larger than the ones on heavy grit blasted samples. However, there were also rather smooth areas through the interface (Figure 85b), which were not observed for the heavy grit blasted specimens.

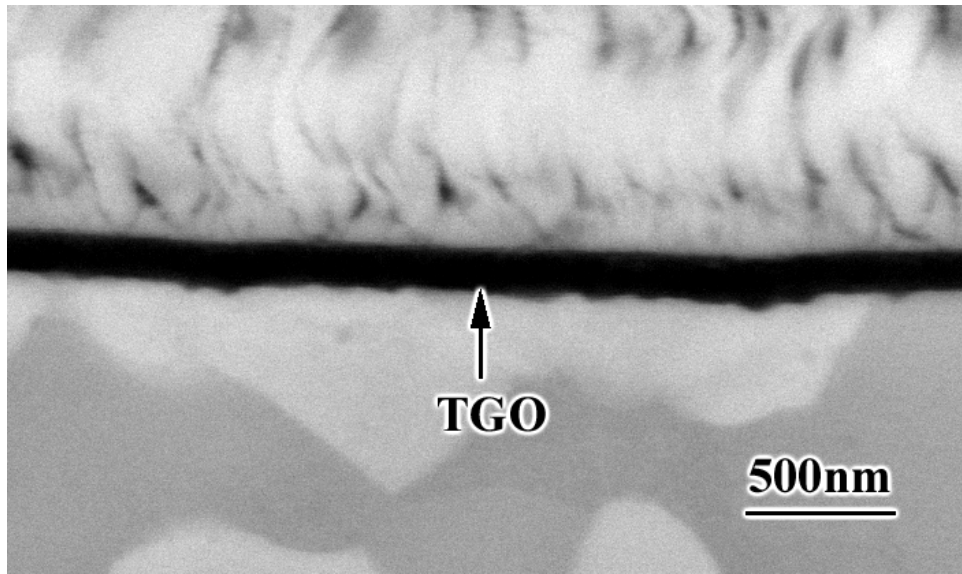
The failure was mainly along the TGO/bond coat interface with numerous excursions into the TGO and TBC in the vicinity of the pronounced TBC defects as evident from the fracture surface as well as cross sectional micrographs given in Figures 86a and 86b, respectively. The cracks initiating in the vicinity of these, occasional but pronounced defects, were sufficient to cause early failure of these specimens despite the presence of smooth areas along the interface. Therefore, these results indicate the importance of a uniformly smooth interface to get improved lives.

Media Finished NiCoCrAlY Bond Coats: Media and vibro finish are two different names given to basically the same processes performed at two different companies. Therefore, media finish

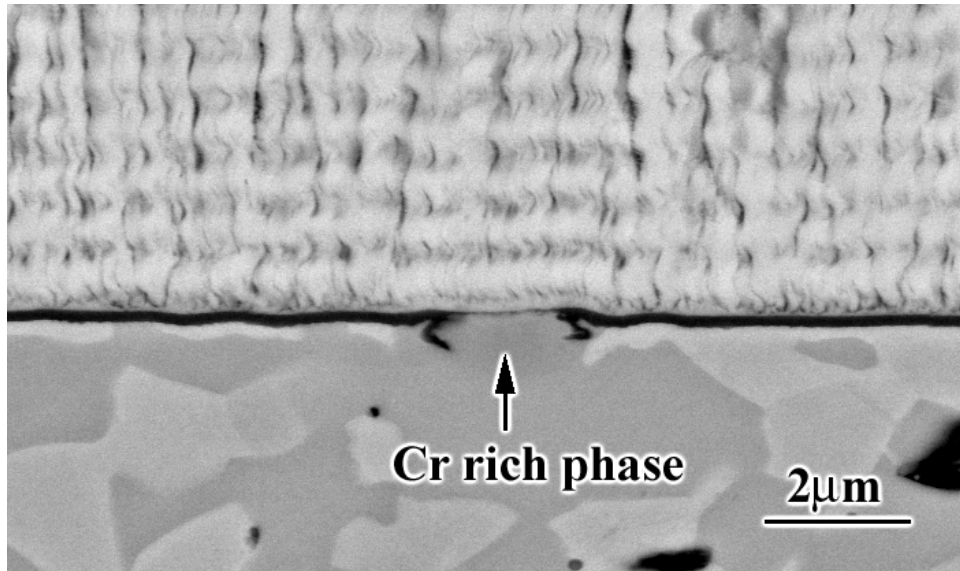
operation was also not successful in providing a uniformly smooth interface.(Figure 87)
Accordingly, these specimens also failed at relatively short times as can be seen from Table 4
and their failure behavior was similar to the failure of the state of the art and the vibro finished
specimens.



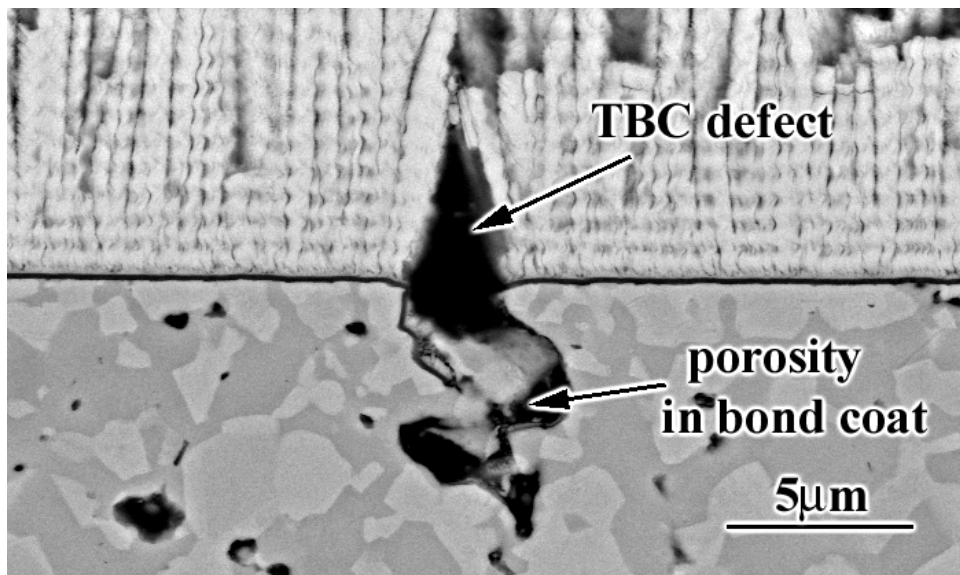
(a)



(b)

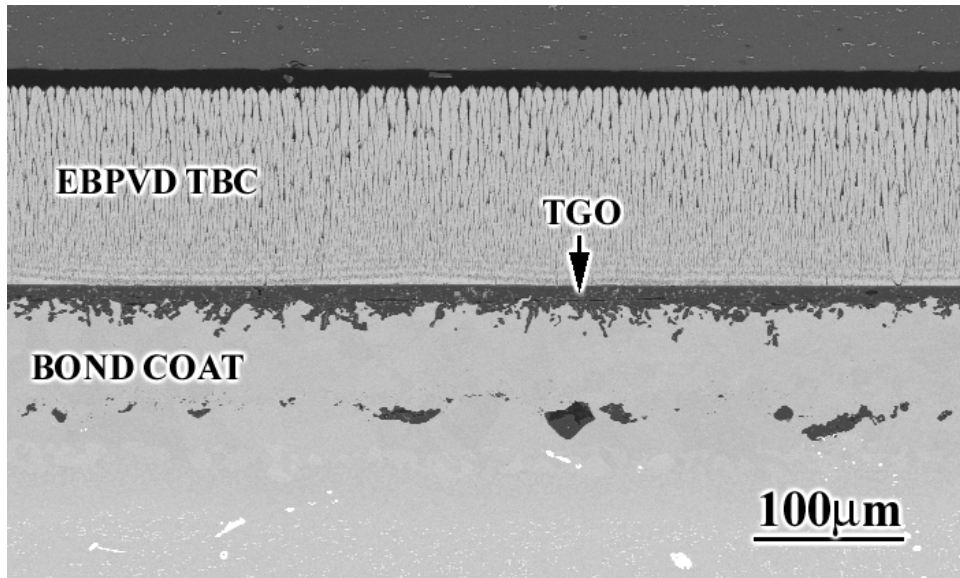


(c)

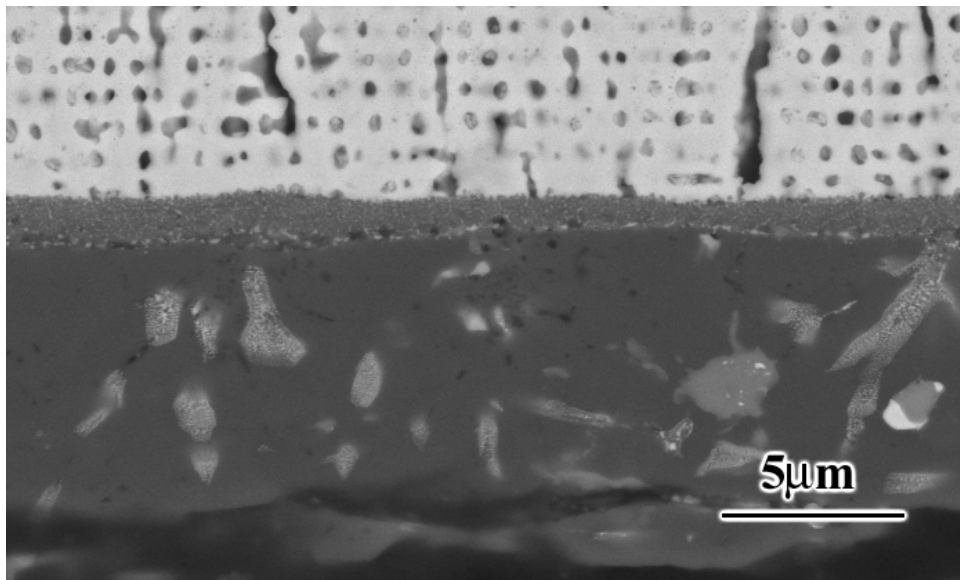


(d)

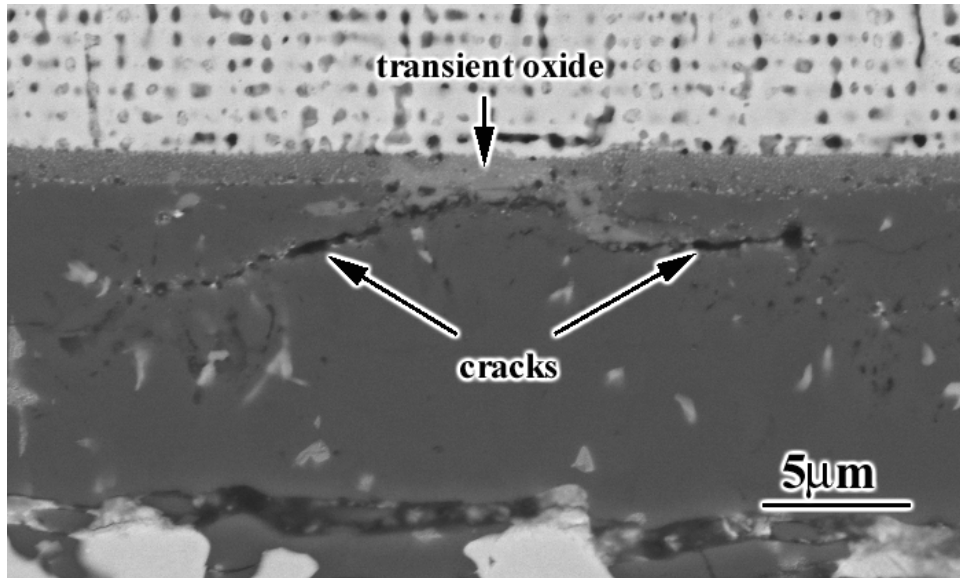
Figure 81 Scanning electron micrographs of a TBC system with hand polished NiCoCrAlY bond coat in the as processed condition, at (a) low and (b) high magnifications, showing a very smooth interface which is free of many defects identified for the state of the art systems except at some localized areas where the continuity of the TGO is interrupted above the Cr rich phases, (c), and where the porosity in the bond coat intersected the surface, (d).



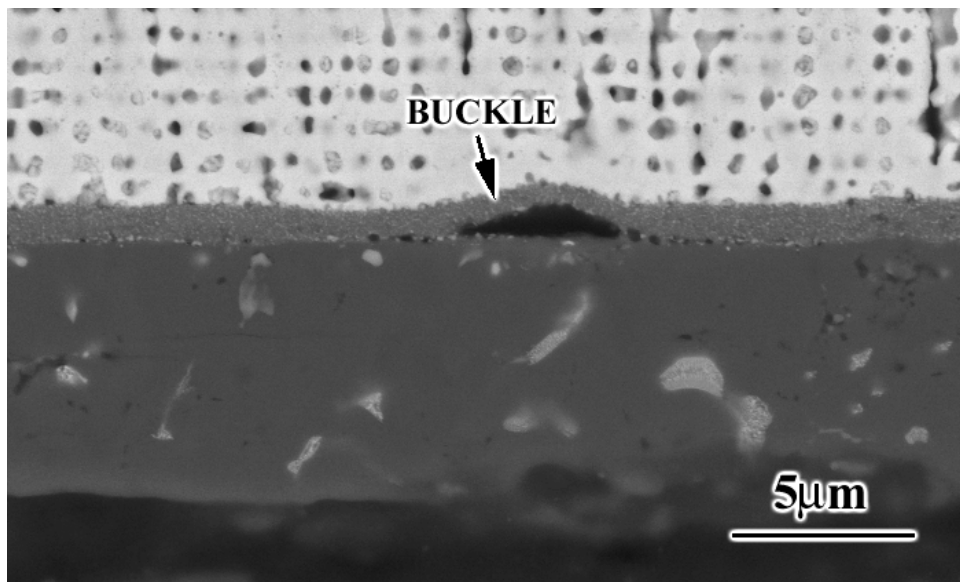
(a)



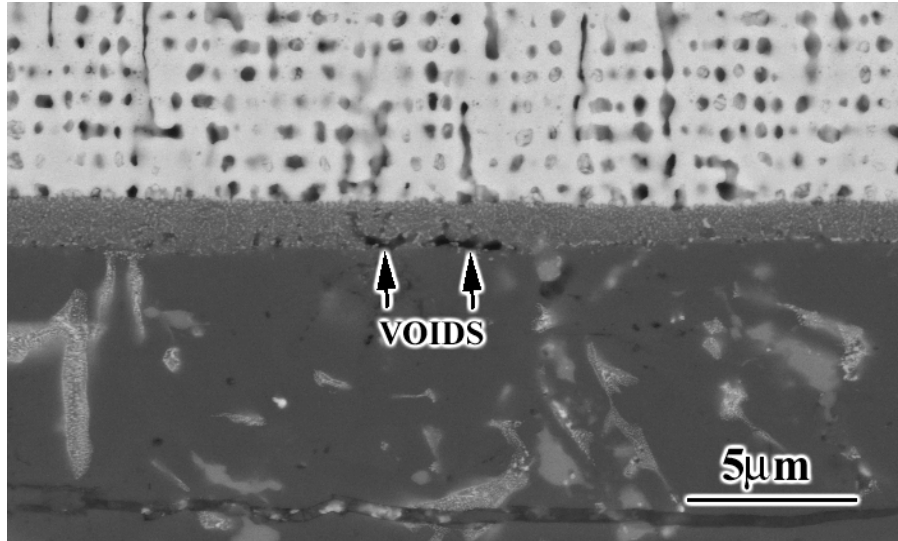
(b)



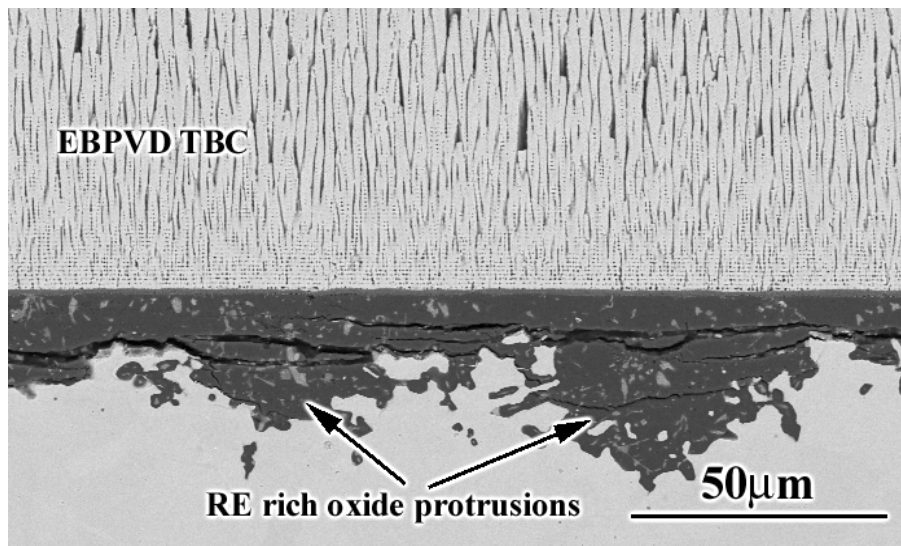
(c)



(d)

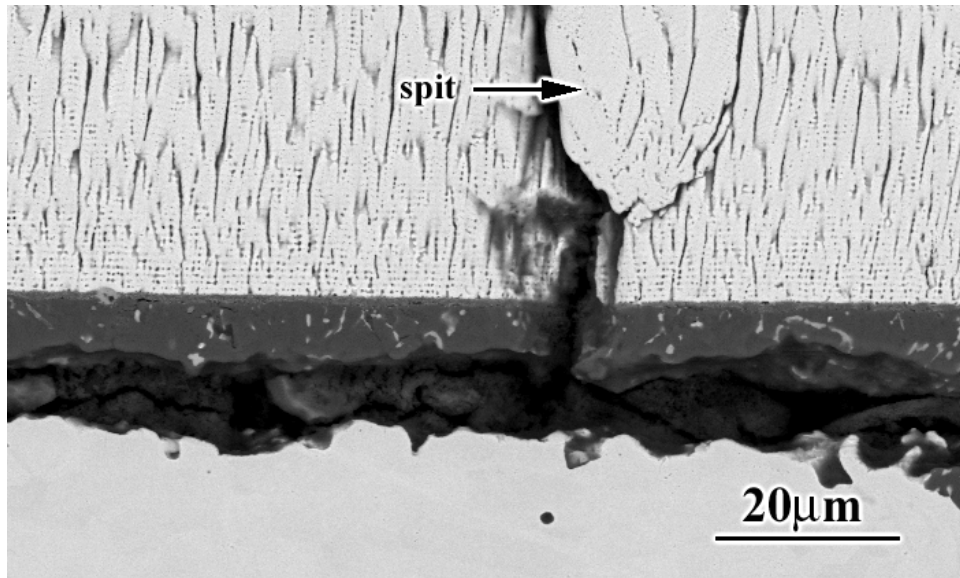


(e)

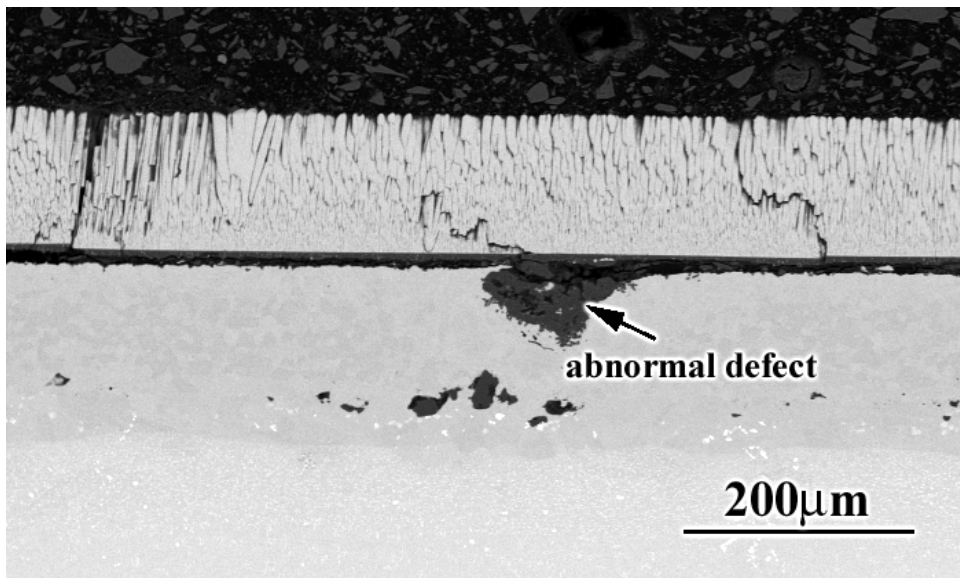


(f)

Figure 82 SEM micrographs of a TBC system with hand polished NiCoCrAlY bond coat after 1520 cycles of exposure at 1100°C before failure showing the presence of a very thick TGO with significant amounts of RE rich oxide protrusions, (a). The TGO/TBC interface was almost free of defects, (b), except at localized areas with transient oxides, (c), and small buckles along the TGO/intermixed zone interface, (d), which seemed to develop by linking up of small voids along this interface, (e). Cracks were present in the vicinity of RE rich oxide protrusions, (f)

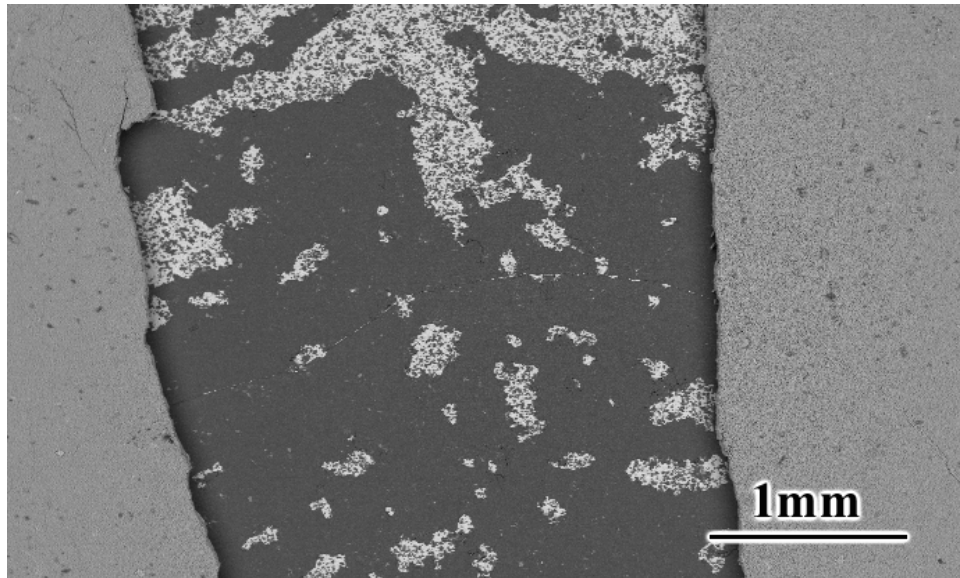


(a)

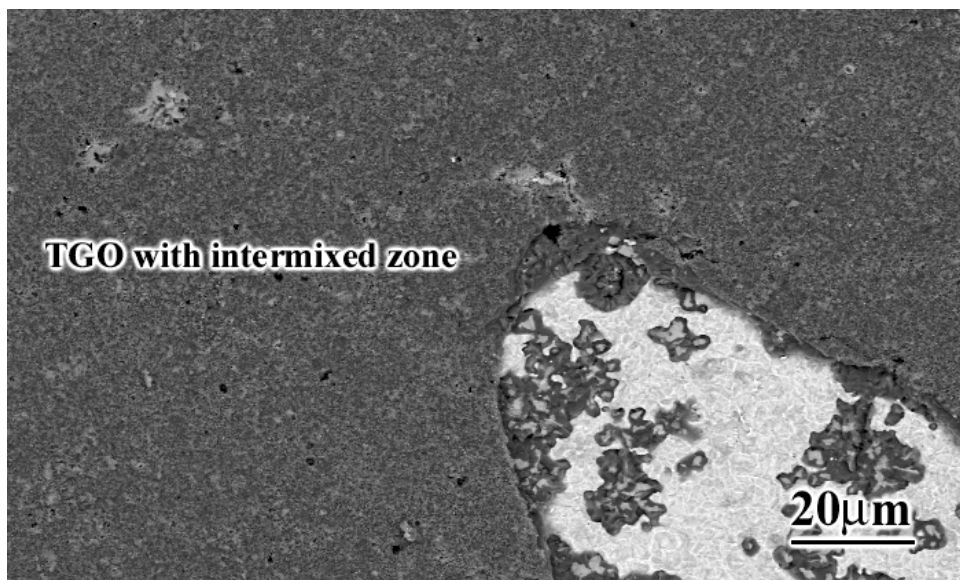


(b)

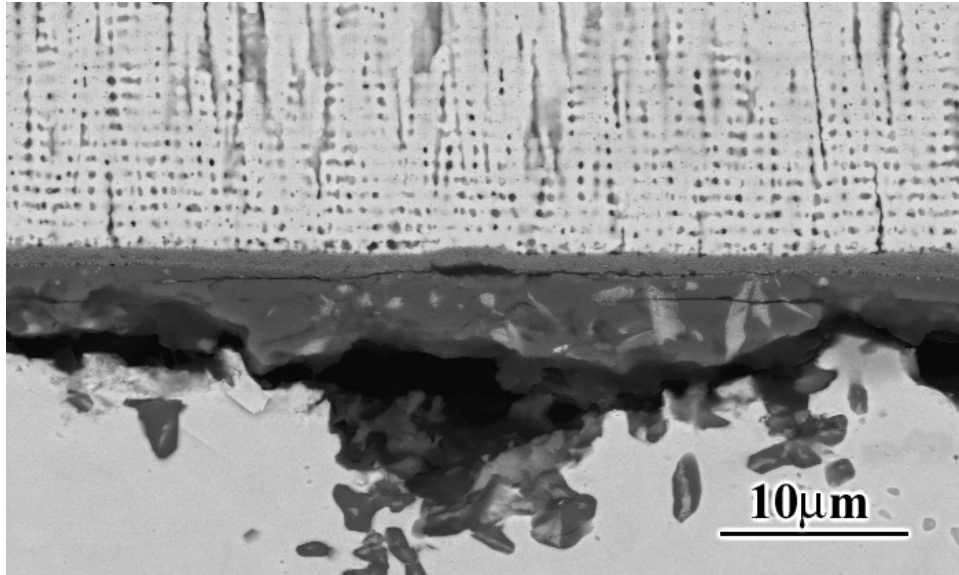
Figure 83 Scanning electron micrographs of TBC systems on hand polished NiCoCrAlY bond coats which failed after 720 cycles of exposure at 1100°C. Spits, (a), as well as an abnormal defect, (b), were observed.



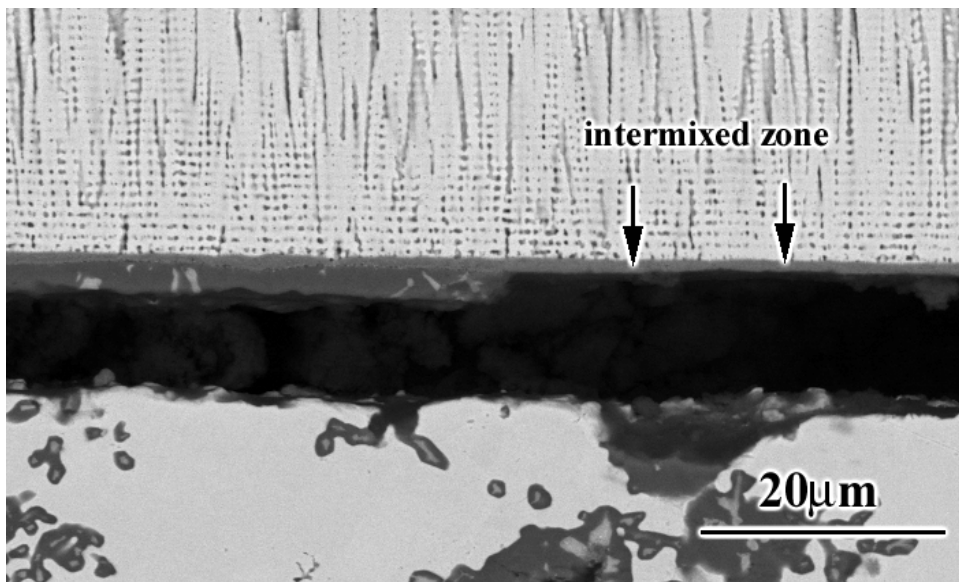
(a)



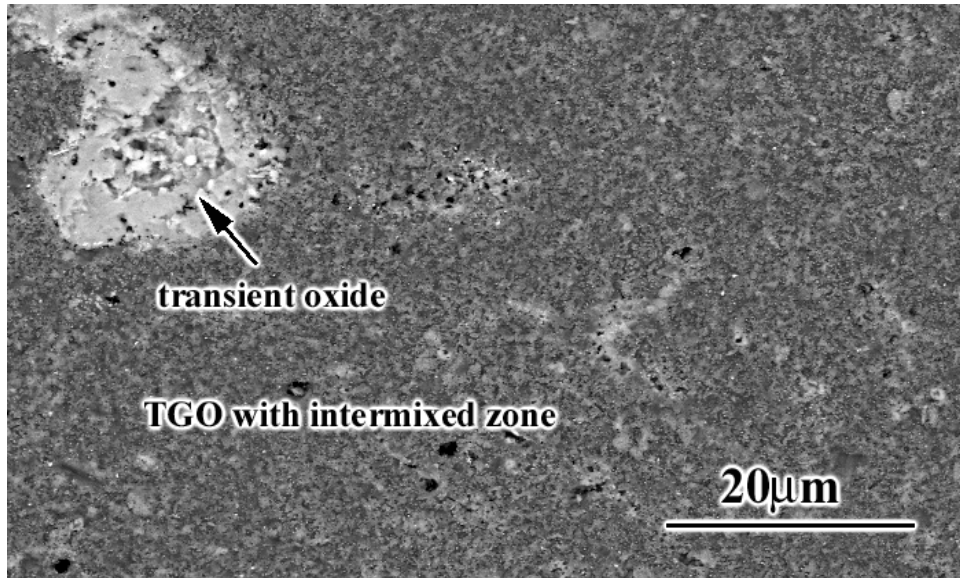
(b)



(c)

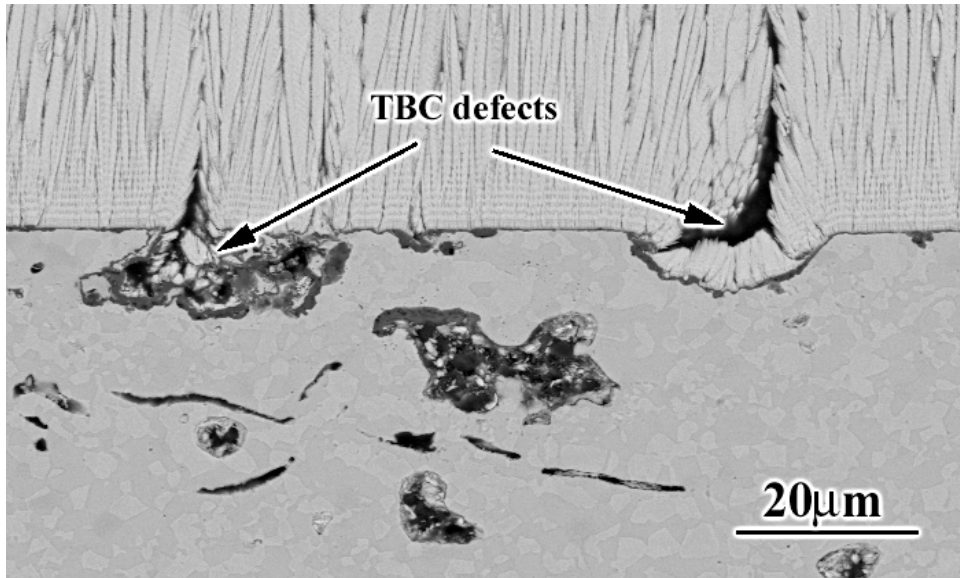


(d)

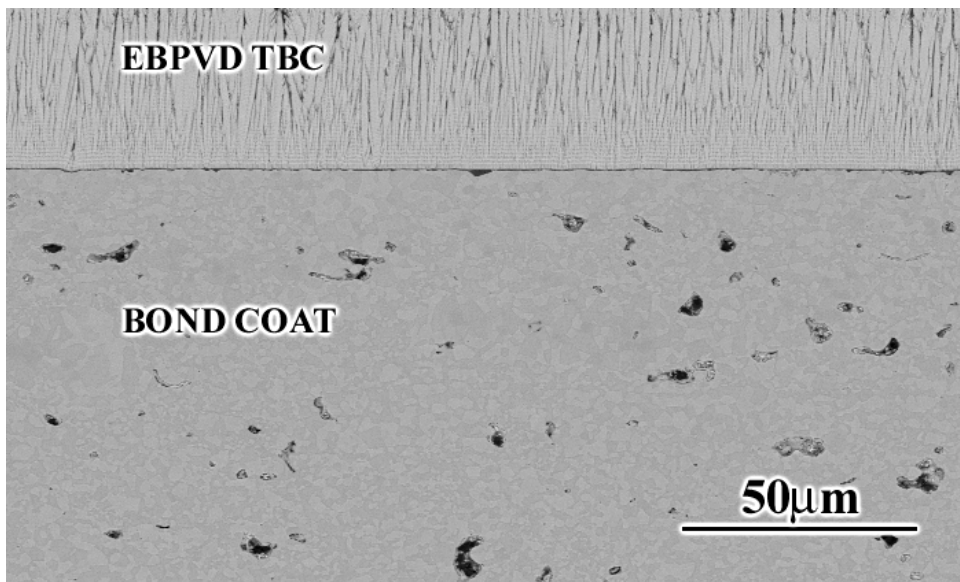


(e)

Figure 84 Scanning electron micrographs of a TBC system on hand polished NiCoCrAlY bond coat which failed after 220 cycles of exposure at 1100°C. Significant amount of failure was along the TGO/intermixed zone interface as can be seen at (a) low and (b) high magnification micrographs from the fracture surface, as well as cross sectional micrographs, (c) and (d). Transient oxides were also present embedded in the intermixed zone, (e).

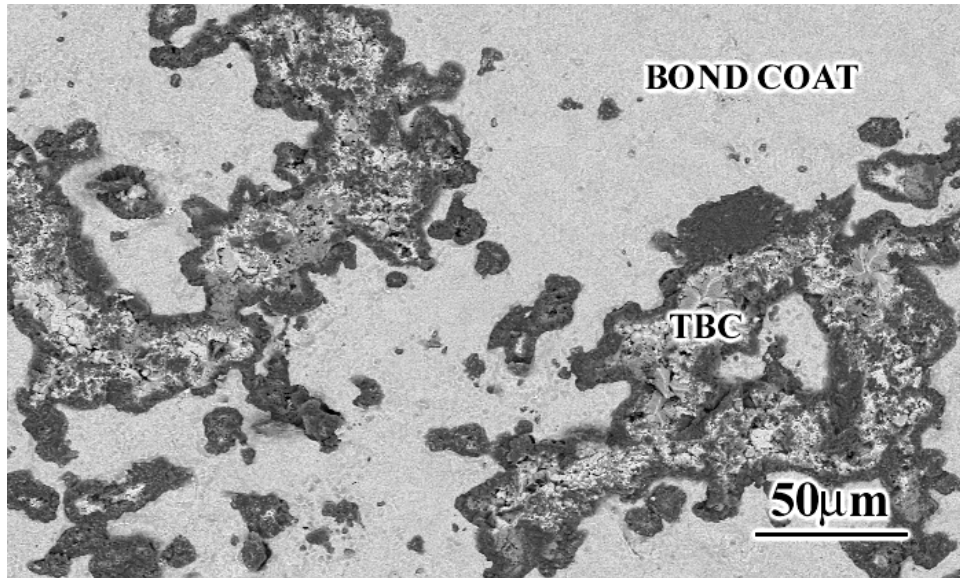


(a)

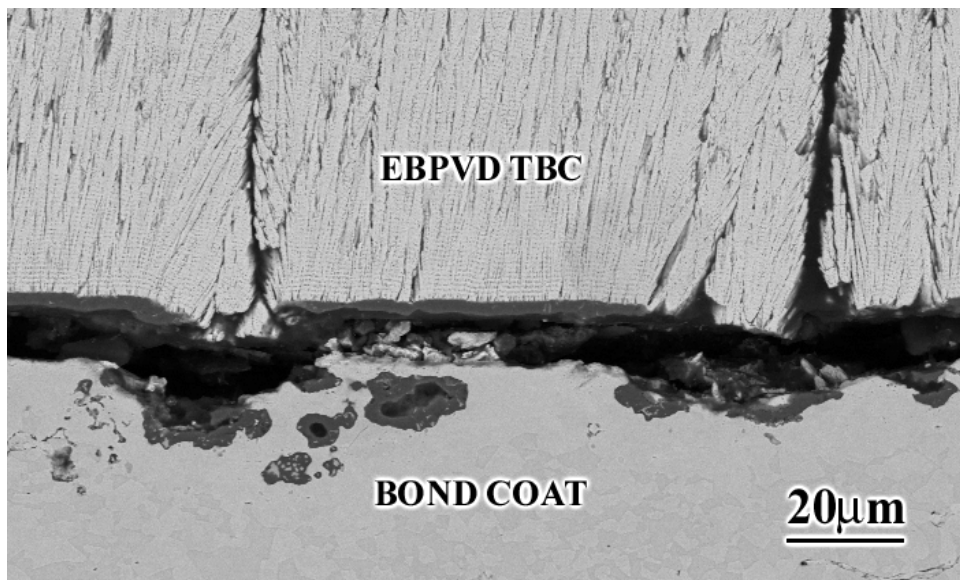


(b)

Figure 85 Scanning electron micrographs of a TBC system with vibro finished NiCoCrAlY bond coat in the as processed condition showing large TBC defects, (a). There were also smooth areas along the interface, (b).



(a)



(b)

Figure 86 Scanning electron micrographs of a TBC system with vibro finished NiCoCrAlY bond coat from the fracture surface, (a), and cross section, (b), showing failure in the vicinity of pronounced TBC defects.

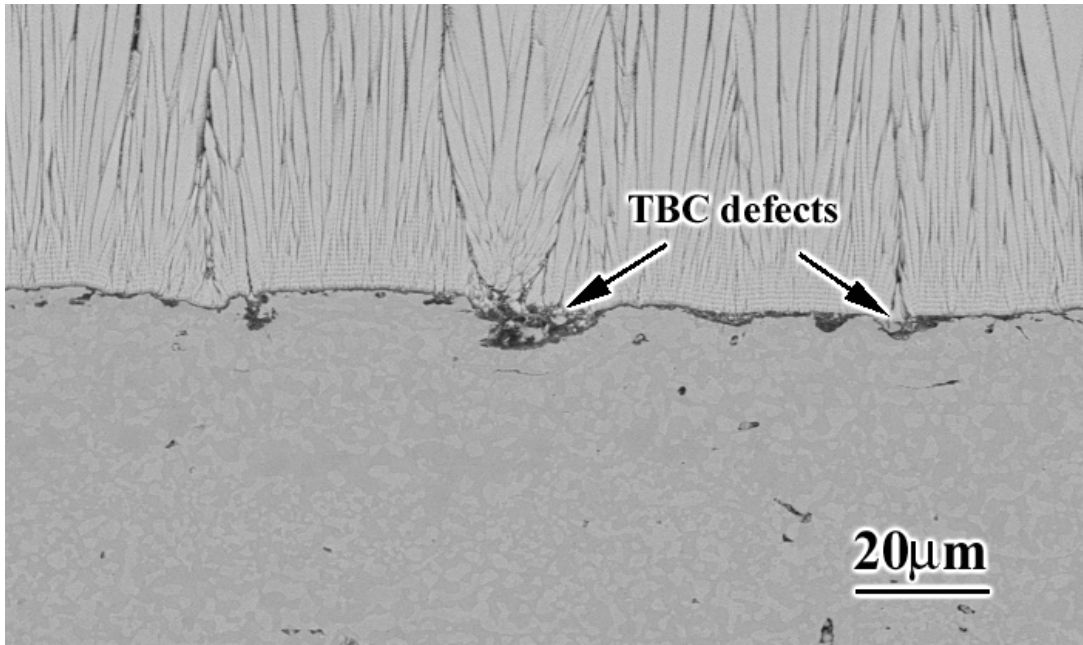


Figure 87 Scanning electron micrograph from a TBC systems with media finished NiCoCrAlY bond coat in the as processed condition showing the presence of TBC defects.

4.2.4.2 Platinum Aluminide Bond Coats Based upon the results obtained on the failure of the state of the art Pt aluminide systems, various modifications were performed. These modifications included: deposition of different thicknesses of Pt and aluminide layers as well as utilizing various surface preparation techniques. The general characteristics of these modified systems will be given next.

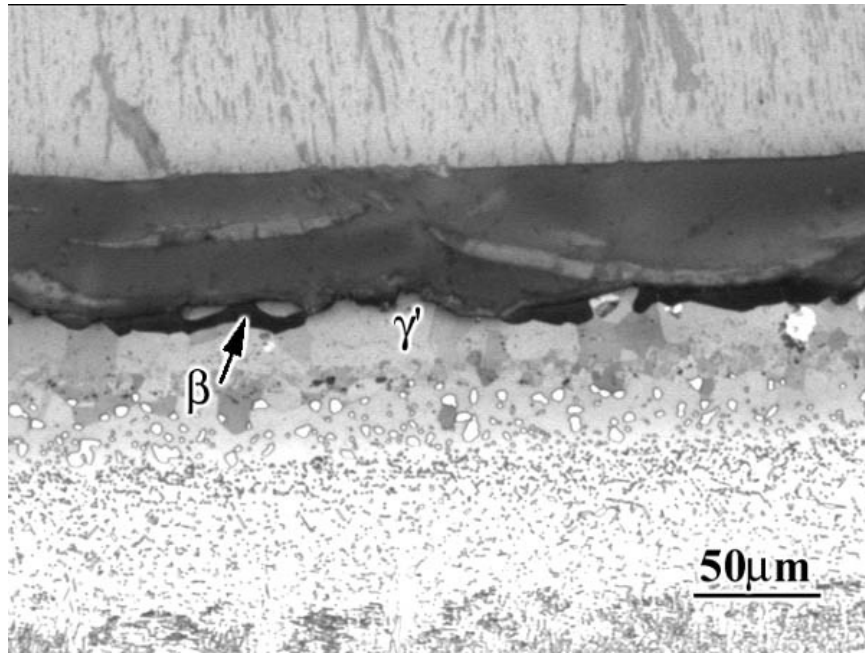
- **Pt and Aluminide Thickness Variations** - The failure times for the TBCs on Pt aluminide bond coats with different thicknesses of Pt and aluminide layers did not show any trend as can be seen from Table 5. It has also been observed that for some specimens the actual thicknesses of the bond coats as well as the TBCs were different than the nominal values given in Table 5. Moreover, some of the specimens had premature failures due to some abnormal defects and/or contamination. All these factors made the analysis of thickness effects complicated. On the other hand, surface preparation was found to have a pronounced effect on the failure times as well as the failure characteristics, which will be explained in more detail.

One general observation that could be obtained on the thickness variations was less Al depletion for the specimens with thicker layers of Pt as well as aluminides. Figure 88a is from a specimen with normal thickness of Pt and aluminide layers (6.35 μ m Pt, 38.1 μ m aluminide) after 1080 cycles of exposure and the microstructure consisted of mainly γ' phase with small amounts of β phase left whereas the specimens with double thickness of aluminide (Figure 88b) as well as double thickness of Pt and aluminide layers (Figure 88c), after 1240 and 860 cycles of exposures at 1100°C, respectively, consisted of mainly β phase with some γ' phase at the grain boundaries. These microstructural differences are expected to cause a marked difference in failure for longer lives where Al depletion becomes a major issue. However, Al depletion of the bond coats examined under this study did not seem to be the major factor for their failures.

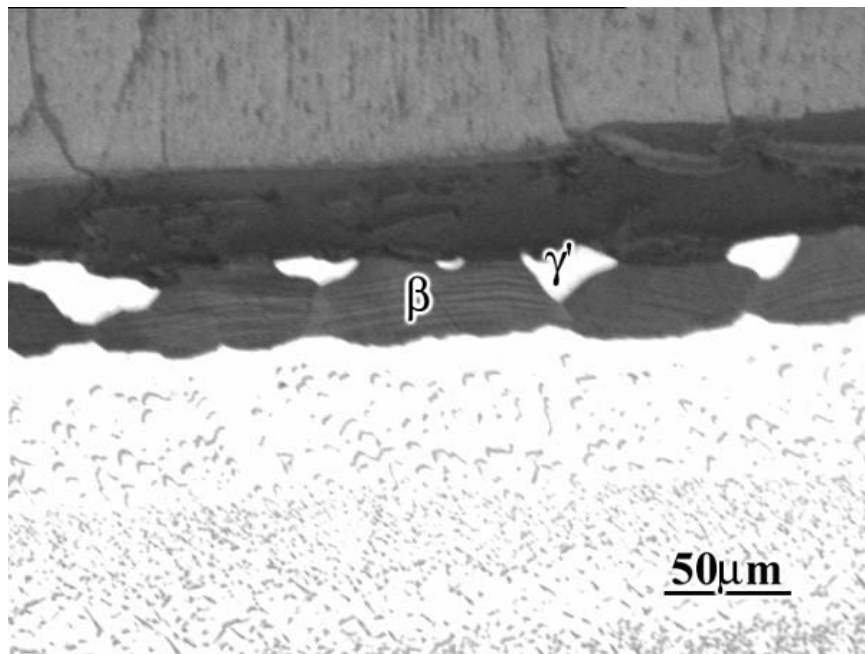
One other observation was the reduced void density for the specimens with thicker Pt and aluminide layers, which were light grit blasted. This seems to be a result of diffusion kinetics which was effected by varying thicknesses of Pt and aluminide layers, as also mentioned before.

Table 5 Failure Times for TBC systems with modified Pt Aluminide Bond Coats

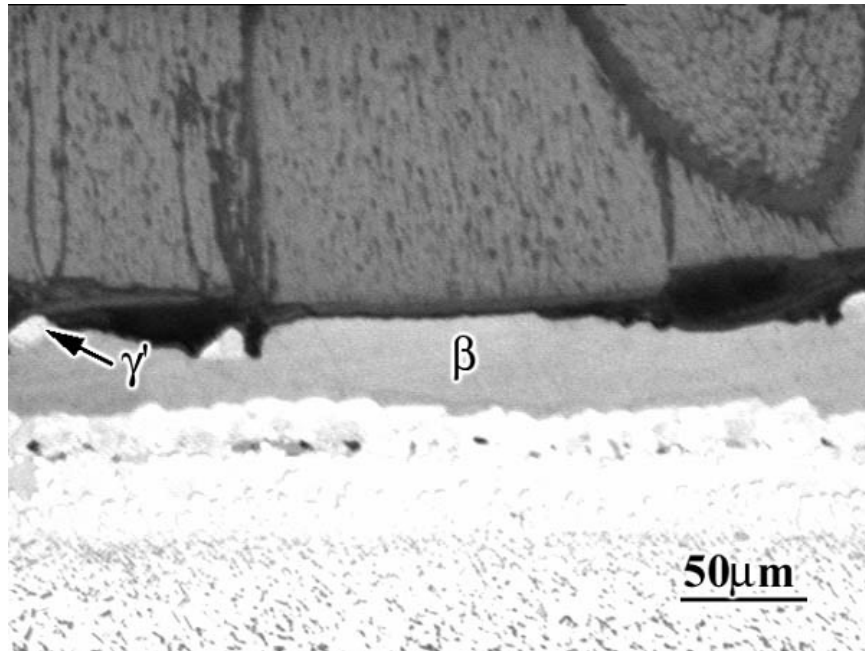
	Failure Time at 1100°C (# of 1 hr cycles to failure)			
	0.25mil Pt 1.5mil Aluminide	0.25mil Pt 3mil Aluminide	0.5mil Pt 1.5mil Aluminide	0.25mil Pt 1.5mil Aluminide
Pt Aluminide As Aluminized	680, 1080	1240, 1260	---	860, 860
Pt Aluminide HGB	840, 1005, 1040, 1100, 1120, 1220, 1280	1340	---	---
Pt Aluminide LGB preoxidation	1600, 3460	360, 1040, 2140	1780, 1920,3780+	---
Pt Aluminide MF preoxidation	---	---	---	2280



(a)



(b)



(c)

Figure 88 Optical micrographs of TBC systems with as aluminized Pt aluminide bond coats with varying thicknesses of Pt and Aluminide layers after exposure at 1100°C. The bond coat with normal thickness of Pt and aluminide layers consisted of significant amounts of γ' phase after 1080 cycles, (a), whereas the specimens with double thickness of aluminide, (b), and with double thickness of Pt and aluminide layers, (c), after 1240 and 860 cycles of exposure, respectively, had much less γ' phase.

●**Surface Modified Platinum Aluminide Bond Coats** - In this part, the specimens will not be differentiated in terms of the various thicknesses of Pt and aluminide layers, instead, the general behavior, which is believed to be surface condition related, will be presented.

As Aluminized Platinum Aluminide Bond Coats: The Pt aluminide bond coats without any surface modification have ridges at the grain boundaries. It has been shown previously that these grain boundary ridges act as crack initiation sites due to tensile stresses generated at the peak of these ridges.

Figure 89a shows a typical cross section of TBC systems on as-aluminized Pt aluminide bond coats. The TBC was very dense close to TGO ($\sim 10 \mu\text{m}$) with parallel rows of pores (Figure 89b). This morphology is probably a result of an initially very flat interface except at the ridges. TBC deposition conditions may also be playing a role for the development of this dense TBC. Small openings developed in the TBC above these ridges (Figure 89c), and then they enlarged with exposure resulting in the formation of vertical separations in the TBC (Figure 89d).

When these specimens were exposed to cyclic exposure conditions, small buckles, which were visible even by the naked eye, formed on the surface at early stages of their lives. Figures 90a through 90c are macrographs taken from the same specimen as a function of time. As can be seen from this sequence of macrographs, the specimens did not fail until the small localized buckles got larger and then linked together forming a critical sized buckle. Figure 90d is a cross sectional micrograph showing these buckles.

Examination of the fracture surface showed that the failure was mainly in the TBC (Figure 91a). Higher magnification micrographs of the fracture surface (Figure 91b) as well as the cross sections (Figure 91c) clearly showed the cracks that developed at these grain boundary ridges. These cracks, once initiated, propagated along the weak points, which were the row of

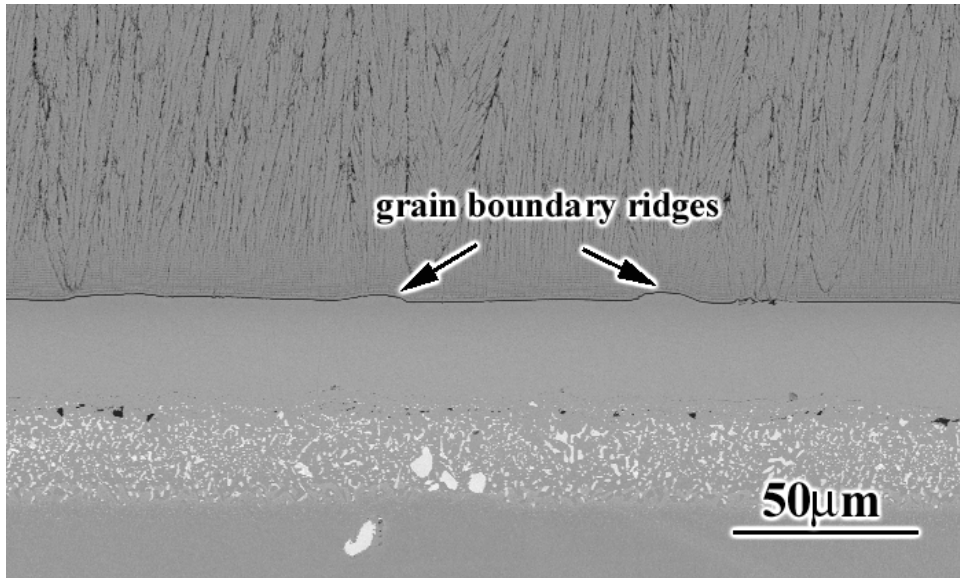
pores in the TBC just above the TGO for these samples. Thus, the formation of buckles at localized areas at early stages of their lives seems to be related to crack formation at the ridges and their propagation in the TBC. In these specimens, vertical separations also developed in the TBC above the ridges. The presence of these vertical separations might also have contributed to crack initiation and/or propagation. However, examination of another set of as-aluminized specimens which developed smaller amounts of vertical separations, also showed crack initiation at the ridges that were not associated with vertical separations (Figure 91d). This set of specimens did not develop a continuous layer of intermixed zone either (Figure 92a) as the first set of specimens did (Figure 92b). These observations also confirm the role of TBC deposition conditions on both development of vertical separations and the intermixed zone.

Cross sectional examination of these specimens showed a highly deformed bond coat surface (Figure 93a) except at areas where the bond coat was still in contact with the TBC at the time of failure (Figure 93b) This observation can be explained by the presence of a TBC constraint to deformation of the bond coat. Therefore, once the TBC separated from the TGO as a result of crack initiation at the ridges and their propagation in the TBC, the bond coat beneath it could deform freely without the constraint given by the TBC. In other areas where the TBC was in contact with the bond coat, the interface remained smooth. Similar observations on TBC constraint to the deformation of the bond coats were also reported by Tolpygo and Clarke [74].

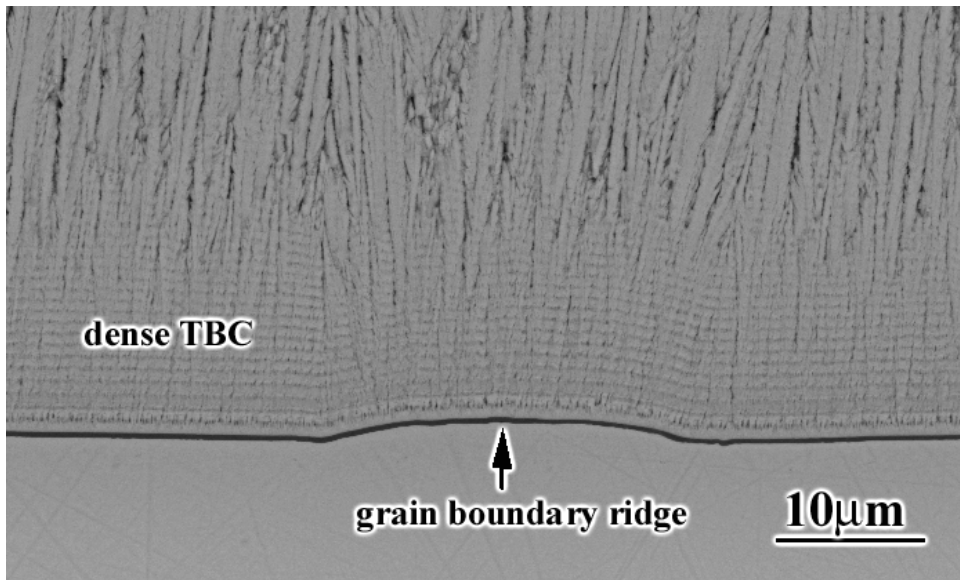
The TGO on top of the ridges also cracked vertically (Figure 94a) and then with continued exposure, the cracks propagated along the TGO/bond coat interface (Figure 94b) followed by reoxidation along this interface (Figure 94c) Preferential oxidation, probably at the grain boundaries, was observed in some areas (Figure 94d).

Some of the specimens were also tested under 15 hour cycles. Cracks, that initiated at the grain boundary ridges, were also observed for these specimens (Figure 95a) However, the cracking along the TGO/bond coat interface and then reoxidation was not present in contrast to specimens exposed to 1 hour cycles. Thus, the failure of this specimen under 15 hour cycles, even after shorter hot times, without separation along the TGO/bond coat interface may indicate that the failure of these specimens were mainly due to linking up of the cracks in the TBC.

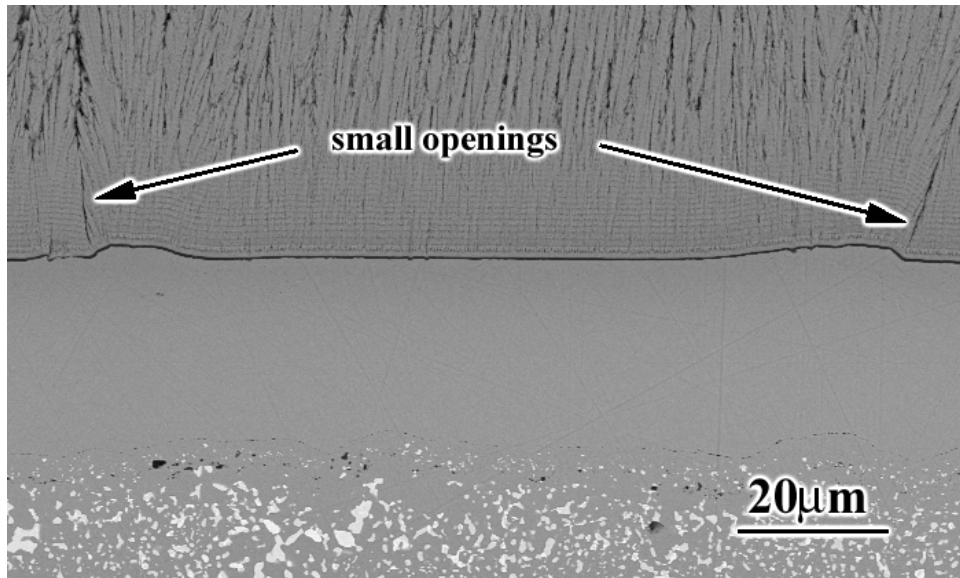
One other specimen was exposed to an isothermal test at 1100°C for 1125 hours, which is a little bit longer than the time at temperature for the cyclically tested specimens. This specimen did not fail. Examination of the cross section showed that there was not much cracking in the TBC and the separation during metallographic preparation was mainly along the TGO/bond coat interface (Figure 95b). These results also show the importance of thermal cycles on crack formation at the ridges. In the absence of these cracks, the failure is expected to be more along the TGO/bond coat interface as the stored energy in the TGO increases.



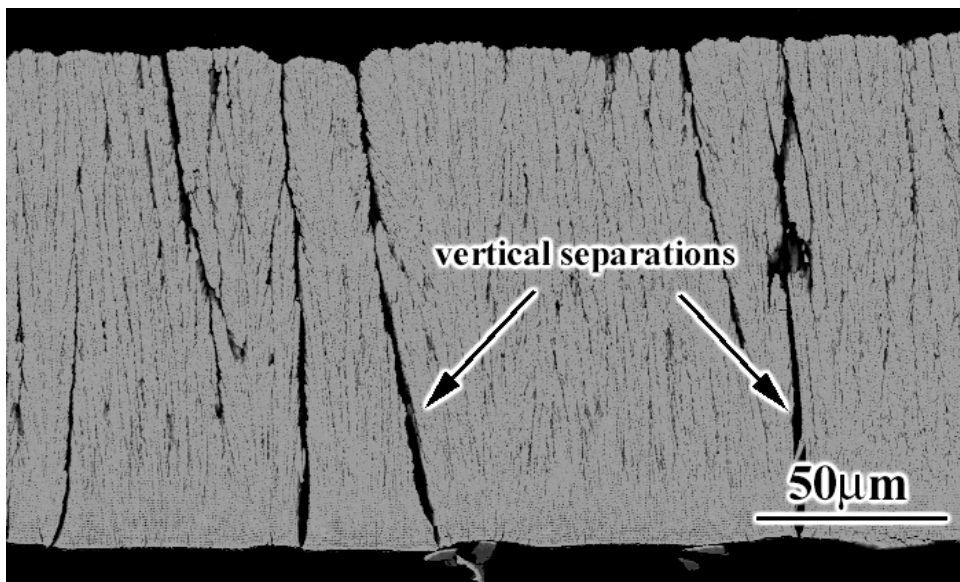
(a)



(b)



(c)



(d)

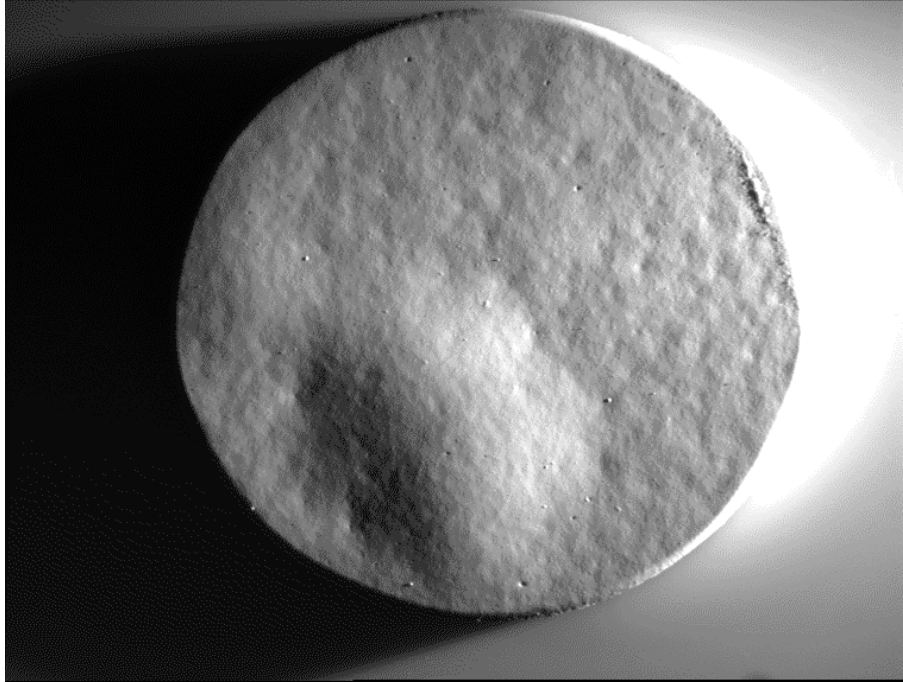
Figure 89 Scanning electron micrographs of TBC systems with as aluminized Pt aluminide bond coats in the as processed condition showing grain boundary ridges, (a), dense TBC with parallel row of pores, (b) and small openings in the TBC above the ridges, (c), which enlarge with exposure resulting in the formation of vertical separations in the TBC, (d).



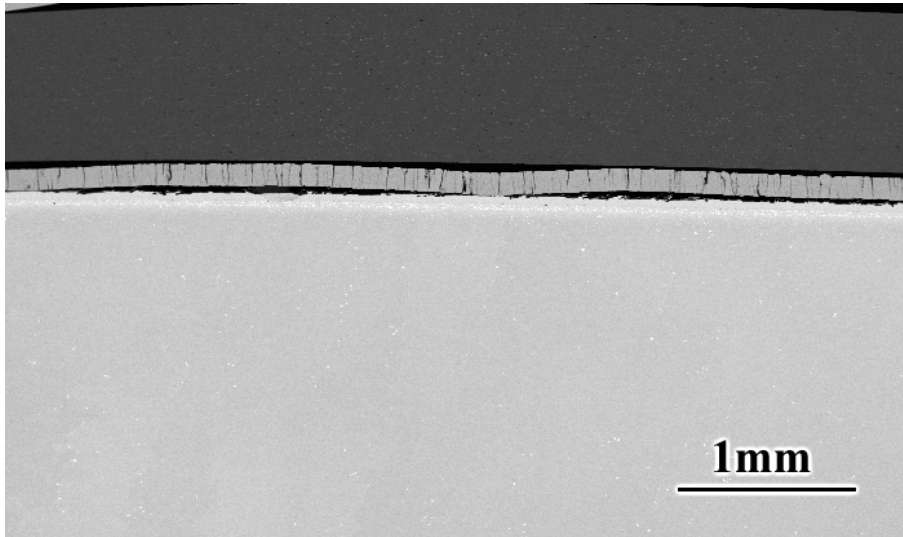
(a)



(b)

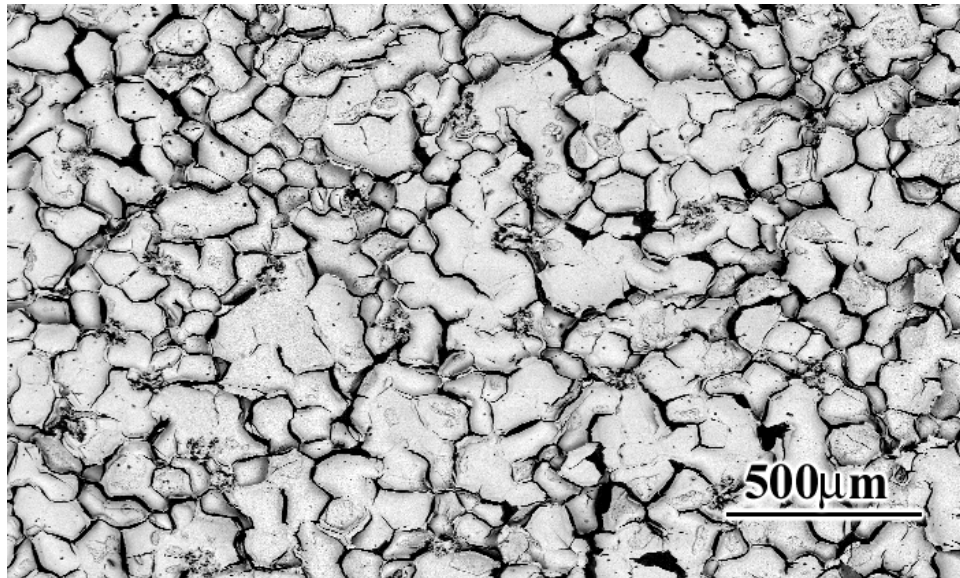


(c)

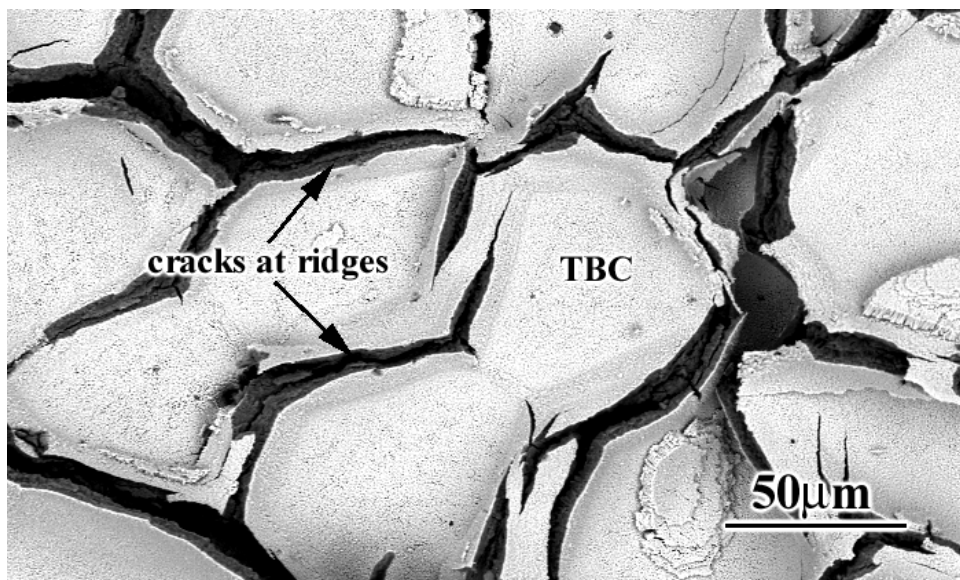


(d)

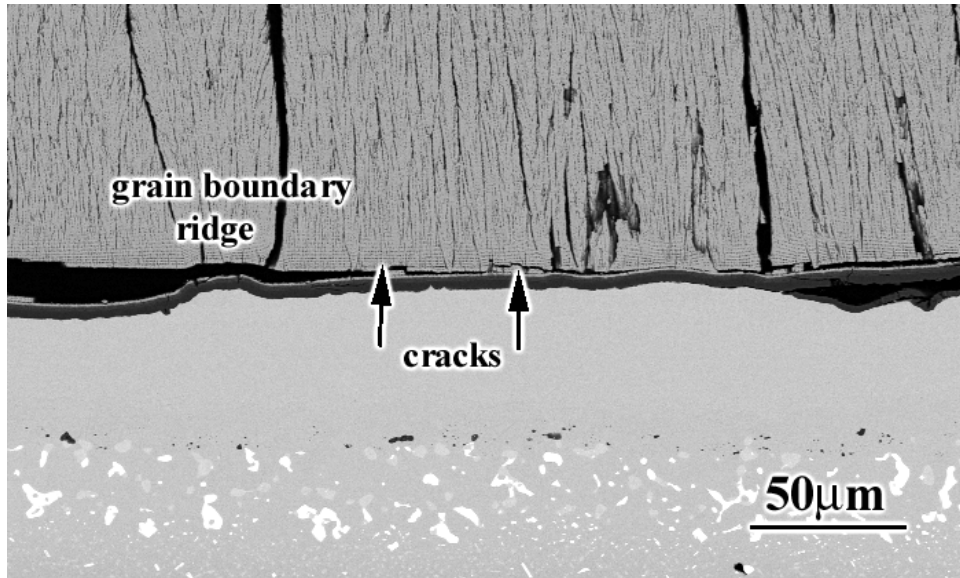
Figure 90 Macrographs of a TBC system on as aluminized Pt aluminide bond coat after exposure at 1100°C for 360 (a), 680 (b) and 860 cycles, (c), showing propagation of failure with time. The SEM micrograph in (d) shows the buckles in cross section.



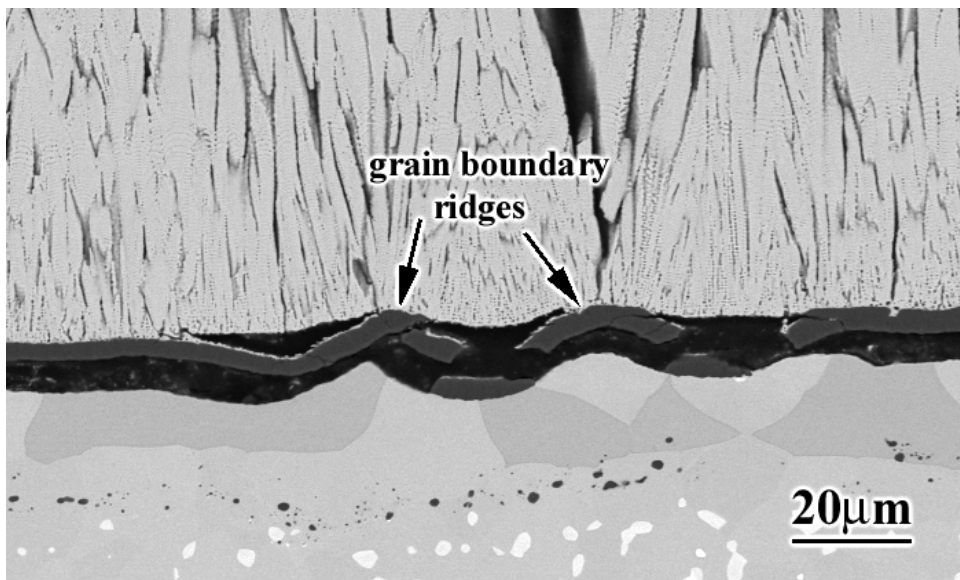
(a)



(b)

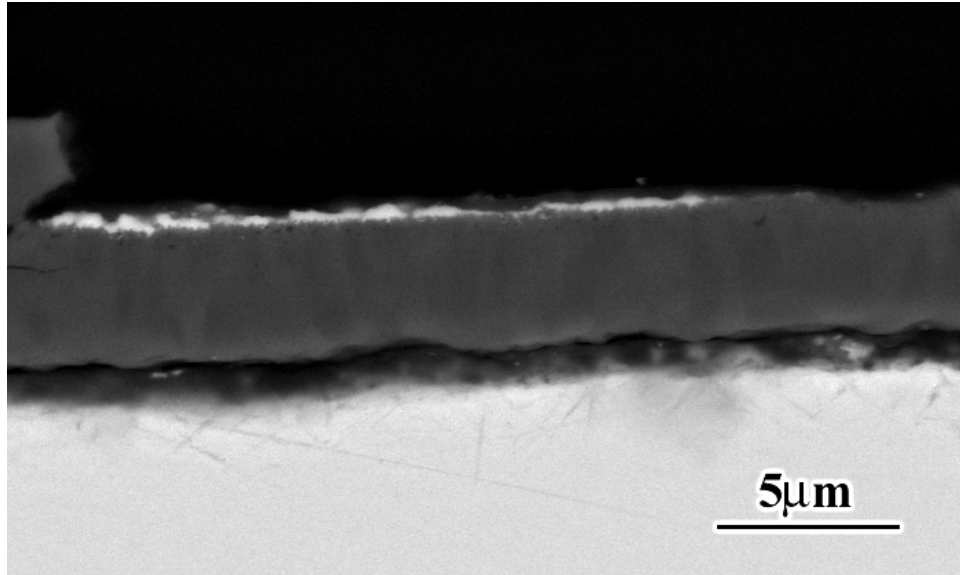


(c)

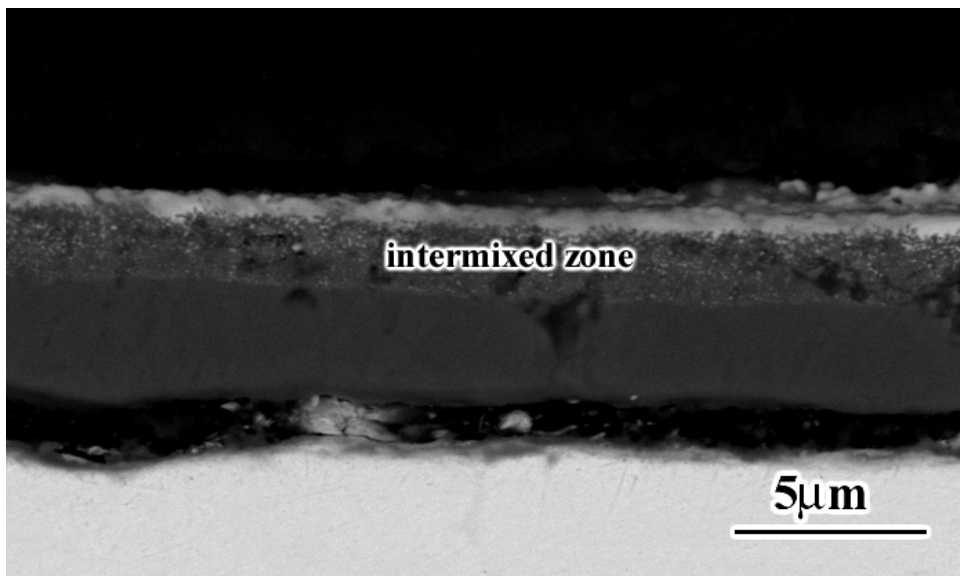


(d)

Figure 91 Scanning electron micrographs of TBC systems on as aluminized Pt aluminide bond coats after failure. The failure was mainly in the TBC, (a), and cracks were present at the grain boundary ridges as can be seen from the fracture surface, (b), as well as cross section, (c). Cracks at the ridges were also present in the absence of vertical separations in the TBC, (d).

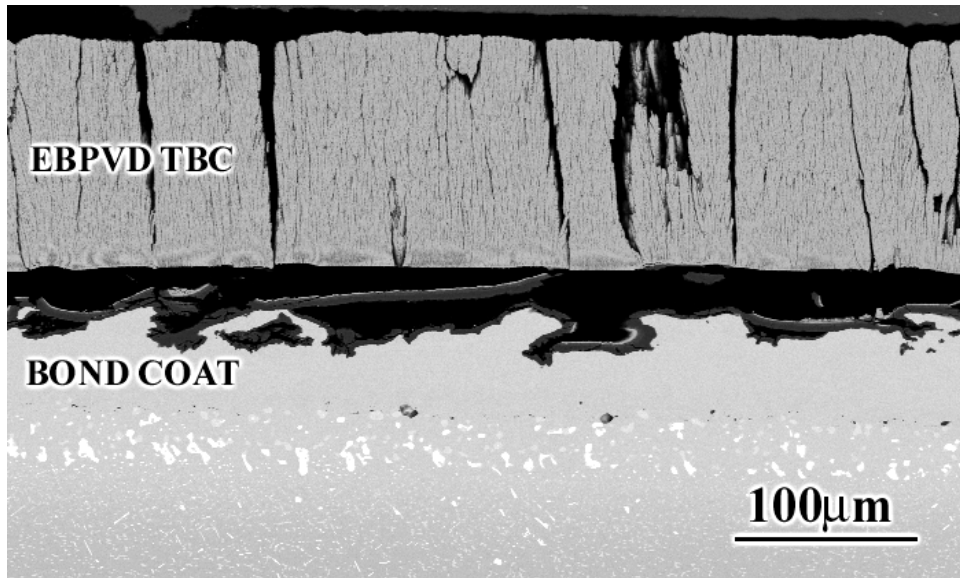


(a)

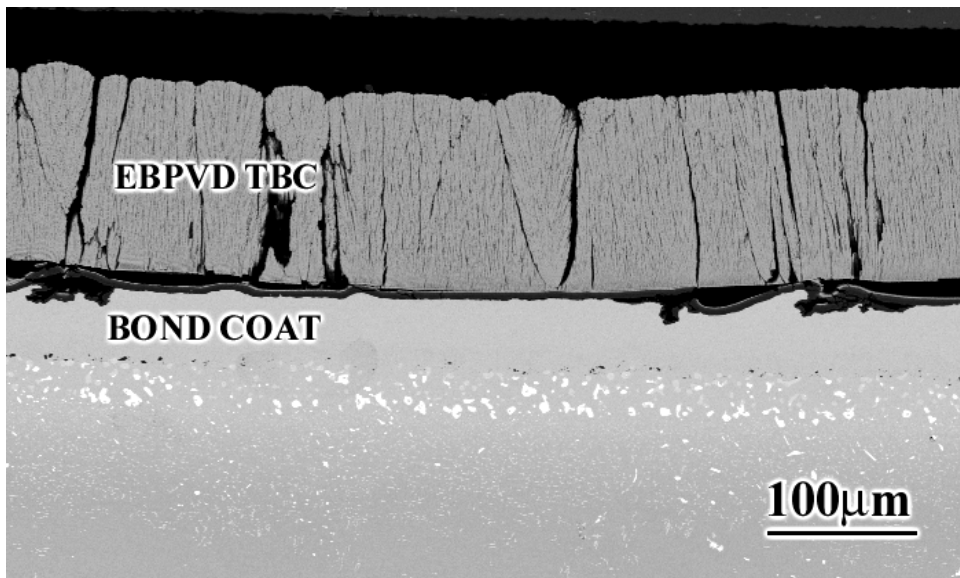


(b)

Figure 92 Scanning electron micrographs of TBC systems on as aluminized Pt aluminide bond coats with TBCs deposited by different companies. There was not any evidence of an intermixed zone for one set of specimens, (a), whereas there was a continuous layer of intermixed zone for the other set of specimens, (b)

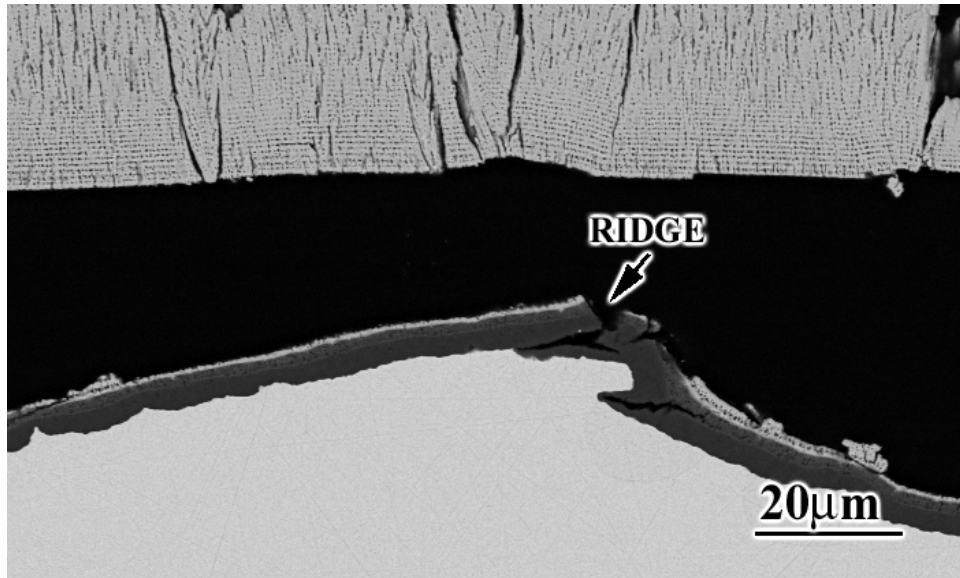


(a)

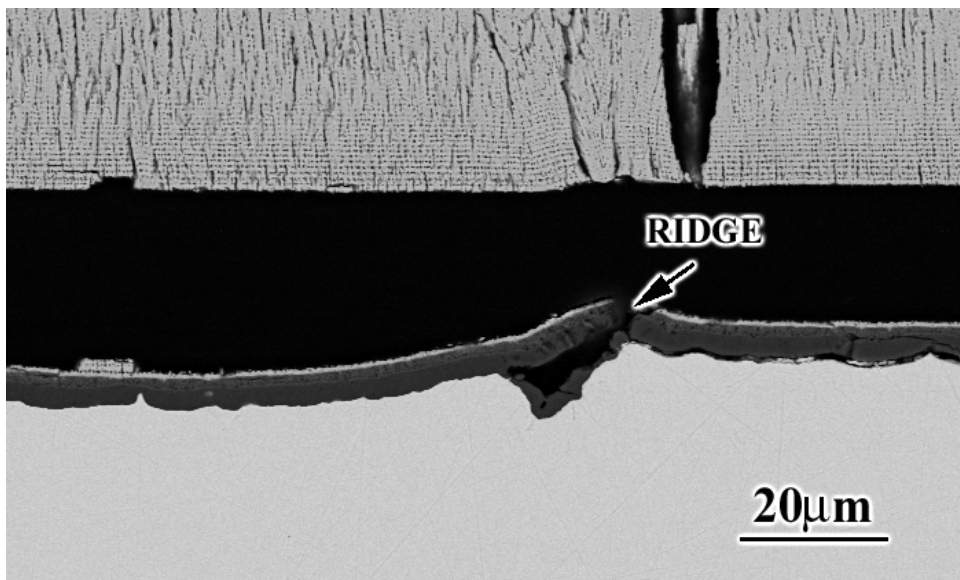


(b)

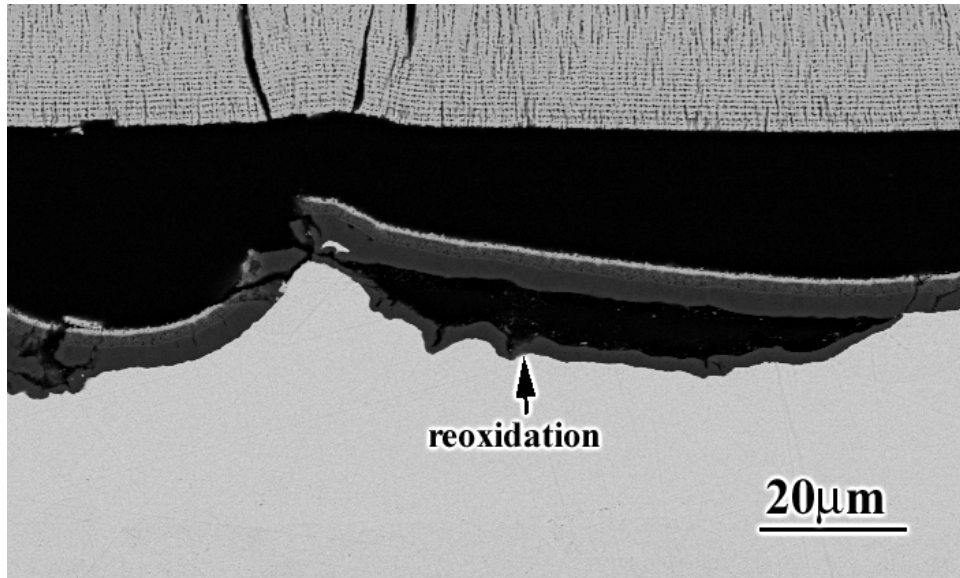
Figure 93 Scanning electron micrographs of TBC systems with as aluminized Pt aluminide bond coats after failure showing a highly deformed bond coat surface, (a), except at areas where the bond coat was still in contact with the TBC at the time of failure, (b).



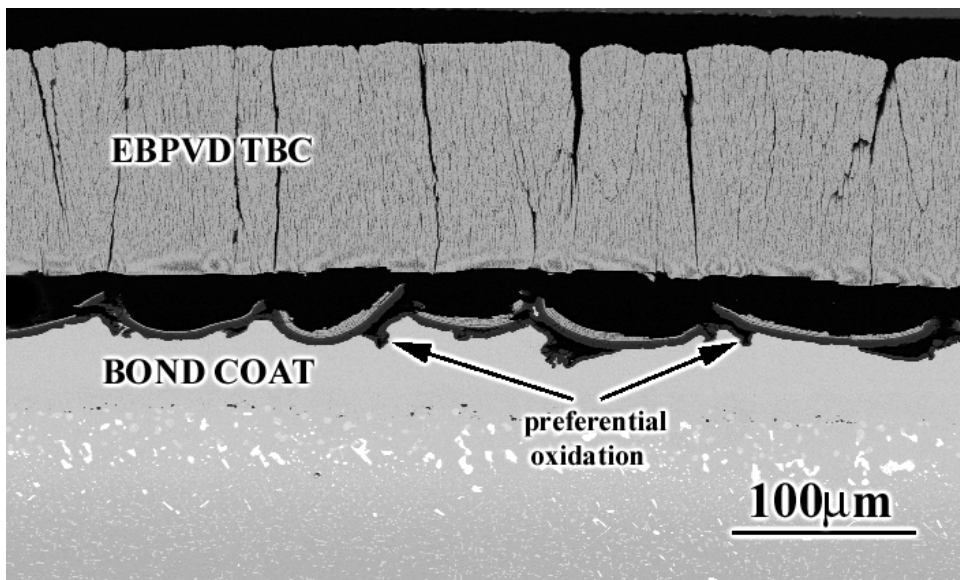
(a)



(b)

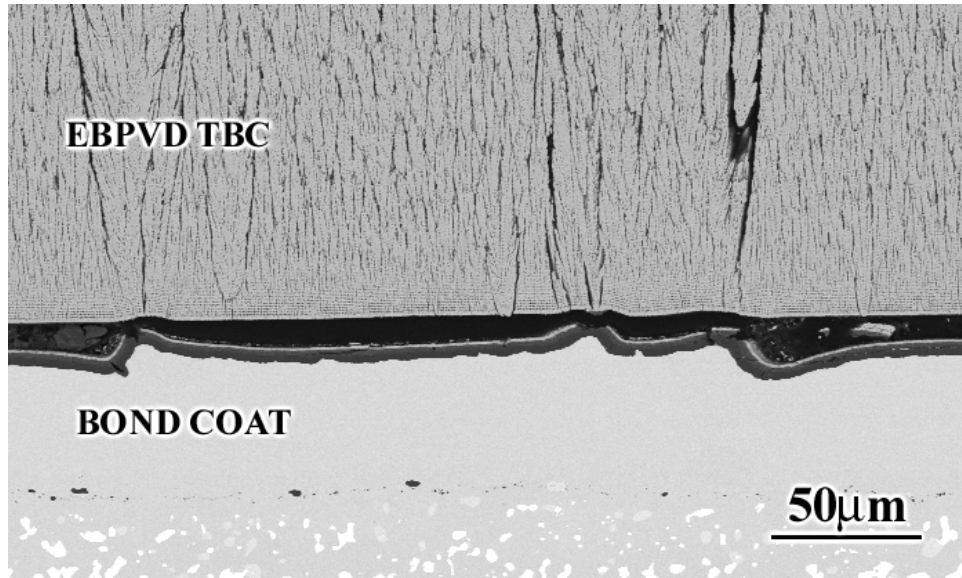


(c)

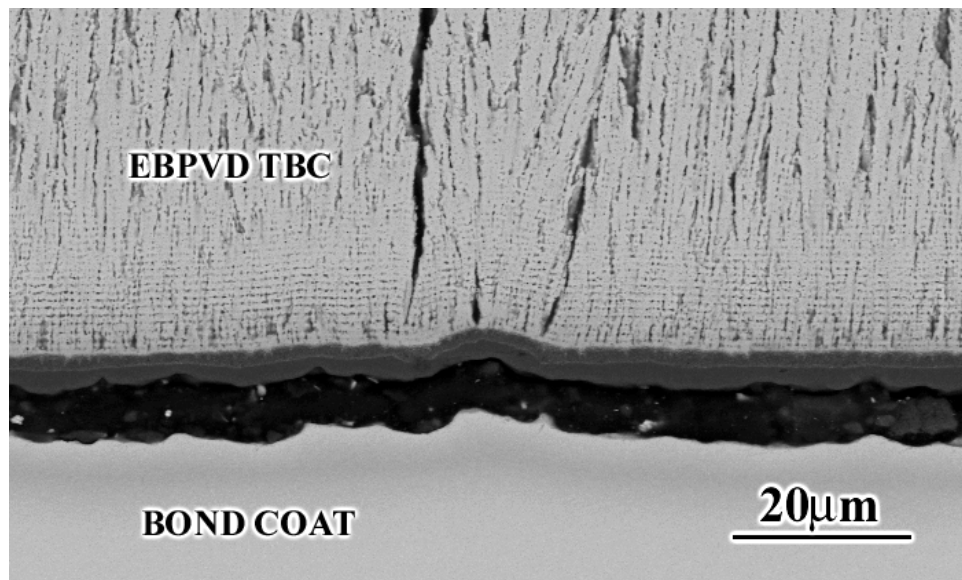


(d)

Figure 94 Scanning electron micrographs of TBC systems with as aluminized Pt aluminide bond coats showing vertical crack formation at the ridges, (a), and their propagation along the TGO/bond coat interface, (b), followed by reoxidation along this interface, (c). Preferential oxidation, usually at the grain boundaries, was observed in some areas, (d).



(a)



(b)

Figure 95 Scanning electron micrographs of TBC systems with as aluminized Pt aluminide bond coats after exposure under 15 hr cycles, (a), as well as under isothermal conditions, (b). Separation along the TGO/bond coat interface followed by reoxidation was not observed for these specimens. Cracking at the grain boundary ridges was not evident for the isothermally tested specimen.

Heavy Grit Blasted Platinum Aluminide Bond Coats: The failure behavior of the heavy grit blasted Pt aluminide bond coats were explained previously in subsection 4.2.3.2.

Light Grit Blasted Platinum Aluminide Bond Coats: The Pt aluminide bond coats that were given light grit blasting and preoxidation prior to TBC deposition outperformed the others. The interface in the as-processed condition was smooth compared to the ones that were given heavy grit blasting (Figure 96) Accordingly, the morphology of the TBC close to the TGO was also more uniform and columnar with much fewer “Corn Kernel TBC defects” commonly observed with the heavy grit blasted specimens.

When these specimens failed after relatively long amounts of time compared to the failure of other Pt aluminides, the failure was mainly along the TGO/bond coat interface (Figure 97a). The interface remained relatively smooth with few ratchets (Figure 97b). Examination of the fracture surface as well as the cross section revealed the presence of a large amount of voids, many of which seemed to develop at the grain boundaries (Figure 97c). In some localized areas, the voids as well as the flat bond coat surfaces around them were reoxidized before final failure (Figure 97d). This indicates that some separation along the TGO/bond coat interface prior to failure occurred in the vicinity of these voids. However, it should be mentioned here that the void density changed for specimens with thicker Pt and aluminide layers as mentioned previously. Void formation in bond coats must be due to vacancy condensation at preferred sites such as grain boundaries in the bond coat. It also appears that some voids may also be caused by phase transformations whereby volume changes arise.

Since these specimens had thick TGOs as a result of their relatively long lives, the stored energy in the TGO is expected to have a significant contribution on the failure. Therefore, void development as well as the stored strain energy in the TGO is believed to interact to cause failure

of these systems. In the presence of abnormal defects and/or contamination, some specimens were observed to fail earlier.

The most significant factor that improves the lives of these systems compared to state of the art heavy grit blasted Pt aluminide systems seems to be the prevention of the ratcheting type of failure due to stronger constraint of the TBC in the absence of “TBC defects” in the as-processed condition.

Media Finished Platinum Aluminide Bond Coats: Another conventional surface preparation technique used was media finishing. The media finished specimens were also preoxidized prior to TBC deposition. In the as-processed condition, the interface was smooth, nevertheless, there was some evidence of grain boundary ridges, which could not be removed completely as evident in Figure 98.

When they failed, the failure was mainly along the TGO/bond coat interface as in the case of light grit blasted specimens (Figure 99a). The interface was relatively smooth except at areas of preferential oxidation, most of which are believed to be along the grain boundaries (Figures 99b and 99c).

The buckles seemed to be associated with the areas that had pronounced amounts of preferential oxidation as evident in Figures 100a and 100b. Therefore, it is possible that the failure initiated in the vicinity of these localized areas of preferential oxidation. The macrograph taken after the specimen failed also indicated failure initiation at localized areas. In other areas, the TBC was still adherent (Figure 100c).

The preferential oxidation may be a consequence of cracking in the vicinity of the remnants of the grain boundary ridges. Preferential oxidation along the grain boundaries has also been shown to follow cracking at the grain boundary ridges for the as aluminized systems by Gell et al. [65].

The TGOs that developed on these specimens were thinner compared to the TGOs that developed on the grit blasted specimens. The slower TGO growth rate in addition to inhibition of the ratcheting type of failure appear to be contributing factors to the improved lives of these systems. The comparatively faster TGO growth on grit blasted samples may be due to incorporation of impurities during grit blasting as proposed by Tolypgo and Clarke [75]. Another possible explanation can be the effect of surface condition on the microstructure of the TGO which can directly affect the TGO growth rate.

Hand Polished Platinum Aluminide Bond Coats: The specimens were hand polished with a final surface finish of 3 microns. Some difficulties were encountered during polishing due to coating build up at the edges of the specimens. This unevenness of the surface resulted in more material removal at the edges, whereas some remnants of the grain boundary ridges were still present close to center of the specimen. There were only 2 hand polished platinum aluminide bond coats that were tested and both of them failed by formation of a buckle close to the center of the specimen exactly where the remnants of the grain boundary ridges were present (Figures 101a and 101b) . Other areas away from the buckles still looked adherent. Examination of the fracture surface below the buckles (Figure 101c) as well as the underside of the TBC (Figure 101d) also showed some areas with grain boundary networks, which may be another indication of failure in the vicinity of grain boundaries. The lives of these 2 specimens were still relatively long compared to the lives of heavy grit blasted specimens even in the presence of defects. These

observations also show the importance of the smooth surface in the improved lives of these systems

The cross sectional examination showed that the TGO/TBC interface remained relatively flat (Figure 102a). However, the TGO/bond coat interface was irregular as a result of thickness variations in the TGO (Figure 102b). Small pores were present in the TBC close to the TGO (Figure 102c). In localized areas, these pores linked up causing separations in the TBC. The bond coat underneath deformed as evident in Figure 102d. This is consistent with the proposed mechanism about TBC constraint where the bond coat deforms as long as it loses contact with the TBC. However, it is not clear why these separations formed in the TBC in the first place. The relatively high stored energy in the TBC due to its denser microstructure on smooth surfaces may be responsible for the initiation and then propagation of these defects.

The TGO growth rates were also slower compared to grit blasted samples as observed for the media finished specimens. Possible explanations for this difference were given previously.

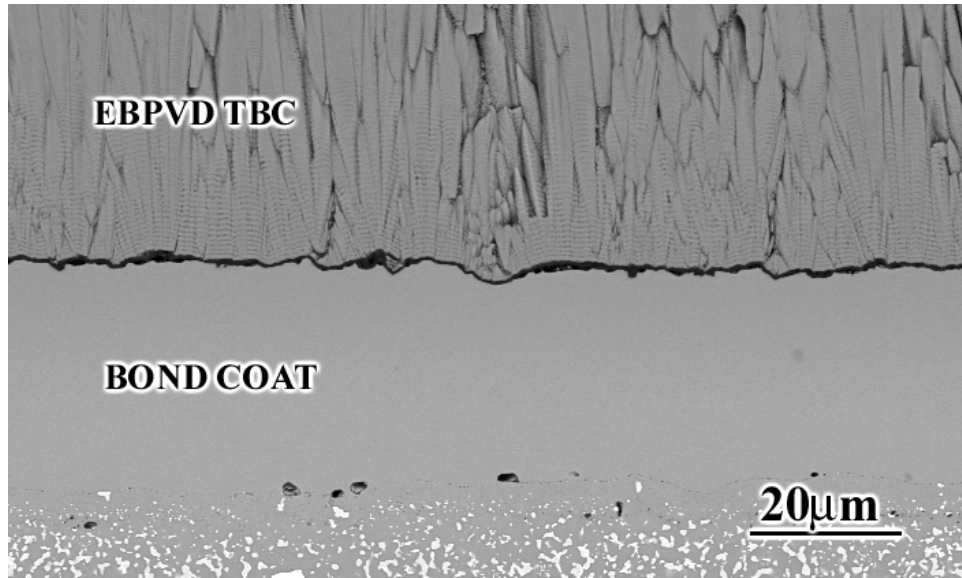
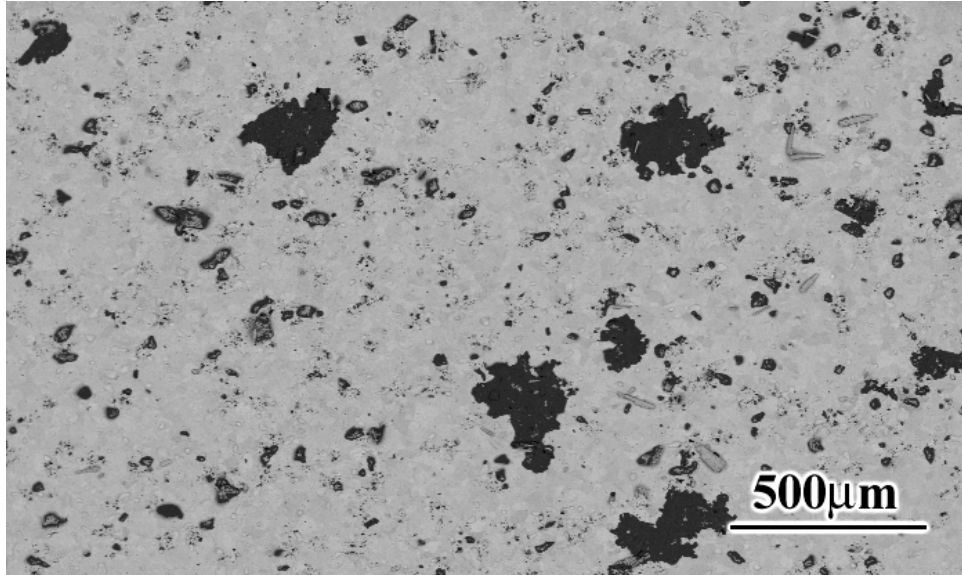
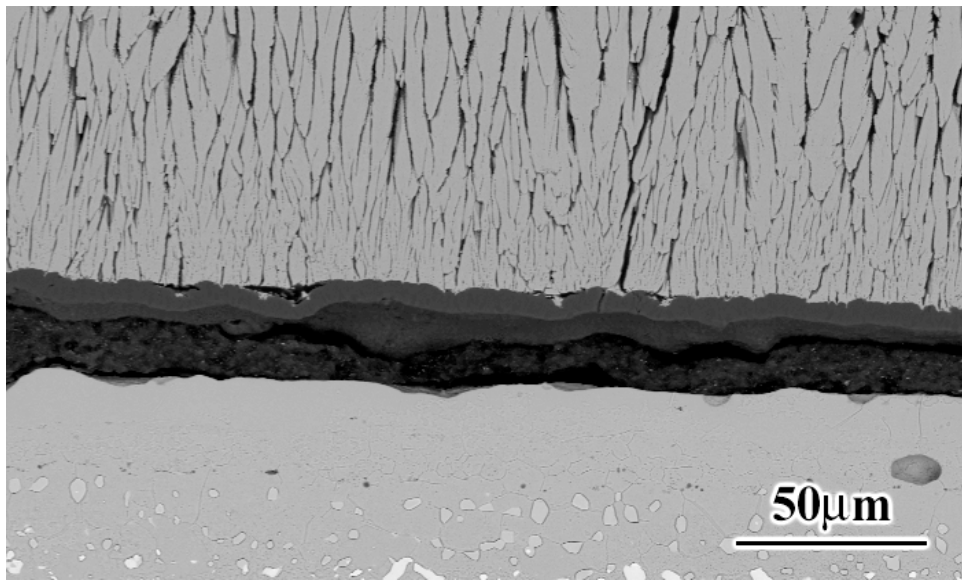


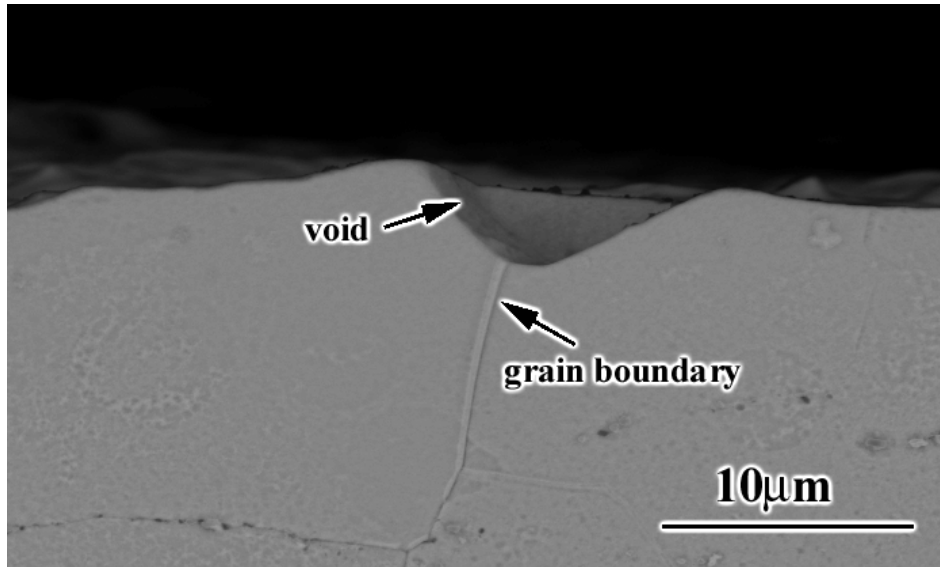
Figure 96 Scanning electron micrograph of a TBC system with light grit blasted Pt aluminide bond coat in the as processed condition showing a relatively smooth interface compared to the interfaces of heavy grit blasted Pt aluminides.



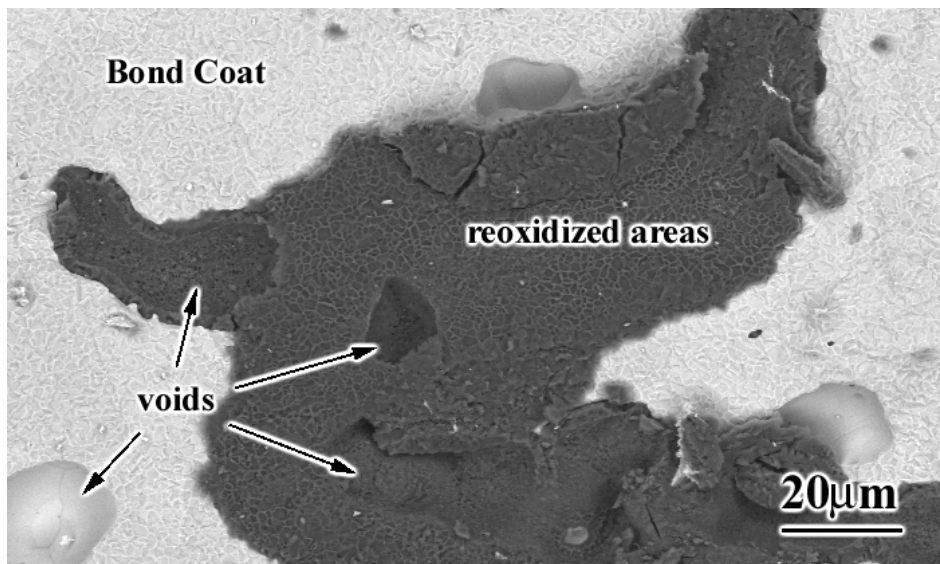
(a)



(b)



(c)



(d)

Figure 97 Scanning electron micrographs of TBC systems with light grit blasted Pt aluminide bond coats after failure showing that the failure was mainly along the TGO/bond coat interface, (a). The interface remained smooth with very few ratchets, (b), and voids, which were usually at the grain boundaries of the bond coat, were evident (c). There were indications of separations along the TGO/bond coat interface in the vicinity of the voids prior to failure, (d).

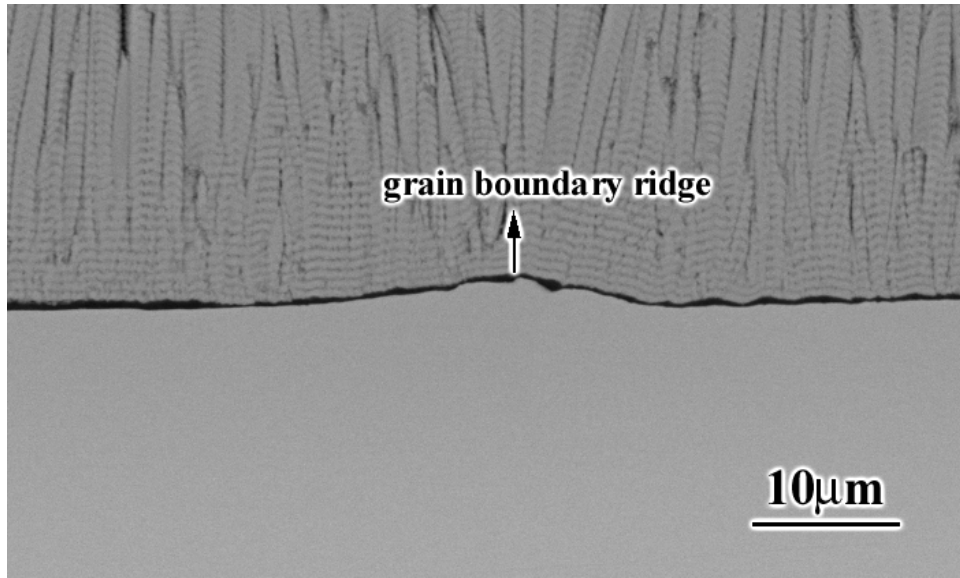
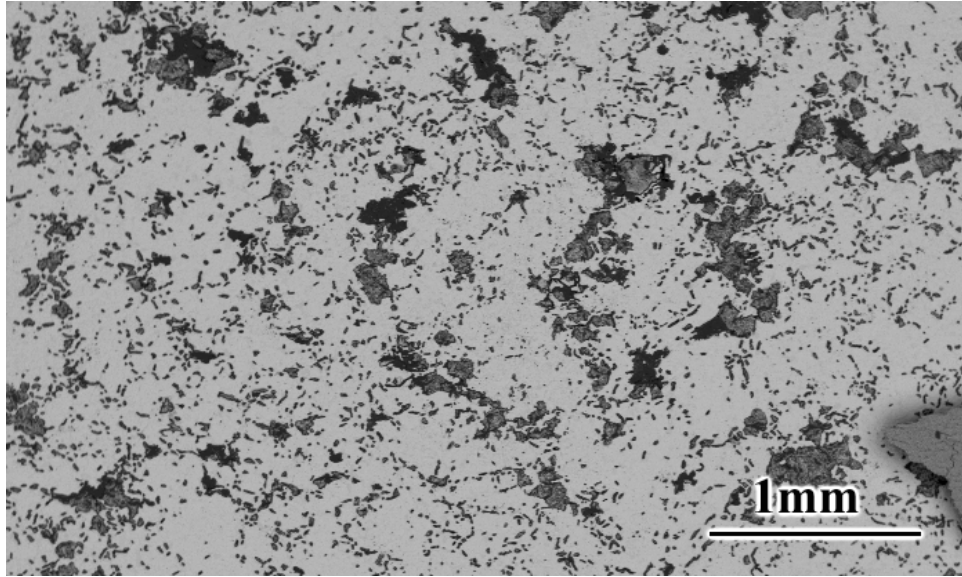
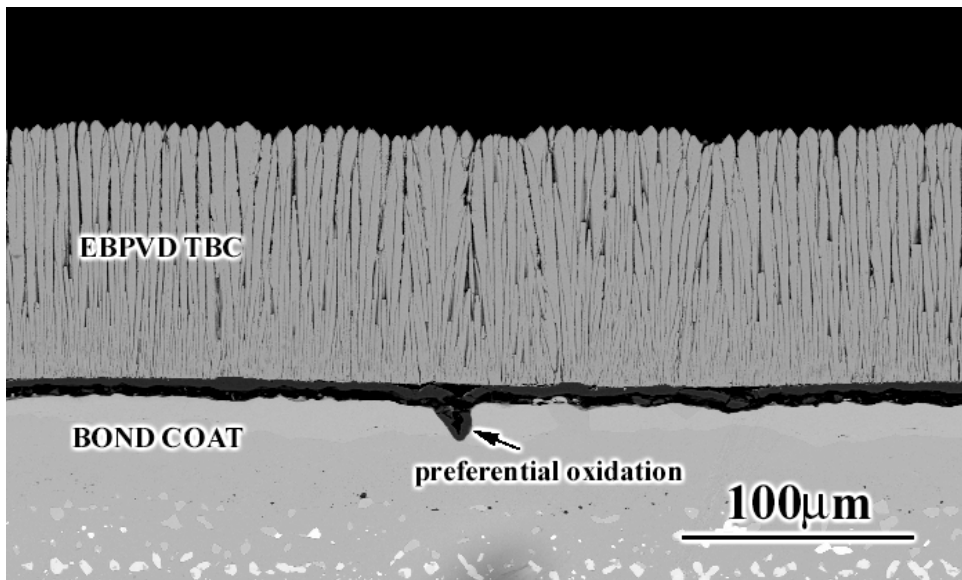


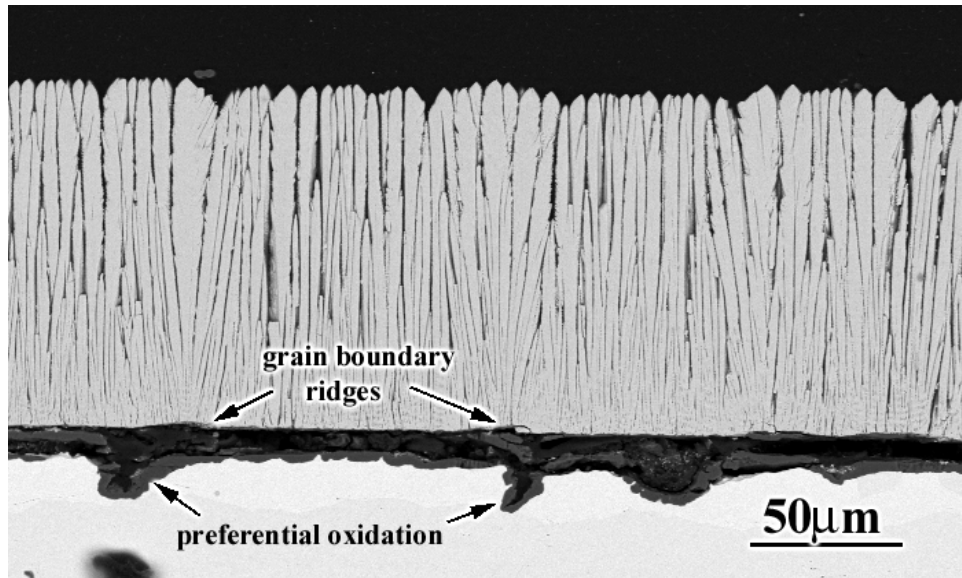
Figure 98 Scanning electron micrograph of a TBC system with media finished Pt aluminide bond coat in the as processed condition showing the presence of remnants of grain boundary ridges.



(a)

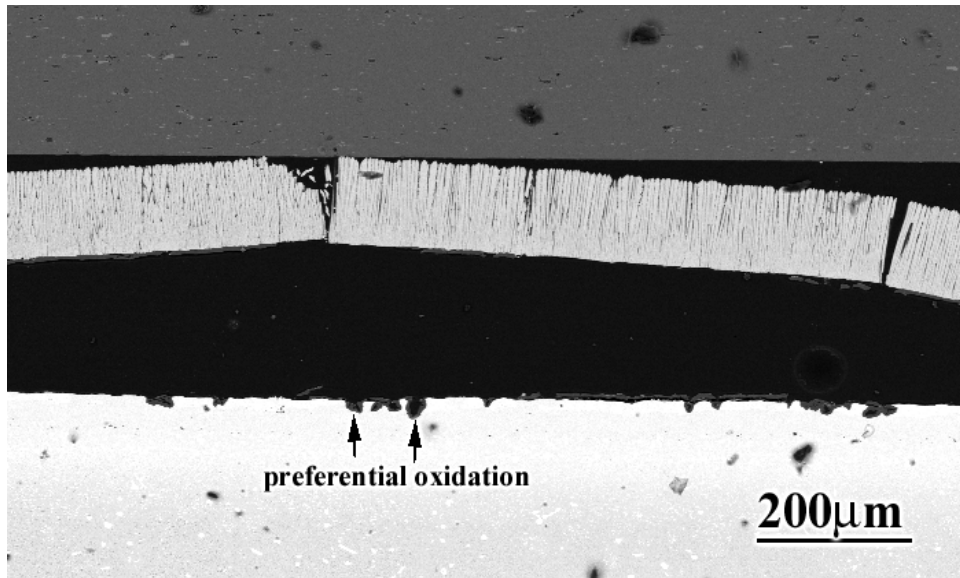


(b)

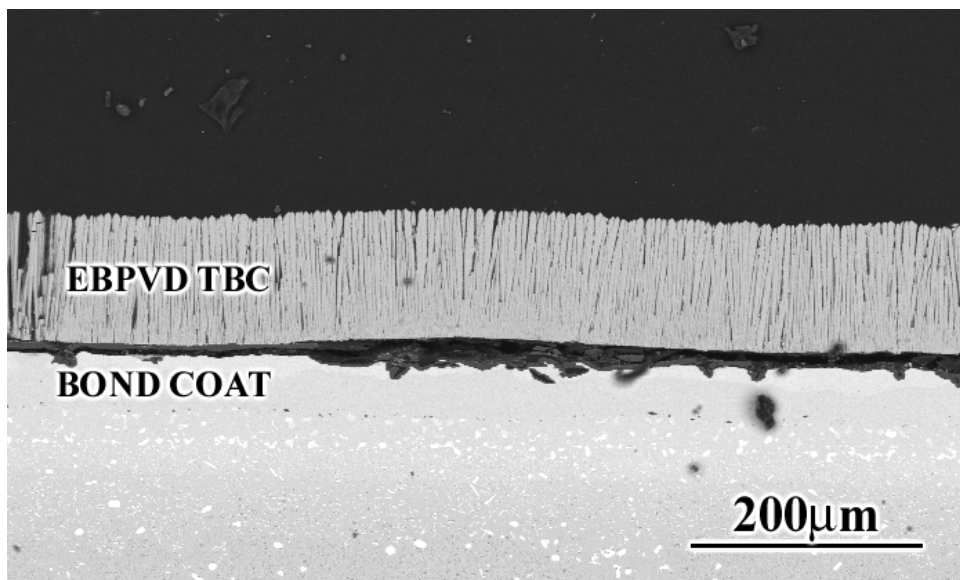


(c)

Figure 99 Scanning electron micrographs of a TBC system with media finished Pt aluminide bond coat after failure. The failure was mainly along the TGO/bond coat interface, (a), and the interface was relatively smooth compared to heavy grit blasted Pt aluminides except at areas of preferential oxidation which were usually observed to be along the grain boundaries, (b) and (c).



(a)



(b)

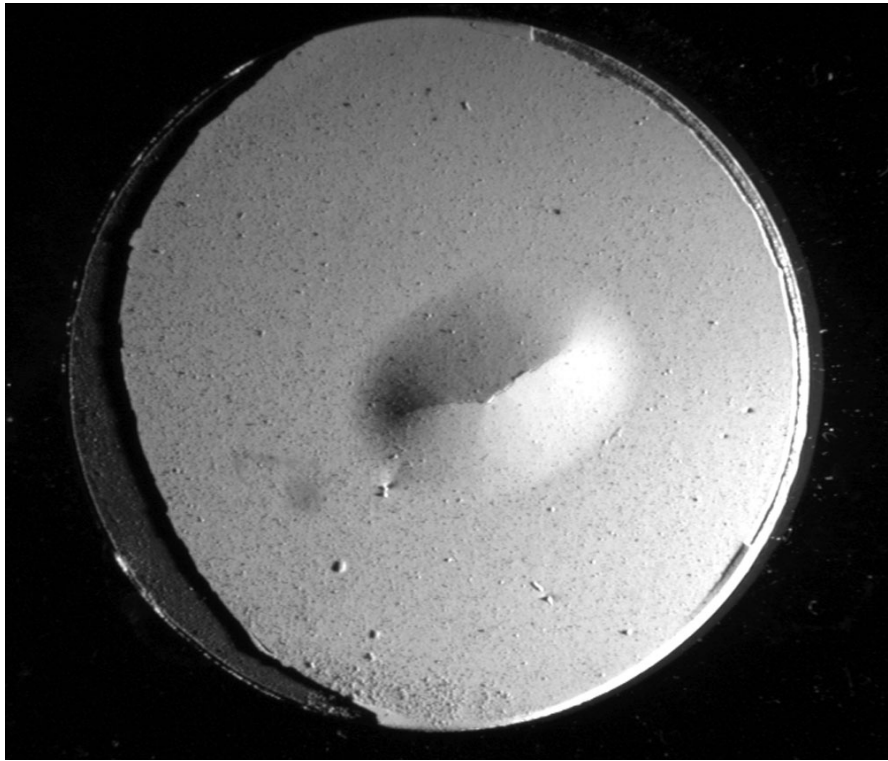


(c)

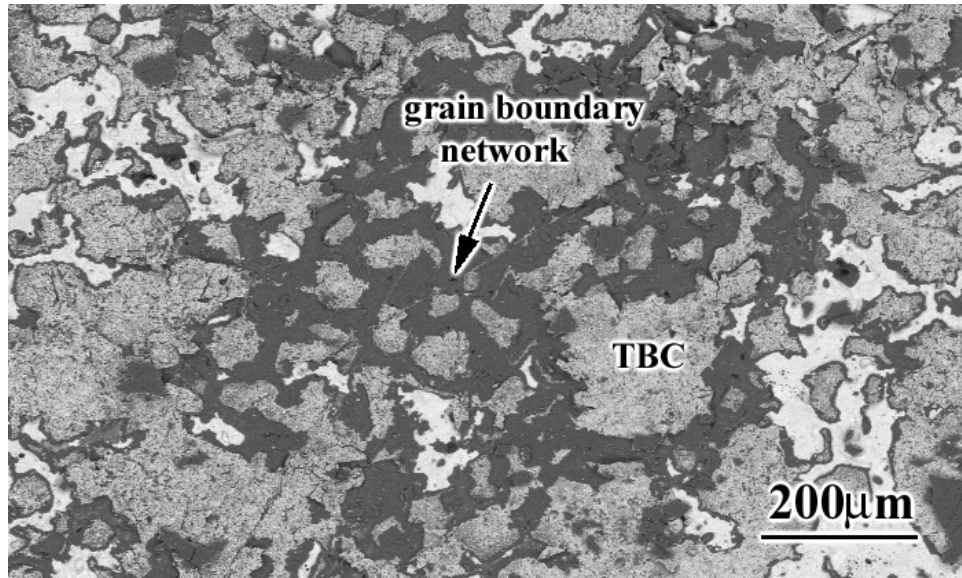
Figure 100 Scanning electron micrographs of a TBC system with media finished Pt aluminide bond coat after failure showing buckles above areas with pronounced amounts of preferential oxidation, (a) and (b). The macrograph of this specimen after failure also indicated failure initiation at localized areas, (c).



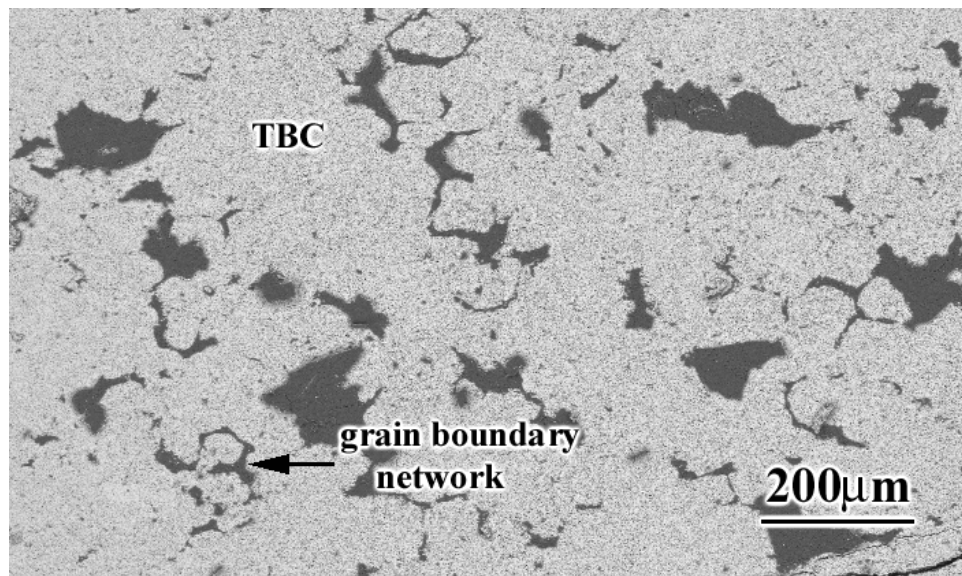
(a)



(b)

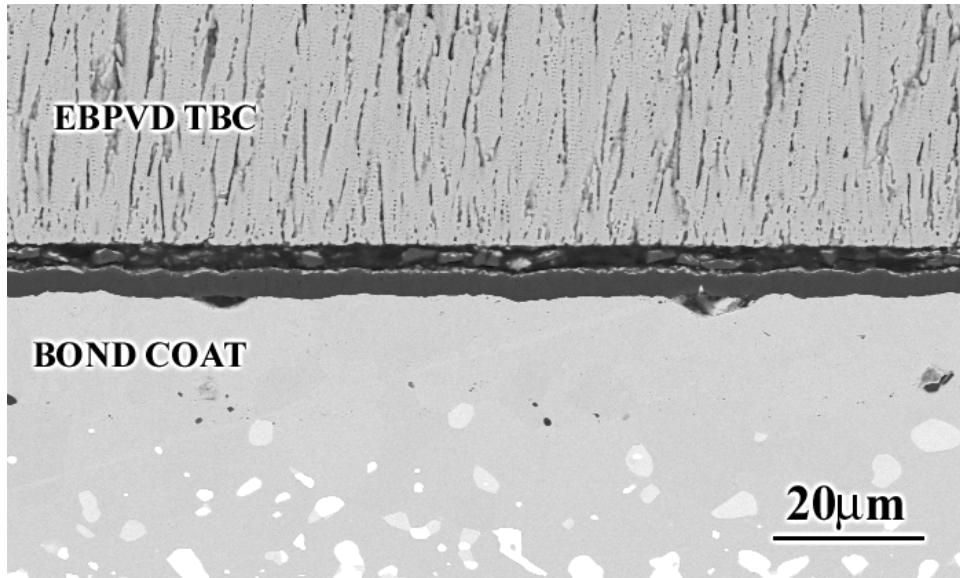


(c)

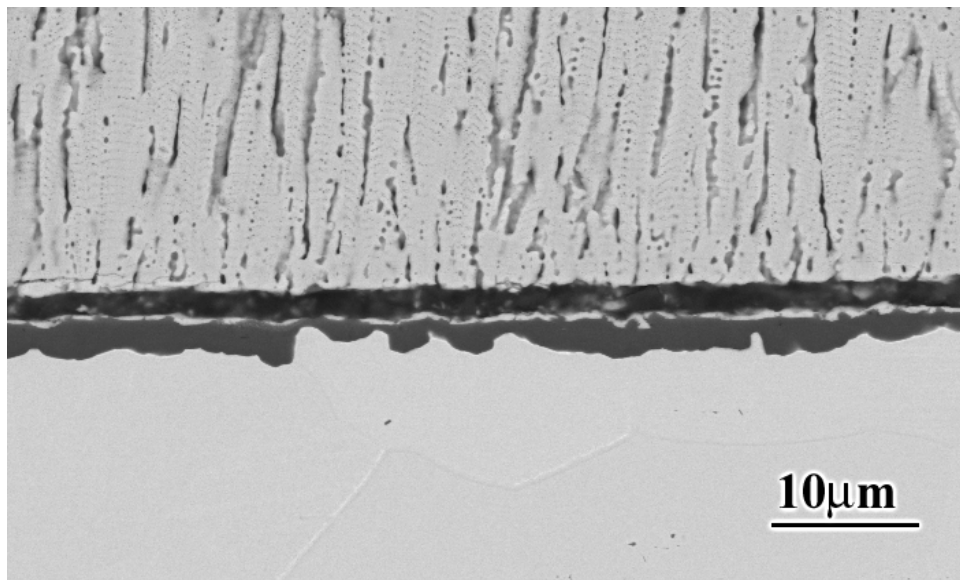


(d)

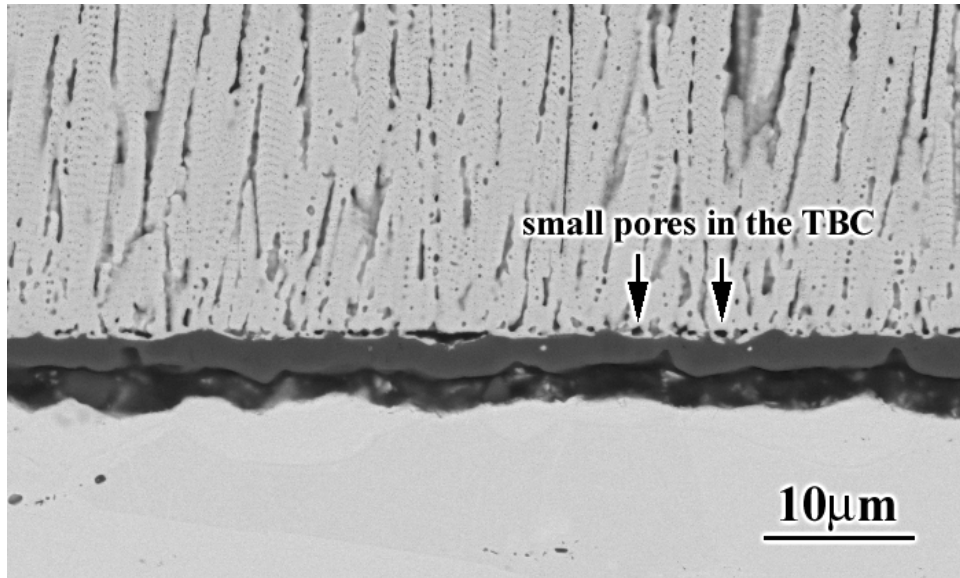
Figure 101 Macrographs of TBC systems with hand polished Pt aluminide bond coats showing buckles formed close to the center of the specimens, (a) and (b). Examination of the fracture surface, (c), as well as underside of the TBC, (d), under these buckles showed a grain boundary network.



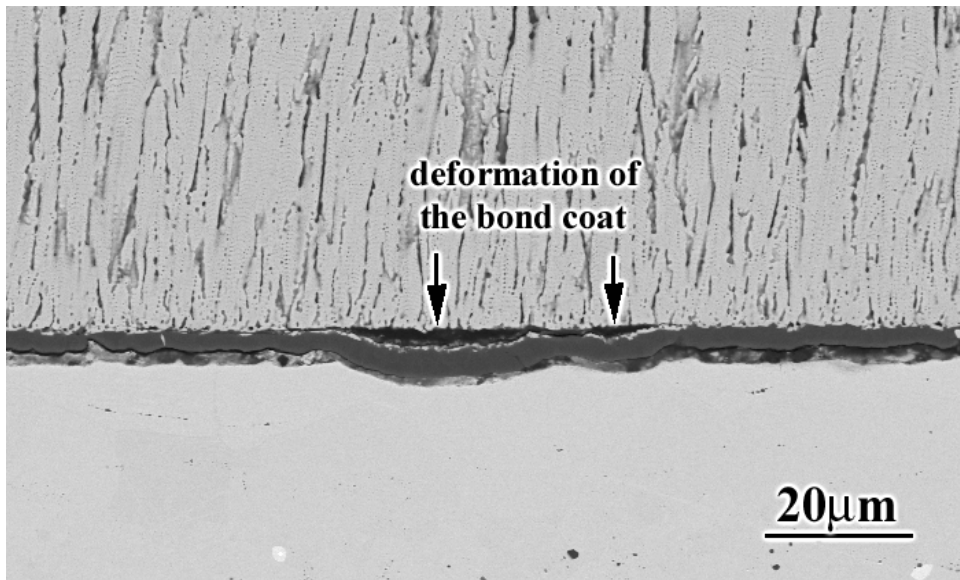
(a)



(b)



(c)



(d)

Figure 102 Scanning electron micrographs of TBC systems with hand polished Pt aluminide bond coats after failure. The TGO/TBC interface remained smooth, (a), whereas the TGO/bond coat interface was irregular due to thickness variations in the TGO, (b). Small pore like openings developed in the TBC, (c), which then linked up causing larger separations which were followed by deformation of the bond coat underneath, (d).

4.2.4.3 No Bond Coat Systems The lives of no bond coat TBC systems were surprisingly long as can be seen from the failure times given in Table 6. They were not expected to perform well due to poor oxidation resistance of the superalloys. However, it has been observed that the poor oxidation resistance could be offset by some other characteristics for TBC performance, which will be discussed next.

There were two different batches of no bond coat TBCs. The first batch was given a preoxidation heat treatment prior to TBC deposition whereas the second batch was just heavy grit blasted without any preoxidation. The cross sectional examination of these specimens in the as-processed condition showed that the specimens from the first batch did not develop a continuous layer of TGO (Figure 103a) whereas the ones from the second batch did (Figure 103b). Some irregularity of the interface was evident as a result of grit blasting, which also left numerous grit particles embedded at the interface (Figure 103c).

The first batch of specimens had relatively shorter failure times compared to the second batch of specimens. The failure of one of the specimens from the first batch after 140 cycles at 1100°C was entirely along the TGO/TBC interface. Significant amounts of transient oxides were observed at this interface (Figure 104a). Cross sectional examination of this specimen showed that the transient oxides formed as a thick and continuous layer and were poorly bonded to the TBC (Figure 104b). This observation explains the early failure of this specimen all along this interface. There was a good trend showing improvements in lives with decreased amounts of transient oxides. Figure 104c is a cross sectional micrograph from one of the specimens, also from the first batch, showing fewer amounts of transient oxides which did not develop as a continuous layer. This specimen failed after 1280 cycles and the failure was more along the TGO/superalloy interface (Figure 104d). The specimens from the second batch had even longer

lives, the shortest being 1580 cycles. One of these specimens was examined after 1840 cycles before failure and this one had even fewer transient oxides compared to the longest lived specimen from the first batch (Figure 104e). This observation also confirms the improved lives of no bond coat TBC systems with smaller amounts of transient oxides. The other specimens from the second batch had lives longer than 3500 cycles. The test was stopped before they failed.

The surfaces remained smooth after long exposure times such as after 1840 cycles as evident in Figure 105. The high strength of the superalloy, which did not let the surface deform, seems to play a crucial role for the significantly long lives of these specimens. However, our results also showed that premature failures could occur if significant amounts of transient oxides were present. Therefore, it is very important to determine the optimized processing conditions that result in the formation of as few transient oxides as possible for the expected durability and the reliability of these systems.

Some of the superalloys were electroplated with Pt prior to TBC deposition. There were also two different batches of these systems. The cross sectional examination of the as-processed specimens from the first batch showed the presence of a non-continuous TGO (Figure 106a) as in the case of the first batch of no bond coat TBCs. On the other hand, the specimens from the second batch had a continuous layer of TGO as evident in Figure 106b. The interfaces were irregular, probably due to electroplating of Pt as mentioned earlier.

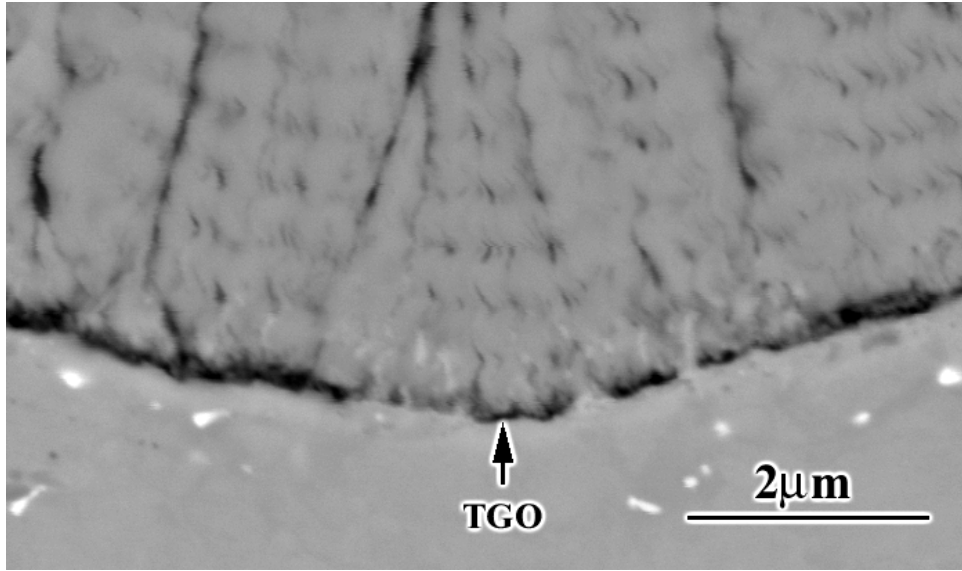
The first batch of specimens had relatively shorter lives compared to the very long lives of the second batch of specimens (Table 6) Figure 107a is from the fracture surface of a specimen from the first batch, showing significant amounts of voids. Transient oxides in addition to voids were also present (Figure 107b). The significant amounts of voids seem to be responsible for the relatively early failure of these specimens, mainly along the TGO/Pt overlayer interface

compared to the second batch. None of the specimens from the second batch failed up to date. However, examination of one specimen after 2300 cycles of exposure before failure indicated the presence of a rather pure TGO (Figure 108a) with intermittent areas of transient oxides (Figure 108b) Separation along the TGO/Pt overlayer interface occurred during metallographic preparation, however, the TGO/TBC interface looked quiet adherent, except at localized areas of transient oxides, despite the presence of numerous vertical separations (Figure 108c).

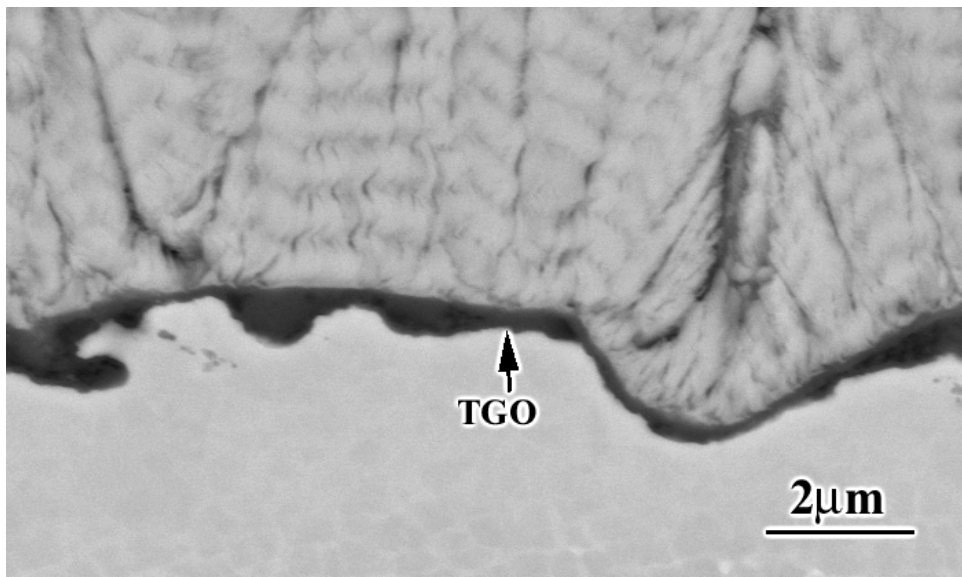
The significantly improved lives of these specimens, despite the initially irregular interface and numerous vertical separations in the TBC, as well as some transient oxides might be a consequence of a very high interfacial toughness, which still remains to be validated.

Table 6 Failure Times for no Bond Coat TBC systems

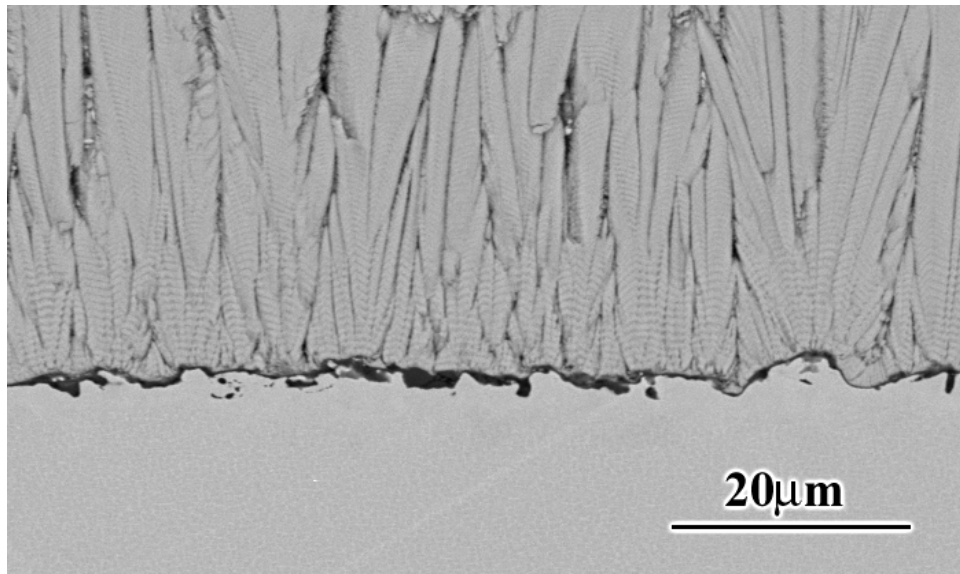
	Failure Time at 1100°C (# of 1 hr cycles to failure)
N5 (first batch)	140, 1280, 700+
N5 (second batch)	1580, 4100, 1840+, 3660+
N5-Pt Overlayer (first batch)	500, 660
N5-Pt Overlayer (second batch)	2300+, 4300+



(a)

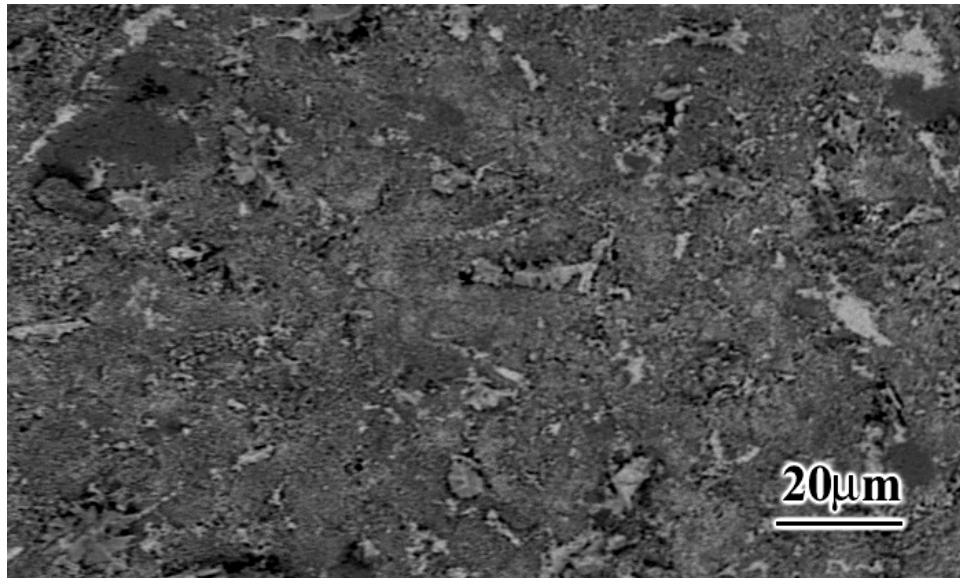


(b)

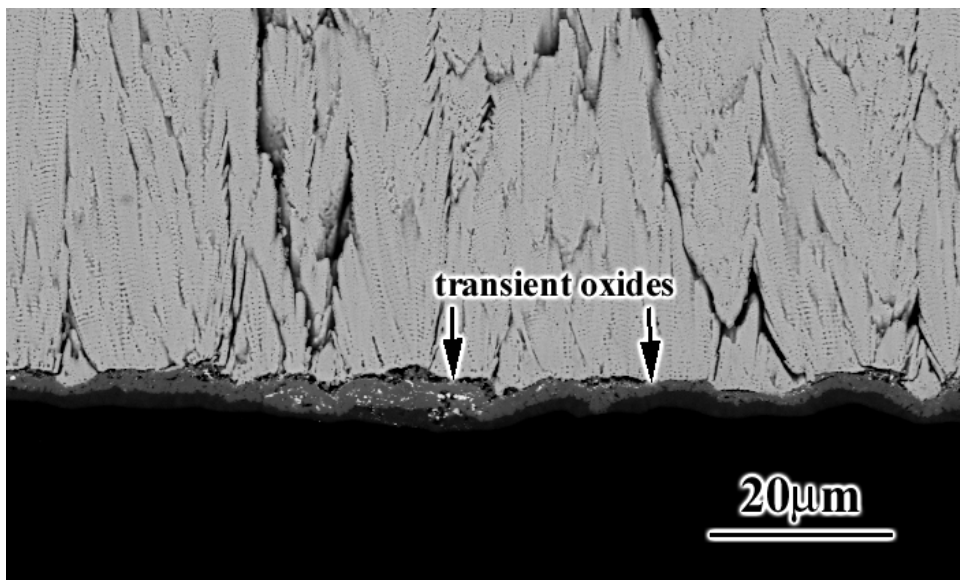


(c)

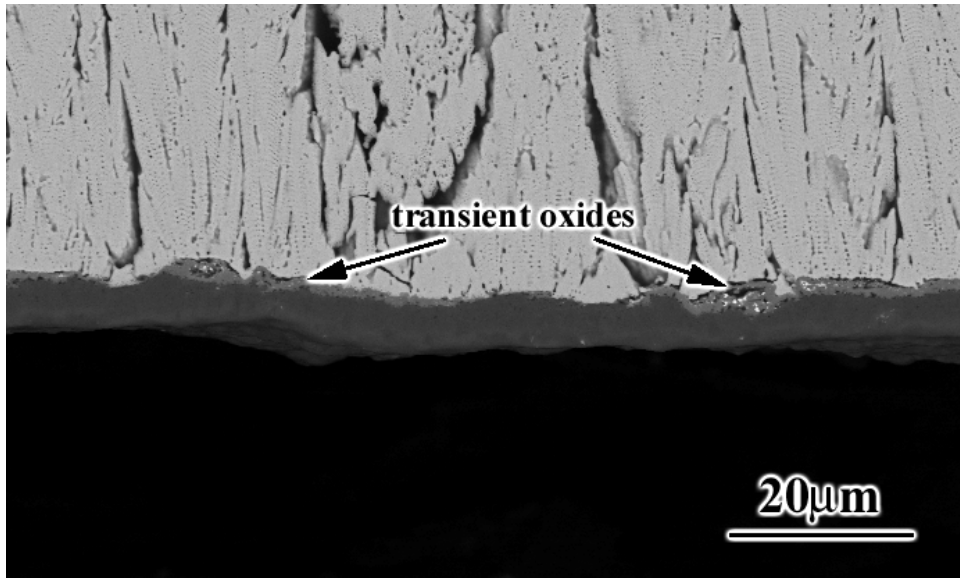
Figure 103 Scanning electron micrographs of no bond coat TBC systems in the as processed condition. The specimens from the first batch did not develop a continuous layer of TGO, (a), whereas the ones from the second batch did, (b). Some irregularity of the interface was evident as a result of grit blasting, (c).



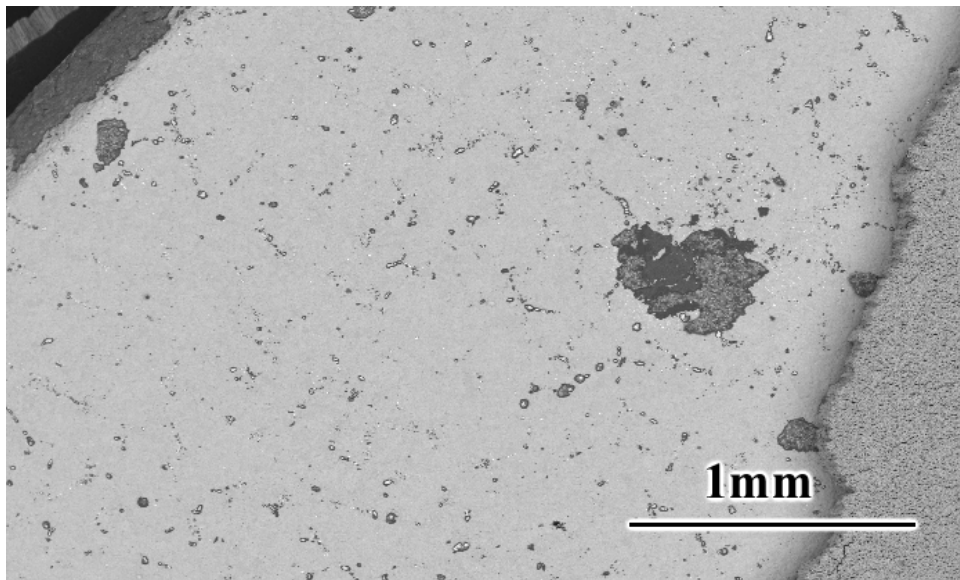
(a)



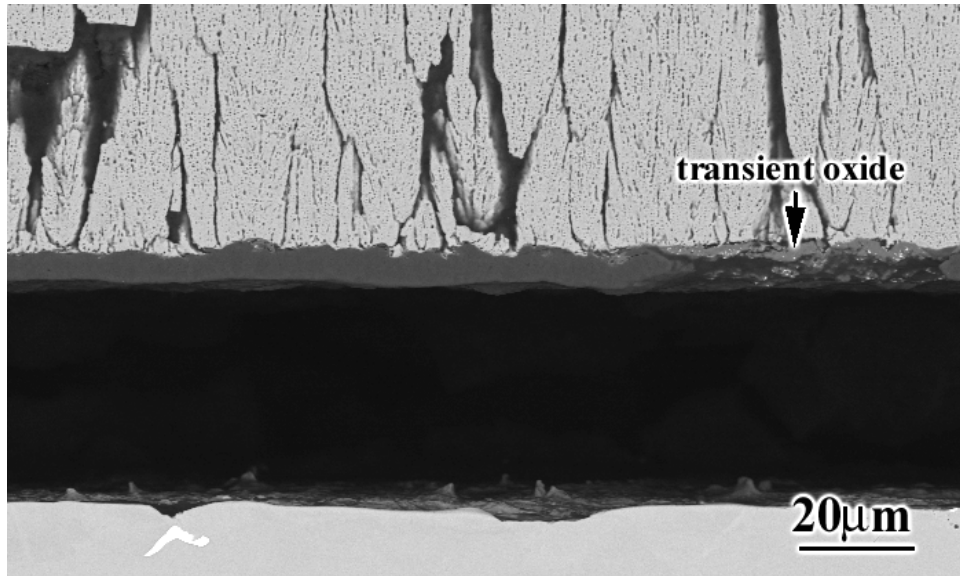
(b)



(c)



(d)



(e)

Figure 104 Scanning electron micrographs from no bond coat TBC systems after 140 cycles, (a) and (b), 1280 cycles, (c) and (d), as well as after 1840 cycles before failure, (e). There was a good trend showing improvement in lives with less transient oxides.

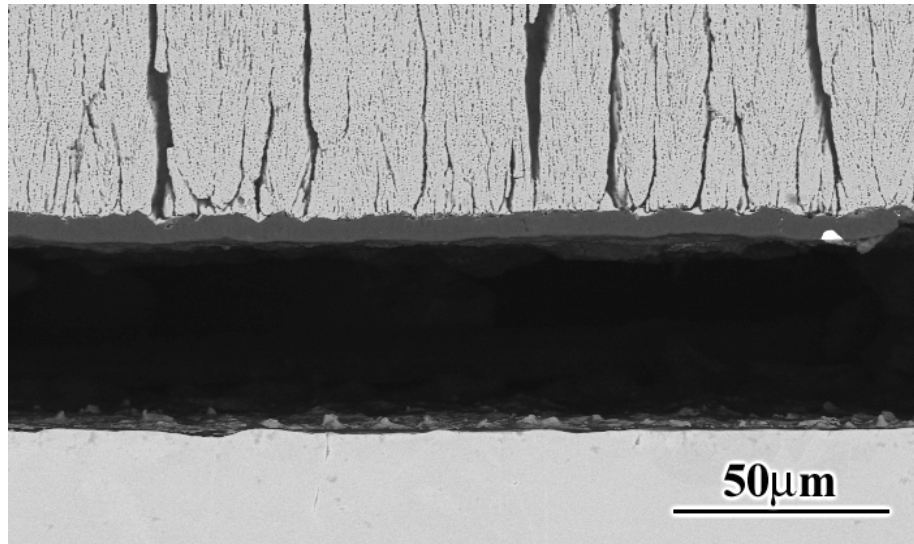
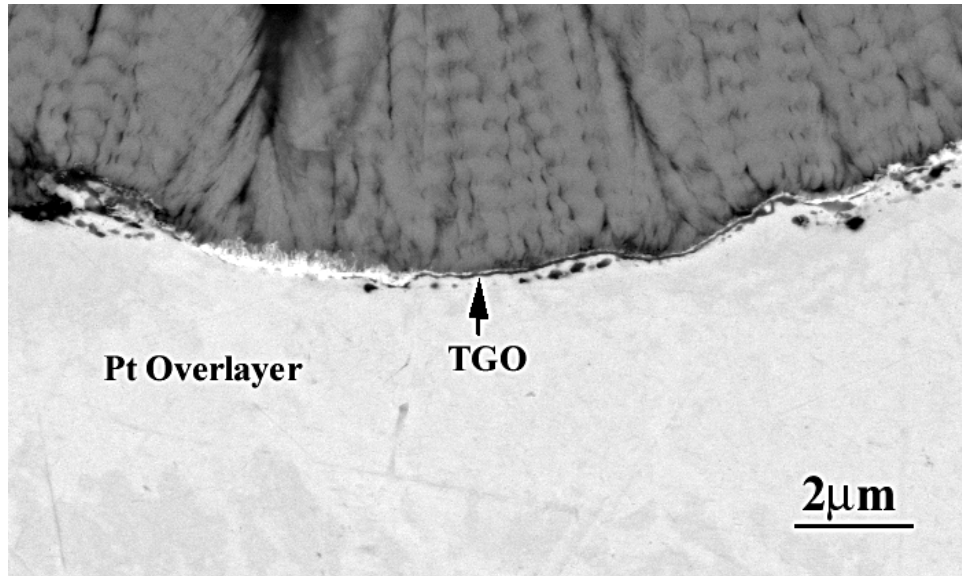
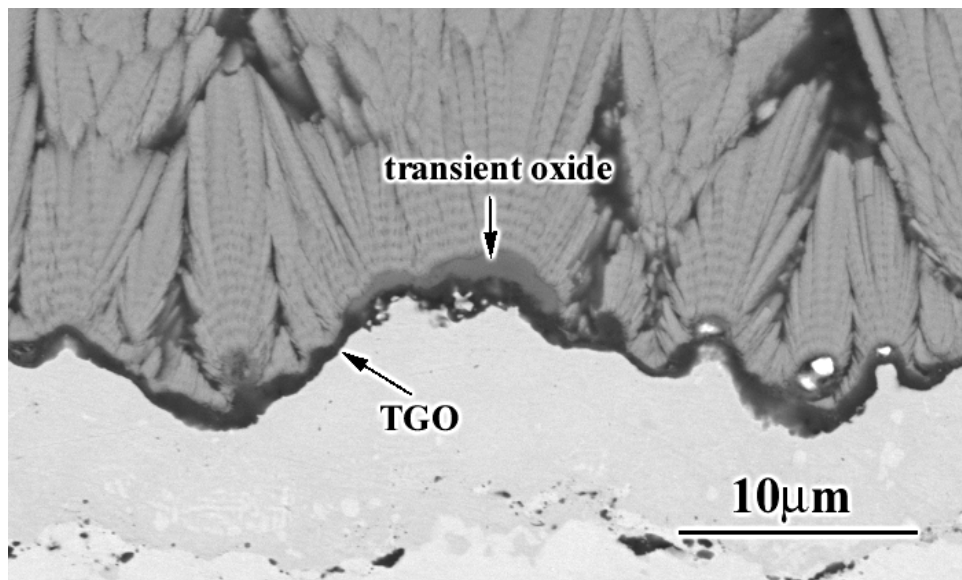


Figure 105 Scanning electron micrograph from a no bond coat TBC system after 1840 cycles of exposure before failure showing the presence of a very smooth interface.

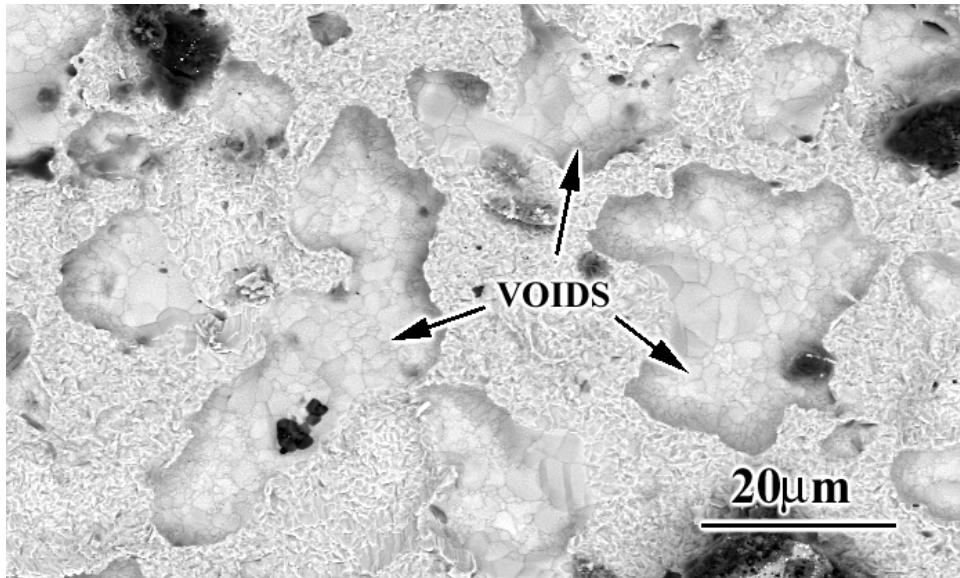


(a)

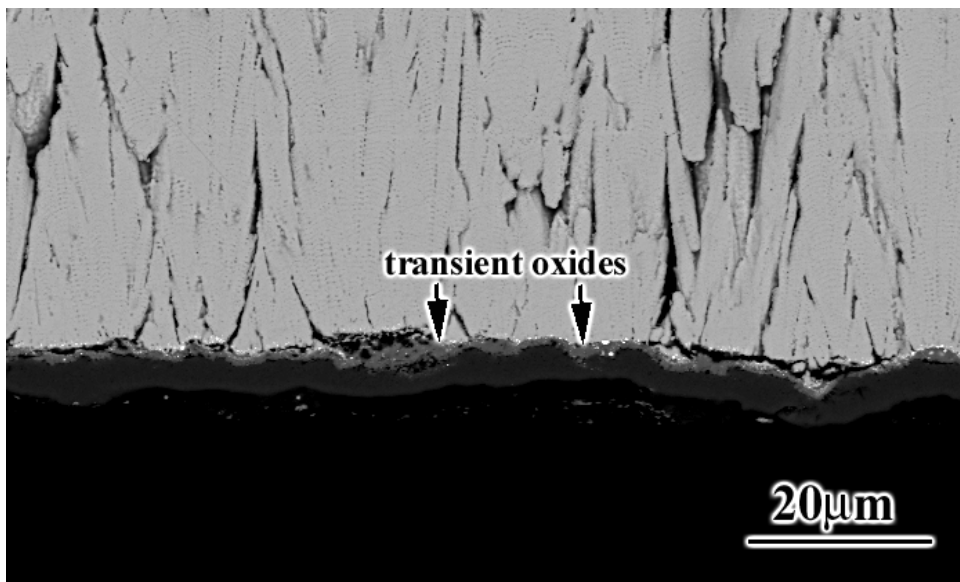


(b)

Figure 106 Scanning electron micrographs of no bond coat TBC systems with Pt overlayers in the as processed condition. The specimens from the first batch did not develop a continuous layer of TGO, (a), whereas the ones from the second batch did, (b).

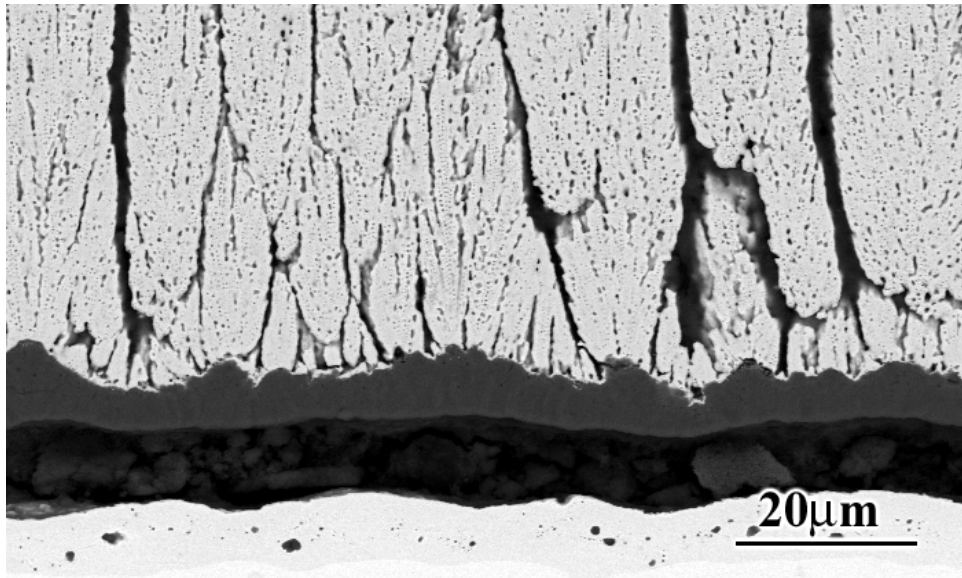


(a)

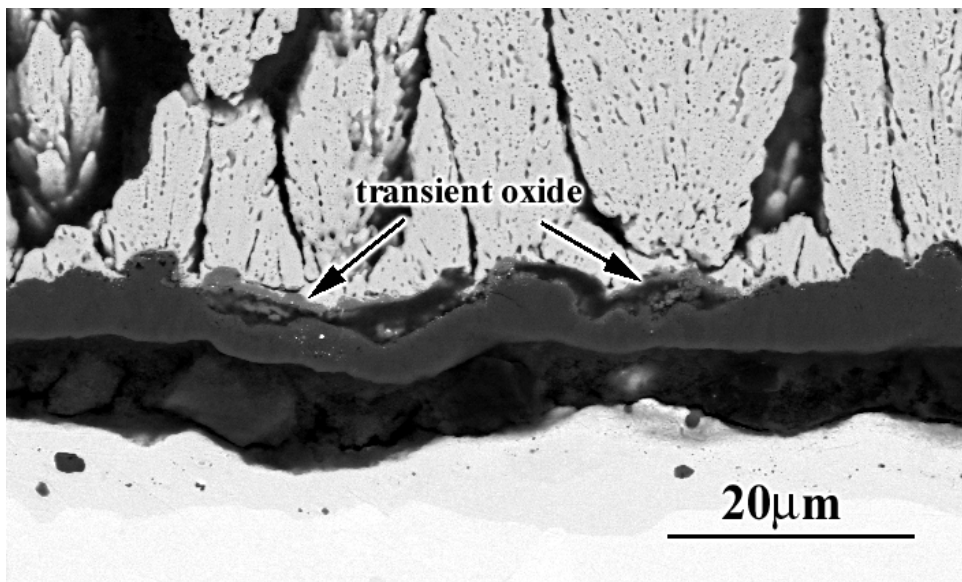


(b)

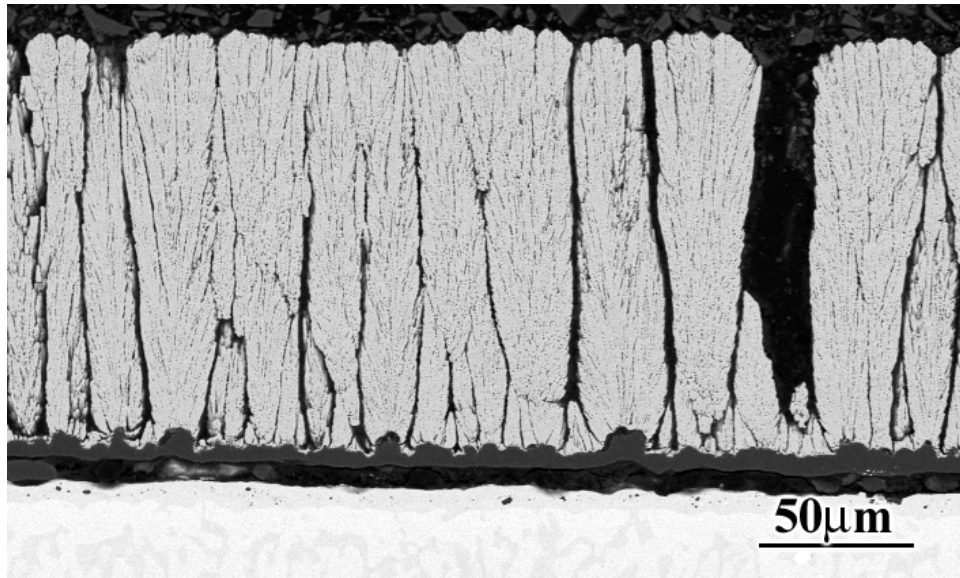
Figure 107 Scanning electron micrographs of no bond coat TBCs with Pt overlayers from the first batch showing the presence of voids, (a), and transient oxides, (b), after failure.



(a)



(b)



(c)

Figure 108 Scanning electron micrographs of second batch of no bond coat TBCs with Pt overlayers after 2300 cycles of exposure before failure. The TGO was rather pure, (a), with intermittent areas of transient oxides, (b). Numerous vertical separations were present in the TBC, (c).

4.3 SOME MICROSTRUCTURAL OBSERVATIONS

This sections involves some general microstructural observations which are not directly related with the failure of these systems, however, may be important for other reasons.

The morphology of the TGO underside of the spalled TBC is different depending on whether it was in contact with the bond coat during exposure or not as evident from Figure 109. The ridge like TGO morphology observed above a void seems to develop by the reaction of incoming oxygen through the TGO with Al available from the vapor phase or surface diffusion above the void.

It is also possible to determine if the TGO had spalled and reformed before the final failure by examining the morphology of the TGO on the fracture surface. If it has a ridge like morphology, it was not in contact with the TBC at the time of failure (Figure 110). These observations may give important clues on where the separations occurred before final failure. However, it is also important to know the history of the specimen, since similar morphologies may develop if the TBC spalls in the furnace and the exposed bond coat reoxidizes.

For some of the specimens there was evidence of sintering between the spalled and the reformed alumina. (Figure 111a and 111b).

The TGO developed on some of the specimens was observed to be non-uniform in thickness (Figure112). The origin of these thickness variations is not clear. However, one possible explanation may be the more rapid transport of oxygen through the grain boundaries of the TGO resulting in the formation of thicker oxides at these sites. These thickness variations in the TGO became less apparent as the TGO grew, probably due to conversion of small bond coat protrusions into oxides .

When the specimens with thickness variations in the TGO failed along the TGO/bond coat interface, the fracture surface consisted of small protrusions of bond coat (Figure 113a). Cross sectional examination as well as examination of the underside of the spalled TBC showed that the failure could sometimes cut through these protrusions of bond coats leaving them isolated in the TGO (Figures 113b and 113c, respectively).

Thickness variations in the TGO can sometimes be a consequence of an initially highly irregular interface such as is evident in Figure 114a. The protrusions of bond coat into the TBC, due to the irregularity of the interface, are converted into oxide quickly as a result of increased surface/volume ratio. This results in thickness variations in the TGO. The TGO/bond coat interface gradually becomes smoother as a result of this process whereas the TGO/TBC interface tries to retain the initial surface roughness (Figure 114b).

Grain imprints of the TGO were observed on the bond coat surfaces if the TGO was in contact with the bond coat during exposure (Figure 115a). It is an effective way to determine the grain size of the alumina at the bond coat interface by measuring the size of the grain imprints. It is also sometimes possible to observe the grain growth if the reformed alumina also spalls, leaving new grain imprints. Figure 115b shows the grain imprints of the reformed alumina that developed on the previous grain imprints of the spalled alumina. The difference in the grain size showed a significant amount of grain growth that took place in the TGO upon exposure. Figure 115c is another example showing the grain imprints of both original and reformed alumina side by side.

The γ' phase was usually observed to form at the grain boundaries of the β -phase of Pt Aluminide bond coats (Figure 116a). One set of specimens cooled slowly in the furnace due to some problems that developed during a cyclic test. The γ' was then observed to form not only at

the grain boundaries but also in the β -phase (Figure 116b). Another observation was the absence of γ' phase after 15 hours of exposure at 1200°C followed by quenching the specimen in cold water (compare Figures 116c and 116d where the former was quenched and the latter was not) All these results indicate the importance of cooling rate on γ' formation.

During metallographic sample preparation, separation along the interfaces as well as cracking in the bond coat may occur. The cracking along the β grain boundaries and/or β/γ' interfaces, as evident in Figures 117a and 117b, may be an indication of weaknesses at these sites.

Segmentation can take place in the TBC upon exposure (Figure 118) This seems to be an undesirable situation since the TBC segments, which are not connected to the rest of the TBC, can come off leading to localized failure of TBCs. These segments are believed to have formed by a mechanism similar to the development of vertical separations in the TBC, where small separations present in the as-processed condition enlarge with exposure as a consequence of sintering.

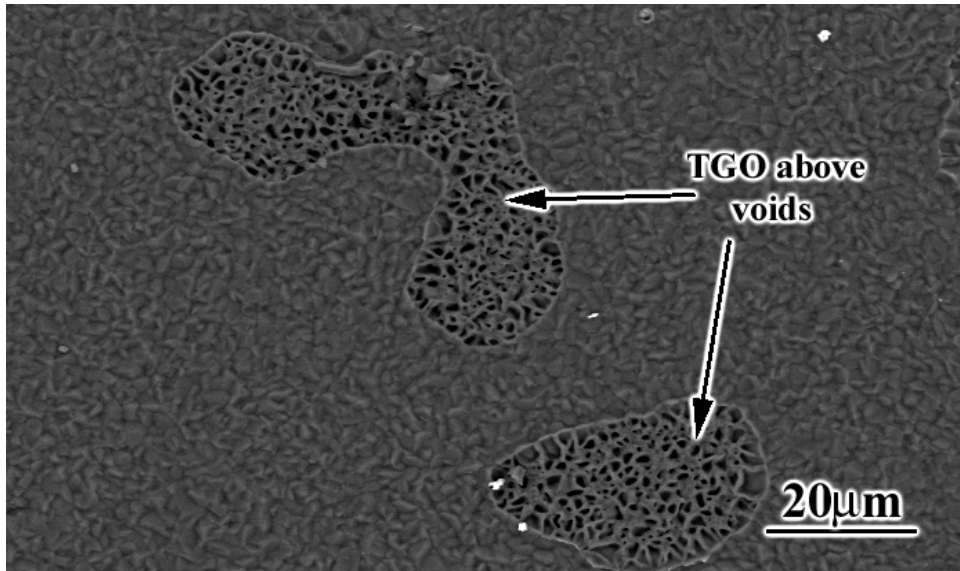


Figure 109 Scanning electron micrograph from the underside of a spalled TBC showing the ridge like morphology of the alumina that developed above voids.

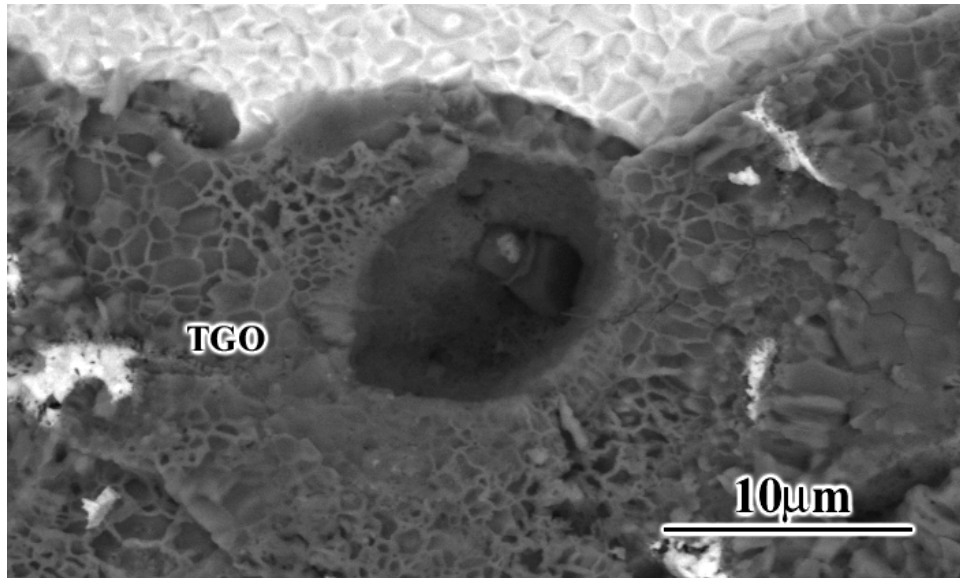
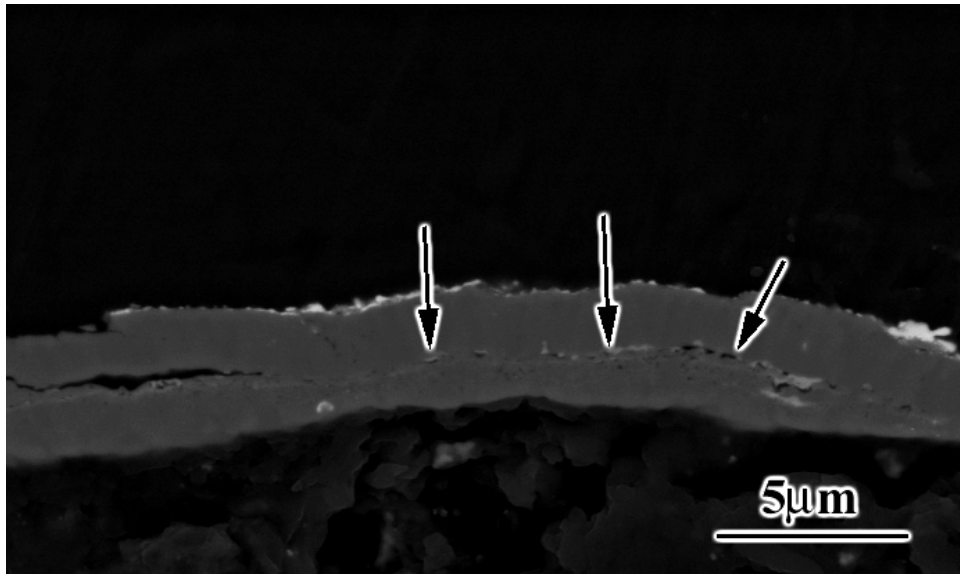
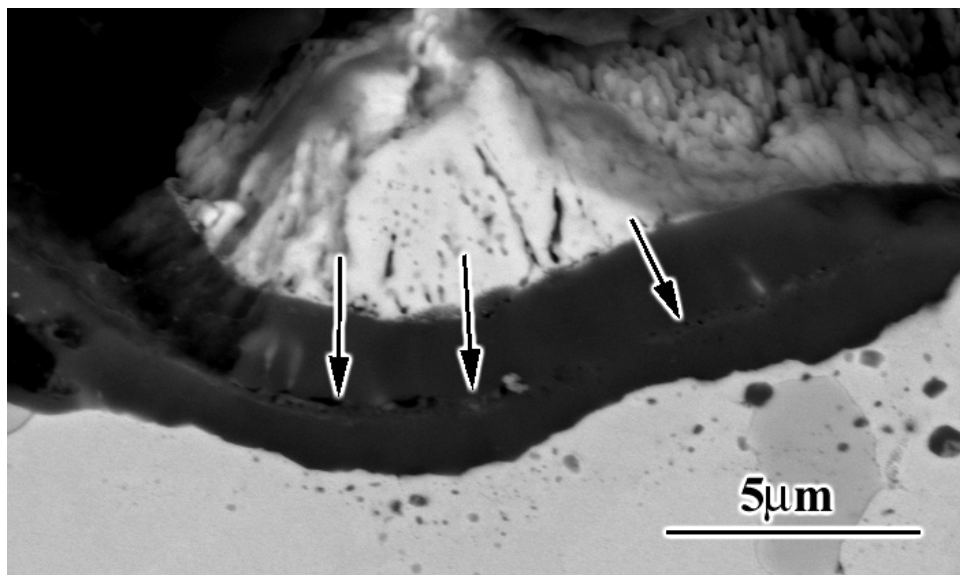


Figure 110 Scanning electron micrograph from the fracture surface of a specimen showing a ridge like alumina morphology which indicates that the TGO was not in contact with the TBC at the time of failure.



(a)



(b)

Figure 111 Scanning electron micrographs showing examples to sintering between the spalled and the reformed alumina. The arrows point to the interfaces where sintering occurred.

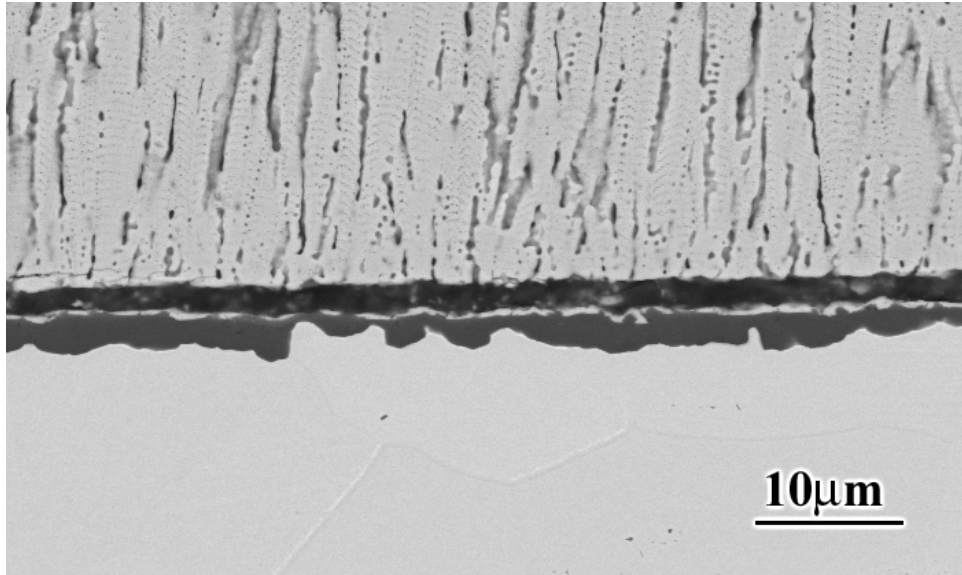
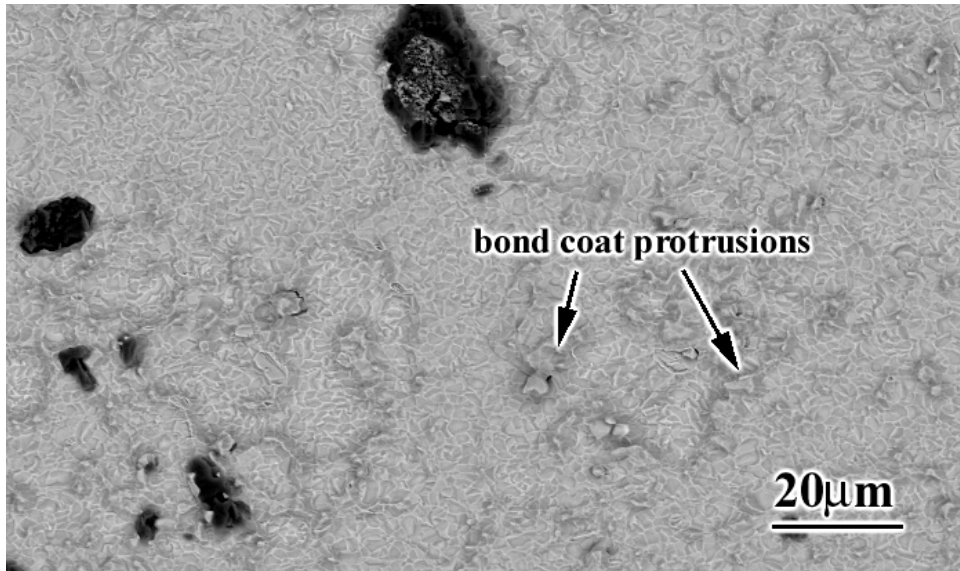
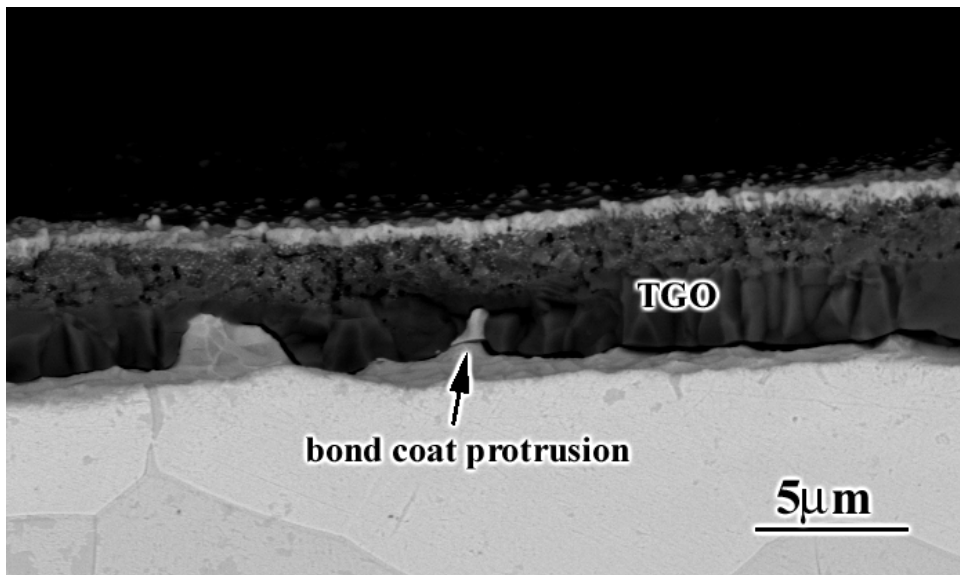


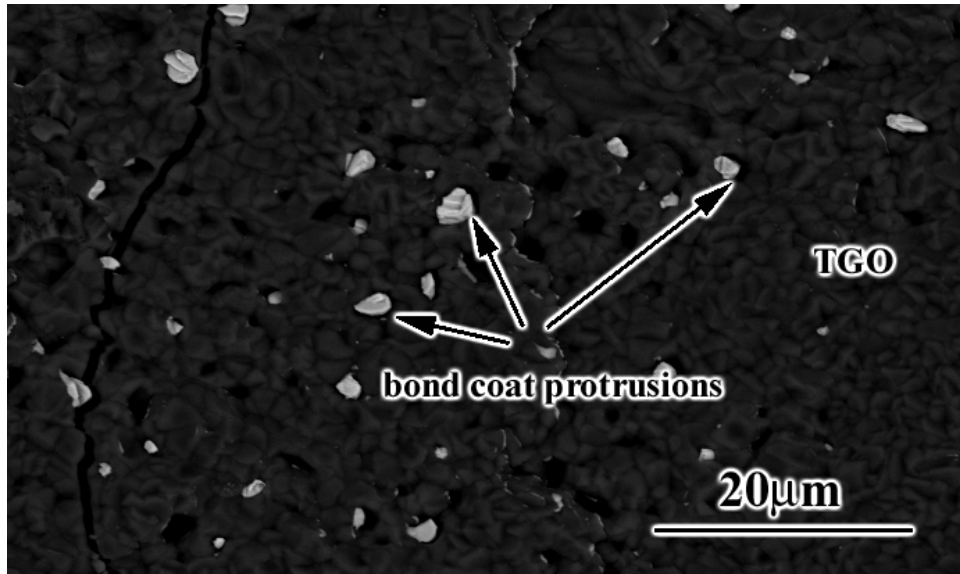
Figure 112 Scanning electron micrograph showing an example to thickness variations in the TGO.



(a)

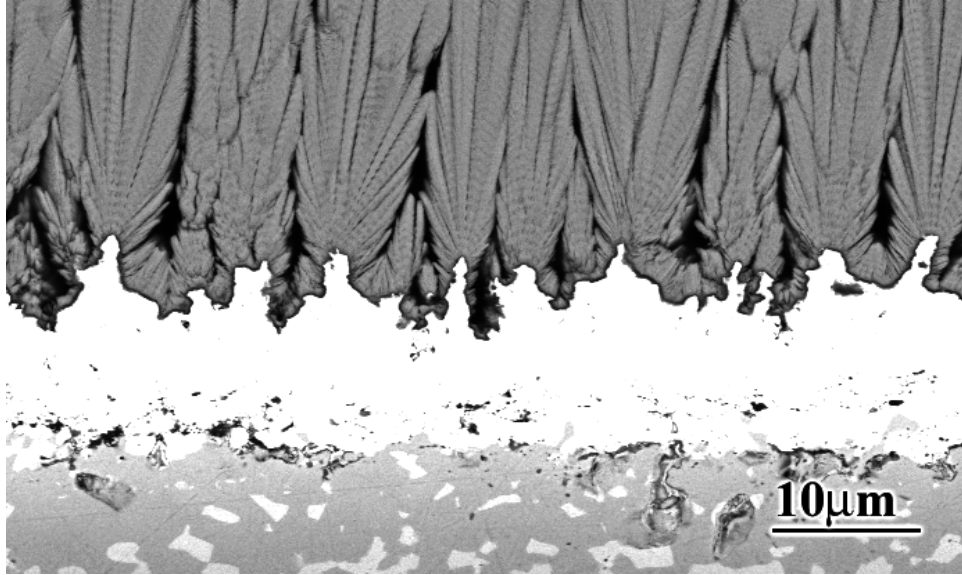


(b)

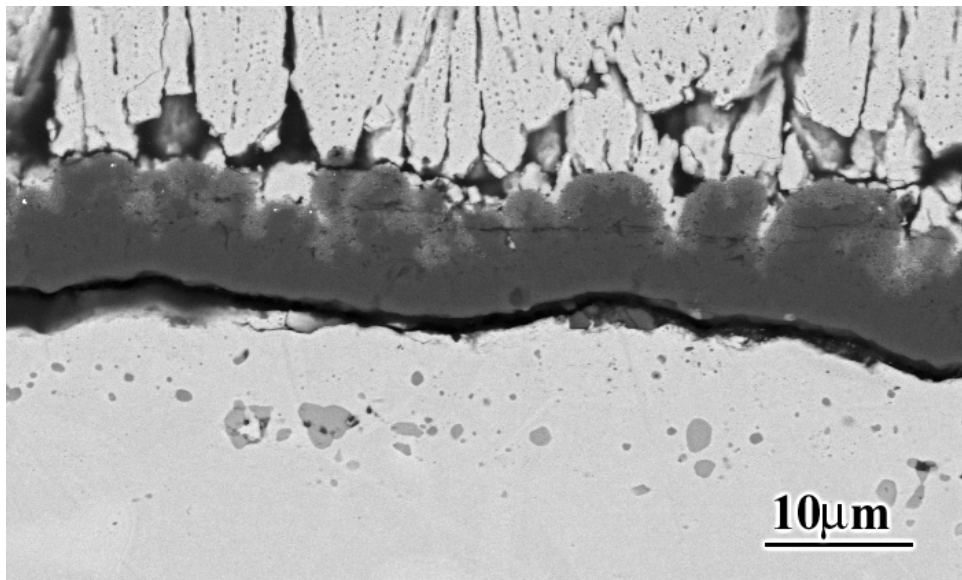


(c)

Figure 113 Scanning electron micrographs from the fracture surface, (a), cross section, (b) and underside of the spalled TBC of a specimen which developed bond coat protrusions. The failure sometimes cut through these bond coat protrusions leaving them isolated in the TGO as can be seen in (b) and (c).

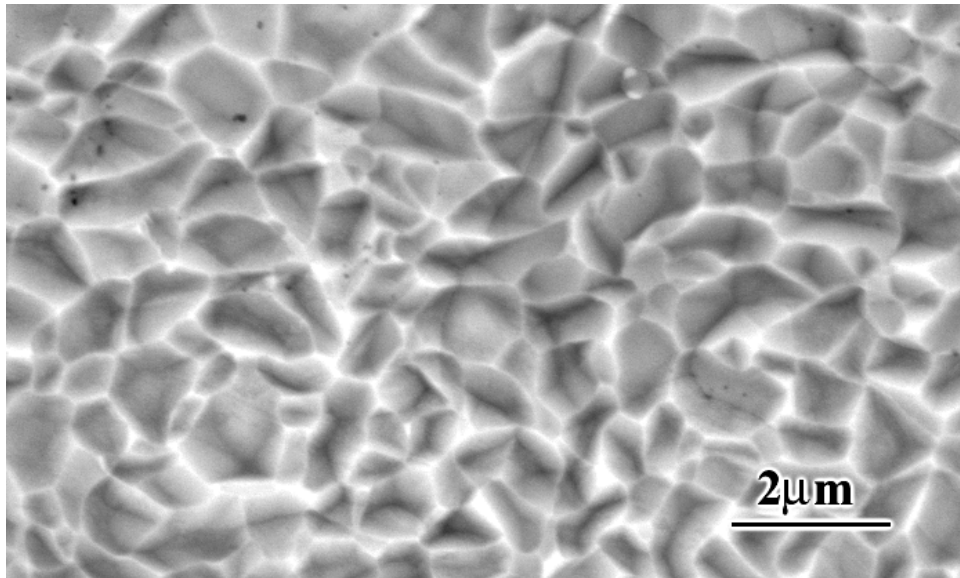


(a)

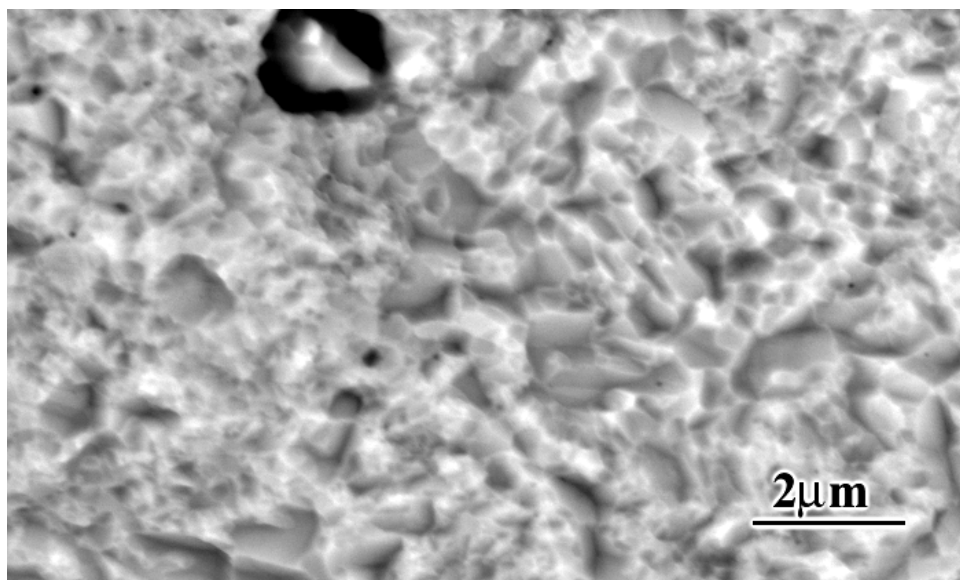


(b)

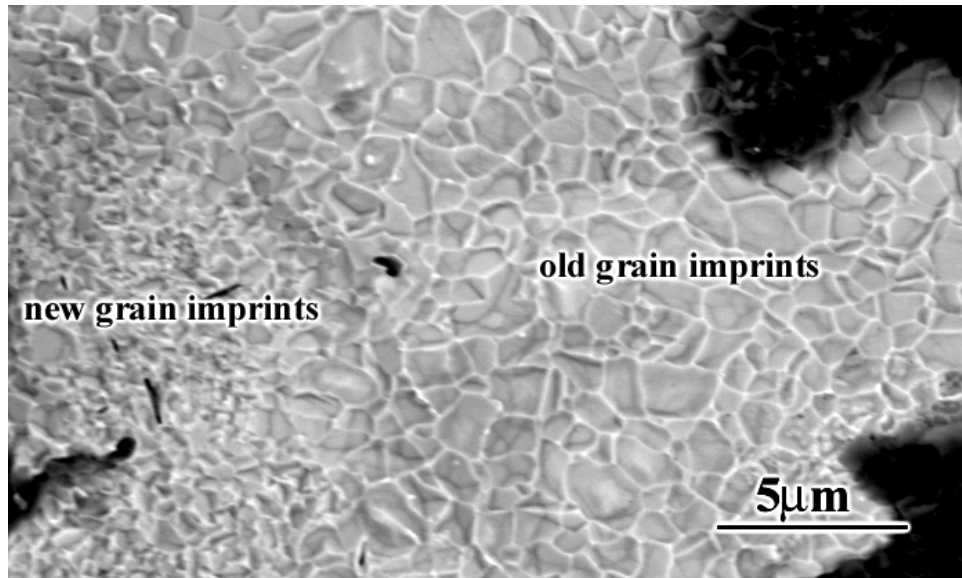
Figure 114 Scanning electron micrographs from a specimen which had a highly irregular interface in the as processed condition, (a). Upon exposure, thickness variations in the TGO developed as a result of the initially irregular interface, (b).



(a)

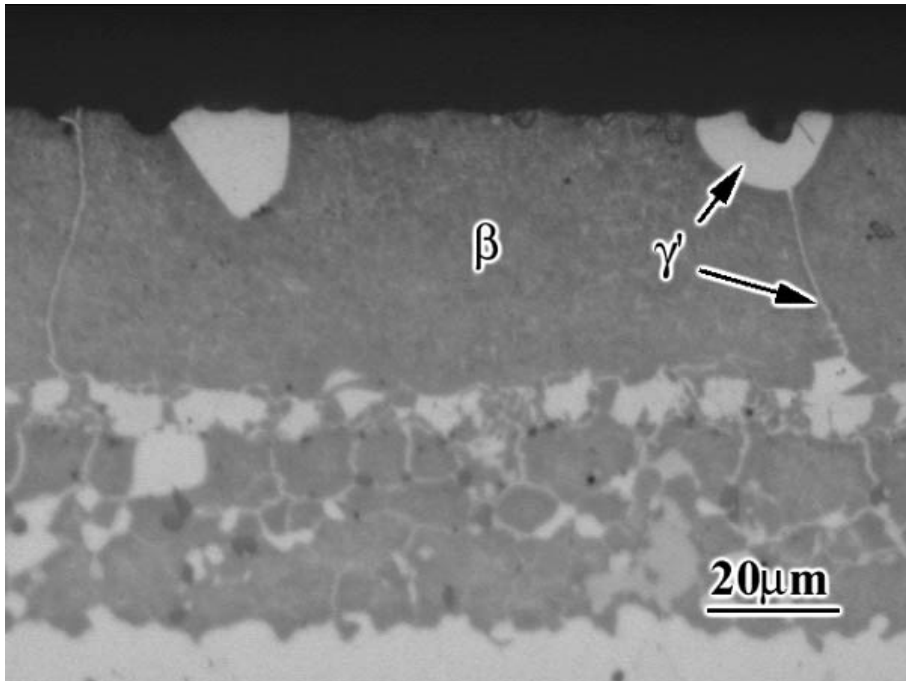


(b)

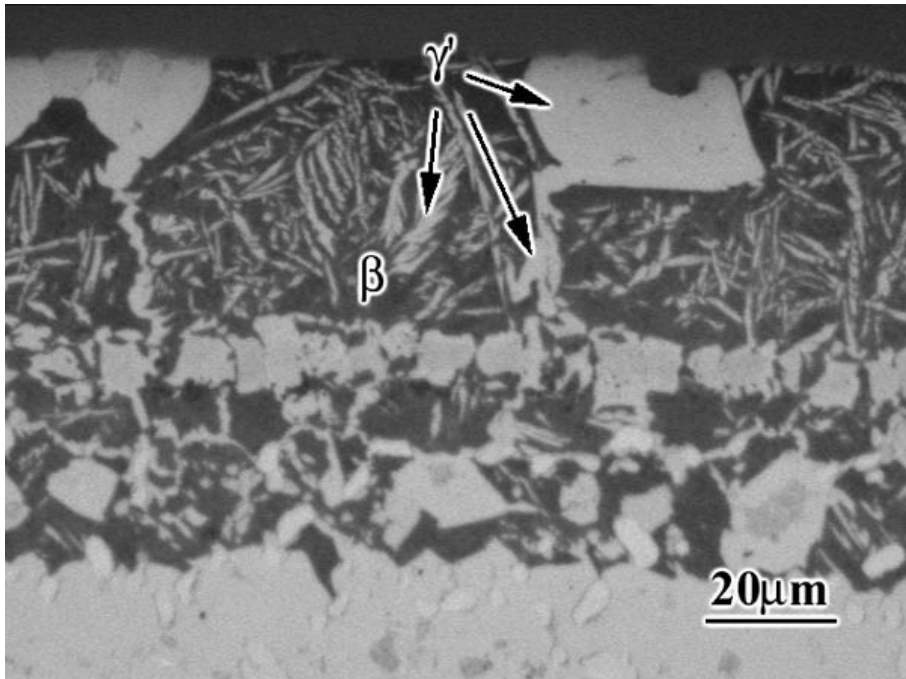


(c)

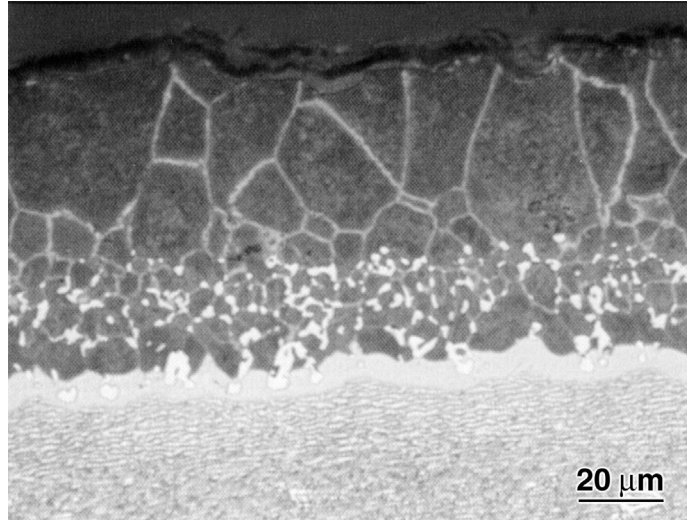
Figure 115 Scanning electron micrographs from the fracture surface of a specimen showing grain imprints of the original TGO, (a), as well as the grain imprints of the reformed and then spalled TGO, (b). The grain imprints of the original and reformed TGO can be seen side by side in (c).



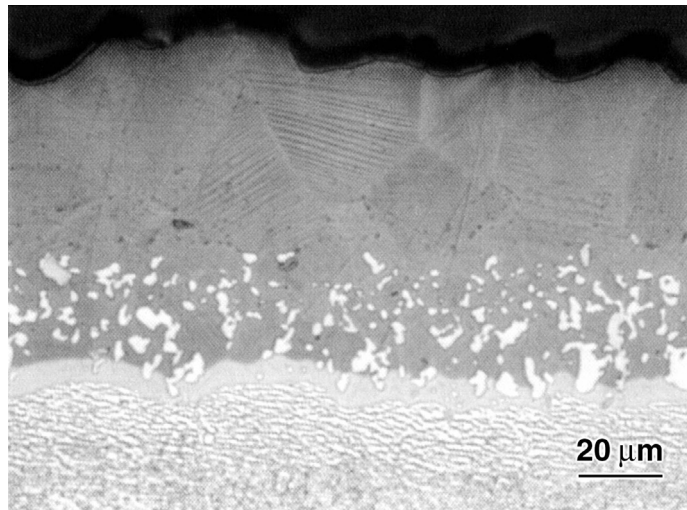
(a)



(b)

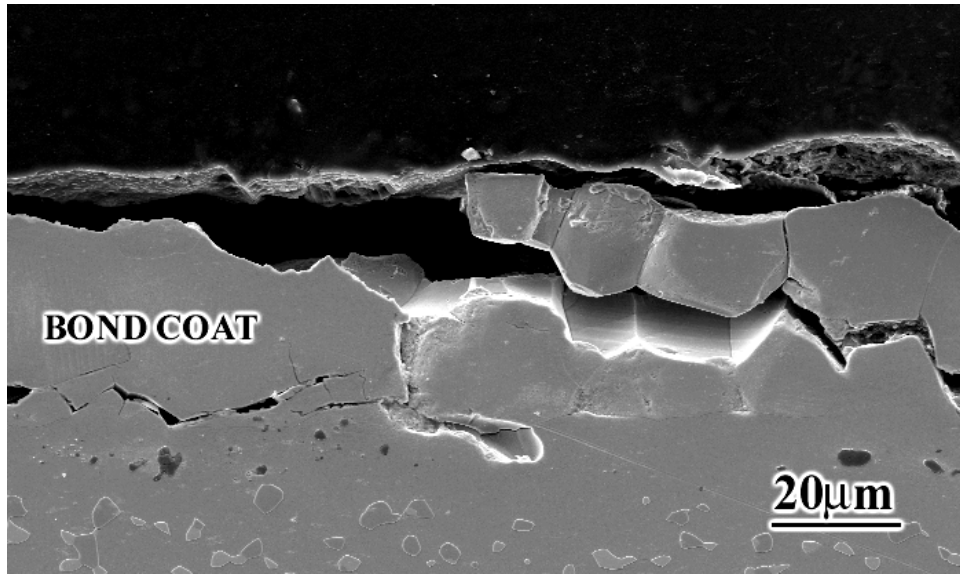


(c)

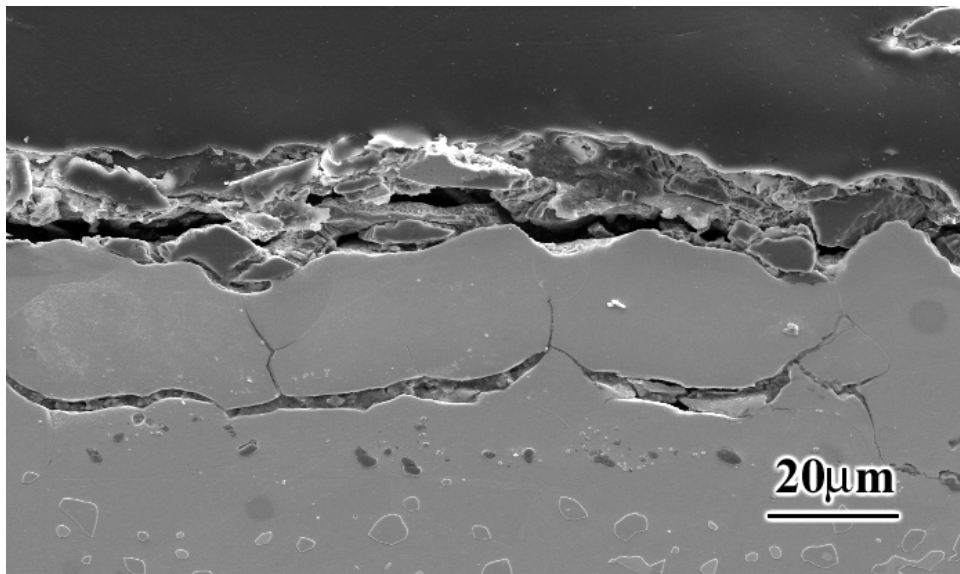


(d)

Figure 116 Optical micrographs showing the effect of cooling rate on the formation of γ' phase. The γ' phase usually developed along the grain boundaries after air cooling, (a), whereas it developed in the β phase as well as along the grain boundaries after furnace cooling, (b). One of the specimens that was air cooled after 15 hrs of exposure at 1200°C developed γ' phase along the grain boundaries, (c), whereas the other specimen which was quenched after same exposure did not develop γ' phase , (d).



(a)



(b)

Figure 117 Scanning electron micrographs showing cracking along the β grain boundaries and/or β/γ' phase boundaries during metallographic sample preparation.

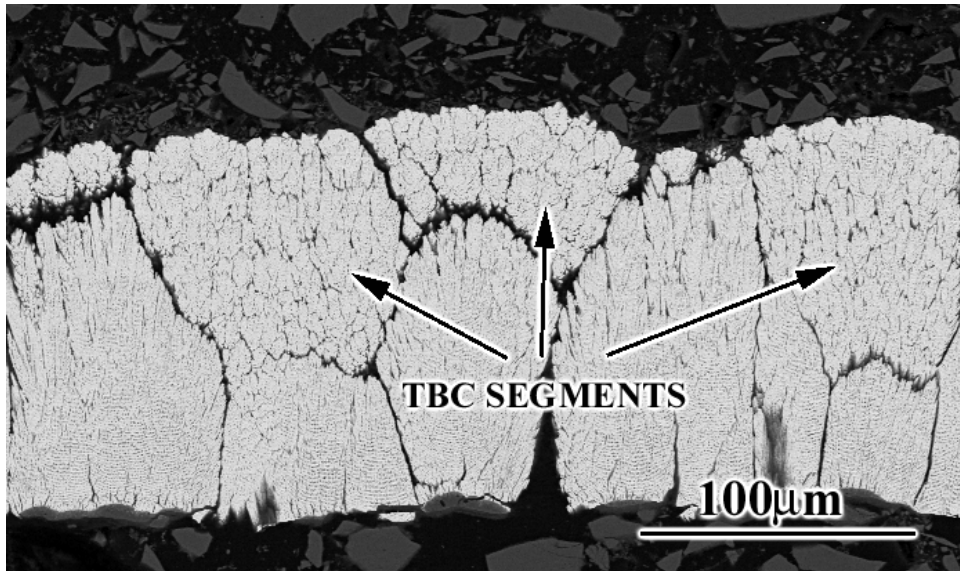


Figure 118 Scanning electron micrograph showing TBC segmentation.

4.4 IMPORTANT CONDITIONS NECESSARY FOR OPTIMIZED PERFORMANCES AND RECOMMENDATIONS FOR FUTURE WORK

Based upon the results obtained by examining a variety of TBC systems, the defects as well as the important factors in the failure of TBC systems were determined. The findings from this study opened another area of research on how to control the processing conditions to fabricate the TBC systems with optimized performances. Moreover, some important issues that still need more in depth studies for elucidation have been defined.

The surface condition of the bond coats as well as the morphology of the TBC close to the TGO, which may be a function of both surface condition and TBC deposition parameters, have been found to be very important factors that determine the performance of these TBC systems. Based upon the observations from this study, the surface preparation techniques for improved performance should result in surfaces which are smooth enough to prevent the development of TBC defects but not so smooth that they result in the development of less strain tolerant, dense TBCs. In addition to leading to formation of less strain tolerant dense TBCs, very smooth interfaces might also have the disadvantage of acting as fast propagation sites for cracks due to lack of obstacles in their paths. Therefore, the critical defect density, above which the system fails, might be less in the case of very smooth interfaces. One experiment to test this hypothesis may be performed by having a controlled amount of defects, if possible, in systems with a very smooth and a rough interface, and examine the damage in the vicinity of these defects upon exposure. Results from such a test would be very valuable to understand the reliability of the systems with very smooth interfaces. However, it should also be mentioned here that a significant number of defects is eliminated only by having smooth surfaces. Therefore,

even if the hypothesis given above is correct, the specimens with very smooth surfaces may still perform better than the ones with rough surfaces.

Light grit blasting (followed by preoxidation) was found to be an effective surface preparation technique that meets the two criteria, which were mentioned in the above paragraph, in the case of Pt aluminide bond coats and resulted in improvements in the lives of these systems compared to the current state of the art heavy grit blasted TBC systems. Media finishing also improved their lives despite the presence of remnants of grain boundary ridges. The TGO growth was slower on the media finished specimens compared to the grit blasted ones. Slower TGO growth rate can make this surface preparation technique a better candidate for the future applications. However, it still needs to be examined whether complete removal of the grain boundary ridges, which may be possible by varying the processing parameters, will result in more improvement in lives. Moreover, the effects of very smooth interfaces on premature failures, if any, still need to be ascertained. Hand polishing also resulted in the development of slow growing TGOs. However, it is not a practical surface preparation technique that can be used in industry, and its use was limited only to laboratory studies to help understand the surface condition effects. Unfortunately, hand polishing was the only surface preparation technique that resulted in improvement in the lives of TBC systems with NiCoCrAlY bond coats in this study. Since their surfaces were highly irregular in the as-processed condition, the techniques such as media finishing and vibrofinishing were not effective in smoothening the surface. Developing practical surface preparation techniques that will result in improved performance of these systems seems to be a very important area for future work if the very significant improvements obtained with smooth surfaces for these systems are to be utilized.

The TBC defects as well as the unfavorable TBC morphologies did not develop as a consequence of surface condition only, but also the TBC deposition conditions were important. Substantial variations in TBC morphologies and TBC defects were observed for specimens from different companies as well as for specimens from the same company but from different batches. Some examples of the undesirable TBC morphologies and/or defects identified in this study were given throughout the text. More work can be performed on specimens with the only difference being the TBC deposition conditions. Such a study would be important to better understand the role of different TBC morphologies on the performance of these systems. Moreover, it would also help to determine the optimized TBC processing parameters for improved lives. If the TBC deposition conditions can be standardized for optimum performance, this would also increase the reproducibility and reliability.

Once improved lives are obtained by optimizing the surfaces as well as the TBC deposition conditions, which are believed to have a first order effect on the failure of TBC systems, then other issues also become important to get more significant improvements

The characteristics of the TGO, such as growth rate and composition, have also been found to have a pronounced effect on the performance of the TBC systems as mentioned previously. Preoxidation of the bond coats prior to TBC deposition may be one possible way to control the TGO characteristics as also reported elsewhere [56, 58]. However, our results showed that even shorter lives can be obtained as a result of preoxidation treatments given prior to TBC deposition. Therefore, it is important to define the correct preoxidation conditions. It would be very valuable if preoxidation conditions that result in the development of slow growing pure TGOs (i.e. α -alumina) could be defined. It should also be kept in mind that each system may need different preoxidation treatments for improved performance. Therefore, extensive studies

on this issue seem to be essential to be able to get beneficial effects from preoxidation treatments.

The temperature dependence of the state of the art TBC failures, which suggests the role of TGO growth on the failures, was mentioned previously. In this study the modified systems were tested only at 1100°C, data points of which were also shown in Figure 21. Therefore, more testing of the modified systems (i.e. hand polished specimens) at different temperatures would be very important to see whether a similar temperature dependence holds or not.

The failures of the TBC systems with Pt aluminide bond coats used in this study have also been shown to be affected by the bond coat properties. Deformation of the bond coat by ratcheting was observed to be less pronounced for the specimens with larger grain size. Consequently, the failure times were relatively longer. However, the fact that the specimens with different grain sizes were from different companies with some other minor differences and the number of samples tested was limited, more work must be performed to confirm these observations by using specimens with the only difference being the bond coat grain size. Another important issue related to bond coat properties is the void development, which is believed to be diffusion related. Therefore, it is also important to optimize the bond coat compositions in order to eliminate or at least minimize the void development. Based upon the observations in this study, increasing the thickness of Pt and aluminide layers was found to minimize void development. Nevertheless, diffusional studies are required for the fundamental understanding of void development.

Pt is believed to improve the interfacial toughness. Better understanding of this effect may lead to new ideas for further improvements in interfacial toughness, which is believed to be a very important parameter in the failure of TBC systems.

In the case of NiCoCrAlY bond coats, further studies are required to optimize the reactive element effect. It would be very valuable if the processing conditions as well as the compositions of the bond coats could be adjusted to result in the development of a fine and uniform distribution of reactive element oxide protrusions.

Very significant TBC lives have been obtained without a bond coat, however, the results were not reproducible. Development of significant amounts of transient oxides for some of the specimens was believed to cause premature failures for these systems. Therefore, further studies to define the processing conditions that result in the development of as few transient oxides as possible may be very important to increase the reliability of no bond coat TBC systems. No bond coat TBCs are important. First, because they provide information on factors that affect TBC failures. Secondly, no bond coat TBCs could be cheaper. However, designers may never be willing to go without a bond coat due to corrosion problems upon TBC failure.

High strength of the superalloys is believed to be the key factor in the improved lives of no bond coat TBC systems. Then, strengthening the bond coats may be an alternative choice to get the beneficial effects of no bond coat systems without the rapid oxidation problems upon TBC failure.

5.0 CONCLUSIONS

5.1 BOND COATS WITH NO TBCS

- The NiCoCrAlY bond coats without TBCs developed transient oxides during cyclic oxidation sooner than Pt aluminides. Spalling of the oxide was evident. The depletion of the bond coat was due to both oxidation and interdiffusion with the substrate. The surfaces became wavy during early exposure times, but then became more smooth with longer exposure times. Surface polishing as well as preoxidation resulted in the development of more adherent and purer alumina scales.
- On the other hand, the Pt aluminide bond coats without TBCs developed more adherent and pure alumina scales. The coating depletion due to interdiffusion with the substrate was more pronounced as a result of more adherent alumina scales. With long exposure times, the surfaces became highly irregular, and large voids developed along the oxide/bond coat interface as well as along the initial superalloy/bond coat interface.
- The surfaces of the NiCoCrAlY bond coats that remained relatively smooth as well as the absence of large voids after long exposure times seems to compensate for the initially poor oxidation characteristics of NiCoCrAlY bond coats making them comparable to Pt aluminide bond coats in terms of the total oxidation lives.

5.2 CURRENT STATE OF THE ART TBC SYSTEMS

- The current state of the art TBC systems with Pt aluminide bond coats outperformed those with NiCoCrAlY bond coats.
- TBC defects associated with the initially highly irregular interface, transient oxides, reactive element rich oxide protrusions and surface defects as well as stored strain energy in the TGO were found to contribute to the failure of TBC systems with NiCoCrAlY bond coats.
- The state of the art TBC systems with Pt aluminide bond coats failed by propagation and then linking up of cracks that initiated in the TBC at areas where the bond coat underneath deformed. This is known as the ratcheting mechanism. The stored energy in the TGO was also a contributing factor in the failure of these systems. The initial interface irregularities and associated TBC defects were found to be prerequisites for ratcheting to occur. Grain size of the bond coat, type of thermal exposure and TBC deposition conditions were observed to affect the amount of ratcheting.

5.3 MODIFIED TBC SYSTEMS

- The surface condition of the bond coats was found to have a first order effect on the failure of TBC systems with both NiCoCrAlY and Pt aluminide bond coats.
- Having smooth surfaces minimized the TBC defects, which were found to play very important roles in the failure of TBC systems with NiCoCrAlY bond coats. Moreover, the surface defects in the bond coat were also eliminated. Therefore, significant improvements in lives were obtained with hand polishing the bond coat surfaces
- The failure times of the TBC systems with hand polished NiCoCrAlY bond coats varied significantly among the specimens tested, the shortest still being longer than the average failure

times of the state of the art TBCs. Examination of these specimens suggested that the failure occurred mainly along and/or close to the TGO/bond coat interface due to cracking in the vicinity of RE rich oxide protrusions as well as stored strain energy in the TGO, unless there were some other defects in the systems, which seemed to contribute to relatively early failures.

- Surface preparation techniques such as vibrofinish and media finish did not improve the lives due to the fact that these techniques could not produce a uniformly smooth surface.

- All the other modifications performed on NiCoCrAlY bond coats (depositing Pt overlayers and Pt underlayers, aluminizing the bond coat surfaces) improved the lives to some extent, with Pt overlayers having the most significant effect. The improvement in lives in the presence of Pt overlayers and aluminizing the surfaces was attributed to the development of pure and adherent alumina scales with fewer defects compared to the state of the art systems. On the other hand, the slight improvement in lives in the presence of Pt underlayers is attributed to the improved inherent TGO/ bond coat interfacial toughness.

- None of these modifications eliminated the TBC defects, which are believed to play significant roles in the failure of TBC systems. Therefore, cracking in the vicinity of the TBC defects contributed significantly to the failure of these systems. Void development in the case of aluminized NiCoCrAlY systems and the presence of all other defects (surface defects, transient oxides, RE

rich oxide protrusions) in the case of NiCoCrAlY systems with Pt underlayers were other contributing factors in the failure of these modified systems.

- The amount of Al depletion as well as void density was less pronounced for Pt aluminide bond coats with thicker layers of Pt and aluminide layers.

- The grain boundary ridges, which are present on the as aluminized Pt aluminide bond coats, acted as crack initiation sites. The cracks that initiated at these sites propagated in the TBC followed by formation of localized buckles at the early stages of their lives. Failure occurred when these localized buckles progressively got larger with time and coalesced to form a critical sized buckle.
- The surface of the bond coat beneath the localized buckles deformed whereas it remained smooth at areas where the TBC was still in contact with the bond coat at the time of failure. These observations indicated the presence of TBC constraint to deformation of the bond coat.
- All surface preparation techniques used in this study for Pt aluminide bond coats (light grit blast, media finish and hand polish) resulted in relatively smooth surfaces compared to the state of the art Pt aluminide systems. The improvement in lives was attributed mainly to the prevention of the ratcheting type of failure. Moreover, the TGO growth was found to be slower on media finished and hand polished specimens.
- Void development as well as the stored strain energy in the TGO are believed to be the main factors in the failure of light grit blasted and preoxidized Pt aluminide bond coats. On the other hand, the media finished as well as hand polished Pt aluminide bond coats failed in the presence of remnants of grain boundary ridges, which were shown to act as crack initiation sites.

5.4 NO BOND COAT TBC SYSTEMS

- The significantly long lives of no bond coat TBCs was attributed to the high strength of the superalloy, which did not permit the surface deform.

- A trend was observed whereby earlier failures could be associated with the presence of substantial amounts of transient oxides.

BIBLIOGRAPHY

1. Meier, S.M., D.K. Gupta, and K.D. Sheffler, "Ceramic Thermal Barrier Coatings for Commercial Gas Turbine Engines", Journal of Metals, Vol (1991), pp. 50-53.
2. Mutasim, Z., C. Rimlinger, and B. W., "Characterization of Plasma Sprayed and Electron Beam Physical Vapor Deposited Thermal Barrier Coatings", in the proceedings of International Gas Turbine and Aeroengine Congress and Exhibition, 1997, Orlando, Florida.
3. Scott, H.C., "Phase Relationships in the Zirconia-Yttria System", J. Mater. Sci., Vol 10, (1975), pp. 1527-35.
4. Taylor, T.A. and R.E. Taylor, "Testing of Stability and Thermal Properties of Thermal Barrier Coatings". in ASM Handbook, Surface Engineering. 1994, ASM: Materials Park, OH.
5. Wood, J.H. and E.H. Goldman, "Protective Coatings", in the proceedings of Superalloys 2, 1987, John Wiley and Sons, pp. 359-383
6. Strangman, T.E., "Thermal barrier coatings for turbine airfoils", Thin Solid Films, Vol 127, (1985), pp. 93-105.
7. Teer, D.G., "Evaporation and Sputter Techniques", in the proceedings of Coatings for High Temperature Applications, 1983, Netherlands, Applied Science, pp. 79-121
8. Mattox, D.M., "Growth and Growth Related Properties of Films Formed by Physical Vapor Deposition". in ASM Handbook, Surface Engineering. 1994, ASM: Materials Park, OH.
9. Goward, G.W., "Diffusion Coatings for Gas Turbine Engine Hot Section parts". in ASM Handbook, Surface Engineering. 1994, ASM: Materials Park, OH.
10. Duret, C. and R. Pichoir, "Protective Coatings for High Temperature Materials: Chemical Vapor Deposition and Pack Cementation Processes", in the proceedings of Coatings for High Temperature Applications, 1983, Netherlands, Applied Science, pp. 33-79
11. Warnes, B.M. and D.C. Punola, "Clean diffusion coatings by chemical vapor deposition", Surface and Coatings Technology, Vol 94-95, (1997), pp. 1-6.

12. Punola, D., D. Sikkenga, and M. Sutton, "Platinum Aluminide Coating Enhances Durability", Advanced Materials and Processes, Vol 12, (1995), pp. 29-30.
13. Goward, G.W. and D.H. Boone, Oxidation of Metals, Vol 3, (1971), pp. 475-495.
14. Das, D.K., V. Singh, and S.V. Joshi, "Evaluation of Aluminide Coating Microstructure on Nickel-Base Cast Superalloy CM-247 in a Single Step High-Activity Aluminizing Process", Metallurgical and Materials Transactions A, Vol 29A, (1998), pp. 2173-2188.
15. Jackson, M.R. and J.R. Rairden, Metall. Trans. A, Vol 8, (1977), pp. 1697-1707.
16. Krishna, G.R., *et al.*, "Role of Pt content in the microstructural development and oxidation performance of Pt-aluminide coatings produced using a high-activity aluminizing process", Materials Science & Engineering A (Structural Materials: Properties, Microstructure and Processing), Vol A251, (1998), pp. 40-7.
17. Farrell, M.S., D.H. Boone, and R. Streiff, "Oxide adhesion and growth characteristics on platinum-modified aluminide coatings", Surface and Coatings Technology, Vol 32, (1987), pp. 69-84.
18. Schaffer, J., *et al.*, "The effects of Precious Metals on the Oxidation and Hot Corrosion of Coatings", in the proceedings of The Role of Active Elements in the Oxidation Behaviour of High Temperature Metals and Alloys, 1988, Netherlands, Elsevier Applied Science, pp. 231-267
19. Lin, K.L. and C.M. Hwang, "Interdiffusion of the Aluminized and Pt-aluminized Coatings on Mar-M247 Superalloy", Surface and Coatings Technology, Vol 56, (1992), pp. 81-87.
20. Tawancy, H.M., *et al.*, "Thermal stability of a platinum aluminide coating on nickel-based superalloys", Journal of Materials Science, Vol 27, (1992), pp. 6463-74.
21. Tawancy, H.M., *et al.*, "Comparative thermal stability characteristics and isothermal oxidation behavior of an aluminized and a Pt-aluminized Ni-base superalloy", Scripta Metallurgica et Materialia, Vol 33, (1995), pp. 1431-8.
22. Niu, Y., *et al.*, "Oxidation Behaviour of Simple and Pt-modified Aluminide Coatings on IN738 at 1100C", Journal De Physique 4, Vol 3, (1993), pp. 511-519.
23. Wood, G.C. and F.H. Stott, "The Development and Growth of Protective Alumina Scales on Alloys", in the proceedings of High temperature Corrosion, 1981, San Diego, California, National Association of Corrosion Engineers, pp. 227-51
24. Tucker, R.C., "Thermal Spray Coatings". in ASM Handbook, Surface Engineering. 1994, ASM: Materials Park, OH.

25. Steffens, H.D., "Spray and Detonation Gun Technologies, Laser Assited Techniques", in the proceedings of Coatings for High Temperature Applications, 1983, Netherlands, Applied Science, pp. 121-139
26. Wood, G.C., Oxidation of Metals, Vol 2, (1970), pp. 11-57.
27. Stott, F.H., "Principles of Growth and Adhesion of Oxide Scales", in the proceedings of The Role of Active Elements in the Oxidation Behaviour of High Temperature Metals and Alloys, 1988, Netherlands, Elsevier Applied Science, pp. 3-21
28. Meier, G.H., private communication
29. Pint, B.A., "Experimental Observations in Support of the Dynamic Segregation Theory to Explain the Reactive Element Effect", Oxidation of Metals, Vol 45, (1996), pp. 1-37.
30. Huntz, A.M., "Effect of Active Elements on the Oxidation Behaviour of Alumina Formers", in the proceedings of The Role of Active Elements in the Oxidation Behaviour of High Temperature Metals and Alloys, 1988, Netherlands, Elsevier Applied Science, pp. 81-109
31. Allam, I.M., D.P. Whittle, and J. Stringer, "The oxidation behaviour of CoCrAl systems containing active element additions", Oxidation of Metals, Vol 12, (1978), pp. 35-66.
32. Allam, I.M., H.C. Akuezue, and D.P. Whittle, "Influence of Small Pt Additions on Alumina Scale Adherence", Oxidation of Metals, Vol 14, (1980), pp. 517-531.
33. Gupta, D.K. and D.S. Duvall, "Efects of Coating-Substrate In-Diffusion on the Performance of Plasma Sprayed M-Cr-Al-Y Coatings", Thin Solid Films, Vol 73, (1980), pp. 477-480.
34. Giggins, C.S. and F.S. Pettit, "Oxidation of Ni-Cr-Al Alloys Between 1000 and 1200 C", J. Electrochem. Soc., Vol 118, (1971), pp. 1782-1790.
35. Tolpygo, V.K. and D.R. Clarke, "Microstructural Study of the Theta-Alpha Transformation in Alumina Scales Formed on Nickel Aluminides", Materials At High Temperature, Vol 17, (2000), pp. 59-70.
36. Felten, E.J. and F.S. Pettit, "Development, growth, and adhesion of Al/sub 2/O/sub 3/ on platinum-aluminum alloys", Oxidation of Metals, Vol 10, (1976), pp. 189-223.
37. Zhang, Y., *et al.*, "Synthesis and cyclic oxidation behavior of a (Ni,Pt)Al coating on a desulfurized Ni-base superalloy", Metallurgical and Materials Transactions A (Physical Metallurgy and Materials Science), Vol 30A, (1999), pp. 2679-87.
38. Fountain, J.G., *et al.*, "The Influence of Platinum on the Maintenance of Alumina as a Protective Scale", Oxidation of Metals, Vol 10, (1976), pp. 341-345.
39. Lipkin, D.M. and D.R. Clarke, Oxidation of Metals, Vol 49, (1996), pp. 187-211.

40. Schumann, E., *et al.*, Oxidation of Metals, Vol 53, (2000), pp. 259.
41. Sarioglu, C., *et al.* in the proceedings of Microscopy of Oxidation 3, 1997, The Institute of Materials, London, , pp. 41
42. Evans, A.G., *et al.*, "Mechanisms Controlling the Durability of Thermal Barrier Coatings", Progress in Materials Science, Vol 46, (2001), pp. 505-553.
43. Miller, R., Journal of American Ceramic Society, Vol 67, (1984), pp. 517.
44. Miller, R., "Thermal Barrier Coatings for Aircraft Engines- History and Directions", in the proceedings of Thermal Barrier Coating Workshop, 1995, Cleveland, Ohio.
45. Miller, R.A. and C.E. Lowell, "Failure mechanisms of thermal barrier coatings exposed to elevated temperatures", Thin Solid Films, Vol 95, (1982), pp. 265-73.
46. Bartlett, A.H. and R.D. Maschio, "Failure mechanisms of a zirconia-8 wt.% yttria thermal barrier coating", Journal of the American Ceramic Society, Vol 78, (1995), pp. 1018-24.
47. Meier, S.M. and D.K. Gupta, "The Evaluation of Thermal Barrier Coatings in Gas Turbine Engine Applications", Journal of Engineering for Gas Turbines and Power, Vol 116, (1994), pp. 250-257.
48. Sohn, Y.H., R.R. Biederman, and R.D. Sisson, Jr., "Isothermal oxidation of physical vapor deposited partially stabilized zirconia thermal barrier coatings", Journal of Materials Engineering and Performance, Vol 3, (1994), pp. 55-60.
49. DeMasi-Marcin, J.T., K.D. Sheffler, and S. Bose, "Mechanisms of Degradation and Failure in a Plasma Deposited Thermal Barrier Coating", Journal of Engineering for Gas Turbines and Power, Vol 112, (1990), pp. 521-526.
50. Rabiei, A. and A.G. Evans, "Failure mechanisms associated with the thermally grown oxide in plasma-sprayed thermal barrier coatings", Acta Materialia, Vol 48, (2000), pp. 3963-76.
51. Mumm, D.R. and A.G. Evans, "On the role of imperfections in the failure of a thermal barrier coating made by electron beam deposition", Acta Materialia, Vol 48, (2000), pp. 1815-27.
52. Evans, A., private communication
53. Wu, B.C., *et al.*, "Microstructures, properties and failure analysis of (ZrO₂-8 wt.% Y₂O₃)/((Co,Ni)-Cr-Al-Y) thermal barrier coatings", Materials Science & Engineering A, Vol (1989), pp. 201-10.
54. Wu, B.C., *et al.*, "The oxide pegging spalling mechanism and spalling modes of ZrO₂-8 wt.% Y₂O₃/Ni-22Cr-10Al-1Y thermal barrier coatings under various operating conditions", Journal of Materials Science, Vol 25, (1990), pp. 1112-19.

55. Anton, R., Cyclic Oxidation of High Temperature Materials. 1999, London: Carlton House Terrace.
56. Lih, W., *et al.*, "Effects of bond coat preoxidation on the properties of ZrO₂-8wt.% Y₂O₃/Ni-22Cr-10Al-1Y thermal-barrier coatings", Oxidation of Metals, Vol 36, (1991), pp. 221-38.
57. Lih, W., *et al.*, "Effect of pre-aluminization on the properties of ZrO₂-8 wt.% Y₂O₃/Co-29Cr-6Al-1Y thermal-barrier coatings", Oxidation of Metals, Vol 38, (1992), pp. 99-124.
58. Lih, W., *et al.*, "Effect of bond-coat pre-aluminization and pre-oxidation duplex pretreatment on the performance of ZrO₂-8wt.% Y₂O₃/Co-29Cr-6Al-1Y thermal-barrier coatings", Oxidation of Metals, Vol 40, (1993), pp. 229-43.
59. Shillington, E.A.G. and D.R. Clarke, "Spalling failure of a thermal barrier coating associated with aluminum depletion in the bond-coat", Acta Materialia, Vol 47, (1999), pp. 1297-305.
60. Haynes, J.A., *et al.*, "Mechanical properties and fracture behavior of interfacial alumina scales on plasma-sprayed thermal barrier coatings", Materials at High Temperatures, Vol 16, (1999), pp. 49-69.
61. Tolpygo, V.K. and D.R. Clarke, "Surface rumpling of a (Ni,Pt)Al bond coat induced by cyclic oxidation", Acta Materialia, Vol 48, (2000), pp. 3283-93.
62. Chen, M.W., *et al.*, "Microstructural Evolution of Platinum Modified Nickel Aluminide Bond Coat During Thermal Cycling", Surface and Coatings Technology, Vol 163-164, (2003), pp. 25-30.
63. Zhang, Y., *et al.*, "Martensitic Transformation in CVD NiAl and (Ni,Pt)Al Bond Coatings", Surface and Coatings Technology, Vol 163-164, (2003), pp. 19-24.
64. Darzens, S., *et al.*, "Observations and Analysis of the Influence of Phase Transformations on the Stability of the Thermally Grown Oxide in a Thermal Barrier System", Metallurgical and Materials Transactions, Vol 34A, (2003), pp. 511-522.
65. Gell, M., *et al.*, "Mechanism of spallation in platinum aluminide/electron beam physical vapor-deposited thermal barrier coatings", Metallurgical and Materials Transactions A, Vol 30A, (1999), pp. 427-35.
66. Tawancy, H.M., *et al.*, "Comparative performance of selected bond coats in advanced thermal barrier coating systems", Journal of Materials Science, Vol 35, (2000), pp. 3615-29.
67. Schaffer, J.C., in the proceedings of TBC Workshop, 1997, NASA Levis Research Center, Materials Division, Cleveland, OH.

68. Clarke, D.R., V. Sergo, and M.Y. He, "Precursor to TBC failure caused by constrained phase transformation in the thermally grown oxide", Elevated Temperature Coatings: Science and Technology III. Proceedings of Symposium, Vol (1999), pp. 67-78.
69. Vasinonta, A. and J.L. Beuth, "Measurement of interfacial toughness in thermal barrier coating systems by indentation", Engineering Fracture Mechanics, Vol 68, (2001), pp. 843-860.
70. Stiger, M.J., *et al.*, "Mechanisms for the failure of electron beam physical vapor deposited thermal barrier coatings induced by high temperature oxidation", in the proceedings of Elevated Temperature Coatings: Science and Technology III. TMS Annual Meeting, 1999, San Diego, CA, TMS, pp. 51-65
71. Kim, G.M., *et al.*, "The effect of the type of thermal exposure on the durability of thermal barrier coatings", Scripta Materialia, Vol 46, (2002), pp. 489-495.
72. Gleeson, B., private communication
73. Schaffer, J.C., M.S. Thesis, The Effect of Platinum on the Behaviour of Diffusion Aluminide Coatings, Materials Science and Engineering, University of Pittsburgh, 1987
74. Tolpygo, V.K. and D.R. Clarke, "Morphological Evolution of Thermal Barrier Coatings Induced by Cyclic Oxidation", Surface and Coatings Technology, Vol 163-164, (2003), pp. 81-86.
75. Tolpygo, V.K., D.R. Clarke, and K.S. Murphy, "The effect of grit blasting on the oxidation behavior of a platinum-modified nickel-aluminide coating", Metallurgical-and-Materials-Transactions, Vol 32A, (2001), pp. 1467-78.